Deliverable 8.2: Updated State-of-the-art report

Work Package 8

The project leading to this application has received funding from the European Union's Horizon 2020 research and innovation programme under grant agreement No 847593.

Document information

Project Acronym	**EURAD**
Project Title	**European Joint Programme on Radioactive Waste Management**
Project Type	**European Joint Programme (EJP)**
EC grant agreement No.	**847593**
Project starting / end date	**1st June 2019 – 30 May 2024**
Work Package No.	**8**
Work Package Title	**Spent Fuel Characterisation and Evolution Until Disposal**
Work Package Acronym	**SFC**
Deliverable No.	**8.2**
Deliverable Title	**Updated State-of-the-art report**
Lead Beneficiary	**Nagra** **National Cooperative for the Disposal of Radioactive Waste**
Contractual Delivery Date	**31.05.2024**
Actual Delivery Date	**12.09.2024**
Type	
Dissemination level	**PU**
Authors	**Efstathios Vlassopoulos (Nagra), Ron Dagan (KIT), Luca Fiorito (SCK CEN), Michel Herm (KIT), Peter Jansson (UU), Marjan Kromar (JSI), Márton Király (MTA-EK), Jaakko Leppanen (VTT), Francisco Feria Marquez (CIEMAT), Volker Metz (KIT),** **Dimitrios Papaioannou (JRC KA), Luis E. Herranz (CIEMAT), Dimitri Rochman (PSI), Peter Schillebeeckx (JRC), Marcus Seidl (EON), Augusto Hernandez Solis (SCK CEN), Alexey Stankovskiy (SCK CEN), Francisco Alvarez Velarde (CIEMAT), Marc Verwerft (SCK CEN), Mª Nieves Rodriguez Villagra (CIEMAT), Thierry Wiss (JRC KA), Uwe Zencker (BAM), Gasper Žerovnik (JRC)**

To be cited as:

Final version as of 12.09.2024 of deliverable D8.1 of the HORIZON 2020 project EURAD. EC Grant agreement no: 847593

Disclaimer

Acknowledgement

This document is a deliverable of the European Joint Programme on Radioactive Waste Management (EURAD). EURAD has received funding from the European Union's Horizon 2020 research and innovation programme under grant agreement No 847593.

Status of deliverable		
	By	Date
Delivered (Lead Beneficiary)	Nagra	31.01.2020
Verified (WP Leader)	SKB	31.01.2020
Reviewed (Reviewers)	Stefano Caruso (KKG) Henrik Liljenfeldt (Noemi AnalyticsKB David Hambley (NNL, UK) Laura McManniman (IAEA	01.09.2024
Approved (PMO)	Paul Carbol	16.01.2024
Submitted to EC (Coordinator)	Andra (Coordinator)	25.09.2024

EURAD SFC – Project Overview

EURAD is an EC-funded project with a programme of integrated work packages (WPs) spanning many domains of radioactive waste management based on the needs and views of the mandated actors of the Member States. The EURAD scope seeks to be beneficial to national waste management programmes at all stages of advancement by supporting them in their RD&D activities. For that purpose, EURAD has a strong focus on knowledge management with a view to making existing information easily available and to provide means for transfer knowledge.

The project Spent Fuel Characterisation and Evolution Until Disposal (SFC) is WP8 within the framework of the EURAD programme, aiming to provide a better understanding of spent nuclear fuel (SNF) properties from the perspective of pre-disposal activities, but also exploring aspects having an impact on long-term safety. The EURAD/SFC consortium brings together more than 20 partners with a range of skills and competences in spent fuel assessment, from management to experimental work. The consortium consists of national waste management organisations, research institutes, universities, technical support organisations and commercial organisations.

The results obtained within the WP will provide a rigorous scientific approach to developing the technical bases for continued safe and secure storage of spent nuclear fuel, in terms of transport, retrieval and pre-disposal options. These achievements are intended to support national programmes and safety assessments and are made available to all interested stakeholders. Safety aspects (i.e. better acknowledgement of safety-related parameter uncertainties, the contribution and further development of guidance on operational safety for both interim storage and fuel packaging facilities) and optimisation aspects (i.e. optimisation of the number of assemblies for the loading of disposal canisters based on precise determination of decay heat and reactivity of spent fuel assemblies) were addressed by the WP. Extremely valuable are the combination of both numerical calculations and experimental methods, which aims to provide a complete and thorough understanding of the mechanisms driving the behaviour of the SNF in pre-disposal activities, for both normal and accident conditions.

For more information, please visit the EURAD website at: https://www.ejp-eurad.eu/

Executive Summary

The final task of WP8 is dedicated to the update of the state-of-the-art (SOTA) report. Accordingly, this report provides the progress made in the underpinning knowledgebase, it documents the identified technical gaps and provides recommendations for future work. The target of this report is to become a key reference in the field and to gain high recognition and visibility as a key resource for knowledge management programmes and to contribute to demonstrating and documenting the state-of-the-art character from a neutral and purely scientific viewpoint.

Depending on individual back-end country strategies, being programme-based within the framework of their national strategy, spent nuclear fuel (SNF) can be destined for direct geological disposal, for reprocessing or for long-term interim storage. For all cases, a proper characterisation of the spent fuel is required.

A state-of-the-art review on characterisation of SNF properties in terms of source term and inventory assessment (neutron, gamma-ray emission, decay heat, radionuclide inventory, elemental content) and in terms of out-of-core fuel performance (cladding performance and fuel integrity in view of the safety criteria for SNF interim storage, transport and canister packaging) using several numerical and experimental approaches and methodologies is presented.

The ability to reliably predict spent nuclear fuel composition and SNF properties, namely radionuclide inventory and source term, is relevant for both operational and long-term safety assessment in geological disposal, as well as for disposal cost key factors, and relies on ad-hoc calculation schemes.

The calculations require a particle transport code coupled with a depletion solver. A large proportion of the available depletion codes has been reviewed in this work. However, since the results also depend on nuclear data and operational data as well as assay data, nuclear data libraries and uncertainty aspects are also discussed. More specifically, the uncertainty of the fuel inventory can be dominated by several factors: irradiation history of the fuel, exact composition of the fresh fuel/cladding especially the level of impurities, and the large heterogeneities in the fuel design discharged from reactors, as well as modelling limitations, nuclear data libraries and reactor core characteristics such as, e.g., void fractions (in BWR's) and mechanical changes of fuel during irradiation. Therefore, the treatment of all related uncertainties (quantification and propagation) has been part of this review. The availability of experimental data enables testing and validation of codes and models in order to understand how closely models could replicate reality. The updated SOTA focuses on the development of new experimental techniques and on the improvement of depletion code accuracy using experimental data. Also, new highlights on the validation of theoretical calculations and depletion codes with experimental data are given, as well as recommendations to enhance procedures to further reduced related uncertainties in the characterisation and validation process.

Furthermore, when considering operational safety cases for the surface facilities where the fuel must be encapsulated in special disposal canisters, studies and research activities are required to assess spent fuel performance as well as developing concepts for handling of consequence scenarios. Therefore, another part of the updated SOTA report reviews experimental campaigns developed to investigate fuel integrity and highlights the advancements achieved in newly developed methodological approaches to investigate the structural performance of SNF.

Table of content

List of figures

List of tables

Glossary

ARIANE	Actinide Research In A Nuclear Element
ATF	Accident Tolerant Fuels
BDBA	Beyond Design Base Accident
BU	Burnup
BUC	Burnup Credit
BWR	Boiling Water Reactor
CIRFT	Cyclic Integrated Reversible-bending Fatigue Tester
CRAM	Chebyshev Rational Approximation Method
DA	Destructive Analysis
DBA	Design Basis Accidents
DBTT	Ductile-to-Brittle Transition Temperature
DDEP	Decay Data Evaluation Project
DHC	Delayed Hydride Cracking
DBRC	Doppler-Broadening Rejection Correction
EGADSNF	Expert Group on Assay Data of Spent Nuclear Fuel
EGBCC	Expert Group on Burnup Credit Criticality
ENDF	Evaluated Nuclear Data Files
EOL	End Of Life
ESARDA	European Safeguards Research and Development Association
FA	Fuel Assembly
FCCI	Fuel/Cladding Chemical Interaction
FDC	Final Disposal Canister
FEA/FEM	Finite Element Analysis/Finite Element Modelling
FIP	Fuel Integrity Project
FP	Fission Product
IAEA	International Atomic Energy Agency
ICP-SF-MS	Inductively Coupled Plasma – Sector Field – Mass Spectrometer
ICPS	Inductively Coupled Plasma Spectrometer
IE	Initial Enrichment
INL	Idaho National Laboratory
JRC	Joint Research Center
LWR	Light Water Reactor
MCNP	Monte Carlo N-Particle Transport Code
NDA	Non-Destructive Analysis
NEA	Nuclear Energy Agency

NPP	Nuclear Power Plant
ORNL	Oak Ridge National Laboratory
PGET	Passive Gamma Emission Tomography
PCI	Pellet-Cladding Interaction
PCMI	Pellet-Cladding Mechanical Interaction
PIE	Post-Irradiation Examination
PNNL	Pacific Northwest National Laboratory
PWR	Pressurised Water Reactor
RCT	Ring Compression Test
RHCF	Radial Hydride Continuity Factor
SCC	Stress Corrosion Cracking
SCIP	Studsvik Cladding Integrity Project
SNF	Spent Nuclear Fuel
SPAR	Spent fuel Performance Assessment and Research
TIMS	Thermal Ionisation Mass Spectrometer
TSC	Transport Storage Cask
UFDC	Used Fuel Disposition Campaign

1. Introduction

The ability to reliably predict spent nuclear fuel composition in terms of radionuclide inventory, elemental content, decay heat and radiation source term is relevant for both operational and long-term safety assessment in geological disposal and has an important influence on the cost of disposal. Ad-hoc calculations are thus required to fully characterise the SNF. The calculations involve a neutron transport code coupled with a depletion solver. The results depend on nuclear data and assay data. More specifically, the uncertainty of the fuel inventory can be dominated by several factors: irradiation history of the fuel, exact composition of the fresh fuel/cladding, such as the level of impurities, and the large heterogeneities in the fuel design discharged from reactors, as well as code modelling limitations and reactor physics code characteristics themselves. However, the availability of experimental data allows testing and validation of codes and models in order to be able to simulate the irradiation conditions quite closely to reality, or at least to assess a solid baseline as a starting point for further uncertainty assessments. If the baseline (i.e. code and fuel model) is known, being properly characterised by a well determined uncertainty, further assumptions can be analysed and incorporated in such a way as to encompass variables in a conservative way, but avoiding bringing the final estimates to a level of over-conservativism.

Depending on individual back-end country strategies, being programme-based within the framework of their national strategy, spent nuclear fuel (SNF) can be destined for direct geological disposal, for reprocessing or for long-term interim storage. For all cases, a proper characterisation of the spent fuel is required, even if the fuel changes its basic form, as in the reprocessing case where the final waste form is a glass and/or compacted metals.

For the case of geological disposal, safety assessments are required to cover a temporal spectrum typically of 1 million years, which implies the development of a qualification process using appropriate research programmes to reasonably reduce the level of uncertainties in the characterisation of the SNF. In particular, the spent nuclear fuel composition must be determined in terms of radionuclide inventory, elemental content, decay heat and radiation source term. Some observables can be determined by Non-Destructive Analysis (NDA) methods (such as decay heat by calorimetric measurements); however, such assays are time-consuming and are almost impracticable for addressing the entire SNF inventory produced over the lifetime of one or more Nuclear Power Plants (NPPs). Therefore, the ability to reliably simulate and predict the SNF source term are extremely important.

Nevertheless, the assessment can have different levels of relevance when considering operational safety cases at the level of surface facilities where the fuel must be encapsulated in special disposal canisters, or for long-term safety assessment where the SNF is encapsulated in canisters embedded in bentonite (or other buffer materials), surrounded by a host rock.

Pre-disposal activities such as SNF transport after interim storage and/or unloading/loading and handling operations for the packaging of the SNF from the transport/storage casks (TSC) into the final disposal canisters (FDC) are safety-relevant operations. Therefore, studies and research activities aimed at assessing spent fuel performance, and developing concepts for handling of consequence scenarios, are required by many countries. Experimental campaigns to investigate fuel integrity are extremely valuable. Many aspects are indeed under observation: effect of hydrogen load, hydride distribution and fuel/cladding interaction, mechanical performance of the cladding and cladding integrity, deterioration of the mechanical properties of the cladding material resulting from Delayed Hydride Cracking (DHC) for high burnup, whilst all are relevant for long term dry storage, many aspects are also relevant to other back-end activities such as post storage recovery and transport.

Scope and structure of the updated SOTA report

The report aims to provide an update of the initial state-of-the-art (SOTA) report published at the beginning of this project. The updated SOTA provides the progress made in the underpinning knowledgebase, it documents the identified technical gaps and provides recommendations for future work.

The target of this report is to become a key reference in the field and to gain high recognition and visibility as a key resource for knowledge management programmes and to contribute to demonstrating and documenting the state-of-the-art character from a neutral and purely scientific viewpoint.

The report is based on the structure of the initial SOTA and is composed of three main sections: 1) Characterisation of the fuel, fuel inventory and source term; 2) Performance of spent nuclear fuel during pre-disposal activities and experimental characterisation; 3) Accident scenarios.

Chapter 2 focuses on the SNF properties characterisation and related uncertainty analysis. The main objective of this task is to produce experimentally verified and validated procedures to determine reliable source terms of SNF, including realistic uncertainties. The focus is on source terms which are of primary importance for safe, secure, ecological, and economical handling, transport, intermediate storage, and final disposal of SNF. The main advancements in this field are captured in this chapter. Those concern the improvement of experimental methods for characterising spent nuclear fuel and evaluating the performance of depletion codes. Key focuses include developing experimental techniques for neutron and gamma-ray emission measurements, assessing the decay heat rate, and improving depletion code accuracy using experimental data. New highlights on the validation of theoretical calculations and depletion codes with experimental data are given, especially for different fuel types and conditions (e.g., UOX, BWR, PWR). Recommendations are provided to enhance the procedures and reduce uncertainties in the characterisation and validation process.

The second section, Chapter 3, is devoted to out-of-core fuel performance, in particular to the performance of the cladding and fuel integrity in view of the safety criteria for SNF interim storage, transport and canister packaging. Insights on newly developed characterisation techniques are provided, including both experimental and numerical approaches. In addition, an extended list of recommendations for further studies is given. Emphasis is given on highlighting technical gaps, indicating that experiments with irradiated fuel and corrosion studies are required to better understand spent fuel integrity.

Finally, Chapter 4 provides updates in the area of accident scenarios analysis. Great advancements have been achieved related to the development of different methodological approaches to investigate the structural integrity of SNF during postulated accident scenarios, utilising state-of-the-art tools. In addition, new insights are provided with regards to assessment of the probability and impact of various postulated accident scenarios during dry storage on the structural integrity of the SNF. The chapter also highlights the importance of enhanced collaboration between industry partners and regulatory bodies aiming to integrate advanced methods into standard safety practices and ensure the continued safety of SNF storage and transport systems.

2. Characterisation of the fuel, fuel inventory and source term

2.1. Observables and nuclides of interest

Due to the number of radionuclides that are present in spent nuclear fuel, spent fuel assemblies need to be characterised for their neutron and γ-ray emission properties and decay heat in view of the safety criteria for casks and canisters for transport, interim storage, and final disposal. Systematic studies in [Hu, 2016; Žerovnik, 2018] reveal that these observables are the result of complex contributions of radionuclides with strongly differing characteristics. This is illustrated in Figure 1 and Figure 2 for a simulated PWR UO_2 fuel sample with an initial ^{235}U enrichment of 4.8 wt.-% and a burnup of 45 GWd/t. Figure 1 shows the specific total decay heat rate (or thermal power) as a function of cooling time together with the contributions due to the emission of α- and β-particles and γ-rays [Žerovnik, 2018]. The relative contributions of individual radionuclides are identified in Figure 2. The largest contribution for cooling times in the range of 1 – 10 years is due to relatively short-lived fission products (FPs), mainly the decay chains $^{144}Ce/^{144}Pr$ and $^{106}Ru/^{106}Rh$. For cooling times between 10 and 30 years, contributions from short-lived FPs become negligible and the largest contribution is due to the decay chains of $^{90}Sr/^{90}Y$ and $^{137}Cs/^{137m}Ba$. With increasing cooling time the ^{241}Am contribution becomes dominant. This is due to the build-up of ^{241}Am from ^{241}Pu decay. Other contributions are due to the decay of $^{238,239,240}Pu$. The contributions from light nuclides reduce over time and eventually become negligible for cooling times longer than ~ 300 years.

Similar figures are reported in [Žerovnik, 2018] for the neutron and γ-ray emission properties of the same simulated fuel sample. For cooling times in the range of 1 – 80 years, the spontaneous fission of neutrons by ^{244}Cm represents the largest contribution to the neutron emission rate, with a relatively small contribution from (α,n) reactions due to decay of ^{238}Pu, ^{242}Cm and ^{241}Am. For cooling times longer than 100 years, neutron emission is mainly due to the spontaneous fission of $^{240,242}Pu$ and ^{246}Cm and (α,n) reactions due to ^{241}Am decay. Hence, for cooling times in the range of 1 − 80 years, the observed total neutron emission rate reflects the quantity of ^{244}Cm. Decay of FPs is the main contributor to spent fuel γ-rays emission for cooling times between 10 and 30 years, with the main contributors being ^{134}Cs, $^{137}Cs/^{137m}Ba$ and ^{154}Eu. For longer cooling times, i.e. 30 – 200 years, the spectrum is dominated by the 661 keV γ-ray due to $^{137}Cs/^{137m}Ba$ decay. Hence, for such cooling times a measurement of the total γ-ray emission rate provides information on the total amount of ^{137}Cs, which is directly proportional to the burnup.

In addition to the FPs and actinides, other dose-relevant and safety related radionuclides are generated, mainly by neutron activation of fuel/cladding impurities (e.g. ^{14}C, ^{36}Cl, ^{41}Ca, ^{59}Ni, ^{63}Ni, ^{93}Mo and ^{94}Nb). These nuclides are of importance for long-term safety assessments in waste disposal conditions up to about one million years. The different production roots are discussed below:

- The primary source is the cladding and related structural components; Modern cladding material is generally Zr-based, with minor amounts of alloying elements (Sn, Fe, Cr, Ni, Nb, O). Structural components (such as the spring material, guide thimbles, grids, hold down springs, etc.) are manufactured from stainless steel, Ni-based alloys, and Zr-based alloys.
- At the outer surface of the cladding (and possibly the inner surface of the shroud), surface deposits generally coming from corrosion products (e.g. $(Ni, Fe)OH^+$) from out-of-core regions may deposit as solid particles (e.g. ferrous hydroxide $(Fe,M)(OH)_2$ or ferrite $M^{II}Fe_2O_4$ with M = Fe, Ni, Co, Mn...). Various compounds may be formed and are collectively referred to as "crud" or "crud deposits".
- A further source of activation products stems from impurities in either the fuel or the cladding, such as N, Mg, Al, Si, Cl, Ca, Cr, Fe, Ni and Th.

Activation products of the above elements are mainly β-active and, with the exception of ^{60}Co (estimated to be of the order of 1%), their contribution to the spent fuel assembly decay heat is negligible (< 0.01%) over the period of interest.

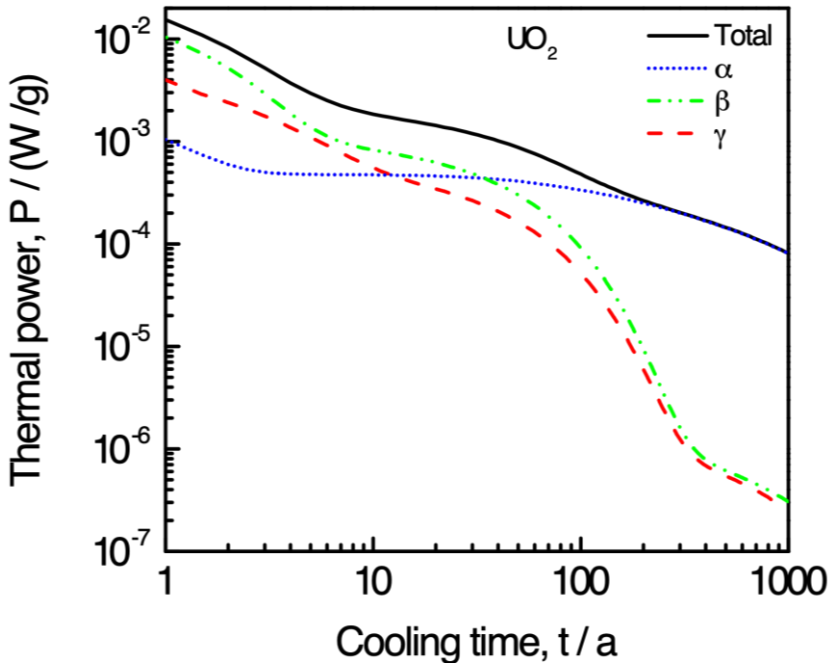

Figure 1 – Specific thermal power (or decay heat rate) of an irradiated fuel sample as a function of cooling time

*The total thermal power per unit mass together with the contribution due to α, β and γ-ray emission is given for a UO_2 sample with initial enrichment of 4.8 wt.-% irradiated in a PWR to a burnup of 45 GWd/t [*Žerovnik, 2018*].*

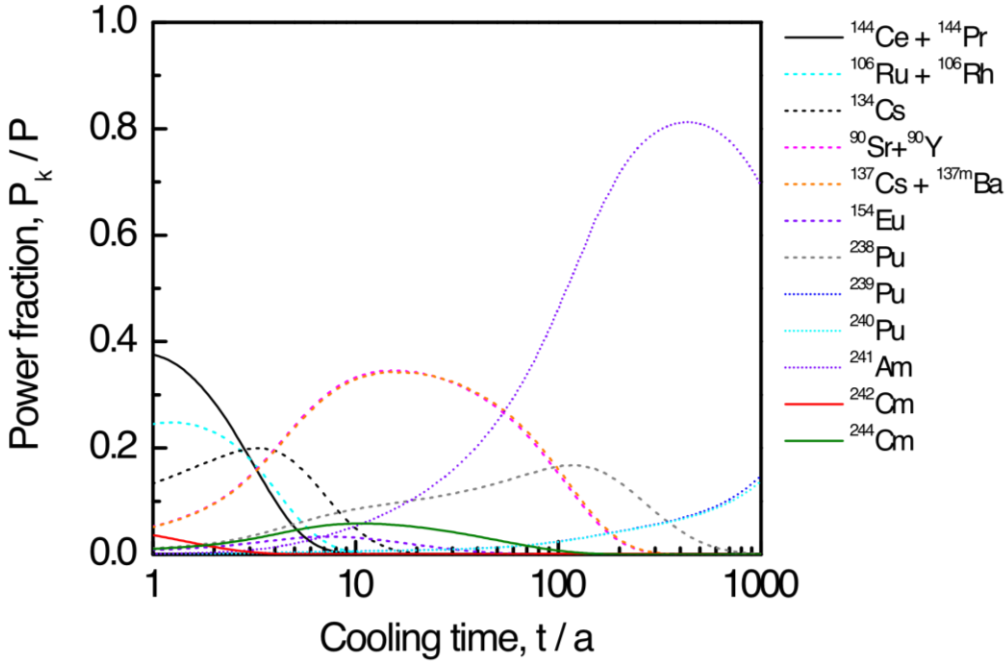

Figure 2 – Relative contribution of radionuclides to the thermal power of an irradiated fuel sample as a function of cooling time

*The data are for a UO2 sample with initial enrichment of 4.8 wt.-% irradiated in a PWR to a burnup of 45 GWd/t [*Žerovnik, 2018*].*

After a cooling time of several thousands of years, the total activity of spent nuclear fuel is dominated by long-lived actinides, in particular ^{235}U, ^{238}U, ^{237}Np and ^{239}Pu. Since plutonium and uranium species are immobile under the reducing conditions of a deep geological repository, they are less important with respect to the long-term safety of spent nuclear fuel disposal. However, the mobility of gaseous or readily soluble and negatively charged species, such as $^{36}Cl^-$, $^{129}I^-$ or gaseous ^{14}C compounds, are not expected to be limited by the (geo-)technical barriers and will move relatively easily through the surrounding rock of the disposal system [Ewing, 2015]. To assess the radiologically relevant inventory, the amount of long-lived activation/fission/decay products, i.e. ^{14}C, ^{36}Cl, ^{79}Se, ^{94}Nb, ^{99}Tc, ^{129}I, ^{135}Cs and ^{226}Ra, as well as the ^{237}Np inventory have to be estimated.

Safe transport, storage or disposal of spent fuel assemblies also requires a (sub-)criticality safety analysis. To avoid unnecessarily over-engineered and expensive transport and storage casks, the loading scheme should account for the reduction in nuclear reactivity of the assemblies. This effect is due to the net reduction of fissile nuclides (fuel depletion) and the production of non-fissile, strongly neutron absorbing actinides and fission products. The concept of taking credit for the reduction in reactivity is referred to as BurnUp Credit (BUC) [Sanders, 1990]. Hence, criticality safety assessments for spent nuclear fuel management based on a BUC approach require a nuclide inventory prediction involving far more nuclides than in a conservative approach based on the inventory of fresh fuel. Nuclides which strongly affect the reactivity of a spent fuel assembly, are: $^{235,236,238}U$, $^{239,240,241}Pu$, ^{95}Mo, ^{99}Tc, ^{101}Ru, ^{103}Rh, ^{109}Ag, ^{133}Cs, $^{147,149,150,151,152}Sm$ [Hicks, 2018; Gauld, 2005]. Other discussions on BUC approaches can be found in e.g. Refs. [Agrenius, 2002; Gauld, 2003; Tardy, 2017; Scaglione, 2009; Herrero, 2015; Vasiliev, 2019].

Spent nuclear fuel is subject to nuclear safeguards to ensure the peaceful use of nuclear materials. It requires a final accounting of special nuclear materials that will be removed from the nuclear fuel cycle for ultimate disposal in a geological repository [Hautamäki, 2000; Mongiello, 2013; IAEA, 2018; Niemeyer, 2016; Lindgren, 2019]. The IAEA will verify the inventory of nuclear material that is declared for disposal. The main nuclear materials of interest are the amount of $^{233,235}U$ and the total amount of plutonium and thorium. In addition, secure transport and storage of spent fuel assemblies implies the prevention of theft, or other malicious acts involving nuclear material. The IAEA lists the development of safeguards equipment to establish and maintain knowledge of spent fuel in shielding/storage/transport containers at all points in their life cycle as a top priority in their R&D needs [IAEA, 2018a]. Evidently, nuclear safety, security and safeguards require similar or complementary measures for documenting, measuring and monitoring spent fuel characteristics. Therefore, synergies inherent in overlapping methods or techniques should be identified to avoid redundancy or duplication of work and equipment [Niemeyer, 2016; Lindgren, 2019].

2.2. Theoretical calculation of the nuclide inventory and observables

The main parameters of interest for the safe, secure, ecological and economical transport, storage and disposal of spent fuel are the decay heat, neutron and γ-ray emission properties and the inventory of some specific actinides, FPs and activation products. Alpha decay of actinides affects the microstructure of the cladding, which is connected to the integrity of the fuel (see section 3). To determine these source terms, the inventory of a large number of nuclides is required. A list of nuclides for which the inventory in spent fuel has to be determined can be found in [Ewing, 2015; Broadhead, 1995; NEA, 2011; Gauld, 2001] and Appendix A [Govers, 2019]. The latter contains radionuclides identified from safety studies of a long-term storage installation for Belgian waste performed by NIRAS/ONDRAF [Vandoorne, 2018].

Due to the complex contributions of radionuclides with different characteristics, estimates of the decay heat, neutron and γ-ray emission properties at any cooling time cannot accurately be derived by simply extrapolating from estimations at shorter cooling times. In addition, the complete nuclide vector of a spent fuel assembly cannot be measured directly; it can only be obtained from theoretical calculations. Such calculations require validated codes that determine the time evolution of the nuclide inventory

during reactor operation. This can be done by coupling a neutron transport and a nuclide production and depletion code.

When the nuclide vector at a cooling time t_0 is known, the nuclide vector at a cooling time $t > t_0$ can be derived by solving the set of linear differential Bateman equations [Bateman, 1910]:

$$\frac{dN_k(t)}{dt} = \sum_{ik} b_{ki_i} N_i - l_k N_k(t) \quad (1)$$

with N_k the number of nuclei of nuclide *k*, l_k its decay constant and b_{ki} the probability that nuclide *i* decays to nuclide *k*. Once the nuclide vector is known, the thermal power $P(t)$, neutron emission rate $S_n(t)$ and γ-ray emission energy distribution $S_g(E_g, t)$ as a function of cooling time *t* can be obtained from:

$$P(t) = \sum_k N_k(t) \lambda_k E_{r,k} \quad (2)$$

$$S_g(E_g, t) = \sum_k N_k(t) \lambda_k s_g(E_g) \quad (3)$$

$$S_n(t) = \sum_k N_k(t) (s_{sf,k} + s_{,k}) \quad (4)$$

with $E_{r,k}$ the recoverable energy per decay of nuclide k and $s_g(E_g)$ the energy distribution of the γ-rays emitted per decay of nuclide k. The specific neutron emission rates, or neutron rate per nuclide, due to spontaneous fission and α-decay of nuclide k are denoted by $s_{sf,k}$ and $s_{,k}$, respectively. The specific spontaneous fission rate is defined by:

$$s_{sf,k} = \lambda_{sf,k} \bar{n}_k \quad (5)$$

with $\lambda_{sf,k}$ the decay constant for spontaneous fission of nuclide *k*, and $\bar{n}_k$ the corresponding average number of neutrons per fission. The specific emission rate of neutrons due to (α,n) reactions in mainly light nuclides can be derived from:

$$s_{,k} = \lambda_{\alpha,k} \sum_{i,j} P_k(E_{\alpha,i}) Y_j(E_{\alpha,i}) \quad (6)$$

where $l_{a,k}$ is the decay constant for α-decay of nuclide k, $P_k(E_{\alpha,i})$ the probability that this decay leads to the emission of an α-particle with an energy $E_{\alpha,i}$ and $Y_j(E_{\alpha,i})$ the probability that the emitted α-particle creates a neutron by an (α,n) reaction with material j.

2.2.1. Principles

Neutron transport calculations can be performed in a deterministic way by solving the Boltzmann transport equation, or in a stochastic way by performing Monte Carlo (MC) simulations using codes such as MCNP [Briesmeister, 2000], SERPENT [Leppänen, 2015] and TRIPOLI [Petit, 2008; Brun, 2015]. In principle, MC transport calculations can be performed with less approximations than by a deterministic approach. However, up to now MC simulations are often applied to systems involving one or a few assemblies. In the case of a full core (with burnup calculations), deterministic transport methods are still the only practical way for routine applications and within a reasonable calculation time.

From the neutron transport calculation, the spatial and energy distributions of the neutron fluence are derived. These distributions are used to calculate energy averaged neutron-induced reaction cross-sections, which are required to deplete and produce nuclides by solving a set of Ordinary Linear Differential Equations (ODEs). Since the energy and spatial distributions depend on the nuclide inventory an iterative procedure is required.

In the case of Light Water Reactors (LWRs), the production and depletion of nuclides by nuclear reactions and radioactive decay in a homogenised material as a function of time form a set of ODEs. These equations can be expressed in matrix notation by:

$$\frac{d\boldsymbol{N}(t)}{dt} = \boldsymbol{A}\boldsymbol{N}(t) \quad (7)$$

with $\boldsymbol{n}(t)$ the number density vector of the nuclides presents in the fuel and $\boldsymbol{A}$ the transition or burnup matrix. The diagonal elements a_{kk} of this matrix are the removal rates of each nuclide:

$$a_{kk} = -(f\,\bar{s}_k + l_k) \quad (8)$$

and the off-diagonal elements a_{kl} are the production rates by other nuclides:

$$a_{kl} = b_{kl} l_l + f\, b_{kl,r} \bar{s}_{l,r} \quad (9)$$

The decay constant of nuclide k is l_k. Its removal rate due to neutron interactions is the product of the total neutron fluence rate and the spectrum-averaged Doppler broadened removal cross-section denoted by f and $\bar{s}_k$, respectively. The matrix element defining the production of nuclide k from nuclide l is due to a decay contribution, defined by the decay constant l_l and branching probability b_{kl},and a contribution due to neutron-induced interactions with nuclide l resulting in the production of nuclide k. The latter is the product of the total neutron fluence rate , the spectrum averaged Doppler broadened neutron-induced interaction cross-section $\bar{s}_{l,r}$ and the probability $b_{kl,r}$ that this interaction produces nuclide k.

The most probable nuclide production interactions are neutron-induced fission and capture reactions. In the case of neutron-induced fission reactions, fission products are produced and the probability $b_{kl,r}$ is the independent fission yield of the fission product k. Examples of such production chains for fission products are given in [Nichols, 2002]. Most of the fission products are neutron-rich and decay mostly by β^-. Other nuclides are generated via a combination of different decay processes and neutron-induced reactions, e.g. a combination of neutron-induced capture reactions and β^- decays are the main processes producing actinides such as Pu, Am and Cm starting from ^{238}U. Several analytical/numerical solutions have been proposed [Moler, 2003; Isotalo, 2011; Hykes, 2013], but only a few are applicable to estimate the nuclide inventory of spent nuclear fuel. A comparison of some of the methods that are implemented in nuclear depletion codes can be found in [Moler, 2003; Isotalo, 2011; Hykes, 2013].

Applying the Transmutation Trajectory Analysis (TTA) method [Cetnar, 2006], also referred to as the linear chain method, the complex nuclide transmutation scheme is considered as a set of individual linear sub-chains that can be solved analytically, following the original work of [Bateman, 1910]. The final result is the sum of the solutions for the individual chains. It involves an enormous network of complex chains that often generate cyclic chains that cannot be linearised. Assumptions are made to terminate unimportant chains based on multiple criteria, e.g. ignoring cyclic chains or terminating them after a few loops. The choice of the termination criterion plays a role in the trade-off between computation speed and accuracy. This method is implemented in the BISON [Cetnar, 2000], CINDER [Wilson, 2007] and VCINDER [Kum, 2018] codes and included as an option in SERPENT [Leppänen, 2015a; Leppänen, 2015b].

The set of first order differential equations can be solved by numerical integration methods such as the Runge-Kutta type of methods [Hairer, 2996; Hairer, 1999]. The primary disadvantage is the relatively high computing time. The 4th order Runge-Kutta scheme was implemented in earlier versions of the MENDEL [Tsilanizara, 2016] and DARWIN/PEPIN2 [Tsilanizara, 2000] systems. The ALEPH2 code [Stankovskiy, 2012] is based on the RADAU IIA implicit Runge-Kutta method of order 5.

The solution of the ODEs can be found by the matrix exponential method, resulting in [Pusa, 2010; Pusa 2011]:

$$\boldsymbol{N}(t) = e^{\boldsymbol{A}t}\boldsymbol{N}_0 \quad (10)$$

where the exponential of the matrix is defined as a series expansion

$$e^{\boldsymbol{A}t} = \sum_{k=0}^{\infty} \frac{1}{k!} (\boldsymbol{A}t)^k \quad (11)$$

with $\boldsymbol{I} = \boldsymbol{A}^0$ the identity matrix and the initial nuclide vector denoted by $\boldsymbol{N}_0$. There are numerous algorithms to compute the matrix exponential, but many of them are computationally expensive and of dubious numerical quality [Moler, 2003]. Given the complexity of the process, the burnup matrix has a wide spectrum of eigenvalues. The presence of short-lived nuclides is problematic since they produce eigenvalues of large magnitude, creating a matrix norm of up to 10^{27} [Pusa, 2010; Pusa, 2011].

The matrix exponential in Eq. 11 can be approximated by a truncated Taylor expansion [Bell, 1973] or a rational Padé approximation [Nigham, 2005], both combined with scaling and squaring. These approximations can only work well when the matrix norm $\|\boldsymbol{A}t\|$ is sufficiently small. This problem can be solved by excluding the short-lived nuclides from the burnup matrix and treating them separately. This results in a kind of hybrid linear chain-matrix exponential method that is used in ORIGEN2 [Croff, 1983]. It is also used in the MOCUP [Moore, 1995] and MONTEBURNS [Poston, 1999] codes which couple MCNP and ORIGEN2 [Croff, 1983]. The latest version of the PHOENIX burnup module solves the ODEs either with a 4th order Runge-Kutta method, a Taylor series development of the matrix exponential, or a Krylov subspace-based algorithm [Haeck, 2012]. The latter is also applied in the AEGIS code [Yamamoto, 2007].

One of the most advanced matrix exponential methods is the Chebyshev Rational Approximation Method (CRAM) [Pusa, 2010; Pusa, 2011; Pusa, 2013; Pusa, 2016; Isotalo, 2016]. It is based on a ratio of polynomials using complex coefficients and provides very accurate solutions without excluding nuclides. The main difficulty in using CRAM is to determine the coefficients of the rational approximant for a given order. [Pusa, 2016] provides CRAM coefficients for approximation of orders 4, 8, 12, …, 48. It is shown that the higher-order CRAM can be used to solve the burnup equations accurately for large time steps. CRAM is implemented as an option in SERPENT [Leppänen, 2015a; Leppänen, 2015b] and in the latest versions of ORIGEN [Gauld, 2011b; Rearden, 2016] and MENDEL [Lahaye, 2017].

2.2.2.Burnup codes

A variety of codes/systems are available to determine the nuclide inventory and decay heat and neutron and γ-ray emission properties of SNF assemblies. Only the codes/systems that will be used within the activities of the spent fuel characterisation work package of the EURAD project will be discussed here in detail.

ALEPH2/MCNP

ALEPH2 is a depletion code developed at SCK•CEN [Stankovskiy, 2012] that makes use of any version of the general Monte Carlo N-Particle Transport Code MCNP [Briesmeister, 2000; Werner, 2017] for MC transport calculations to obtain particle spectra. The reaction rates are handled outside MCNP by ALEPH2 using the same continuous energy nuclear data as MCNP. This ensures consistent use of nuclear data by transport and depletion modules. The depletion module is based on the solver RADAU5 [Hairer, 1996; Hairer, 1999], which uses an implicit 5th order Runge-Kutta method. The power-to-fluence rate conversion takes into account the energy deposited by fission and neutron capture reactions, making it possible to accurately model systems containing burnable absorbers. The code is able to reflect in a single run the time evolution of many parameters, such as fuel expansion, fuel reshuffling, changes in material temperature and density, control rod movement and changes in boundary conditions. Besides the nuclide inventory evolution, various radiation source terms such as decay heat, delayed radiation sources and dose rates can be derived.

CASMO/SIMULATE/SNF

The CMS/SNF methodology is based on the coupled CASMO/SIMULATE/SNF code sequence and used for evaluating the nuclide composition of spent nuclear fuel. It inherently applies a 3D core model to any assembly irradiated in the core, accounting for realistic irradiation conditions [Bahadir, 2009]. The nuclide library, generated by the lattice physics code CASMO5 [Rhodes, 2006], provides nuclide concentrations, cross-sections and reaction rates, tabulated via exposure, moderator density, control blade and fuel temperature histories. The nodewise exposure and accumulated history parameters, obtained from qualified operational reactor data and core simulation using the nodal reactor code SIMULATE [Grandi, 2011], are used as entry points in the interpolation routines and, together with the power history model in SNF [Børresen, 2004], are used to compute the nuclide concentrations at the time of assembly discharge. CMS5/SNF computes the nuclide concentrations and all relevant spent fuel parameters such as decay heat rate, activity, neutron and photon sources on a nodal basis following the axial nodalisation of the reactor core model.

SIMULATE and SNF share the same cross-section library, generated by CASMO5 and based on ENDF/B-VII.1. The basic decay data in SNF are also based on ENDF/B-VII.R1. The SNF decay library includes basic data such as decay constants and nuclide transmutation chains; radiation emission spectra for photons from radioactive decay, (α,n) reactions, bremsstrahlung, and spontaneous fission; electrons and α particles from radioactive decay; neutrons from radioactive decay, spontaneous fission, and (α,n) reactions; decay heat production; and others. These data are compiled from data libraries (e.g. ENDF/B-VII.1 [Chadwick 2011], ENSDF [Tuli, 2001], TENDL-2012 [Koning, 2012]) and processed sources (ESTAR and ASTAR [Berger, 2015]) for 890 nuclides. The evaluation and validation of the decay data in SNF is reported in [Simeonov, 2017].

DRAGON

DRAGON [Hébert, 2006] is a lattice deterministic code developed at École Polytechnique de Montréal. It uses different models and algorithms to solve the neutron transport equation. In order to find the best trade-off between accuracy and calculation speed, the Collision Probability method (CP) using the DRAGON formatted library is recommended. For self-shielding, the interface current method (SYBILT) can be used to perform the geometry tracking together with a subgroup method (USS module) with physical probability tables. In the subgroup or multiband method, the detailed energy-dependent cross-section behaviour in each coarse energy group is replaced by its probability density representation. An accurate discretisation of each probability density can be obtained, which leads to probability tables which are subsequently used within the fluence rate solution algorithm of the subgroup method. The SYBILT module can also be used for the fluence rate calculation using the fixed Laplacian option and without leakage model. The default option for solving the depletion equations is the 4th order Kaps-Rentrop algorithm of the Runge-Kutta family. The power-to-fluence rate conversion is done taking into account a constant power with the total energy released in the complete geometry (GLOB option), by accounting for (n,γ) reactions outside the fuel. In this case, the power released per initial heavy element at the beginning and at the end of each time step can be set to a constant.

EVOLCODE

EVOLCODE 2.0 is a combined neutron transport and depletion evolution simulation code to describe the burnup evolution of either critical or subcritical reactors operating in any neutron spectrum [Álvarez-Velarde, 2014]. The code has been focused on the estimation of a large variety of nuclear reactor parameters, with a particular interest in the nuclide composition evolution of the fuel in a nuclear reactor. The evolution with burnup of any material present in the design can be followed for activation purposes. Burnup problems are solved by using a time interval method consisting of the successive calculation of first the neutron fluence rate for fixed material densities at a given time and later the depletion of these densities, using the hypothesis of constant neutron fluence rate. These hypotheses are considered valid

only for relatively short irradiation times. Hence, several iterative calculations are needed to solve the system for the whole irradiation period. Each iteration, corresponding to a partial irradiation period, is called an EVOLCODE cycle.

In the present version of the code, the neutron transport calculations are performed by any version of the general MC transport code MCNP/X [Werner, 2017], which is able to model complex 3D geometries. The depletion of the geometry zones, requested by the user, is carried out by the activation code ACAB [Sanz, 2008]. This code is implemented in the EVOLCODE 2.0 system to provide best estimates together with their uncertainties resulting from a propagation of uncertainties of cross-sections, decay data and fission yields, and to enlarge the number of nuclear reactions taken into account by the irradiation calculations. ACAB is a point-depletion and radioactive decay computer code that solves the ODEs using a method similar to the one implemented in ORIGEN2 [Croff, 1983]. The depletion code ORIGEN can be used instead of ACAB. The user chooses which depletion code or version of MCNP/X is used in the simulations.

The spatial dependence of the neutron fluence rate is determined by the MCNP cell definition, which, together with the entire geometry definition, allows for an important degree of the heterogeneity description in the reactor core model. The energy dependence is obtained by means of the energy distribution of the neutron fluence rate for each of these cells. On the one hand, the neutron fluence rate is normalised by means of a predictor/corrector method, so that the depletion is simulated using the proper value of the system thermal power. Finally, the neutron fluence energy distributions are used for creating (outside MCNP) spectrum averaged cross-section libraries for depletion.

EVOLCODE 2.0 uses the same basic libraries as MCNP to ensure consistency in the use of the data. From these basic libraries, the information on those reactions suitable for ACAB and available in the database is selected, disregarding the information about elastic collisions. Additionally, since isomers may have very different half-lives and reaction cross-sections compared with the ground state nuclide (leading to different transmutation chains), the information on the isomer producing reactions is provided to the code by a separate file containing the information on the branching ratios. Finally, the fission yields library is supplied to the code as an external sub-library. Currently, sub-libraries are defined for neutron-induced fission product yields and for yields from spontaneous fission. Besides, independent and cumulative yields are also included in the sub-library. EVOLCODE 2.0 only considers neutron-induced independent fission product yields since these are the data required by the depletion code.

MCNP-CINDER

The MCNP code in general, and in particular the recent version MCNP6, is widely used for neutron transport calculations from which the neutron fluence energy distribution is obtained and reaction rates can be generated. As far as burnup codes are concerned the depletion part can be disintegrated from the neutron transport code, that is, the reaction rates are calculated separately and several systems operate in this way, e.g. ALEPH2 [Stankovskiy, 2012] and EVOLCODE [Álvarez-Velarde, 2014].

The depletion code that was coupled to earlier versions of MCNP is the MONTEBURNS module [Poston, 1999]. The recent MCNP6 versions integrate the depletion part CINDER [Wilson, 2007] within the transport solution. Hence, the reaction rates are based on the nuclear input data of the MCNP code itself. As a weak point, CINDER uses a pre-calculated 63-group cross-section library obtained externally. CINDER belongs to the group of codes which use the so-called linear chains approach based on the Markov method, i.e. TTA method described in Section 2.2.1. The linearisation considerably simplifies the complexity of the exponential matrix but in return, one should be careful with the burnup time steps to maintain the accuracy of the nuclide inventory. On the other hand, it offers the possibility of handling many nuclides with longer depletion chains.

SCALE

One of the most widely used computer codes for the prediction of spent fuel source terms (nuclide composition, neutron and γ-ray emission and decay heat) is the SCALE code package developed at the Oak Ridge National Laboratory (ORNL). The latest available version, as of September 2019, is SCALE 6.2.3 [Rearden, 2016; Grandi, 2011]. It is described in detail in [Gauld, 2011]. Most of the geometrical systems studied with the SCALE package are related to a limited number of assemblies.

SCALE is a multi-purpose code package offering a range of options for performing source term calculations: starting with pre-packaged LWR libraries in the ORIGEN-ARP module or alternatively determining simplified but assembly-specific cross-sections with the SAS2H control sequence in combination with the one-dimensional discrete ordinate code XSDRNPM-S or computing nuclide vectors with the T6-DEPL control sequence and the KENO lattice physics solver.

The package includes built-in cross-section libraries (e.g. ENDF/B-VII.0 and ENDF/B-VII.1) in Multi Group (MG) approximation (56 or 252 groups) and in pointwise Continuous Energy (CE) detail. These are recommended for general-purpose reactor physics and LWR analysis [Rearden, 2016], along with complementary data from the JEFF-3.0/A library. The latest covariance data are based on the covariance evaluations of ENDF/B-VII.1 and other sources. These covariances, along with perturbation factors, can be used to generate perturbed MG libraries for the cross-sections, decay and fission yield data (see Section 2.4). For nuclide data not covered by ENDF/B-VII.1, "low-fidelity" covariances were estimated using simple procedures in a collaborative project by nuclear data experts of the Brookhaven National Laboratory (BNL), Los Alamos National Laboratory (LANL) and ORNL.

SCALE offers several modules for depletion calculations:

- TRITON couples one of the neutron transport modules to the ORIGEN depletion module in an iterative time-stepping sequence. One can choose between a deterministic 2D approach (NEWT) and a 3D MC simulation (KENO). The latter runs in multi-group or continuous-energy mode. TRITON is also used to generate problem-specific cross-sections that are used by the ORIGEN-ARP module for transmutation and decay calculations [Caruso, 2014b].
- POLARIS is a 2D lattice physics module that is used for the analysis of LWR fuel assemblies [Rearden, 2016]. POLARIS uses the Embedded Self Shielding Method [Williams, 2012a] for evaluating the self-shielded, multi-group cross-sections based on the Bondarenko interpolation, and a Method of Characteristics (MoC)-based transport solver [Williams, 2012a]. The outputs of POLARIS are the critical spectrum, few-group homogenised and condensed cross-sections, and one group condensed microscopic cross-sections.
- ORIGEN – Oak Ridge Isotope GENeration (ORIGEN) code is coupled to TRITON and POLARIS to perform the depletion and decay calculations, and therefore to simultaneously generate the time-dependent nuclide concentrations. POLARIS and TRITON are coupled to ORIGEN by one-group, zone-averaged fluence rates and one-group fluence-weighted cross-sections and reaction yields to compute the stepwise change in the problem-dependent nuclide vector. The coupling is done at the end of each depletion step using the predictor-corrector method, which is then used to update the depleted materials composition for the next self-shielding and transport calculation. ORIGEN can also be used stand-alone for activation, depletion and/or decay calculations using the pre-developed macroscopic cross-section libraries [Caruso, 2016].
- ORIGEN-ARP uses pre-packaged LWR libraries available in the SCALE package. It also allows user-defined libraries to be imported which can be developed with the TRITON module.
- SAMPLER is a module for uncertainty analysis. It is a stochastic sampling super-sequence that was developed for the SCALE system by ORNL in collaboration with GRS on the basis of the XSUSA code [Williams, 2013b]. SAMPLER can be used to perform uncertainty analysis for POLARIS. SAMPLER works by stochastically sampling input parameters (MG nuclear data, depletion data, decay data as well as model parameters such as nuclide concentrations, geometric specifications, operational history). Afterwards, SAMPLER will repeat numerous

passes through the employed module (or sequence of modules), output distributed response parameters (or their uncertainties), and finally analyses these distributions to evaluate the correlations between different response parameters (e.g. different radionuclides) or the correlations between simultaneously modelled systems (similarity studies).

SERPENT

SERPENT [Leppänen, 2015a; Leppänen, 2015b] is a multi-purpose three-dimensional continuous energy MC particle transport code developed at the VTT, Technical Research Centre of Finland since 2004. The latest version, as of September 2019, is SERPENT 2, Version 2.1.31. SERPENT can be used for various reactor physics analyses and decay heat, activity and nuclide inventory calculations. In addition, SERPENT is capable of performing multi-physics simulations and neutron, photon and coupled neutron-photon transport calculations.

The geometry description in SERPENT is handled by a universe-based constructive solid geometry (CSG) model. Different elementary and derived surface types can be used in combination with Boolean operators (intersections, unions and complements) to define homogeneous material cells of practically any shape desired. Special surface types are defined for several lattice structures. In addition to CSG-type universes, SERPENT has the option to import CAD and unstructured mesh based geometries.

Particle transport in SERPENT is based on the combination of conventional ray-tracing based surface tracking and the Woodcock delta-tracking method [Woodcock, 1965] – the rejection sampling based delta-tracking method [Morgan, 2015]. Surface-tracking is used when necessary, e.g. in the presence of localised heavy absorbers which may cause efficiency problems for the delta-tracking method [Leppänen, 2010].

SERPENT has built-in state-of-the-art routines for depletion calculations and no coupling to external solvers is needed. The primary method used for solving the Bateman depletion equations is based on the CRAM method, an advanced matrix exponential solution developed for SERPENT at VTT [Pusa, 2010; Pusa, 2011, Pusa, 2013; Pusa, 2016; Isotalo, 2016].

The main capabilities of the code are:

- Geometry: SERPENT is capable of calculating nuclide inventories on assembly level in two (2D) and three (3D) dimensions. Whole core depletion calculations are also possible for small cores, such as research reactors. Serpent includes 2D lattice structures for square (PWR, BWR), hexagonal (VVER) and circular (AGR, CANDU, MAGNOX, RBMK, TRIGA) lattices. There is also a structure for a 1D vertical stack and 3D cuboidal and hexagonal lattices. Other structures are also possible to create by the user. Reflective, periodic and vacuum boundary conditions can be used. Support for spatial domain-decomposition for very large burnup calculations is currently in development.
- Physics options: SERPENT includes several modelling options affecting the physics of the modelled problem. One of them is the Doppler-broadening preprocessor routine [Viitanen, 2009] that allows for adjustment of the temperatures of ACE format cross-sections. This results in a more accurate description of the interaction physics in temperature-sensitive applications, as the data in the cross-section libraries are typically available in 300 K intervals. The Doppler-Broadening Rejection Correction (DBRC) method (see Section 2.3.1) is available.
- Irradiation history: The irradiation history is defined in units of time or burnup. Reaction rates are normalised to total power, specific power density, neutron fluence rate, fission or source rate, and the normalisation can be changed by dividing the irradiation cycle into a number of separate depletion intervals. Other parameters such as fuel temperature, moderator temperature and density, boron concentration, etc. must apply constant values during a single depletion calculation. However, these parameters can be changed, and fuel shuffling is possible by writing different inputs for each change in the parameters and using SERPENT's restart feature. The effect of the uncertainty of different irradiation history parameters on the source

terms can be investigated e.g. by refining the accuracy of which irradiation history is defined in the calculation. Boron history can be modelled using first one average value and then changing the boron concentration during the calculation with increased precision.

- Depletion calculation: SERPENT handles every material as an individual depletion zone and provides nuclide inventories separately for each material. In addition, burnable materials in lattices can be automatically sub-divided into depletion zones, e.g. a lattice comprising one fuel material can be automatically sub-divided into depletion zones separately for each fuel pin. A fuel pin can also be automatically sub-divided into further depletion zones to better account for effects such as Gd burning. The depletion calculation can be followed by a decay calculation of any desired length. All nuclides included in the nuclear data libraries are available in the depletion and decay calculations. The output of the depletion calculation includes total and material-wise volume and burnup. Nuclide-wise output for every depleted material includes: atom and mass density, activity, decay heat, spontaneous fission rate, photon emission rate, ingestion toxicity, and inhalation toxicity.
- Activation analysis: in addition to fuel burnup calculations, SERPENT is capable of calculating the activation of any material defined in the geometry. Materials of interest are the fuel cladding and structural materials such as the spacer grid.
- Nuclear data: SERPENT reads continuous-energy cross-sections from ACE format data libraries based on JEFF-2.2, JEFF-3.1, JEFF-3.1.1, JEFF-3.2, ENDF/B-VI.8, ENDFB/B-VII.1 and JENDL-4.0. In addition, any other continuous-energy ACE format data library generated for MCNP can be added to SERPENT. Radioactive decay data and incident-neutron energy-dependent fission yields and isomeric branching ratios for neutron-induced reactions are read from data libraries in ENDF-6 format. The nuclear data used can be easily changed between different runs.
- Shielding calculations: SERPENT provides a radioactive decay source mode to perform shielding calculations for spent fuel and other irradiated materials. The source term is formed automatically by combining the nuclide composition from a previous burnup or activation calculation and the emission spectra from ENDF decay data. The methodology includes photons and neutrons emitted in radioactive decay, as well as secondary photons produced by β-decay by applying the thick-target bremsstrahlung (TTB) approximation.

Various other codes/systems have been developed such as FISPACT [Sublet, 2017], MENDEL [Lahaye, 2017], MOCUP [Moore, 1995], MONTEBURNS [Poston, 1999], STREAM [Ebiwonjumi, 2019], SWAT [Kashima, 2015], and VESTA [Haeck, 2012]. Information on these codes is available from the quoted references.

2.2.3. Code comparison

Recently, the performance of ALEPH2, SCALE, DRAGON and SERPENT were compared using the same nuclear data, fuel design and composition and irradiation history parameters. The code versions used in the exercise are specified in Table 1. All codes were used in combination with the ENDF/BVII.1 library. Details about the exercise are given in [Žerovnik, 2019].

Code	Neutron transport	Solver	Version
ALEPH2	MC	Runge-Kutta (RADAU IIA)	ALEPH2/MCNP6.2
SERPENT	MC	CRAM	V2.1.29
DRAGON	Deterministic	Runge-Kutta (4th order Kaps-Rentrop)	Version 5
SCALE	Deterministic	CRAM	TRITON/NEWT

Table 1 – Burnup codes used in the comparison exercise reported by Žerovnik et al.

A reference 2D model representing a typical 17x17 PWR fuel assembly with reflective boundary conditions was considered. The fuel pins consisted of a stack of 4wt.-% ^{235}U enriched UO_2 pellets in a Zircaloy-4 cladding. The fuel was irradiated for 4 cycles of 300 days each, with interim cooling periods of 30 days. Simplified operating conditions were considered, with:

- constant power levels of 50, 50, 40 and 30 MW/t during each cycle
- coolant density of 0.655 kg/cm^3 with a constant boron level of 800 ppm
- fuel smeared density (95% of the theoretical density): 10.4 g/cm^3
- constant material temperatures: fuel and gap at 900 K and coolant and cladding at 600 K

The following approximations were adopted in all codes:

- the neutron transport calculations for each fuel cycle were rerun at time steps of: 1 day, 10 days, 14 days, 3 × 25 days and 4 × 50 days,
- to account for neutron self-shielding effects the fuel pins were divided into 4 radial regions.

The abundance of key nuclides at a cooling time of 5 years is compared in Table 2. Uncertainties due to MC counting statistics are given for the results obtained with SERPENT. The results obtained with the MC codes ALEPH2 and SERPENT are very similar. The largest difference, about 3%, is observed for the abundance of ^{149}Sm and the second largest, about 1.2%, for ^{246}Cm. The good agreement between ALEPH2 and SERPENT confirms the good performance of the RADAU IIA Runge-Kutta type of ODE solver used in ALEPH2.

Differences between SERPENT (& ALEPH2) and DRAGON, and SERPENT (& ALEPH2) and SCALE are larger. In general, the differences between DRAGON and SERPENT are smaller for the fission products than for the actinides, with the exception of ^{149}Sm. Substantial differences are observed for ^{242m}Am and $^{244,245,246}Cm$ isotopes. Differences between results from SCALE and SERPENT (& ALEPH2) are even more pronounced. There are no clear similarities between the differences observed with DRAGON and SCALE, except for ^{149}Sm and $^{245,246}Cm$. Similar observations were made by comparing SCALE and SERPENT in [Kromar, 2019]. To clarify these differences, more systematic studies including results from calculations with the KENO module of SCALE are required.

Nuclide	SERPENT	ALEPH2		DRAGON		SCALE	
	c_1 / g/t	c_2 / g/t	100x$\Delta c/c_1$	c_3 / g/t	100x$\Delta c/c_1$	c_4 / g/t	100x$\Delta c/c_1$
^{90}Sr	678.56 (2)	678.86	0.04	679.08	0.08	675.43	-0.46
^{106}Ru	7.357 (<1)	7.294	-0.86	7.286	-0.96	7.321	-0.49
^{133}Cs	1621.7 (2)	1624.2	0.15	1624.3	0.16	1637.9	1.00
^{134}Cs	43.86 (2)	43.68	-0.43	43.64	-0.51	41.11	-6.28
^{137}Cs	1638.0 (<1)	1640.2	0.13	1639.8	0.11	1643.2	0.32
^{144}Ce	4.386 (<1)	4.364	-0.51	4.363	-0.53	4.356	-0.68
^{148}Nd	567.92 (1)	569.51	0.28	569.29	0.24	567.45	-0.08
^{149}Sm	3.536 (2)	3.645	3.08	3.703	4.72	4.080	15.36
^{234}U	178.69 (8)	178.02	-0.37	180.54	1.04	190.23	6.46
^{235}U	7109.9 (14)	7064.5	-0.64	7119.6	0.14	7283.3	2.44
^{236}U	5620.5 (6)	5612.7	-0.14	5560.7	-1.07	5627.0	0.12
^{238}U	920116 (33)	920234	0.01	920143	0.00	919950	-0.02
^{237}Np	765.76 (37)	766.47	0.09	795.13	3.84	741.58	-3.16
^{238}Pu	426.44 (18)	426.55	0.03	434.35	1.85	429.22	0.65
^{239}Pu	6747.4 (18)	6786.5	0.58	6825.4	1.16	6947.2	2.96
^{240}Pu	3065.2 (13)	3044.1	-0.69	3056.1	-0.30	2976.3	-2.90
^{241}Pu	1556.7 (6)	1561.8	0.33	1570.8	0.91	1608.5	3.33
^{242}Pu	970.92 (30)	967.77	-0.32	963.26	-0.79	990.42	2.01
^{241}Am	499.66 (17)	499.79	0.03	503.06	0.68	516.77	3.43
^{242m}Am	1.253 (<1)	1.261	0.68	1.389	10.85	1.346	7.43
^{243}Am	242.95 (24)	242.87	-0.03	238.63	-1.78	225.35	-7.24
^{242}Cm	0.015 (<1)	0.015	-0.21	0.015	0.71	0.016	2.00
^{243}Cm	0.912 (1)	0.909	-0.37	0.878	-3.74	0.905	-0.83
^{244}Cm	109.38 (8)	108.80	-0.52	106.84	-2.32	102.37	-6.41
^{245}Cm	11.73 (2)	11.71	-0.19	10.820	-7.79	11.145	-5.02
^{246}Cm	1.302 (2)	1.286	-1.18	1.199	-7.91	1.208	-7.18

Table 2 – Comparison of the abundance of key nuclides present in a spent nuclear fuel sample of after a cooling time of 5 years

*The irradiation conditions are summarised in the text. To illustrate the observed differences between codes the relative difference with respect to the valued obtained with SERPENT are given. They are given in the column: 100 x $\Delta c/c1$ = 100 x (cx-c1)/c1. The results are taken from [*Žerovnik, 2019*]*

2.3. Sources of bias effects and uncertainties

The discussion in Section 2.2 reveals that various codes/systems are available to calculate source terms of spent nuclear fuel. Bias effects can be due to the methodology that is applied to solve the neutron transport and nuclide production and depletion processes. Independent of the methodology that is applied the final accuracy depends on input data which can be classified into nuclear data and fuel history data. The latter include the initial fuel composition and design and reactor operation and irradiation conditions.

2.3.1. Methodology

A detailed model of the irradiation conditions of a fuel assembly is not always possible. One of the reasons is that the full core information is mostly not publicly available and only limited information is provided by the plant operator or fuel vendor. Another reason concerns the tools used to perform the calculations. As mentioned earlier, Monte Carlo transport simulations, which are generally preferred to simulate irradiations, can hardly be applied to a large number of assemblies. Therefore, depending on the method used and depending on the degree of detail known from reactor operation, a simplified description of the irradiation history of a fuel assembly is necessary. For example, the effect of neighbouring fuel assemblies often cannot easily be described. In-core reactor measurements are typically made only for relatively few fuel assembly positions. Moreover, the fuel temperature, the moderator temperature or the moderator boron concentration history are often condensed into a few average values per cycle. In the case of 1D or 2D calculations, the axial profile is typically ignored in favour of a given node average burnup value provided by the power plant's in-core fuel management. This approach ignores shielding effects due to control rod position changes or the neutron fluence suppression at spacer or mixing grid positions. The impact of these factors on the nuclide inventory has been addressed for example in [NEA, 2011]. However, more quantitative studies of possible bias effects due to these assumptions are still needed.

The Doppler effect seems to be well understood, as far as its impact on the broadening of resonance structures is concerned. The broadening of ^{238}U resonance profiles has a strong influence on the self-shielding effect and the production of ^{239}Pu. Hence, it is important for reactor licensing and for spent fuel characterisation. Both the scattering and absorption cross-section are Doppler broadened. Until a decade ago, the scattering kernel, that is, the change in energy and angle of the scattered neutron, was simulated for a target nucleus at rest, namely at a temperature of 0K. Temperature-dependent scattering kernel theories which started by Wigner and Wilkins [Wigner, 1944], were further developed by [Rothenstein, 1998]. On the practical side, [Rothenstein, 2004] and later [Becker, 2009] found a technique to include the energy-dependent scattering kernel in stochastic transport calculations. This technique, known as Doppler-Broadening Rejection Correction (DBRC), was validated by a dedicated experiment in [Becker, 2009] and was implemented in MCNP, SERPENT and TRIPOLI [Zoia, 2013]. In the KENO code of SCALE, the angular part is missing. It can be shown that the inventory of ^{239}Pu in a thermal LWR is underestimated by 1.5% when the impact of the Doppler effect on the scattering kernel is not properly taken into account [Dagan, 2005]. Evidently this bias of 1.5% will affect the inventory of all other actinides that are produced in the chains following the ^{239}Pu production and the source terms depending on this inventory. More efforts should be made to study possible bias effects due to the use of spectrum-averaged cross-sections in the ODEs and in particular, the present assumptions made regarding the energy and angle differential scattering cross-sections for energies above the resolved resonance region.

Different approaches can be applied to account for resonance self-shielding in case of deterministic transport calculations [Williams, 2011]. Two different methods implemented in SCALE were compared in [Ilas, 2012]. The results show a substantial difference in the inventory of Sm-isotopes and ^{245,246}Cm obtained with the two different methods. The effect increases with increasing burnup. For a burnup of 50 GWd/t, the inventory of ^{239,240,241}Pu can be biased by more than 3%. Methods to account for self-shielding in the unresolved resonance region are discussed and compared in [Sublet, 2009]. At present

a detailed systematic study assessing the methods used in the different codes is not reported in the literature.

2.3.2. Nuclear data

Different types of nuclear data are required to calculate the spent nuclear fuel source terms: neutron interaction cross-sections, fission product yields, decay data and neutron and γ-ray emission properties. Most of these data are available in the main general purpose Evaluated Nuclear Data Files (ENDF) such as the ENDF/B, JEFF and JENDL libraries. The decay data in these files are mostly adopted from the ENSDF library or result from international collaborative efforts such as the Decay Data Evaluation Project (DDEP) [Kellett, 2017]. The general purpose libraries can be complemented by data from special purpose libraries that are dedicated to specific applications, such as the International Reactor Dosimetry and Fusion File (IRDFF) file for neutron dosimeter reactions or activation cross-sections in the European Activation File (EAF). The TENDL library can be used to fill the remaining gaps. An overview of evaluated nuclear data libraries can be found on the website of the Nuclear Energy Agency of the OECD (OECDNEA) and the Nuclear Data Section of the IAEA (IAEA-NDS).

The general purpose libraries contain mainly calculated data resulting from an evaluation process that is based on nuclear reaction formalisms or theories involving model parameters which are adjusted to experimental data. Calculated cross-sections are required to ensure consistency and to account for the Doppler effect. The term "general purpose library" is not always appropriate. Some of the cross-sections are adjusted based on results of integral benchmark experiments. Such data are often biased due to compensating effects and can only be used for specific applications. An example of a biased cross-section due to a compensating effect is given in [Sirakov, 2017].

Nuclear data in general purpose libraries are stored in the internationally adopted ENDF-6 format. This format is not adequate for neutron transport or inventory calculations. Therefore, data processing codes are used to transfer the data into a format that is suitable for use in transport and burnup codes. The NJOY nuclear data processing system [MacFarlane, 2010] is widely used to convert evaluated data from the ENDF-6 format into a format useful for practical applications. One of these formats is the ACE format which is the most used format for MC transport codes. The AMPX code is a modular system for processing ENDF-6 formatted data into data that are ready for use in the SCALE system.

The primary goals of projects supporting the production of evaluated nuclear data were not to fulfil requirements for a spent fuel characterisation. For example, various projects to improve decay heat predictions have been organised or coordinated by both the IAEA-NDS [Dimitrou, 2014] and the [NEA, 2007]. However, they concentrated on decay heat predictions at short cooling times and resulted in a substantial improvement of specific decay heat data for short-lived radionuclides. Measurements to produce such data are very complex. Unfortunately, the results are not relevant for the prediction of the thermal power of a SNF assembly at cooling times longer than one year.

The status and need for nuclear data for spent fuel characterisation is best illustrated by some specific examples. Key nuclides to determine the source terms are e.g. ^{137}Cs and ^{90}Sr. These nuclides are predominantly produced in a single mass chain through neutron-induced fission and β^- decay. The total number of nuclides N_X that are produced during an irradiation period can be approximated by summing the product of the cumulative fission yield $Y_{c,k}$ and total number of fission reactions $N_{f,k}$ due to neutron-induced fission of nuclide k:

$$N_X \approx \sum_k Y_{c,k} N_{f,k} \tag{12}$$

The total number of fission reactions for each nuclide k is given by:

$$N_{f,k} \approx s_{f,k}\, j\, T \tag{13}$$

with T the total irradiation time, the total fluence rate and $s_{f,k}$ the fission cross-section of nuclide k. The main contribution to fission events starting from fresh UO_2 fuel in a LWR is due to ^{235}U(n,f). With

increasing irradiation time, the burnup of the initial fuel and production of ^{239}Pu progresses. This results in an increased contribution of fission events due to ^{239}Pu(n,f). At high burnup the latter can even dominate. Evidently, in the case of MOX the relative contribution of ^{235}U(n,f) and ^{239}Pu(n,f) depends on the composition of the initial fuel.

The approximation in Eq. (12) can be made due to the relatively long half-life and small capture cross-section of ^{137}Cs and ^{90}Sr. Hence, the nuclear data required to derive their inventory are the cumulative fission yields and fission cross-sections. They are reported in Table 3 and Table 4 for thermal neutron-induced fission of ^{235}U and ^{239}Pu. These data suggest that there is a rather good consensus on the fission cross-sections and their uncertainties. However, for the cumulative fission yields there are larger differences. For ^{235}U(n,f) the difference between the yields recommended in JEFF-3.3 and ENDF/B-VIII.0 is almost 2% and their uncertainties differ by a Factor 2. The inventory of these nuclides, as such, is not a key source term. However, ^{137}Cs has a substantial contribution to the γ-ray emission and decay heat. The data used to derive the γ-ray emission spectrum due to the decay of ^{137}Cs are well known and they can be taken from the ENSDF data base [Tuli, 2001]. The total energy that can be transformed into heat, which is also referred to as recoverable energy, is summarised in Table 5. These values are deduced from a combination of decay data. The uncertainty of the recoverable energy due to the decay data is less than 1% for both ^{90}Sr and ^{137}Cs. It is remarkable that all recommended values differ from the value E_r = 1'147 (9) keV that was derived by Ramthun from a direct calorimetric measurement [Ramthum, 1967]. The results in Table 5 suggest that the recommended values might be underestimated with a bias between 1.5% and 3.5%. New measurements are required to resolve these discrepancies.

Library	**σ(n,f) at 2'200 m/s**		**< σ(n,f)>: spectrum-averaged**	
	^{235}U(n,f)	**^{239}Pu(n,f)**	**^{235}U(n,f)**	**^{239}Pu(n,f)**
ENDF/B-VIII.0	586.7 (29) b	747.4 (69) b	33.99 (14)	77.62 (107)
JEFF-3.3	584.5 (38) b	749.3 (65) b	33.49 (23)	78.02 (95)
JENDL-4.0	585.0 (20) b	747.3 (84) b	34.06 (11)	78.53 (59)

Table 3 – Cross-section for neutron-induced fission of ^{235}U and ^{239}Pu recommended in the latest versions of the main data libraries

The cross-section at thermal energy (or at 2200 m/s) is given together with a spectrum-averaged cross-section based on a typical neutron energy distribution in a PWR. Uncertainties are at the 68% confidence limit.

Library	^{90}Sr	^{90}Sr	^{137}Cs	^{137}Cs	^{148}Nd	^{148}Nd
	^{235}U(n,f)	^{239}Pu(n,f)	^{235}U(n,f)	^{239}Pu(n,f)	^{235}U(n,f)	^{239}Pu(n,f)
ENDF/B-VIII.0	0.0578 (5)	0.0210 (4)	0.0619 (3)	0.0661 (3)	0.01674 (6)	0.01662 (8)
JEFF-3.1.1	0.0573 (13)	0.0201 (5)	0.0622 (7)	0.0659 (8)	0.01681 (12)	0.01658 (17)
JEFF-3.3	0.0568 (13)	0.0208 (6)	0.0609 (6)	0.0673 (8)	0.01693 (12)	0.01685 (15)
JENDL-4.0	0.0577 (6)	0.0210 (4)	0.0618 (3)	0.0660 (3)	0.01671 (7)	0.01642 (8)

Table 4 – Cumulative fission yields of ^{90}Sr, ^{137}Cs and ^{148}Nd for neutron-induced fission of ^{235}U and ^{239}Pu at thermal energy (or 2'200 m/s)

The cross-sections recommended in evaluated data libraries are compared. Uncertainties are at the 68% confidence limit.

Library	^{90}Sr/^{90}Y			^{137}Cs/^{137m}Ba		
	E_r / keV	$E_{r,cp}$ / keV	$E_{r,\gamma}$	E_r / keV	$E_{r,cp}$ / keV	$E_{r,\gamma}$ / keV
DDEP [Kellett, 2017]	1'129.4 (14)			813.3 (18)	247.9 (12)	813.3 (18)
ENDF/B-VIII.0	1'128.8	1'128.8	0	805.7	240.1	565.6
JEFF-3.3	1'128.5	1'128.5	0	804.1	237.4	566.7
JENDL/FPD-2011	1'129.6	1'129.6	0	811.2	247.9	563.3

Table 5 – Total recoverable energy (Er) together with that resulting from charged particle (Er,cp) and γ-ray (Er,γ) emission due to the decay of the ^{90}Sr/^{90}Y and ^{137}Cs/^{137m}Ba chains

The energies recommended in nuclear data libraries are compared with the ones derived from the data in the DDEP [Kellett, 2017]. Uncertainties are at the 68% confidence limit.

The capture cross-section of ^{134}Cs is relatively large and cannot be ignored when estimating the abundance of ^{134}Cs. Figure 3 compares the capture cross-section that is recommended in the ENDF/B-V and ENDF/B-VII.0 libraries. It is shown in [Ilas, 2012] that the difference between the cross-sections in ENDF/B-V and ENDF/B-VII.0 results in a 7.5% difference in the ^{134}Cs abundance in case of a 50 GWd/t burnup. Even larger differences of up to 30% are observed for $^{149\text{-}152}$Sm, ^{155}Eu and ^{155}Gd. This shows the importance of estimating the cross-section in the resolved resonance region based on resolved resonance parameters, which can only be derived from a resonance shape analysis of experimental data (see [Fröhner, 2000; Schillebeeckx, 2012]).

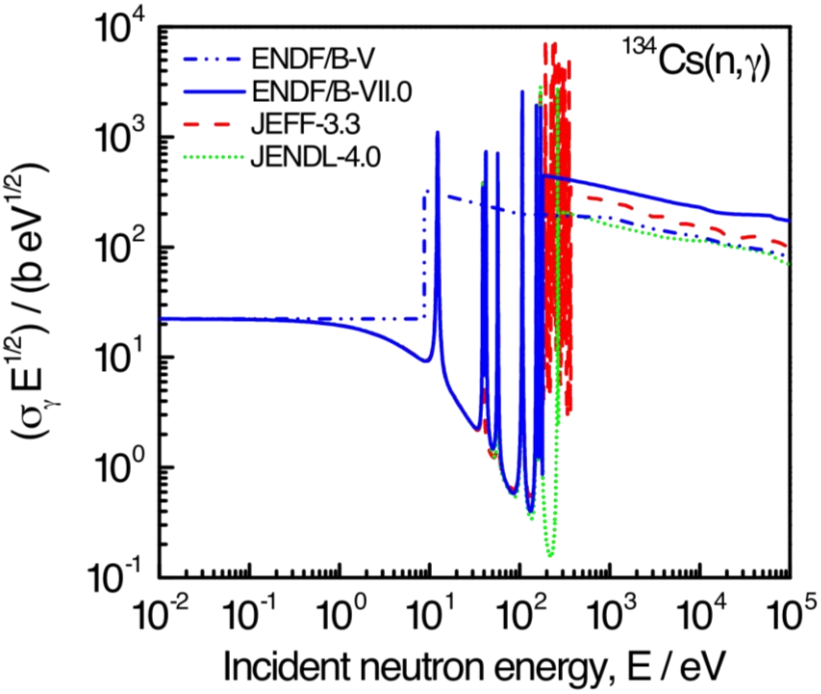

Figure 3 – Comparison of the $^{134}Cs(n,\gamma)$ cross-sections as a function of neutron energy which are recommended in the ENDF/B-V, ENDF/B-VII.0, JEFF-3.3 and JENDL-4.0 libraries

The capture cross-section $\sigma\gamma$ is multiplied with the square root of the energy.

One of the important contributors to the neutron emission rate of spent fuel is ^{244}Cm. Starting from UO_2 based fuel, this curium isotope is produced through a sequence of neutron capture reactions and β^- decay starting from the ^{238}U(n,γ) reaction. The main production chain involves six neutron-induced capture reactions. Several studies [Hu, 2014; Zu, 2016; Leray, 2016; Borella, 2017; Rochman, 2018b] show that the uncertainty of the predicted ^{244}Cm abundance is in the order of 10%. This is mainly due to the uncertainty of the ^{242}Pu(n,γ) and ^{243}Am(n,γ) cross-sections [Hu, 2014; Leray, 2016]. To derive the neutron emission rate, the ^{244}Cm abundance has to be combined with the specific neutron emission per decay, which is 3.74 (11) × 10^{-6} based on data in the JEFF-3.3 library. Hence, at present the total uncertainty of the predicted neutron emission rate due to ^{244}Cm(sf) is dominated by the one of the ^{244}Cm production. This uncertainty can only be reduced by performing new experiments to improve the capture cross-section data for ^{242}Pu(n,γ) and ^{243}Am(n,γ). In the case where the neutron emission is dominated by the production of (α,n) neutrons, there is a substantial contribution to the uncertainty due to the specific (α,n) neutron production which is in the order of 8% [Simakov, 2017]. This uncertainty component is difficult to reduce and requires both improved experimental data and theoretical modelling.

For a criticality safety assessment based on a BUC approach, the concentrations of nuclides with a relatively large absorption cross-section are required together with reliable estimates of the cross-sections. Oscillator experiments [Gruel, 2011] were performed at the MINERVE reactor of CEA Cadarache (FR) to validate the capture cross-section of fission products that are important for such a criticality safety analysis. For most of them, substantial differences were observed between the measured and calculated reactivity-worth. Based on these differences, correction factors are proposed to define criticality safety margins [Tardy, 2015]. However, results derived from such oscillator experiments might be biased due to poor knowledge of the sample properties as discussed in [Šalamon, 2019; Ma, 2019]. Problems with the sample properties could explain the reactivity-worth difference in the order of 10% observed for ^{103}Rh in Ref. [Gruel, 2011]. Since natural rhodium is mono-isotopic and metallic homogeneous samples are easy to produce, its capture cross-section can be determined with an uncertainty of less than 2% [Schillebeeckx, 2012]. Therefore, the use of correction factors is not recommended and reliable safety margins should be derived starting from accurate microscopic absorption cross-sections resulting from an evaluation process that is based on a resonance analysis of experimental data reported in the literature. Unfortunately, the present status of the evaluated libraries does not always reflect the quality of the available experimental data. Table 6 compares the capture cross-section for ^{103}Rh at thermal energy as recommended in the main general purpose libraries. The values are consistent within the quoted uncertainties, except for the one in JENDL-4.0. Nevertheless, it seems that none of the evaluation procedures included the value σ_γ = 144.9 (7) b derived by [Dilg, 1974], even though this value was derived by the same method that was used to derive the value for ^{197}Au(n,γ) [Dilg, 1973], which is still the basis of the present neutron standard [Carlson, 2018].

Library	**^{103}Rh**		
	σ (n,tot) / b	**σ (n,n) / b**	**σ (n, γ) / b**
ENDF/B-VIII.0	146.5	4.34 (87)	142.1 (15)
JEFF-3.3	146.6 (38)	3.88 (92)	142.7 (37)
JENDL-4.0	136.4	3.27	133.1

Table 6 – Total cross-section and cross-section for neutron elastic scattering and capture of ^{103}Rh at thermal energy

The data in recommended data libraries are compared.

2.3.3. Fuel history

The importance of the fuel history, i.e. fuel composition and design, reactor operation and fuel irradiation conditions, is discussed in a state-of-the art report that was issued by the NEA/OECD. This report was the result of an Expert Group on Assay Data of Spent Nuclear Fuel (EGADSNF) [NEA, 2011]. In this report, the impact of modelling approximations due to missing or uncertain fuel history data is discussed based on calculations done using the Takahama PWR 17×17 assembly as a reference. The report discusses how various parameters such as power history, moderator temperature (density), moderator soluble boron, fuel temperature, sample burnup, assembly pitch and surrounding assemblies affect the nuclide inventory.

Assigning an uncertainty to these parameters to propagate them to the uncertainty on the source terms is not evident. It will depend on the quality of the documentation provided by the fuel manufacturer, operators and engineering companies. In the OECD-NEA state-of-the-art report, estimates of representative uncertainties at a 68% confidence limit are given for the initial enrichment (0.05 wt.-%), fuel temperature (50 °C), moderator temperature (2 °C) and fuel sample (local) burnup (2%, relative). The impact of the uncertainty of the initial enrichment and burnup on the inventory of some key nuclides is illustrated in Figure 4 [Schillebeeckx, 2018]. This figure gives the sensitivity of the nuclide inventory to a change in IE and BU for a PWR assembly with an initial enrichment of 4.8 wt.-% ^{235}U and burnup of 45 GWd/t. The results illustrate that the inventory of ^{137}Cs and ^{148}Nd is not sensitive to the initial enrichment and a 1% uncertainty of the burnup results in a 1% uncertainty of the inventory. For a relative variation of 1% of the initial enrichment and burnup, the inventory of ^{244}Cm changes by 2% and 4%, respectively. The impact of burnup increases due to the number of neutron-induced reactions involved in the production process.

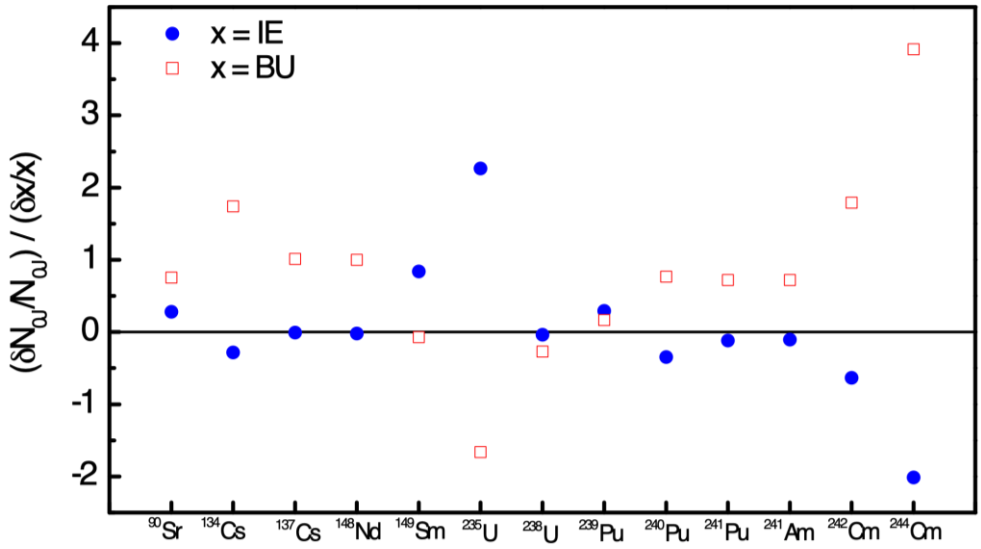

Figure 4 – Relative sensitivity of the nuclide inventory to the initial enrichment (IE) and burnup (BU)

The data are for a UO_2 sample with initial enrichment of 4.8 wt.-% irradiated in a PWR to a burnup of 45 GWd/t.

Burnup is an essential parameter for the calculations. It is related to time integrated the thermal power that is extracted from the nuclear fuel. The thermal power of a system is used to determine the neutron fluence which is required to normalise the theoretical calculations. The relation between thermal power P and neutron fluence rate is [Gauld, 2011]:

$$= \frac{P}{\sum_k N_k (N_{f,k} E_{f,k} + \sum_a N_{a,k} E_{a,k_{\square}})} \quad (14)$$

with $N_{f,k}$ and $N_{a,k}$ the total number of fission and other absorption reactions with nuclide k, respectively, and $E_{f,k}$ and $E_{a,k}$ the corresponding recoverable energies for these reactions. The inventory of nuclide k is denoted by N_k. Table 7 lists the recoverable energy per fission and capture event for ^{235}U and ^{239}Pu, which are recommended in the main data libraries. There is almost no difference between the adopted values. The recoverable energy for some nuclides with a relatively large absorption cross-section are given in Table 8. These energies are the same in the main data libraries and are used in SERPENT and ALEPH2. They are also used in SCALE, except for ^{155}Gd and ^{157}Gd, for which a default energy of 5 MeV is adopted. This can create bias effects in the case of Gd-loaded fuel.

	^{235}U			**^{239}Pu**		
	E_r / MeV	**$E_{r,f}$ / MeV**	**$E_{r,\gamma}$ / MeV**	**E_r :/MeV**	**$E_{r,f}$ / MeV**	**$E_{r,\gamma}$ / MeV**
ENDF/B-VIII.0	200.645	194.1	6.545	205.134	198.6	6.534
JEFF-3.3	200.415	193.87	6.545	205.234	198.7	6.534
JENDL-4.0	200.345	193.8	6.545	206.434	199.9	6.534

Table 7 – Recoverable energy due to neutron-induced interaction with ^{235}U and ^{239}Pu

The energies recommended in evaluated data libraries are compared.

Library	**Recoverable energy, E_r / MeV**				
	^{1}H(n,γ)	**^{16}O(n,γ)**	**^{10}B(n,α)**	**^{155}Gd(n,γ)**	**^{157}Gd(n,γ)**
ENSDF [Tuli, 2001]	2.225	4.143	2.790	8.536	7.937

Table 8 – Recoverable energy for some important neutron absorption reactions

The energies in the decay libraries are adopted in the main evaluated data libraries. They are also used in SCALE, except for ^{155,157}Gd(n,γ).

The burnup is mostly defined as time integrated thermal power per unit initial actinide mass in the fuel and often expressed in gigawatt-days per ton (GWd/t) or megawatt-days per kg (MWd/kg). In the case where samples of irradiated fuel are analysed, the burnup is mostly derived from the total number of Fission reactions per Initial number of heavy Metal Atoms (FIMA). It is often assumed that the burnup defined by the total thermal power is directly proportional to the total number of fissions, with a constant conversion factor. Evidently, this assumption is not always valid and might introduce bias effects Kępisty, 2007; Kenya, 2006]. The recoverable energy depends on the fissioning nuclide such that the average energy released per fission event will change with burnup. A more detailed discussion on the relation between burnup and FIMA is given in [Kępisty, 2007].

The number of fission events of an irradiated sample can be derived by determining the amount of a specific fission product. An ideal fission product to determine the number of fissions should have a cumulative fission yield that is independent from the fissioning nuclide, a low yield from neutron capture, a low neutron absorption cross-section and a relatively long half-life. Under these conditions, the amount of this fission product is directly proportional to the total number of fission reactions, even independent

of the initial enrichment. In addition, it should not be volatile and not be produced through volatile precursors. The use of the stable fission product ^{148}Nd as a FIMA monitor or indicator is generally accepted as a standard method since the issue of the ASTM method E 321-96 [ASTM, 1969; ASTM, 2012]. However, in spite of the short half-life of ^{147}Nd and the small ^{148}Nd(n,γ) cross-section, the production of ^{148}Nd is affected by the ^{147,148}Nd(n,γ) cross-sections [Suyama, 2005]. These capture reactions will have an opposite effect on the ^{148}Nd production. The results in Ref. [Kenya, 2006] show that ignoring the contributions due to the ^{147,148}Nd(n,γ) reactions and the dependence of the recoverable energy, the burnup derived from the amount of ^{148}Nd can be biased by 3%. To reduce bias effects, it is recommended to derive the burnup by theoretical calculations by adjusting the theoretical ^{148}Nd inventory to the experimental value as in Refs. [Zwicky, 2010; Gauld, 2016]. Applying such a procedure, the total number of fission reactions can be determined with an uncertainty of 1.5% (68% confidence limit) [Gauld, 2016].

Evidently, the ^{147}Nd(n,γ) cross-section enters into such a calculation. Although, this reaction contributes less than 2% to the ^{148}Nd production, the results in Figure 5 illustrate the need for a re-evaluation of this cross-section. This figure compares the cross-section recommended in the ENDF/B-VIII.0, JEFF3.3, JENDL-4.0 and TENDL-2017 libraries. The cross-section in TENDL-2017 relies on a re-evaluation of the cross-section at thermal energy in [Rochman, 2016a]. This evaluation is based on the value reported in [Heck, 1974] combined with results of optical model calculations. Unfortunately, the value in [Heck, 1974] is the only experimental value for this reaction at thermal energy that is reported in the literature. Hence, the experimental data available for performing an evaluation are rather scarce.

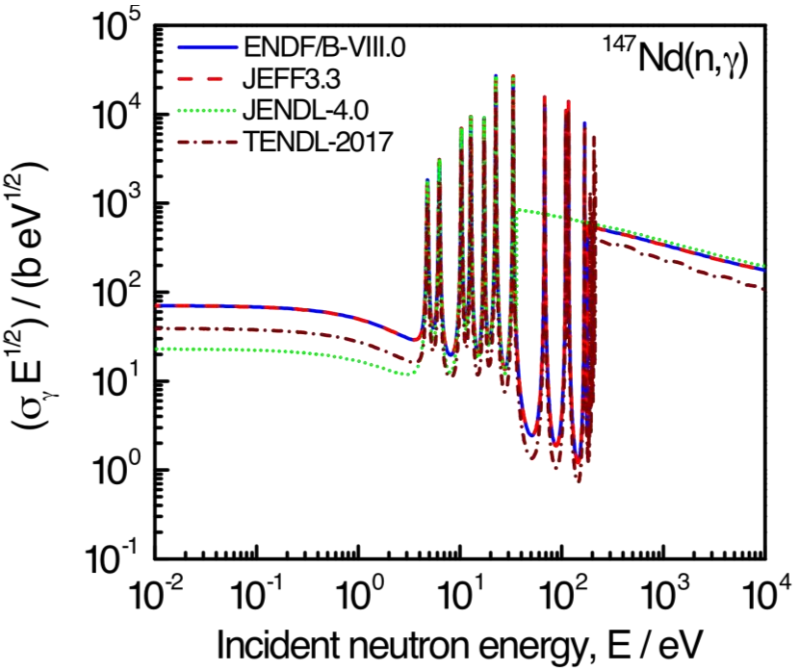

Figure 5 – Comparison of the ^{147}Nd(n,γ) cross-sections as a function of neutron energy that are recommended in the ENDF/B-VIII.0, JEFF-3.3, JENDL-4.0 and TENDL-2017 libraries

The cross-section $\sigma\gamma$ is multiplied with the square root of the energy.

Alternative methods to determine the number of fission events are based on measurements of other Nd isotopes, fission products such as ^{133,137}Cs and ^{235}U or ^{239}Pu [Zwicky, 2010; Gauld, 2016; Kim, 2007; Kim, 2015]. Different methods to are compared in [Zwicky, 2010]. The results are consistent within 3%. The advantage of using γ-ray emitting indicators such as ^{137}Cs is that their inventory can be determined by non-destructive γ-ray spectroscopic methods and used to verify the burnup of an assembly. All these

methods use the inventory of a specific nuclide to normalise the local burnup of the sample being investigated and to compare measured and calculated inventories of other nuclides. However, for final applications, the burnup information provided by the operator has to be used. Unfortunately, no detailed study is available in the open literature that provides an uncertainty assessment to link FIMA to the burnup information of the operator.

2.4. Uncertainty evaluation and sensitivity analysis

A reliable characterisation of spent fuel requires best estimates of the observables together with their uncertainties and covariance matrix. They will finally define the confidence limits and safety margins and influence the decision-making. Hence, a careful evaluation of the covariance matrix of the calculated nuclide vector is required. Unfortunately, the relationship between the nuclide vector and the input data is rather complex. Since the neutron and γ-ray emission rates and thermal power are linear functions of the nuclide vector, their uncertainties can be derived by conventional first order uncertainty propagation, also considering the uncertainty of decay constants, specific emission properties and recoverable energy.

2.4.1. Methods

Propagation of uncertainties can be performed by deterministic or probabilistic methods [Rochman, 2011; Wieselquist, 2013]. Deterministic methods are based on the first order uncertainty propagation formula:

$$\boldsymbol{V}_Y = \boldsymbol{S}\boldsymbol{V}_X\boldsymbol{S}^T \tag{15}$$

with $\boldsymbol{V}_Y$ the covariance matrix of the output, $\boldsymbol{V}_X$ the covariance matrix of the input data and $\boldsymbol{S}$ the sensitivity matrix. The latter is defined by the partial derivatives of the output with respect to the input. Most of the deterministic sensitivity and uncertainty analysis codes used for reactor applications rely on perturbation theory [Kodeli, 2001; Rearden, 2011]. For neutron transport problems, the sensitivity matrix is directly obtained from the forward and adjoint transport equation [Wieselquist, 2013; Kodeli, 2001]. Adjoint equations for depletion calculations were implemented in ORIGEN [Rearden, 2011] based on the work of [Gandini, 1975]. The present version of ORIGEN includes adjoint calculations based on the CRAM method for sensitivity and uncertainty analysis [Isotalo, 2015; Gauld, 2017].

The direct perturbation approach works well for smooth relationships between input and output and when the uncertainties are relatively small. When non-linearity effects are important this approach is not applicable and can be replaced by stochastic sampling-based uncertainty propagation [Rochman, 2011]. This consists of repeating the nominal calculation a large number of times, each time with different input data. The input data are sampled from independent or multivariate probability distributions. These distributions reflect the covariance $\boldsymbol{V}_X$ of the input data. In most cases they are based on multivariate normal distributions. However, this is not a restriction, for example inherently positive data can be sampled from a log-normal or rectangular distribution. The choice of the distributions depends on the available information about the input data and can be based on the Maximum Entropy Principle [Jaynes, 1968]: when only a best estimate of an inherently positive observable is known the data should be sampled from a decreasing exponential distribution; however, when an estimate of the covariance matrix is also available the optimum probability distribution for further inference is a multivariate normal distribution [Fröhner, 2000]. Stochastic sampling offers the advantage that uncertainties of all input data can be propagated, independently of their relationship with the output of interest and of the magnitude of the uncertainty. In addition, it provides the final probability distributions of output quantities from which the uncertainties can be derived.

Various codes and platforms have been developed to propagate uncertainties by stochastic sampling, e.g. SHARK-X [Wieselquist, 2013; Aures, 2017], XSUSA [Aures, 2017; Zwermann, 2014], NUSS [Zhu, 2015], NUDUNA [Diez, 2015], SAMPLER [Williams, 2013b; Rearden, 2015] and SANDY [Fiorito, 2017].

The development and testing of these codes have been motivated by the Benchmark for Uncertainty Analysis in Modelling (UAM) for design, operation and safety analysis of LWRs organised by the OECD-NEA [Ivanov, 2013].

The SHARK-X platform has been developed at the Paul Scherer Institute for sensitivity analysis and uncertainty propagation based on a deterministic perturbation and stochastic sampling approach [Wieselquist, 2013; Aures, 2017]. It is a set of Perl-based tools build around the lattice code CASMO-5. It allows perturbation to nuclear data, i.e. cross-sections for (n,n), (n,n'γ), (n,2n), (n,f) and (n,γ) reactions, the average number of neutrons per fission and the prompt fission neutron energy distribution. In addition, any parameter contained in the input file, e.g. cladding thickness, fuel enrichment, can be perturbed.

The XSUSA Cross-section Uncertainty and Sensitivity Analysis (XSUSA) method [Zwermann, 2014] is based on the random sampling method implemented in the code package Software for Uncertainty and Sensitivity Analysis (SUSA) Krzykacz, 1994]. It enables simultaneous correlated sampling of (n,n), (n,n'), (n,2n), (n,f), (n,γ) cross-sections, fission neutron multiplicities and fission neutron spectra. As a basis for generating the data variations, the SCALE 6.1 covariance data library is used and processed in a multi-group structure with 44 energy groups. Normal distributions are assumed as default distributions. In addition to neutron cross-section uncertainties, uncertainties of data relevant for the production of nuclides and their decay chains can be propagated, i.e. uncertainties of fission yields, decay constants and branching. These uncertainty data are extracted from the ENDF/B-VII library. The XSUSA method is also integrated into the SAMPLER module [Williams, 2013b; Rearden, 2015] of the SCALE code system, where it can be used in combination with the POLARIS sequence. The SAMPLER module uses the XSUSA method to repetitively sample nuclear data in multi-group approximation, execute the sequence and analyse the distributions of e.g. decay heat rate or nuclide vector.

The Nuclear data Uncertainty Stochastic Sampling (NUSS) random sampling tool [Zhu, 2015] combines multi-group uncertainties and pointwise/continuous energy nuclear data. This tool is implemented for the continuous energy ACE format, facilitating direct use by MC codes such as MCNP and SERPENT. It is capable of introducing perturbations to (n,n), (n,n'), (n,2n), (n,f), (n,γ) cross-sections, fission neutron multiplicities and fission neutron energy distribution data using multivariate normal distribution. Caution has to be taken that associated total quantities are updated accordingly, i.e. summation rules are not applied automatically.

The NUclear Data UNcertainty Analysis (NUDUNA) package [Díez, 2015] provides full random sampling of nuclear data inputs for transport and depletion calculations. NUDUNA takes the information provided by nuclear data evaluations in the standardised ENDF-6 format as input, taking into account best estimates and covariances of neutron-induced cross-sections, resonance parameters, fission neutron multiplicities, angular distributions of outgoing particles and decay data, assuming normal or log-normal distribution. The NUDUNA output files can be used as input for different neutron transport and fuel depletion codes, such as SCALE, SERPENT or MCNP.

The random sampling code SANDY [Fiorito, 2017] enables sampling of nuclear data for which covariance data are available: resonance parameters, cross-sections, angular and energy distributions, fission neutron multiplicities, fission yields and decay data. The code includes capabilities for verification of mathematical correctness of the covariance data and automated correction methods to make the covariance matrix positive semi-definite [Higham, 2011]. It uses multivariate normal or log-normal distribution for sampling of correlated parameters. Apart from the basic option of uncertainty propagation, it also includes capabilities for sensitivity analysis using linear regression. This method is analogous to the first order deterministic sensitivity analysis since it is accurate for small uncertainties or (close to) linear functions. It enables simultaneous determination of the entire sensitivity matrix using one set of samples with all input parameters perturbed. Due to the nature of random sampling, this method works for any functional relationship. The SANDY code is freely available and works with nuclear data files in ENDF-6 format.

2.4.2. Examples

The codes presented in Section 2.4.1 have been used for sensitivity and uncertainty analysis of the source terms of spent nuclear fuel, see [Leray, 2016; Borella, 2017; Rochman, 2018b; Zwermann, 2014; Cabellos, 2011; Fiorito, 2015; Rochman, 2013; Leray, 2017; Rochman, 2020a]. They focus on nuclear data uncertainties with the emphasis on cross-sections and fission yields.

Nuclear data

The results in [Cabellos, 2011; Fiorito, 2015] reveal that uncertainties due to decay constants have a negligible contribution to the total uncertainty of the nuclide inventory, except for the production of ^{151}Eu. The results in [Cabellos, 2001; Fiorito, 2015] are based on a recommended half-life of $T_{1/2}$ = 90 (8) for ^{151}Sm. The present recommendation by DDEP is $T_{1/2}$ = 94.7 (6) a. This value is based primarily on results of measurements reported in Ref. [Bé, 2015] and has been adopted in JEFF-3.3 but not in ENDF/B-VIII.0.

Most of the studies verifying the impact of nuclear cross-section data report only final uncertainties. Sensitivity studies to identify the main reactions contributing to the uncertainty of the nuclide inventory are rather scarce. However, such studies are needed to define nuclear data that need to be improved. A study of reaction cross-section data that are important for the production of ^{244}Cm and ^{238}Pu is presented in [Tiehun, 2016] and [Gauld, 2017], respectively. These studies show the convenience of the adjoint equations for the depletion calculations for such a sensitivity study.

Efforts are made to propagate uncertainties of fission yields. Table 9 compares reported uncertainties for the predicted ^{137}Cs and ^{148}Nd inventory due to the propagation of fission yields covariance data for UO_2 in a PWR [Leray, 2016; Rochman, 2018b; Rochman, 2013; Leray, 2017b]. The results reveal strong differences, e.g. for ^{137}Cs the uncertainty varies between 0.3% and 7.0% and for ^{148}Nd between 0.4% and 14%. Part of these differences is due to the use of independent fission yields which are needed for a complete consistent burnup calculation. Unfortunately, independent fission yields are generally more complicated to measure compared to cumulative yields. Therefore, they have larger uncertainties. Methods have been proposed and developed to produce covariance data for independent fission yields that are consistent with cumulative yields, that is, to maintain the cumulative yields together with their uncertainties [Fiorito, 2014; Fiorito, 2016; Rochman, 2016b]. However, given the difference between the evaluated data discussed in Section 2.3, a difference of a Factor 2 will remain. Hence, a consensus on the evaluated cumulative yields and their uncertainties is required.

An uncertainty assessment of decay heat predictions for BWR SNF assemblies is reported by Ilas and Liljenfeldt [Ilas, 2017]. The impact of uncertainties due to nuclear data and fuel history parameters were verified using the SAMPLER module of SCALE. The results, which are summarised in Table 10, suggest that for a cooling time of about 15 years, the total uncertainty of the predicted heat is about 1.3%. The contribution of the uncertainties due to both nuclear data and fuel history is about 0.9%. 70% of the decay heat at such cooling times derives from the decay chains of ^{137}Cs and ^{90}Y. The discussion on the fission yields and recoverable energy in Section 2.3.2 suggests that an uncertainty of less than 1% is questionable. Using the data in Table 4 and Table 5, a difference of about 2.5% in estimated thermal power only due to nuclear data can be expected for the conditions considered in [Ilas, 2017]. A study in [Rochman, 2016] reports for similar conditions an uncertainty of at least 3% by propagating only cross-section and fission yield uncertainties. In addition, the discussion in Section 2.3 suggests that an absolute prediction of the burnup with an uncertainty of less than 1% is questionable. Hence, a more detailed uncertainty assessment of decay predictions is required to define realistic confidence limits that can be presented to licensing authorities.

Ref.	Library	Con-straint	Reactor	Fuel	BU (GWd/t)	IE (wt.-%)	^{90}Sr	^{137}Cs	^{148}Nd
[Zwermann, 2014]	SCALE-6.1		PWR	UO_2	40	4.1	5.0%	1.7%	14%
[Fiorito, 2016]	ENDF/B-VII.0		PWR	UO_2	40	4.1	5.6%	2.0%	12%
[Leray, 2016]	ENDF/B-VII.1	Y	PWR	UO_2	54	3.4	1.5%	4.0%	0.4%
[Rochman, 2018b]	ENDF/B-VII.1	Y	PWR	UO_2	54	3.4	0.7%	6.2%	0.4%
[Rochman, 2018b]	ENDF/B-VII.1	Y	PWR	UO_2	40	4.1	0.7%	7.0%	0.4%
[Leray, 2017b]	ENDF/B-VII.1	Y	PWR	UO_2	60	4.1	3.6%	0.3%	0.9%
[Leray, 2017b]	JEFF-3.1.1	Y	PWR	UO_2	60	4.1	9.3%	0.8%	0.6%

Table 9 – Uncertainties of the inventory due to the propagation of nuclear data uncertainties

All results are for UO_2 fuel in a PWR. The burnup (BU) and initial enrichment (IE) are specified together with the nuclear data library that is used. The 3rd column specifies whether the covariance of the independent fission product yields was based on boundary conditions (constraints) (see [Fiorito, 2014; Fiorito, 2016; Rochman, 2016]).

Uncertainty component		**Relative uncertainty** (68% confidence limit)
Fuel history	Fuel design	0.20%
	Operation history	0.85%
	Total	0.87%
Nuclear data	Cross-sections	0.88%
	Fission yields	0.26%
	Total	0.92%
Total		***1.27%***

Table 10 – Uncertainty evaluation of the decay heat estimated by theoretical calculations

Reported in [Ilas, 2017]. The uncertainties are for a UO_2 assembly with an initial enrichment of 2.9 wt.-% that was irradiated in a BWR to a burnup of 36.9 GWd/t. The results are for a cooling time of 15.6 years.

Fuel history

The impact of fuel history data on the inventory of a PWR spent fuel assembly is discussed in the state-of-the-art report issued by OECD-NEA [NEA, 2011]. The OECD-NEA started a new initiative to produce a guidance report on "Code validation for decay heat application". This report will include a section discussing the impact of fuel history data on the calculated decay heat [Fiorito].

Kromar and Kurinčič performed a sensitivity analysis for UO_2 spent fuel from the Krško nuclear power plant using SERPENT [Kromar, 2015; Komar, 2017]. They verified the influence of several factors, such as initial enrichment, burnup, fuel temperature, moderator temperature and density, soluble boron concentration, average power density and burnable absorbers on the decay heat and neutron and γ-ray emission. The main conclusions drawn from this analysis are valid for any PWR fuel in the form of low-enriched UO_2.

Change the burnup of 50 GWd/t by 20% changes the thermal power and γ-ray emission rate by ~ 20% and the neutron emission rate by ~ 35% at the end of irradiation. Hence, around a burnup of 50 GWd/t the thermal power and γ-ray emission rate are almost linearly dependent on burnup (i.e. the relative sensitivity ~ 1), whereas the neutron emission rate has a stronger dependence on burnup (i.e. absolute relative sensitivity ~ 2). This is expected since, at the end of irradiation, the dominant contributions to the thermal power and γ-ray emission is due to the decay of fission products whose build-up depends almost linearly on the number of fissions, whereas the neutron emission comes entirely from actinides whose build-up as a function of burnup can typically be approximated as a higher order polynomial dependence.

Changing the initial enrichment of 3.525 wt.-% by 20% changes the thermal power by ~ 5%, the γ-ray emission rate by ~ 3.5% and the neutron emission rate by 25% at the end of irradiation. The relative sensitivities of the decay heat and γ-ray emission to the initial ^{235}U enrichment at short cooling times are small. The sensitivity of the neutron emission rate from spent fuel on initial enrichment is higher ~ - 1.3 due to the build-up of higher actinides.

The effects of other operational parameters on decay heat, neutron and γ-ray emission were smaller. Moderator density (due to thermal expansion) and the presence of boron in the moderator and burnable absorbers are important, while the sensitivity of the observables to the fuel temperature and the specific power is smaller and needs to be considered only in very detailed cases.

In addition to the sensitivity study itself, non-linearity (departure from the first-order sensitivity approximation) was examined. Such analyses are important, since they indicate the errors produced in the averaging process, which is usually applied in practical applications. Results show that simple averaging of the enrichment and burnup domains can induce errors of several%. To avoid this, a sufficiently heterogeneous problem decomposition (several axial and perhaps even radial regions) is required.

2.5. Experimental determination of SNF source terms and observables

As discussed in Section 2.1, the ability to calculate the nuclide inventory of spent nuclear fuel is essential for many licensing aspects of the back-end of the fuel cycle, such as spent nuclear fuel transport, interim storage and final disposal. The nuclide inventory that is required cannot be determined directly from measurements; it can only be derived from theoretical calculations using codes as described in Section 2.2. Independently of the progress made to improve the calculation methodologies and capabilities, a code validation and assessment of the accuracy based on a comparison with experimental data is required. This is essential for having procedures relying on such calculations accepted by licensing and nuclear safeguards authorities.

Due to the importance of having experimental data for code validation, the Expert Group on Burnup Credit Criticality (EGBUC) formed by the NEA/OECD supported the development of the SFCOMPO-2.0 database [Michel-Sendis, 2017]. It includes experimental data for 750 spent nuclear fuel samples resulting from material that was irradiated in a wide variety of reactors. The data are supplemented with reviewed fuel design information, irradiation conditions and characteristics of the host reactors. At present, the data-base contains only results of Destructive Analyses (DA), which are mostly part of complex Post Irradiation Examination (PIE) studies [Degueldre, 2016]. However, the possibility to

include results of Non-Destructive Assay (NDA) methods is considered, in particular, results of direct decay heat measurements by calorimetry, such as those produced in [SKB, 2006; Maeda, 2004; Jaboulay, 2012].

Promising NDA data result from the SKB-50 campaign organised at the interim storage facility CLAB in Sweden [Tobin, 2016]. In this campaign, characterisation of 50 PWR and BWR fuel assemblies using a calorimeter [SKB, 2006], a γ-ray spectroscopic scanning device [Vaccaro, 2016] and two advanced neutron based systems, a Differential Die Away (DDA) [Martini, 2016] and Differential Die Away Self-Interrogation (DDSI) system [Trahan, 2020], have been performed. An integrated NDA system [Tobin, 2018b] that combines the capabilities of a Passive Gamma-ray Emission Tomography (PGET) [White, 2018], a Passive Neutron Albedo Reactivity (PNAR) instrument [Tobin, 2018] and a load cell has been developed in Finland. This system will be used to verify BWR and VVER-440 assemblies in Finland. Results of the calorimetric measurements provide useful data for code validation. NDA methods based on the detection of gamma-rays and neutrons emitted by spent fuel assemblies can be used to verify fuel design parameters or irradiation history conditions to improve the nuclide inventory calculation prior to the encapsulation of the assemblies. A verification of the burnup of a SNF assembly by NDA is required for criticality safety analysis to avoid criticality safety problems due to misloading of assemblies [Bevard, 2009]. Another field of research is the development of NDA detection systems to verify the presence of fuel assemblies in transport or storage casks.

2.5.1. Analysis of fuel rods and segments

Most of the code validation studies reported in the literature are based on nuclide inventories of segments of a spent fuel rod determined by destructive chemical and radiochemical analysis methods (for example in Refs. [Gauld, 2016; Zwicky, 2010; Gauld, 2011; Hu, 2017]). It involves a series of steps including the selection of representative samples, dissolution of the sampled material and chemical separation of elements, followed by a combination of different analysis techniques to determine the elemental and isotopic compositions.

The selection of a representative sample is performed on the basis of a full-rod γ-ray scanning of the axial total activity or activity of specific nuclides, e.g. ^{134}Cs, ^{154}Eu and ^{137}Cs. Ideally, a large enough sample or segment from the fuel rod is taken that includes both pellets and pellet gaps. For UO_2 and MOX fuels, digestion of the sampled material is performed in concentrated, boiling HNO_3 under reflux. Where iodine is to be measured, a dedicated iodine trap is installed to condense the iodine in the off-gas. Often, a residue consisting mostly of hard-to-dissolve metallic fission products (Mo, Ru, Rh, Pd, Tc, Ag) is filtered off and digested in a second step with higher molarity HNO_3 to which a catalytic amount of HF is added. If full dissolution of the metallic precipitates is desired, a third, alkaline melt based, step is sometimes applied to the residue remaining after the second step. The concentrations of specific nuclides are measured by various analytical techniques. The most common techniques are:

- radiation detection techniques: applying α- and γ-ray spectroscopy and liquid scintillation counting
- mass spectroscopy: using a thermal ionisation mass spectrometer (TIMS) or inductively coupled plasma mass spectrometer (ICP-MS) combined with the Isotope Dilution technique (IDMS), addition of a standard solution or an external calibration

The state-of-the-art report prepared by the OECD-NEA [NEA, 2011] discusses these techniques and provides recommendations for measurements of some key nuclides. In [Hu, 2017], a table with experimental techniques, measured nuclides and associated uncertainties is given and the problem of determining the inventory of nuclides with low abundance by ICP-MS is discussed. The uncertainties range from 1% to 5%, with the smallest uncertainty for data derived by IDMS.

Radiochemical-based analysis methods are time-consuming and expensive to study the characteristics of a full rod or to determine axial and radial distributions of fuel characteristics. For such studies, NDA techniques are preferred. The MOSAÏC calorimeter was used in the MERCI experiment to measure the

decay heat of PWR fuel rods with a thermal power between 4 W and 200 W with an uncertainty below 2% (68% confidence limit) [Jaboulay, 2012]. The results were used to validate burnup calculations performed with TRIPOLI-4 [Petit, 2008] combined with the PEPIN2 solver of the DARWIN system [Tsilanizara, 2000].

The axial distribution of fission products and actinides can be obtained by non-destructive high resolution γ-ray spectroscopic scanning as shown in [Matsson, 1997]. Such axial profiles are used to study fission gas release and to determine the axial burnup and power profiles by analysing full energy peaks of γ-rays emitted by ^{85}Kr, ^{137}Cs and ^{140}La [Matsson, 1997]. Other radionuclides that provide useful γ-ray spectroscopic signatures are ^{134}Cs, ^{144}Ce and ^{154}Eu [Berndt, 1988; Caruso, 2007].

Axial and radial spatial information of spent fuel rods can be derived from γ-ray emission tomographic measurements. Details about techniques and methods for imaging can be found in [Parker, 2015]. One of the first two-dimensional γ-ray scanning measurements of spent fuel rods to determine the spatial distribution of radionuclides (fission and activation products) were carried out at LANL by [Barnes, 1970; Barnes, 1982; Philipps, 1979]. Other examples are the ISARD program developed at Grenoble [Ducros, 1985] and the measurement campaign at the VENUS facility of the SCK•CEN [Borms, 1999]. A γ-ray tomographic analysis of fuel cladding to verify its integrity has been performed by [Dobrin, 1997]. Tomographic measurements to determine within-pin distributions of ^{134}Cs, ^{137}Cs, and ^{106}Ru are reported in [Buurveld, 1993]. A γ-ray tomography cell station has been designed and developed at the Paul Scherrer Institute (PSI) for the investigation of individual LWR spent fuel rod segments at a within-rod level of resolution [Caruso, 2014a]. This computerised tomographic system benefits from an advanced high-resolution γ-ray spectrometry methodology [Caruso, 2008]. Transmission tomography, relying on the absorption of an external source (e.g. neutron, γ-ray or X-ray) crossing an object, is able to assess the internal morphology of an object. It is applied for quality control of radioactive waste packages [Tanke, 1991; Camp, 2002]. The use of γ-ray transmission tomography to determine the within-rod spatial distribution of the fuel density and γ-ray attenuation coefficients was demonstrated on a commercial nuclear fuel rod in [Caruso, 2014a; Caruso, 2009] using a ^{60}Co source. These spatial properties were used in combination with results of γ-ray spectroscopic emission tomography to determine the radial and axial distribution of ^{134}Cs, ^{137}Cs and ^{154}Eu in spent fuel rod segments with a burnup between 52 GWd/t and 121 GWd/t [Caruso, 2014a].

The best results for code validation are those from an international programme including an inter-comparison exercise involving different laboratories and techniques to identify potential bias effects and define realistic uncertainties. The different measurements should include all stages of the process starting from the fuel dissolution to the data reduction. Examples of such programmes are: ARIANE [Belgonucléaire, 2000], MALIBU [Boulanger, 2004], REBUS [Baeten, 2003] and REGAL [Govers, 2015]. The aim of the ARIANE (Actinide Research In A Nuclear Element) programme was to improve the knowledge of the inventories of actinides and fission products in UO_2 and MOX fuels irradiated to various burnups in PWRs and BWRs. Spent fuel samples were analysed using different techniques to determine the inventory of 49 different nuclides [Belgonucléaire, 2000]. The MALIBU programme, a successor of the ARIANE programme, was designed to obtain assay data for high burnup UO_2 and MOX fuel from both PWR and BWR [Boulanger, 2004]. The REBUS programme was dedicated to the validation of codes for criticality calculations involving BUC. It included DA measurements to determine the nuclide inventory of the irradiated fuel and a measurement of the reactivity in the VENUS critical facility at SCK•CEN [Baeten, 2003]. The objective of the REGAL (Rod-Extremity and Gadolinia AnaLysis) programme is to investigate rod extremity effects and the study atypical shielding patterns in gadolinia-doped fuel rods [Govers, 2015]. The data of the ARIANE, MALIBU and REBUS programmes were used to validate SCALE and the ENDF/B libraries [Ilas, 2010; Ilas, 2012; Gauld, 2013]. The use of the REBUS data to validate SCALE and MONTEBURNS is reported in [Töre, 2013].

2.5.2. Non-destructive assay of spent fuel assemblies

Most of the NDA systems used for quantitative characterisation of SNF assemblies have been developed to verify the amount of fissile material for nuclear materials safeguards applications [Hue, 1978; Tarvainen, 1997; Lebrun, 2013] and to verify burnup for nuclear criticality safety applications applying a BUC approach [Bevard, 2009; Lebrun, 2001a].

Conventional nuclear safeguards NDA systems

At present NDA systems that are routinely in use are limited to total neutron counting, γ-ray counting and γ-ray spectroscopy. The main detectors are fission and ionisation chambers measuring the total neutron and γ-ray emission rate, respectively, and γ-ray spectrometric detection systems based on HPGe, CdTe and CZT detectors, recording a spectrum of γ-rays emitted by the spent fuel assembly.

The FORK detector type of instrument is one of the main NDA detection systems used by safeguards inspectorates, providing quantitative signatures of the SNF. The first model was designed and constructed at LANL [Phillips, 1983; Rinard, 1988; Bosler, 1991]. The detector consists of two arms that can be positioned around a LWR fuel assembly. Each arm contains three detectors: two fission chambers, one surrounded by a thin sheet of cadmium, and one ionisation chamber. These signals are used through calibration curves to estimate the burnup and cooling time [Rinard, 1988]. The main signature is the total neutron count which is mainly due to spontaneous fission of ^{244}Cm. The sensitivity of the total neutron count rate to the burnup is illustrated in Figure 6, which shows the ^{244}Cm inventory as a function of burnup for a UO_2 sample with an initial enrichment of 4.8 wt.-% irradiated in a PWR to a maximum burnup of 60 GWd/t. The strong sensitivity to the burnup is due to the total number of neutron-induced capture reactions in the production of ^{244}Cm. Evidently, the results strongly depend on the declaration of the operator. The importance of having fuel history data to use the FORK detector for partial defect verification of LWR spent fuel assemblies is demonstrated in [Tiitta, 2002].

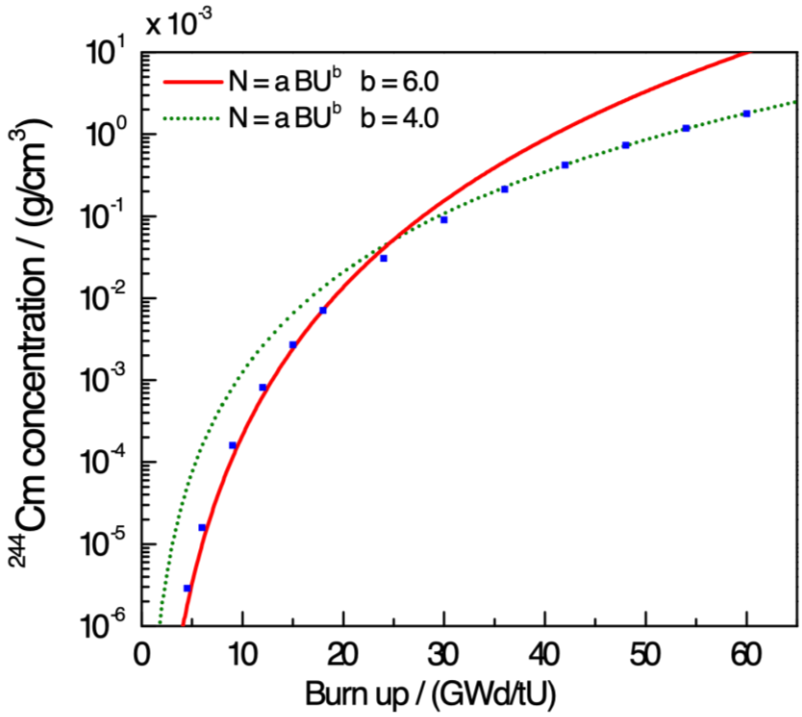

Figure 6 – Concentration of ^{244}Cm as a function of burnup for a UO_2 sample with initial enrichment of 4.8 wt.-% irradiated in a PWR to a burnup of 45 GWd/t

The potential to predict the output of the FORK detector by burnup codes is demonstrated in [Gauld, 2015; Gauld, 2006; Vaccaro, 2018] based on measurements of 15 PWR and 15 BWR assemblies as part of the SKB-50 exercise at CLAB. The experimental response is compared with the one obtained using the Integrated Review and Analysis Program (iRAP). This program, which is developed jointly by EURATOM and IAEA in collaboration with ORNL, is based on the ORIGEN module [Gauld, 2011] of SCALE [Bowman, 2011]. To account for the experimental details such as the absolute detection efficiency a normalisation was applied based on the average ratio between calculated and measured data [Vaccaro, 2018]. For PWR assemblies, the ratios of the observed and calculated neutron emission and γ-ray emission have a standard deviation of 4.6% and 2.4%, respectively. For BWR assemblies, the standard deviations for the neutron and γ-ray emission rates become 5.7% and 5.2%, respectively. The results in [Gauld, 2015; Gauld, 2006; Vaccaro, 2018] show the importance of accounting for neutron multiplication in the assembly and for the non-linear response of the ionisation chamber to the γ-ray intensity. The FORK detector is also suitable to determine the axial profile of the total neutron and γ-ray emission rate with limited special resolution. This provides additional information on burnup profiles.

Variants of the original LANL design are reported by [Lee, 2015; Tiitta, 2001]. The fission chambers in the system of Lee et al. [Lee, 2015] are replaced by ^{10}B proportional counters. The use of ^{10}B counters avoids logistic problems related to transport and use of fission chambers containing fissile material. However, due to their higher sensitivity to γ-rays, they require additional shielding against the γ-rays emitted by the spent fuel assembly. In the system proposed by [Tiitta,2001], a CZT detector is included that offers the possibility to perform γ-ray spectroscopic analysis and separate the contribution due to ^{134}Cs, ^{137}Cs and ^{154}Eu. The Safeguards MOx PYthon (SMOPY) system was developed by the French Support Program to IAEA Safeguards. It includes fission chambers to determine the total neutron emission rate and a CZT detector to perform γ-ray spectroscopic measurements.

The added value of γ-ray spectroscopic data for a more quantitative assessment of the SNF is demonstrated in [Vaccaro, 2016; Willman, 2006a; Willman, 2006b]. At CLAB a γ-ray spectroscopic scanning system using an HPGe detector is installed that measures the γ-ray spectrum from a SNF assembly with an axial resolution of about 15 mm. From these measurements, the total γ-ray emission rate of ^{137}Cs together with the abundance ratios ^{106}Ru/^{137}Cs, ^{134}Cs/^{137}Cs, ^{144}Ce/^{137}Cs and ^{154}Eu/^{137}Cs were derived and combined with model calculations to provide information about the initial enrichment, burnup and cooling time [Vaccaro, 2016].

Tomographic systems

A γ-ray emission tomographic system, referred to as Passive Gamma Emission Tomography (PGET), was developed by the IAEA for partial defect verification of spent fuel assemblies [Tobin, 2018]. The development started in the early nineties as part of the Finnish support programme to the IAEA [Lévay, 1993; Honkamaa, 2014]. It consists of an array of collimated CdTe γ-ray detectors and two neutron detectors, which are rotated in the horisontal plane. Measurements are performed with a spent fuel assembly placed in the centre of the toroidal shaped detector platform. The PGET system was used at spent fuel ponds in Finland and Sweden to verify VVER-440, BWR, and PWR spent fuel assemblies with burnups ranging from 5.7 GWd/t to 57.8 GWd/t and cooling times between 1.9 years and 26.6 years. These tests confirm that missing rods inside an assembly can be identified. The IAEA is studying new reconstruction processing techniques that should result in a more accurate localisation of missing rods and calculation of the relative γ-ray activities of individual rods.

With a tomographic device such as PGET, it is difficult to produce activity levels of specific radionuclides in individual rods due to the limited energy resolution of the γ-ray detectors. Using high-resolution Ge-detectors rod-wise activity distributions of specific radionuclides, i.e. actinides, fission and activation products, can be obtained. Such distributions can be used to study fuel properties, e.g. burnup and power profiles of individual rods [Svärd, 2005], fission gas release [Holcombe, 2016] and fuel behaviour under loss-of-coolant accident conditions [Andersson, 2016], from a measurement of an entire fuel

assembly. This avoids the need for dismantling the fuel to measure each rod separately. An example of such a tomographic system is described by [Holcombe, 2015]. This system was used to characterise an assembly consisting of rods that were irradiated at the Halden Boiling Water Reactor. The assembly contained four rods with a burnup of 26 GWd/t and five rods with a burnup of 50 GWd/t. The system of Holcombe et al. [Holcombe, 2015] is based on a single detector, which limits the spatial resolution due to time constraints. Using a segmented HPGe detector increases the efficiency such that a better spatial resolution can be reached in the same measurement time [Andersson, 2020].

Advanced neutron based detection systems

The Next Generation Safeguards Initiative – Spent Fuel (NGSI−SF) established by the Department Of Energy (DOE) of the United States triggered the development and testing of new NDA techniques to characterise spent nuclear fuel assemblies [Tobin, 2009; Tobin 2011]. A total of 14 detection techniques, covering passive and active measurements including both γ-ray and neutron detection, were identified within NGSI−SF. A review of these systems is given in [Bolind, 2015]. A first assessment of the techniques was based on results of simulations using a spent nuclear fuel library which was established as part of the NGSI−SF [Trellue, 2013]. Three neutron-based detection systems, i.e. Partial DEfect Tester (PDET) [Ham, 2011; Henzl, 2013], Differential Die-Away (DDA) [Martinik, 2016; Henzl, 2013; Martinik, 2015] and Differential Die-away Self-Interrogation (DDSI) [Trahan, 2020; Menlove, 2009; Kapklan, 2014], were constructed and used at the CLAB facility as part of the SKB-50 project [Tobin, 2016]. The performance of a Passive Neutron Albedo Reactivity (PNAR) system was tested at the Fugen power plant in Japan [Eigenbrodt, 2014, Eigenbrodt, 2016] and at the spent fuel interim storage facility at the Olkiluoto power plant in Finland [Tobin, 2019]. At present, the analysis procedures of these systems concentrate on nuclear safeguards applications. The main objective is the detection of partial defects (missing fuel rods) and the determination of the plutonium content.

PDET is a passive NDA device that relies on the detection of neutrons spontaneously emitted by a spent fuel assembly [Ham, 2011; Ham, 2015]. It is designed for the detection of missing fuel rods in an assembly. The present version has been prototyped for a PWR 17×17 spent fuel assemblies [Ham, 2011]. It consists of a set of fission chambers and ionisation chambers to measure the total neutron and γ-ray emission rate. The detectors are placed in a construction that can be inserted in the guide tubes of a PWR assembly that are used for the insertion of the control rods. Results of measurements at the CLAB facility in Sweden show that the instrument can be used to verify average burnup levels and to detect partial defects [Ham, 2015].

The PNAR concept was first proposed by [Lee, 1982] and demonstrated by measurements of fresh fuel by [Menlove, 1997]. It is a passive NDA technique that relies on the emission of neutrons spontaneously emitted by the assembly. The neutrons are measured in two configurations. One configuration is designed to enhance the multiplication of primary neutrons due to mainly spontaneous fission of ^{244}Cm. In the second configuration this multiplication is suppressed. In other words, in one configuration the albedo is maximised while in the other it is minimised. The amount of fissile material present in the assembly is estimated from the ratio of the count rates obtained from measurements with the two configurations [Bolind, 2014]. Two prototype detection systems have been developed to test the PNAR concept. The first prototype was used for measurements of seven irradiated MOX assemblies at the Fugen power plant in Tsuruga, Japan [Eigenbrodt, 2014; Eigenbrodt, 2016]. The second was designed as part of an integrated system that includes a PGET device [Tobin, 2018; Tobin, 2018; Tobin, 2019; Tupasela, 2009; Tobin, 2018c]. This system is optimised for measurements of BWR fuel irradiated in the Olkiluoto power plant. Results of measurements on 23 BWR spent fuel assemblies are reported in [Tobin, 2019].

The DDA technique is an active NDA technique that uses a pulsed external neutron source that interrogates the assembly by neutron-induced fission. The prompt fission neutrons from the fission chain reactions initiated by the source neutrons are detected by a set of neutron detectors surrounding the assembly. DDA is a well-known technique that is used for characterisation of nuclear waste drums

[Caldwell, 1985] and cargos [Jordan, 2008]. It mostly uses a D-T neutron generator producing a 14 MeV pulsed neutron source. The detected neutrons are registered as a function of the difference between the time of detection and of the creation of the neutron pulse. This distribution in time is analysed to determine the rate of fission events induced by thermal neutrons, which is proportional to the fissile content of the assembly. The results of an active measurement are combined with a passive measurement providing an estimate of the total number of neutrons spontaneously emitted by the assembly. The NGSI-SF spent nuclear fuel library was used to simulate the response for PWR assemblies for a broad range of initial enrichments, burnups and cooling times [Henzl, 2013, Martinik, 2015]. The results of these studies confirm that DDA is a suitable instrument for verifying the fissile content of spent fuel assemblies with a limited number of calibration constants depending on the fuel history [Henzl, 2013]. A prototype DDA device was designed for measurements at the CLAB facility taking into account the requirements of the Swedish regulator and constraints given by the industrial environment of the facility [Martinik, 2016]. Experiments with this device have been finalised and the data analysis is in progress.

The DDSI technique is a passive NDA technique that uses the neutrons spontaneously emitted by the assembly as an internal interrogating neutron source [Menlove, 2009]. These neutrons are thermalised in the water of the storage pool and induce fission in the fissile material present in the assembly, which results in the emission of prompt fission neutrons. The neutrons emitted by the assembly are detected by an array of ^{3}He proportional counters surrounding the assembly and the time correlation technique is applied to construct a Rossi-α distribution. The resulting time distribution consists of a sum of two main components which "die away" as a function of time. The two components have different time constants. This feature is used to separate the contribution of spontaneous fission neutrons and neutrons from neutron-induced fission. The former is related to the amount of ^{244}Cm and the latter provide information about the fissile content in the assembly. The NGSI-SF library was used in [Menlove, 2009] to simulate the response of a DDSI system for a variety of PWR assemblies. An analysis of these data reveals that the neutron multiplication, which is related to the fissile content in the assembly, can be derived from the observed Rossi-α distribution [Kapklan, 2014]. A system based on the design of [Kapklan, 2014] was constructed and used for measurements of 50 PWR and BWR spent fuel assemblies at the CLAB facility in Sweden [Trahan, 2020].

The calorimeter installed at the CLAB facility [SKB, 2006] is at present one of the most valuable instruments for determining the thermal power of an entire fuel assembly. It is based on the design of the calorimeter that was constructed and tested by General Electric's Morris Operation [McKinnon, 1986]. Results of decay heat measurements of BWR assemblies with this calorimeter are reported Ref. [McKinnon, 1986]. The procedure applied at CLAB is similar to the one described in [McKinnon, 1986]. It relies on a measurement of the temperature increase as a function of time. The gradient of the temperature increase is translated into the thermal power produced by a fuel assembly through a calibration curve that is obtained from measurements with an electrical heater. Two corrections are required: a correction to account for the difference in heat capacity of the electrical heater and the fuel assembly and a correction to account for heat losses due to γ-rays that escape from the calorimeter. In the SKB R-05-62 report [SKB, 2006] calorimetric measurements of 34 PWR and 50 BWR assemblies are reported. The assemblies cover a burnup range of 14 − 51 GWd/t, cooling times between 12 years and 27 years and initial enrichments between 2.2 wt.-% and 3.4 wt.-% ^{235}U. Details about the fuel design and composition and irradiation history are given in Refs. [SKB, 2006; Murphy, 2009]. Other results of the measurements at CLAB are summarised in [Ilas, 2008; Ilas, 2014; Ilas, 2022]. A blind test was organised by SKB Sweden to assess the quality of decay heat predictions by burnup codes. For these tests five 17×17 PWR assemblies were measured. Details of the measurements are described in [Jansson, 2020].

The experiments at CLAB provide important benchmark data for decay heat calculations. Unfortunately, no detailed uncertainty evaluation has been carried out for the calorimeter at CLAB. A study to improve the analysis procedures together with a performance assessment and uncertainty evaluation has started

as part of the EURAD project. The result of this study should make from the calorimeter at CLAB a reference instrument for decay heat measurements of spent fuel assemblies.

2.5.3. Verification of transport and storage casks

At present only Finland and Sweden have taken a final decision to open a deep underground geological repository for final disposal of spent fuel assemblies. Due to a lack of well-defined strategies by other countries, there is an accumulation of dry storage casks at temporary/interim storage facilities. Current safeguards approaches for dry storage casks rely heavily on containment and surveillance to maintain Continuity of Knowledge (CoK). However, failures of the seals cannot be excluded. The growing number of casks increases the probability of loss of CoK. A reverification of the contents by opening the cask is an extremely costly and time consuming procedure. Therefore, there is a strong interest in NDA techniques to verify casks. It is one of the top priority R&D needs of the [IAEA, 2018]. The minimum requirement is the possibility to detect the removal or missing of one Significant Quantity, which is approximately equivalent with one PWR and four BWR spent fuel assemblies.

Application of conventional NDA techniques based on the detection of radiation emitted by the spent fuel is not trivial, if not impossible, since the casks are designed to limit radiation exposure outside the cask. Nevertheless studies have been made to use the neutrons and γ-rays emitted by the fuel as fingerprints [Ziock, 2005; Peerani, 2007; Santi, 2010; Harkness, 2018; Ham, 2019]. Other complications are the neutron and γ-ray emission rates which change with cooling time and the background from neighboring casks. To account for the change in neutron emission characteristics, i.e. change in contributions of spontaneous fission and (α,n) neutrons, the use of a spectroscopic system is proposed [Harkness, 2018]. A fast neutron counting detection system with limited spatial resolution is proposed in [Ham, 2019]. All these methods suffer from the low intensity of the radiation escaping from the casks. [Peerani, 2007] concluded from simulation studies that it is not evident to detect the removal of a PWR assembly from a CASTOR V21/A based on neutron intensities outside the cask. Conventional neutron detection spectroscopy systems such as Bonner spheres remain useful instrumentations to monitor the neutron exposure of the personnel during transportation and storage of the casks [Rimpler, 2002].

The use of cosmic muons as an external source to verify the contents of spent fuel casks is very promising [Chatzidakis, 2016; Checchia, 2017; Kaiser, 218; Poulson, 2018; Durham, 2018; Checchia, 2018; Ancius, 2019]. Cosmic muons can penetrate meters of dense material and therefore can be used to image the contents of spent fuel held in heavily-shielded containers. In addition, they are an external probe which do not suffer from background from other casks and do not require any prior knowledge. The use of muons to verify the contents of a cask is discussed in [Chatzidakis, 2016; Checchia, 2017; Poulson, 2018]. Most of these studies are based on results of Monte Carlo simulations. Experimental verification of the potential of imaging with muons are reported in Refs. [Durham, 2018; Checchia, 2018]. Further work to quantify the sensitivity of the technique to complicated diversion scenarios is still required.

2.6. Code validation

2.6.1. ALEPH2

ALEPH2 [Stankovskiy, 2012] has been validated using various sets of experimental data. The REBUS programme [Baeten, 2003] provides nuclide concentrations from a radiochemical analysis of samples from UO_2 spent fuel that was irradiated for four full cycles in a PWR nuclear power plant at Neckarwestheim in Germany. The data were compared with predictions based on calculations with the previous version of ALEPH2 and the ORIGEN 2.2 and WIMS codes. The best results were obtained with ALEPH2. Nevertheless, an overall overestimation of fission product abundances was observed. This overestimation is most probably due to the limitations of the fission product yield data [Stankovskiy, 2010].

The nuclide inventories of two samples from a spent fuel rod which was irradiated in the Gösgen nuclear power plant in Switzerland were predicted using ALEPH2, MONTEBURNS and SCALE in [Massinon, 2018]. The results were compared with results of a destructive analysis carried out at the JRC-Karlsruhe and SCK CEN. Calculations with ALEPH2 were repeated using different nuclear data libraries, i.e. ENDF/B-VII.1, JEFF-3.2 and JEFF-3.3T. The libraries used with MONTEBURNS and SCALE were JEFF-3.1 and ENDF/B-VII.1, respectively. The overall best agreement between calculated and measured inventory was obtained for the calculations with ALEPH2 using the JEFF-3.2 and ENDF/BVII.1 libraries.

The potential of ALEPH2 for prediction spent fuel decay heat was demonstrated in [Gérard, 2018] by the results of decay heat measurements of 25 PWR and 34 BWR spent fuel assemblies at CLAB [SKB, 2006]. ALEPH2 combined with the JEFF-3.2, JEFF-3.3, ENDF/B-VII.1 and ENDF/B-VIII.0 libraries was used to predict the decay heat. A clear distinction between the average ratio of calculated and experimental decay heat for BWR and PWR assemblies was observed. The calculated values obtained for the BWR assemblies are on average higher compared to experimental data, and for the PWR assemblies they are lower. This trend was observed for all nuclear data libraries and was confirmed by independent calculations using the TRITON and SAS2H modules of SCALE. It is not clear if this difference is due to a systematic effect of the experimental data or of the theoretical estimates.

A similar exercise was carried out in [Broustaut, 2012] based on the results of decay heat measurements for fast reactor spent fuel from the JOYO MK-II core experimental program [Maeda, 2004]. An ALEPH2 simplified model was used which was based on open data for the average neutron fluence rate and burnup. The experimental and theoretical estimated decay heat were compared as a function of cooling time for a period of about 800 days. The predicted and experimental value were normalised at the first measurement point (almost zero cooling time). Even after this normalisation the predicted values are on average about 4% lower compared to the measured ones. This systematic difference was observed for the calculations using the JEFF-3.1.2 and ENDF/B-VII.1 libraries [Broustaut, 2012].

2.6.2. CASMO and SIMULATE

The code system consisting of CASMO and SIMULATE [Bahadir, 2009; Rhodes, 2006] is regularly used at PSI to support the Swiss safety authority ENSI for cycle reloading licenses [Rochman, 2019a; Rochman, 2019b]. Over the years, a large database of validated models for the five Swiss reactors has been developed [Ferroukhi, 2008], containing CASMO and SIMULATE models, and experimental data (in-core measurements such as boron concentrations and aerobal data) for various code versions. This represents a tremendous source of validation, spanning over hundreds of reactor cycles and many decades of operations, for both PWR and BWR. Such an automated and validated chain of calculations opens up the possibilities for core calculations with uncertainties due to nuclear data [Rochman, 2018b; Leray, 2017a] and transient calculations with uncertainties [Dokhane, 2018]. Additionally, it is relatively straightforward to extend such a validation chain for spent nuclear fuel calculations with the addition of the SNF code [Borresen, 2014]. With the validated chain CASMO-SIMULATE-SNF, the information

(source term, decay heat…) for all Swiss spent fuel can be calculated at once (with uncertainties and biases due to code versions). With the addition of Monte Carlo calculations for canister criticality [Rochman, 2018a], the complete lifetime of spent fuel can be estimated, with information at the pin-by-pin and segment level. Such general and validated approach represents the state-of-the-art for the calculation of spent fuel source terms.

Additional validations of CASMO are routinely performed based on specific PIE samples from the Swiss nuclear power plants. As a detailed fuel history of the assemblies concerned is known (with surrounding assemblies, and full 3D characteristics), such validations generally go beyond the traditional approach used to calculate PIE data such as from the SF-COMPO database. In the present case, the 13 samples from the LWR-PROTEUS programme, as well as a number of samples from the ARIANE and MALIBU programmes are used for validations, using the core simulator (SIMULATE), avoiding any normalisation to the sample burnup or specific burnup indicator (e.g. ^{148}Nd) [Rochman, 2020b]. A detailed validation exercise based on PIE data of samples from a rod irradiated to an average burnup of 70 GWd/t in a Spanish PWR reactor is reported in [Zwicky, 2010].

Finally, such extensive validations allow for application of the present approach to burnup credit calculations with a high degree of confidence. This is performed for the calculations of loading curves for the waste disposal canisters, together with the Swiss waste management organisation Nagra [Vasiliev, 2019; Herrero, 2017].

2.6.3. DRAGON

DRAGON has been widely employed both by academic institutions and research centres around the world. Due to the fact that DRAGON is able to solve the deterministic multi-group neutron transport equation both in 2D and 3D based in different Eulerian (i.e. collision probability, discrete ordinates) or Lagrangian (i.e. Method of characteristics) methods of solution, some validation test cases have been carried out. For example in [Donnelly, 2000] a code-to-code verification and an experimental validation for a 3D model of a CANDU device is reported. However, most of the validation cases have been carried out at the scale of a 2D lattice representation. Examples are presented in [Hong, 2002; Zain, 2018; Choi, 2018; Yaakoubi, 2019]). Some of them include new core CANDU designs for which DRAGON have already built-in modules for neutron transport studies. Others include PWR type of assemblies as part of a collaborative effort with CEA to test the APOLLO deterministic lattice code. The validation exercise included results obtaind with MCNP calculations [Choi, 2018; Ortensi, 2010] and benchmark data of the International Handbook of Evaluated Criticality Safety Benchmark Experiments [Martin, 2011].

2.6.4. EVOLCODE

The EVOLCODE system has been used extensively at CIEMAT for the simulation of both current and advanced nuclear power plants. Given that in Spain only LWRs have been commissioned, CIEMAT has focused on validating EVOLCODE with published data from such reactors. This effort led to the validation of EVOLCODE [Álvarez-Velarde, 2014] with the Isotope Correlation Experiment (ICE) [Koch, 1981], now available at the SFCOMPO database as Obrigheim-1. This experiment was developed by a working group of the European Safeguards Research and Development Association (ESARDA) to check the feasibility of the isotopic correlation technique. The samples were irradiated to a burnup of about 30 GWd/t. The amount of some actinides and inventory ratios of fission products of irradiated samples were derived by radiochemical analysis at the reprocessing plant WAK at Karlsruhe. The agreement between experiment and theoretical estimate was very good for uranium and plutonium isotopes, with the exception of ^{235}U, ^{236}U and ^{238}Pu. The difference between the calculated and measured inventory was less than 3%, which is smaller than the experimental uncertainties. The calculated fission product ratios were in good agreement with the experimental ones, in particular for the Kr, Xe, Nd and Cs isotopic ratios. A sensitivity/uncertainty method was developed to verify whether the differences between experimental and calculation data were compatible with the uncertainties in the nuclear data. This exercise showed that the uncertainty of the theoretical estimates due to reported

uncertainties in cross-sections is in general smaller than the experimental uncertainty. For some nuclides such as ^{239}Pu and ^{240}Pu, the uncertainty due to the cross-section data is similar to or larger than the differences between experimental and simulated values. For ^{235}U, ^{236}U and ^{238}Pu, the differences between the results obtained with EVOLCODE and the experimental data cannot be explained by the experimental or nuclear data uncertainties.

2.6.5. SCALE

The SCALE code system has been extensively validated in Refs. [Gauld, 2016; Gauld, 2011a; Hu, 2017; Ilas, 2010; Ilas, 2012; Gauld, 2013; Ilas, 2008; Ilas, 2014; Gauld, 2010, Ilas, 2011; Smith, 2013]. Most of the calculation–experiment comparisons for decay heat and nuclide concentrations have been undertaken with samples from commercially irradiated nuclear fuel. In a few cases, single effect tests were used. For example, predicted total energy release rates following the fission of ^{233}U, ^{235}U, ^{238}U, ^{239}Pu, ^{241}Pu, and ^{232}Th during very short cooling times have been compared with results of SCALE in [Gauld, 2010].

Calorimetric measurements of spent fuels at CLAB were used to validate the decay heat predictions of SCALE using the ENDF/B-VII.0 library [Ilas, 2008; Ilas, 2014; 247, Gauld, 2010]. A comparison of the calculated and measured decay heat shows in general a very good agreement. The average ratio between calculated and measured heat (C/E) is 1.002 for PWR and 0.997 for BWR assemblies, with a corresponding standard deviation of 1.2% and 2.4%, respectively [Ilas, 2014]. Considering that the main contribution is due to the decay of ^{90}Sr/^{90}Y and ^{137}Cs/^{137m}Ba, the average ratios will change by almost 2% taking the latest JEFF-3.3 fission yield data. The results in [Ilas, 2014] favour the fission yields used in SCALE which are those adopted in ENDF/B-VIII.0. However, such a conclusion is not straightforward due to possible compensating effects resulting from biases in both the calculations and the experiment. Unfortunately, the uncertainties on nuclide inventories for ^{90}Sr and ^{137}Cs obtained from radiochemistry data are mostly larger than 2% and cannot be used to clarify the situation. This confirms the need of a detailed performance assessment of the calorimeter.

For nuclide inventory validation, more than hundred PWR spent fuel samples were obtained from low-, moderate-, and high-burnup spent fuel assemblies from nine PWRs. Initial enrichments were in the range 2.5 – 4.6 wt.-% ^{235}U and burnup values were between 7 – 70 GWd/t. Many of the experimental programs, such as ARIANE, MALIBU and REBUS, provided measurement data for up to 50 nuclides, including actinide and fission products mostly relevant to burnup credit. These data were used to validate SCALE. The C/E values show a high variance, with fluctuations as high as ± 125% and more around one. In particular, there can be large fluctuations between C/E values for samples with similar burnup, although no obvious dependence of the C/E bias with increasing burnup could be distinguished. Also, often error estimates from the different experimental programs vary widely even though irradiation conditions must have been very similar during irradiation.

Since samples were taken from commercially irradiated fuel, uncertainties from fuel production and irradiation boundary conditions have to be added on top of the microscopic data and model uncertainties. This makes it difficult to pinpoint the root source of the above-mentioned C/E fluctuations in the validation exercise. It underlines the need for high quality validation data if any improvement in the accuracy is desired: either performing single-effects tests or obtaining samples from a fuel assembly with very well-known irradiation history. While the average energy generation of a single fuel assembly during operation inside a reactor can usually be determined with an accuracy better than 5%, there are higher uncertainties for pellet-sized samples due to: control rod movements, local void content, fuel assembly bow, axial power offset, fuel assembly neighbour neutron spectrum.

2.6.6. SERPENT

SERPENT is currently used in some 220 organisations around the world, and even though several users have performed verification and validation studies for their own purposes, only limited systematic V&V has been carried out by the code developers at VTT. Since SERPENT shares the cross-section library format with MCNP, the physics routines are regularly verified by comparison to reference MCNP5 or MCNP6 calculations. This type of calculation is run, for example, when new features are implemented or new cross-section data is produced using NJOY. This type of code-to-code comparison does not guarantee the accuracy of the results, but it does confirm that the interaction physics is handled properly.

Systematic validation has been carried out at VTT for criticality safety by running benchmarks in the International Handbook of Evaluated Criticality Safety Benchmark Experiments, but the cases have been limited to those relevant for Finnish power reactors (VVER, PWR, BWR). Other benchmark calculations include burnup credit, γ-ray shielding and kinetics.

In addition to the validation of the neutron transport part of the calculation, more efforts will be devoted in the future to burnup calculations. This includes both calculations run at VTT, as well as collecting data from the user community.

2.7. Progress and developments made within WP8 of EURAD

This paragraph summarises the progress that was made within WP8 of EURAD to improve and develop experimental methods for the characterisation of spent nuclear fuel and to assess the performance of depletion codes. From the research carried out and corresponding results obtained within WP8, recommendations are given to improve procedures to charactertise spent nuclear fuel, with a focus on spent fuel assemblies under industrial conditions.

2.7.1. Experimental characterisation of spent nuclear fuel

Procedures to characterise spent fuel for the main observables of interest, i.e. the neutron and gamma-ray emission properties, decay heat rate, reactivity and long-term radiotoxicity, strongly rely on theoretical calculations. Such calculations are done with depletion codes, which require two types of input data, i.e. nuclear data and fuel related input data. To validate the procedures high quality experimental data are needed. Within WP8 experimental methods and data to assess the performance of codes including the nuclear data and to verify the fuel related input data were studied, improved and produced [Seidl, 2023]. The principles and performance of NDA systems that can be used for the characterisation of spent fuel samples and assemblies were studied and described in EURAD deliverable D8.4. Experimental data that were produced within WP8 of EURAD to assess the performance of depletion codes are provided in EURAD deliverable D8.5. The deliverable includes references to the fuel related data that are required to perform the depletion calculations.

Experimental data for code validation

At present a performance assessment of depletion codes strongly relies on nuclide inventory data resulting from destructive chemical and radiochemical analysis of spent fuel rod segments, also referred to as Post Irradiation Examination (PIE). The SFCOMPO database contains results of PIE together with the design and fuel operational data that are required to perform depletion calculations [NEA, 2011], [Michel-Sendis, 2017]. Most of the high quality data are for UOX PWR. The restricted availability for BWR and MOX is partly due to commercial property rights. Within WP8 additional data for UO_2 segment samples extracted from BWR and PWR irradiated assemblies were made available together with the decay power or decay heat rate of PWR and BWR spent fuel assemblies derived from measurements at the Clab calorimeter.

The results of radiochemical analyses of 8 samples taken from a GE14 10x10 BWR assembly together with the design properties and irradiation history were provided to the EURAD partners [Muñoz, 2020].

The project was coordinated by ENRESA and the measurements were carried out at the Studsvik Laboratory. The assembly was irradiated in a BWR of the Forsmark (SE) nuclear power plant. The characterisation measurements included a gamma-ray spectroscopic rod scan and Inductively Coupled Plasma Mass Spectroscopy (ICP-MS) measurements, including isotope dilution analysis, to determine the inventory of 60 nuclides covering 21 elements. The ICP-MS measurements were performed after separation by High Performance Liquid Chromatography (HPLC). A second set of similar BWR samples was used to verify the use of laser ablation coupled with ICP-MS (LA-ICP-MS) for characterisation of spent fuel samples [Muñoz, 2022; Muñoz, 2023]. The use of LA-ICP-MS for the characterisation of spent fuel was already reported in e.g. [Restani 2016]. During the development of a first measurement campaign several technical problems related to the laser ablation device and technique were encountered. Therefore, a new measurement campaign was carried out in 2022 to correct and complete the data of 2020. The nuclide inventory derived by LA-ICP-MS was compared with the inventory obtained from depletion calculations using SCALE/Polaris. Finally, the results of these studies reveal that ICP-MS is a valid technique to determine the nuclide inventory of spent fuel provided that a calibration using a matrix-matched material is performed. However, the use of LA-ICP-MS has some limitations, since it cannot manage isobaric overlap, which should be solved by other techniques coupled to it. Given the problems encountered during the laser ablation measurement campaigns only the results of the data given in Ref. [Muñoz, 2020] are recommended for code validation. These data were used within Task2 of EURAD to verify the performance of CASMO5 [Rochman, 2022].

A high burn-up UOX segment sample irradiated in a PWR (Gösgen, CH) was characterised by radiochemical analysis at KIT for its nuclide inventory in the fuel and the cladding material around the plenum which was in contact with the fuel. Several techniques, including ICP-MS, liquid scintillation counting, alpha- and gamma-spectroscopy, were applied to determine the inventory of actinides and fission products. Particular emphasis was given to the difficult to measure volatile activation and fission products ^{36}Cl and ^{129}I, respectively. Details of the performed radiochemical separations and the determined inventories are reported in the PhD Thesis of [König, 2022].

An innovative non-destructive assay (NDA) method was developed within WP8 to determine in an absolute way the neutron emission rate of a spent fuel segment sample avoiding any reference to a representative spent nuclear fuel sample to calibrate the device. The method, experimental and analysis procedures are described in Refs. [Schillebeeckx, 2020; Schillebeeckx, 2023]. The method relies on a transfer procedure that is adapted to the hot cell facilities installed at the Laboratory for High and Medium level Activity (LHMA) of the SCK CEN (BE). A neutron correlation counter was used to separate the contribution of spontaneous fission and (α,n) neutrons. Measurements were performed using a segment sample of a rod that was part of an assembly which was irradiated in the Tihange 1 PWR as part of the REGAL project (Rod-extremity and gadolinia analysis) [Eysermans, 2022]. The neutron production rate of this REGAL sample due to spontaneous fission derived from the direct neutron measurements is S_{sf} = 680 (15) $s^{-1}g^{-1}$. This value is within uncertainties in agreement with the one derived from the nuclide inventory of the adjacent sample, which is S_{sf} = 699 (28) $s^{-1}g^{-1}$. The uncertainty of the value derived from the nuclide inventory is only due to propagating the uncertainty of the experimental determination of the nuclide inventory by radiochemical analysis in [Eysermans, 2022a]. Hence, the emission rate of spontaneous fission neutrons resulting from the direct neutron measurements is determined with an uncertainty that is a factor 2 smaller than the one derived by radiochemical analysis. Hence, this NDA method is a valuable radiometric method to complement radiochemical analysis techniques for depletion code validation. It does not require chemical treatments such as defueling and dissolution of the spent fuel sample and further dilution and/or chemical separation processes. Evidently, this reduces the impact and interference of systematic effects due sample preparation. The results of the neutron emission rate measurements with the REGAL sample together with the databook of the sample [Eysermans 2022b] were used to assess the performance of ALEPH2, the TRITON/KENO-V.a module of SCALE and Serpent 2 [Schillebeeckx, 2023]. After the succesful completion of the first campain an optimised detection system was designed and constructed. It will be used for new measurements of the same sample at LHMA to reduce the uncertainty of the neutron emission rate of the REGAL sample. It is expected that with the new system samples with a low neutron emission rate and relatively high γ-ray

emission rate, such as the segments from the bottom and top part of a fuel rod, and samples taken from irradiated MOX fuel can be measured.

At the interim storage facility Clab (SE) a calorimeter is installed to measure the decay heat rate or decay power of spent nuclear fuel assemblies. This calorimeter is extensively used to validate the potential of depletion codes to predict the decay power of irradiated assemblies [SKB, 2006], [NUREG/CR-6971, 2009]. To improve the use of the data produced by the Clab calorimeter, a detailed study of the measurement principle of the calorimeter was performed within WP8. Optimised analysis procedures including an evaluation of the measurement uncertainty were defined. The procedure was applied to measurement data that were previously analysed based on a procedure defined by [Jansson, 2022]. It is shown that results obtained with the procedure used by Jansson et al. suffers from a systematic error. The experimental decay heat is overestimated by about 2%. This overestimation was confirmed by an independent analysis as part of an EPRI project. The procedure developed within WP8 was applied to determine the decay power of a set of PWR and BWR assemblies which were used as part of blind benchmark that was conducted within WP8. In the blind-benchmark 12 institutions/ organisations participated using different codes combined with different nuclear data libraries. Based on the findings within WP8 and the extensive use of the calorimetric data of the Clab calorimeter for code validation, it is recommended that the results of the measurements reported in the R-05-62 report [SKB, 2006] are reviewed applying the procedures obtained within the EURAD project. Evidently, the results of this study will strengthen the intention to include calorimetric data produced at Clab into the SFCOMPO database.

Experimental data to verify spent fuel assembly properties

Results of depletion calculations depend on the quality of the fuel dependent input data, i.e. design properties and operational history. For spent fuel assemblies from the nuclear power plants in Switzerland this information can be retrieved from the Core Management System (CMSYS) developed at the Paul Scherrer Institut (PSI) [Ferroukhi, 2008; Leray, 2017]. It includes full cycle information up to the latest operated cycle and validated models that are used for full reactor core simulations with SIMULATE or lattice calculations with CASMO5 which can be coupled with the SNF code to calculate the nuclide inventory. Unfortunately, such a database system with an extensive information about the fuel design and history to produce the fuel related input file for the depletion calculation is not always available. To reduce the impact of limited information and identify possible errors in the input data, an experimental verification of the spent fuel properties by NDA can be done.

Passive NDA methods based on the detection of gamma-rays and neutrons emitted by spent nuclear fuel assemblies were reviewed within WP8. The emphasis was on methods and systems that can be applied in routine operation at an industrial facility. This limits the method to techniques relying on the detection of gamma-rays and neutrons emitted by the assembly. Details about these studies are reported in EURAD deliverable 8.4.

Gamma-ray spectroscopy is a powerful tool to verify characteristics of spent fuel as demonstrated for spent fuel elements of research reactors [Ansari, 2007; Vela Mora, 2011; Koleška, 2016] and assemblies of power reactors [Min, 1988; Willma,n 2006a; Willman, 2006b; Jansson, 2016; Vaccaro, 2016; Kirchknopf, 2022]. It is well known that independent information such as initial enrichment, burnup and cooling time can be derived by combining absolute and relative activity ratios of some key radionuclides such as ^{134}Cs, ^{137}Cs and ^{154}Eu [Berndt, 1988; Min, 1998; Willmann, 2006a; Willman, 2006b; Jansson, 2016; Vaccaro, 2016; Kirchknopf, 2022]. This is due to differences in production process and half-life of these radionuclides [Berndt, 1988; Willman, 2006a; Willman 2006b;]. Evidently, the information that can be retrieved depends on the cooling time.

At Clab a gamma-ray spectroscopic scanning using a HPGe detector is installed [Willman, 2006; Vaccaro, 2016; Bengtsson, 2022; Volans, 2023]. This system is used to determine the inventory or acitivity of gamma-ray emitting radionuclides and to derive the axial profile of their inventory with a spatial resolution of about 15 mm. Results of measurements with this system have been used within

WP8 to apply an intrinsic self-calibration method to determine the overall detection efficiency, including gamma-ray attenuation within the assembly, and derive the $^{134}Cs/^{137}Cs$ and $^{154}Eu/^{137}Cs$ inventory ratio [Solans, 2023]. An analysis from measurements on PWR and BWR assemblies show that the ^{137}Cs inventory can be derived with an uncertainty of about 2.5%, provided that the system is calibrated with a reference assembly [Bengtsson, 2022]. Combining the experimental data with model calculations results of such measurement can be used to provide information about the initial enrichment, burnup and cooling time [Vaccaro, 2018].

The detection of neutrons emitted by spent nuclear fuel is one of the most common NDA methods used for the implementation of nuclear safety analysis relying on a burnup credit approach and for nuclear safeguards inspection of spent fuel assemblies. Due to the dominating contribution of neutrons produced by $^{244}Cm(sf)$ results obtained from a passive neutron detection system are extremely sensitive to the burnup. The main instrument is the FORK detector for which a first prototype was designed and developed in the 80-ties at Los Alamos National Laboratory (LANL). The instrument combines two configurations for neutron detection and an ionisation chamber for total gamma-ray counting. In the past the interpretation of the data relied on assembly specific calibration curves. Using data from measurements at the Clab facilty it was demonstrated in [Vaccaro, 2018] that by combining measurement data with depletion calculations the analysis of data derived from FORK measurements can be improved. The data obtained with the FORK detector installed at the nuclear power plant of Doel were used within WP8 to test such a combination. It is shown that by complementing the experimental data with depletion calculations for PWR assemblies the burnup can be derived with an uncertainty of less than 2% independent of cooling time and initial enrichment. The procedure requires only one normalisation factor. In addition, it was shown that combining the results of the neutron and gamma-ray measurements additional information about the assembly type can be derived.

The performance of the PNAR [Tobin, 2018] and DDSI [Kapklan, 2020] systems which were developed at LANL as part of the NGSI programme was investigated. Most of the data for these systems that are presented in the literature are based on results of Monte Carlos simulations. Results of experiments with a PNAR device at the Olkiluoto power plant and with a DDSI device at the Clab facility show that at present they do not provide additional quantitative information about the characteristics of the assembly compared to the measurements of the total neutron output that can be obtained with a conventional FORK detector. A study of the response of the DDSI system within WP8 based on results of simulations reveals that with an improved interpretation of the experimental data additional information about the fuel characteristics can be derived [Solans, 2022]. Unfortunately, the quality of the data derived from the measurements with a DDSI prototype instrument at Clab is not good enough to validate the improved analysis procedure.

2.7.2. Validation of theoretical calculations

The above described PIE data of BWR samples, neutron emission rate of the REGAL sample and calorimetric data obtained at Clab, together with PIE data from the SFCOMPO data base (GU1, GU3, BM1, BM3) were used within WP8 to study the performance of different depletion codes, i.e. ALEPH2, CASMO5, DARWIN, Evolcode, SCALE, SNF and Serpent 2, in combination with different nuclear data libraries. An overview of the studies and related references of publication is given in *Table 11* –. The results of the performance evaluation are summarised in EURAD deliverable D8.6. Based on this evaluation recommendations are formulated in EURAD deliverable D8.7 to further improve state-of-the-art characterisation of spent nuclear fuel.

ID	Reactor	Fuel	BU [MWd/kg]	Composition	Code	Ref.
Samples						
GU1	PWR	UO2	59	3.5 wt% 235U/U	CASMO5	[Rochman, 2021]
GU3	PWR	UO2	52	4.1 wt% 235U/U	CASMO5 ALEPH, Serpent	[Rochman, 2021] [Grimaldi, 2022]
SF95-4	PWR	UO2	36	4.1 wt% 235U/U	Serpent	[Grimaldi, 2022]
SF95-5	PWR	UO2	30	4.1 wt% 235U/U	Evolcode	[Álvarez-Velarde] [Panizo, 2023]
REGAL	PWR	UO2	55	4.5 wt% 235U/U	ALEPH Serpent SCALE/NEWT	[Schillebeeckx, 2023]
BM1, BM3	PWR	MOX	47	2.36 wt% Pu/(U+Pu+Am) 24 wt% 239Pu/Pu 9 wt% 241Pu/Pu	CASMO5	[Rochman, 2021]
ENRESA	BWR	UO2	38 – 51	3.95 wt% 235U/U	CASMO5 SCALE/Polaris	[Rochman, 2022]
Gund-remmingen	BWR	UO2	27	2.5 wt% 235U/U	Serpent	[Häkkingen, 2021]
Assemblies						
Clab-2006	PWR BWR	UO2 UO2	20 – 51 15 – 47	2.1 – 3.4 wt% 235U/U 2.1 – 3.2 wt% 235U/U	SCALE/Polaris SCALE/Origen CASMO5 SNF	[Shama, 2022] [Rochman, 2023]

Table 11 – Overview of studies to validate depletion codes performed within WP8 of EURAD and published in open literature

These studies, together with other work performed in WP8 and published in [Fiorito, 2021; Shama, 2021; Romojaro, 2022; Čalič, 2022; Grimaldi, 2023], reveal that results of depletion calculations strongly depend on the burnup and the moderator density and nuclear data. The dependence on the moderator density makes the modelling of the irradiation conditions in a BWR more complex than those in a PWR. This is due to heterogeneous irradiation conditions, in particular the void fraction and moderator temperature. The main operational parameter of interest for both PWR and BWR is the total number of neutrons seen by the spent fuel object under study which is needed to normalise the calculations. In case of the interpretation of PIE data the normalisation is mostly based on the inventory of one or more burnup indicators, with the main burnup indicator ^{148}Nd. Normalisaton of depletion calculations by the inventory of a burnup indicator is almost impossible in case an assembly has to be characterised. Mostly, the normalisation is based on the average burnup given by the operator, which is derived from calculations with a 3D core simulator. To avoid systematic errors, the assumptions made in the core simulator and the depletion code used to characterise the assembly should be consistent. This implies that the same nuclear data are used to reduce systematic errors. Unfortunately, the nuclear data used by core simulators is often not open-source and not accessible. Given the crucial role of the recoverable energies for depletion calculations, recommended values based on a traceable documented evaluation procedure are required.

Most of the depletion codes rely on a 2D lattice representation of the reactor core with calculations in one zone using an average burnup to normalise the data. Evidently, as long as the observable of interest is determined by nuclides for which the production rate is linear with burnup this will not create an error in the calculations. This was verified for the decay heat produced by PWR and BWR assemblies with a relatively modest maximum burnup of 51 MWd/kg [Ilas, 2008]. The maximum error made on the decay heat rate is in the order of 1% for PWR and 2.5% for BWR. Similar studies, however, limited to PWR assemblies are reported in [Kromar; 2022; Hannstein, 2023]. As mentioned, this error is due to a

deviation from a linear relation between decay heat rate and burnup, which is caused by a non-linear dependence of some radionuclides with burnup. Therefore, the error made depends on cooling time and burnup. Evidently, due to the impact of e.g. the void fraction on the burnup profile the effect will be larger for BWR than for PWR. It is expected that for increasing burnup the contribution of the actinides such as ^{238}Pu, ^{241}Am and ^{244}Cm to the decay heat increases. If the spent fuel assemblies with higher burnups have to be characterised this effect will need to be investigated in more detail.

Nuclear data, i.e. neutron induced cross sections, fission yields and decay data, are together with the burnup and moderator density the main input data affecting the calculated results. The impact of using different nuclear data libraries including the recommended covariance data has been verified for various cases. These studies show that there are significant differences between the observables of interest together with their uncertainties when using different nuclear data libraries [Häkkinen, 2021; Shama, 2021; Čalič, 2022; Grimaldi, 2023]. E.g. it is shown that the uncertainty of the decay power due to the uncertainty of fission yields differs by a factor 10 using the covariance data in JEFF-3.3 and ENDF/B-VII.1 [Shama, 2021]. From detailed studies of the decay heat and neutron emission rate shortcomings for some specific nuclear data such as the ^{147}Nd(n,γ), ^{242}Pu(n,γ) and ^{243}Am(n,γ) reaction cross sections and cumulative fission yields of some fission products as ^{90}Sr, ^{137}Cs and ^{148}Nd were identified [Schillebeeckx, 2023]. In addition, it was noticed that decay data in the ENDF/B and JEFF libraries are not consistent with those recommended by the Decay Data Evaluation Project (DDEP) and results of other high quality evaluation projects [Schillebeeckx, 2023]. This indicates necessity for a project entirely dedicated to nuclear data for depletion calculations. Ideally, the project should start from a detailed sensitivity analysis to identify the main nuclear data of interest. Such a sensitivity analysis is required to avoid problems due to compensating effects which can be introduced to the complex production process of some nuclides [Fiorito, 2021]. Fortunately, the number of nuclides that are important to predict the main of observables of interest are not many. Therefore, the production of a general purpose library including reliable covariance data for the key nuclides of interest to the characterisation of spent nuclear fuel for all users (plant operators, WMO, TSO and RE) is recommended as part of a collaborative effort supported by the EC.

A final validation of depletion codes including the nuclear data requires accurate experimental data. They are needed to make estimates of possible systematic errors in the calculations, i.e. to determine the bias, and to define reliable confidence limits for safety analysis procedures. A comparison of calculated and experimental PIE data used within WP8 indicates obvious systematic errors in the experimental data. They also suggest that experimental uncertainties differ strongly from laboratory to laboratory and that measurement uncertainties are often underestimated. Therefore, a critical evaluation of experimental data to be used for code validation is recommended. In general, more reference data based on independent measurements and analysis of the same observable is required, e.g. the combination of neutron measurements and radiochemical analysis of the REGAL sample and the independent analysis of Clab data within WP8 and EPRI. Given that at present only one calorimeter for fuel assemblies is in operation, an effort should be made to construct an additional calorimeter. Ideally, the system should be mobile such that it can be used at different facilities.

The blind test exercise using the decay heat data at Clab made clear that errors due to a user effect in the use of a code or interpretation of the data book and even errors in the data book provided by the operator cannot be excluded. Therefore, best-practice recommendations and quality assurance procedures are required. The best approach to avoid such errors and enhance confidence in the results is by diversity, that is, by using different independent calculation tools and by combining the theoretical calculations with an experimental verification. Further research is needed to improve and optimise NDA methods to be used for the characterisation of spent nuclear fuel assemblies under industrial conditions. This will result in a reduction of the uncertainties of the observables of interest and related safety margins.

Besides the above-mentioned recommendations, further attention should be devoted to the diversity of burnup, enrichment, cooling time, fuel type and facilities. Finally, a correct use of terminology and

definitions, such as those defined in the Guide to the Expression of Uncertainty in Measurement published by the BIPM, is recommended to avoid miscommunication.

3. Performance of spent nuclear fuel during pre-disposal activities and experimental characterisation

3.1. Introduction about spent nuclear fuel degradation

The main aim of this chapter is to report current progress regarding spent nuclear fuel (SNF) characterisation and its performance with respect to pre-disposal activities. In particular, the behaviour of irradiated cladding, the phenomena ruling the potential SNF degradation, the fuel/cladding chemical interaction (FCCI), and the ageing effect under conditions of extended interim storage, transport and emplacement in a final disposal system are considered through experimental as well as modelling studies. The chapter gives an overview of SNF experimental characterisation methodologies, from destructive assays to non-destructive assays.

As reported by the IAEA [IAEA, 2019a], the potential degradation mechanisms that may affect the cladding integrity of light water reactor (LWR) fuels during dry storage (and subsequent handling and transport operations) under normal operating conditions are:

1. Air oxidation
2. Thermal creep
3. Stress corrosion cracking (SCC)
4. Delayed hydride cracking (DHC)
5. Hydride reorientation
6. Hydrogen migration and redistribution

Other physico-chemical processes may occur during dry cask storage, such as self-radiation damage and He build-up (due to α decay of the actinides). Both processes are temperature-dependent and lead to a volume expansion of the UO_2 structure, in addition to the strain from pressure due to gas accumulation in the crystal structure [Ewing, 2015].

There is a broad spectrum of monitoring techniques for spent nuclear fuel [IAEA, 2019a], including basic visual inspections, portable gas analysers (for the presence of gaseous fission products), pressure monitoring of the seals and radiometric systems (gamma detector of the 514 keV ^{85}Kr γ-line, whose half-life is 10 years).

3.2.Key phenomena

The understanding of spent fuel performance during dry interim storage is indispensable both for the analysis of the failure probability and to characterise the state of the cladding, so that fuel management is conducted with accurate knowledge of the fuel conditions. The main interest is on cladding degradation mechanisms, as it is the first physical barrier between fission products and the environment. A brief description of the key phenomena governing the fuel rod state during dry storage is given here on the basis of the gap analysis carried out by Hanson [Hanson, 2012].

Key phenomena mainly related to the initial conditions of the dry-stored spent fuel are:

- **Hydrogen migration/precipitation:** Hydrogen picked up during irradiation is distributed heterogeneously throughout the zirconium alloy [Feria, 2018] and can precipitate in the form of hydrides according to solubility limits. For burnups greater than 45 GWd/t_{HM}, the concentration of hydrides is much higher close to the cladding waterside; this brittle zone is called the hydride rim. The hydrogen present in the cladding may also affect creep behaviour (hardening or softening effect, depending on the state of hydrogen in the material [Suman, 2018]).
- **Hydride blister formation:** At some point during in-reactor operation, the zirconium oxide layer formed may spall and, as a consequence, a cold spot will form at the outer surface of the cladding. In this situation, the hydrogen will quickly migrate to this spot to form a zone with an

extremely high hydrogen concentration, known as a blister or lens. This brittle morphology may lead to local failure [Martin-Rengel, 2017].

- **Pellet-cladding bonding:** Higher burnup fuels form tenacious layers between fuel pellets and cladding (bonding) that would condition fuel rod performance during dry storage [Lyon, 2018].

Key phenomena that may occur during dry storage are:

- **Creep:** The main contribution to cladding deformation in dry storage is thermal creep. It is considered self-limiting because hoop stress will decrease when creep occurs (stress relaxation due to creep out) and temperature decreases over time. However, even if it does not result in a cladding failure, the corresponding cladding thinning and the change in the pellet-cladding gap are important aspects for the cladding integrity during subsequent handling or transport. Attention should be paid to the following aspects: very long-term effects from fuel swelling on local Pellet-Cladding Mechanical Interaction (PCMI) that could give rise to athermal creep, and the hardening effect during irradiation that could be annealed in dry storage and that, consequently, might enhance creep [Ito, 2004]. On the other side, hydrogen in solid solution can enhance creep by the so-called Hydrogen Enhanced Localiced Plasticity (HELP). At high hydrogen concentrations which persist even at creep relevant temperature, these can then slow down creep [Mallipudi, 2012]. Extensive studies on the impact of hydrogen on plasticity and creep of unirradiated Zircaloy-4 cladding tubes have shown that the creep rate decreases with increasing hydrogen concentration in cold-work stress-relieved Zircaloy-4 [Bouffioux, 2000]. A significant increase in creep resistance due to hardening induced by the presence of hydrides in Zircaloy-4 was observed [Suman, 2020], as hydrides alter the kinematic hardening by increasing the internal stress.
- **Hydride radial reorientation:** During the drying process in preparation for dry storage, the temperature rises and hydrides dissolve. They repreciptate during the slow cooling. Under high hoop stress, induced by rod internal pressure due to fission products, the hydrides may reprecipitate in the radial direction. If there are sufficient radial hydrides, the cladding will become brittle [Billone, 2013b; Billone, 2019].
- **Delayed Hydride Cracking (DHC):** Under long-term dry storage conditions, the potential PCMI mentioned above may cause sufficient stress in the cladding to foster the diffusion of dissolved hydrogen to an incipient crack tip (flaw), followed by nucleation, growth, and fracture of the hydride at the crack tip. This is known as Delayed Hydride Cracking.
- **Oxidation of UO_2:** If the pellet is exposed to an oxidising environment during dry storage due to fuel management operation issues and an undetected defect in the cladding, UO_2 oxidation can occur. The main concern is that if oxidation develops up to the formation of U_3O_8, the fuel will swell and can result in the propagation of the cladding defect due to PCMI enhancement [Hanson, 1998]. Additionally, fission gas release and fuel grain decohesion might be fostered. A number of major parameters affecting UO_2 oxidation are detailed in Section 3.2.1.
- **α decay:** Another potential driver for the enhancement of cladding stress during long-term dry storage is the PCMI resulting from pellet swelling and gas content build-up due to α decay. Additionally, precipitation of helium bubbles at grain boundaries in the pellet could eventually result in the decohesion of the grains and a reduction of the mechanical strength [Rondinella, 2011].

3.2.1. UO_2 oxidation

Temperature and oxygen partial pressure are the major quantifiable variables that promote the oxidation of the nuclear fuel matrix [Olsen, 2018; Herranz, 2009; McEachern, 1998; IAEA, 2019a] with time [Olsen, 2018; McEachern, 1998; Anderson, 1955a; Anderson, 1955b; Bae, 1994; Leinders, 2016b; Leinders, 2016a; Hoekstra, 1961; Taylor, 1980; Elorrieta, 2018a]. From a safety perspective, the loss of inert conditions due to the replacement of the inert cover gas with air should be considered as a potential

scenario during dry storage [IAEA, 2019a]. Moreover, morphometric properties such as the physical form (powders, fragments or pellets) and the grain size have an effect on the rates of oxidation [Herranz, 2009; McEachern, 1998; Anderson, 1955b; Gómez, 2008; Leinders, 2016c; Bannister, 1968; Martin, 1948; Iglesias, 2008; Wood, 1986]. Water in a dry storage container can be found as either bound water (chemically or physically absorbed) or free water (physically trapped or simply unbound) [Patterson, 2015]. Moisture is regarded as a technical issue of concern by several countries in their gap-assessment procedures [Patterson, 2015], as it can lead to Zircaloy cladding corrosion [IAEA, 2019a; Smith, 2011; Jung, 2013] and UO_2 oxidation [Massih, 2018; Olander, 1999; NSFPOISG, 2006; Espriu-Gascon, 2015].

On the other hand, fuel burnup [McEachern, 1998; IAEA, 2019b; Cobos, 1998; NRC, 2019] and composition have been pointed out to delay fuel matrix oxidation [McEachern, 1998; Massih, 2018; Olander, 1976; Thomas, 1993; Wilson, 1961; Kim, 2001; Hanson, 2003; You, 2000; Elorrieta, 2016; Elorrieta, 2018b; Choi, 1996; Park, 1992; Fujino, 1992; Kim, 1995; Kvashnina, 2013; Kleykamp, 1979; Eloirdi, 2018; Norris, 1983; Suresh, 2004; Talip, 2018; Elorrieta, 2017]. Fission reactions during reactor operation produce oxygen and other elements: some of them (i.e., metallic FPs: Y, Zr, Nb, lanthanides and actinides) can react with oxygen to form oxides [Massih, 2018]. The excess oxygen dissolves in the fuel matrix and oxidises the uranium. At first, the net effect of burnup is to generate more hyper-stoichiometric UO_2 fuel than fresh UO_2 and to increase the oxygen potential of the fuel [Massih, 2018; Olander, 1976]. In general, for doped UO_2, the kinetic stability of the cubic U_4O_{9+y} fluorite type structure is then enhanced with respect to U_3O_8 formation [McEachern, 1998] for longer time periods than the undoped UO_2 material [Thomas, 1993].

Other source of impact on fuel matrix oxidation is the aging process, which consists of the alteration of the fuel due to the effect of long-term ambient-air storage. Early studies on unirradiated UO_2 pellets, as the one performed by Campbell et al., have proved that for storage periods up to two years and temperatures of 250°C, the oxidation kinetics experiment significant changes [Campbell, 1989]. However, an increasing of the aging time delays both, the weight gain and the oxidation rate, hindering the solid sample spallation and pulverisation and, in a later stage, the oxidation reaction. It is assumed that these slower rates could be due to the formation of a thin oxidised layer in the sample surface, identified by XPS, that prevents oxygen diffusion inside the pellet. This layer has also been observed on aged CANDU fuel at 150°C (burnup in the range of 7…10 MWd/kg) [Wasywich, 1993].

The intrinsic difficulties associated with collecting empirical data on long-term aged fuels led Wiss et al. 2014 to use artificially accelerated aged-materials. They analysed a set of alpha-doped UO_2 pellets, simulating alpha doses in real spent fuel. With this purpose, they varied the Pu concentration to simulate samples aged from 5 to 30 years, and then, characterised the materials by XRD, thermal desorption spectroscopy and electron microscopy. From their results, a similar behaviour on delaying oxidation of aged fuel would be expected. However, it is necessary to broaden the data set in order to extend the conclusions to different scenarios. More studies about ageing effect on oxidation behaviour are needed to confirm the aforementioned layer hypothesis.

In summary, irradiated fuel undergoes a series of dynamic physico-chemical changes directly influenced by the irradiation history, including irradiation cycles, power history and burnup. The specific features of SNF (inventory, HBS, distribution of fission gas, heat content and state of the protective cladding) will determine its behaviour in case of an incidental event or during predisposal/disposal activities. A detailed picture of the above-mentioned parameters on oxidation behaviour is not completely drawn.

3.2.2. Pellet-Cladding Interaction

Pellet-Cladding Interaction (PCI) should be considered as a mid-priority process in the investigation of the safety approach for water reactor fuel due to the possibility of cladding failure during a power transient. Cladding integrity (as the first FP containment barrier) must be ensured in all operating conditions.

Pellet-Cladding Interaction and Stress Corrosion Cracking (PCI-SCC) remain one of the causes identified as leading to potential fuel failure. The occurrence of PCI-SSC is reduced by fuel vendors'

restrictions on power variations and by using advanced fuels with increasing resistance to PCI-SCC. An option widely applied, specifically in boiling water reactors, is the use of an inner liner, consisting of a purer Zr alloy, mitigating the SCC between pellet and cladding [NEA, 2018]. Another option is the use of so-called doped fuel, which consist of UO_2 with additives (Cr, Al, Si, Zr), leading to softer pellets. These doped fuels are newly also considered as "accident tolerant", because of their potential better behaviour in contact with cladding that is discussed after the Fukushima event to have lower tendency to oxidise and thus form less hydrogen in an accident case. This accident tolerant cladding may be stiffer, and therefore a softer pellet is advantageous.

Irradiation induces fuel densification, with density increasing from the theoretical density of UO_2 pellets of ~ 95 % (3 … 5 % porosity) to a range of 97 … 98 %. Densification (pellet shrinkage) occurs as a consequence of porosity removal and affects the gap size. According to the literature, the amount of densification depends on burnup, initial density, pore size distribution, grain size, temperature, possible dopants and oxygen-to-metal ratio. Due to the thermal gradient (stress), the pellet transitions to an "hourglass shape" [CEA, 2009], which causes irreversible deformation to the cladding (Figure 7). Pellet-cladding contact takes place because of a decrease in the cladding diameter (creep-down due to pressure from the coolant) and an increase in the pellet diameter (thermal expansion and swelling due to the inclusion of solid FP in the matrix and inter- and intra-granular accumulation of fission gas in pores).

Contact first occurs at the inter-pellet spaces while a continuing rearrangement of pellet fragments takes place simultaneously [CEA, 2009]. Thus, due to pellet swelling, the cladding is subjected to tensile hoop stress, and modifies the diametrical strain via creep (thermally and irradiation induced). The probability of cladding damage is extremely low as the equilibrium hoop stress inside the cladding is lower (< 100 MPa) than the creep rupture strength (> 600 MPa) [CEA, 2009]. In the case of an incident (power increase), the temperature at the pellet centre can increase abruptly, leading to exacerbated hourglassing and/or release of volatile FPs such as iodine (prone to attack the cladding). Cladding damage, resulting from excessive thermal creep or high local deformation, could end in a "pinhole" leak followed by depressurisation of the fuel rod. Water ingress into the rod can occur, leading to a secondary damage, i.e. stress corrosion cracking (SCC), often combined with a high local amount of hydrogen / hydrides, at some distance from the primary leak. This may initiate a radial axial crack, propagating in axial direction. At the end, there will be a mechanical failure of the fuel rod, with a potential risk of release of volatile FPs, such as the fission gases, caesium or iodine.

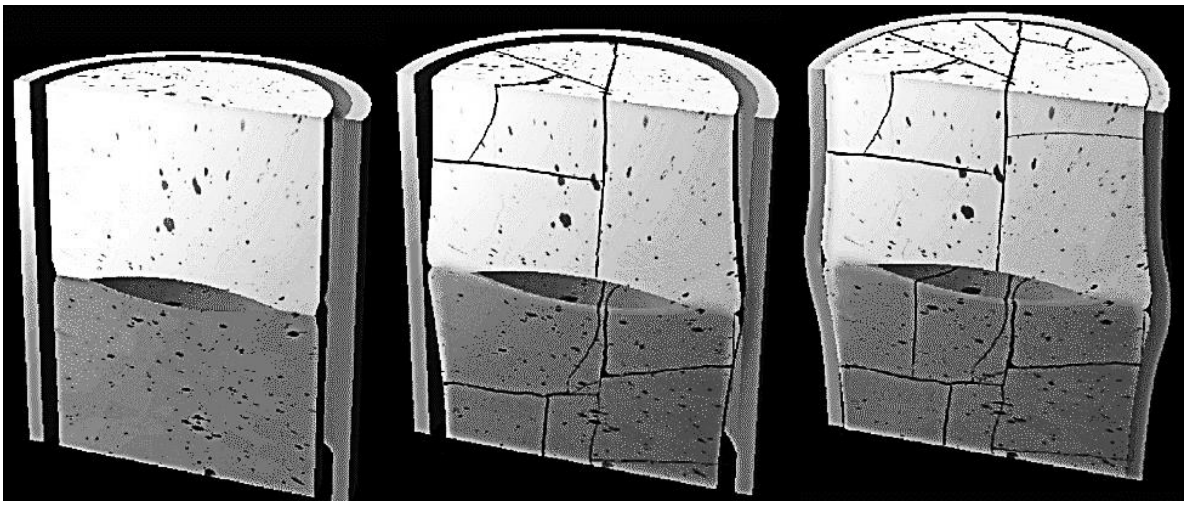

Figure 7 – Schematic representation of pellet cracking, evolution of the "hourglass" shape, and pellet-cladding gap during operation

Figure reproduced from [CEA, 2009].

PCI failure is an in-pile effect during reactor operation. Classical PCI failure does not occur under dry storage conditions. Nonetheless, a combined effect of stress and moisture could possibly lead to a corrosion-induced leaker followed by fission products release. However, with time, the internal pressure in the fuel rod decreases and the potential to disperse fission products decreases as well.

The assessment on the long-term corrosion behaviour of SNF and the impact of storage and disposal of radioactive waste should meet safety criteria. However, the lack of an adequate experimental database for SNF oxidation, especially long-term evaluations, due to problems in the handling of irradiated fuel, have led to study some corrosion scenarios by analysing SNF analogues, i.e., unirradiated materials. A systematic approach to compare surrogates and irradiated fuel behaviour still remains as an uncertainty in some cases. An assessment of the anticipated phenomenon of PCI consequences is essential and requires more studies, especially those that relate to the inner tensile fields, hydride reorientation and creep rupture of the cladding, important to mitigate the effects of the release of volatile FPs or exposition of fuel matrix to an oxidising ambient. In addition, chemically assisted SCC processes on the inner surface of the cladding tubes, induced by e.g. halogens (iodine or chlorine compounds) within the fuel-cladding interaction layer could mitigate the cladding integrity even further [Spykman, 2018].

3.2.3. Helium behaviour in UO_2

Alpha-decay of the actinides produces large quantities of helium in the spent fuel; if it is released into the free volumes in the rod, it would contribute to the rising internal pressure and cladding creep strain. Moreover, helium accumulation in the form of bubbles at the grain boundaries can increase either the pressure in the bubbles, and thus the stresses exerted on the grain boundaries, or the size of the bubbles (by migration of alpha-decay induced vacancies), diminishing the mechanical strength of the grain boundaries. These phenomena could eventually lead to failure at the grain boundaries, releasing the accumulated radionuclides into the free volumes in the rod. Studies of spent nuclear fuel (SNF) evolution in a closed system have concluded that the evolution of the pellet microstructure will strongly depend on He fate in the SNF [Ferry, 2010]. He concentration in SNF depends on Pu concentration in fresh fuel, burnup rate and storage time. Table 12 shows the He concentration in spent UO_2 fuel as a function of storage time for both burnup rates of 52 and 60 GWd/t. The increase during storage is mainly due to the decay of minor actinides. In MOX (8% of Pu) the concentration of these radioisotopes can be 6 times higher for the same burnup rate. Colle et al. found about 0.26 at% He in a 17-year-old irradiated MOX fuel (after discharge from the reactor) with an average burnup of 42.6 GWd/t and a Pu content of 3.5% [Colle, 2014].

Time (years)	UO_2 (52 GWd t^{-1})		UO_2 (60 GWd t^{-1})	
	at cm^{-3} [a]	at.%	at cm^{-3} [a]	at.%
300	4.2×10^{19}	0.06	5.0×10^{19}	0.07
1000	7.0×10^{19}	0.1	8.0×10^{19}	0.11
5000	1.2×10^{20}	0.16	1.3×10^{20}	0.18
10,000	1.5×10^{20}	0.21	1.7×10^{20}	0.24
50,000	2.6×10^{20}	0.37	2.8×10^{20}	0.40

[a] Calculated with a grain density of 10.5 g cm^{-3}.

Table 12 – Mean He concentration in spent UO_2 fuel grains (from Cesars code)

Taken from Table 1 in [Ferry, 2010].

Most studies on the behaviour of He in fuels concern UO_2 in single-crystal, polycrystal or powder form. Luzzi et al. published a critical analysis of data on the diffusivity of He in UO_2 [Luzzi, 2018]. The measured diffusion coefficient depends on the lattice damage: the best estimate is

$D=2.0\cdot10^{-10}\cdot\exp(-2.12/kT)$ $m^2\cdot s^{-1}$ for limited lattice damage and increases to $D=3.3\cdot10^{-10}\cdot\exp(-1.64/kT)$ $m^2\cdot s^{-1}$ with significant damage in the temperature range between about 970…2110K and 1800K respectively. Yakub et al. compared various experimental He solubility data measured on single crystals and powders over a temperature range from 1000...1800K [Yakub, 2010]. Colle et al. determined that the helium solubility in perfect UO_2 was 1.6 at·ppm ($5.8\cdot10^{-9}$ $mol\cdot g^{-1}$) at 1500K [Colle, 2014]. Ab initio simulation [Freyss, 2006] and experiments [Garrido, 2004] suggest that He atoms occupy octahedral position in the UO_2 lattice when dissolved in the matrix. This low solubility and high binding energy of He in vacancy defects can result in a high propensity to form bubbles which are traps for He and can also migrate [Talip, 2014a; Michel, 2020]. In addition, stoichiometry has an important effect on diffusion in uranium oxides. Pure UO_2 oxidises via a two-stage reaction, firstly, from UO_2 to cubic U_4O_9 (for O/U=2.25) or tetragonal U_3O_7 (for O/U=2.33), and secondly to U_3O_8 (for O/U=2.66) [Scheele, 2004]. It has been observed that U_3O_8 can form simultaneously with both U_4O_9 and U_3O_7 phases as oxygen diffuses into the lattice [Olds, 2020]. He release increases for hyperstochiometric U_3O_8 [Talip, 2014b]. In Molecular Dynamics (MD) simulations, Yakub et al. [Yakub, 2010] and Govers et al. [Govers, 2009] showed that He diffusion coefficient increases in $UO_{2\pm x}$, as x increases. The apparent activation energy is calculated at 2.6 eV in UO_2 and is predicted to decrease for hypo-stochiometry and reach 0.3 eV in $UO_{1.91}$ (due to the high V_O concentration) and 1.2 eV in $UO_{2.09}$, where interstitial sites are occupied by additional and displaced oxygen atoms [Yakub, 2010].

Fuel microstructure may also play a role in the He behaviour. Garcia et al. have proposed that grain boundaries can be effective short circuits for He atoms in He implanted UO_2 samples [Garcia, 2012], and that He diffusion towards grain boundaries can be accelerated by the elimination of irradiation-induced defects to these sinks. They introduced the existence of a specific diffusion coefficient in the vicinity of grain boundaries (GB) that becomes weaker (by three orders of magnitude) than that in the grains as the temperature increases above 973 K. This was recently confirmed by Giorgi et al. who implemented a new mechanistic model for the treatment of He behaviour in grain boundaries in the SCIANTIX code [Giorgi, 2022]. Galvin et al. calculated the activation energy for He diffusion, using MD, as a function of several types of GB and it reaches a value close to 0.7 eV for Σ19 grain boundaries at a high temperature of 2300…2600K [Galvin, 2016]. This specific diffusivity at the grain boundaries leads to the increase of He release in small grains. If grain boundaries are considered perfect sinks for the diffusing helium, the average distance helium travels to reach grain boundaries increases with grain size [Talip, 2014a]. Inside the grains, helium mobility depends on He concentration and temperature, from diffusion in the form of interstitials when the concentration of He and vacancy defects (traps) remains low, to trapping in bubbles that slow down He atoms migration. In addition, depending on temperature, pores can trap He if they are closed, or make release easier if they are open.

Information on the behaviour of helium in spent fuel is scarce and can be contradictory. On one hand, Roudil et al. have reported that helium diffusion is negligible within the time and temperature range of long-term dry storage and geological disposal [Roudil, 2004]. On the other hand, Talip et al. observed opening of grain boundaries in a 37 years old $^{238}PuO_2$ sample [Talip, 2014a]. In addition to He production, alpha-decay induces damage in spent fuel [Talip, 2014a], and in particular can create vacancy defects that could impact the behaviour of He due to their properties.

Lanthanide (Ln) doping is currently used to understand the behaviour of spent fuel because, i) Ln are formed in fuel during burnup in reactors, and ii) these elements can be used as surrogates of minor actinides also produced by neutron capture and decay in reactors. The question is whether they will have an effect on the properties of He itself, or indirectly by modifying the properties of defects that might interact with He. These Ln-doped uranium oxides are attracting increasing attention, and several studies have been published on their properties.

The addition of lanthanides (La, and Gd) strongly stabilises oxygen deficiencies in uranium oxides [Yoshida, 2011; Une, 1983]. Osaka et al. determined that oxygen vacancies (V_O) in hypo-stoichiometric Lu-doped uranium oxides $(U\text{-}Lu)O_{2-x}$ were more stable than in other rare-earth-doped UO_2s and that smaller doping cations enabled greater overall V_O stability [Osaka, 2008]. Raman spectroscopy shows that Gd^{III} doping leads to the formation of V_Os and, eventually, MO_8-type complexes, where M is given

for U or Gd [Liu, 2017]. The Gd doping slows down the oxidation of uranium oxide. The O/M ratio of the final oxidation step decreases linearly with increasing Gd content [Kim, 2001]. More generally, lanthanide dopants inhibited oxidation to U_3O_8, particularly for Yb 5 at%, whose oxidation was delayed by a factor of ~180 [Olds, 2020].

In hypo-stoichiometric lanthanide (Ce, Nd, Yb) doped uranium oxides, the average number of coordinations surrounding the (U,Ln) sites – which is compensated by a decrease in U-O bond length – and concomitantly the lattice parameter are reduced [Olds, 2020]. In Raman spectroscopy, the 'defect band', including a component attributed to V_O (~540 cm^{-1}) and the 1LO phonon (~575 cm^{-1}) increases in intensity with increasing dopant concentration and upon oxidation [Olds, 2020]. Talip et al. have confirmed the existence of oxygen vacancies in UO_2 doped with 6, 11, 22 mol% lanthanum (band at ~540 cm^{-1} in the Raman spectra) and an increase in lattice parameter with La content [Talip, 2015a].

With regard to the study of He behaviour in Ln-doped uranium oxides, Talip et al. have shown that the amount of dissolved He increases slightly with increasing oxygen vacancy concentration in hypo-stochiometric La-doped uranium oxide samples [Talip, 2015b]. However, solubility remains very low, suggesting that He bubbles can also be formed in these materials. He release depends on La content, with maximum release in samples with the highest La content between 1300K and 1400K. In the sample with the lowest La content, around 50% of the He is released at higher temperature.

3.2.4. Aging of fuel by alpha-damage

The heat capacity of alpha-damaged uranium and plutonium mixed dioxides $(U_x, Pu_{1-x})O_2$ samples was measured during thermal annealing at the JRC-Karlsruhe. The investigated samples, UO_2 doped with ^{238}Pu, covered equivalent storage time of irradiated LWR fuel (45 GWd/t) of up to 250 years.

The preparation of alpha-doped samples was already described extensively in a publication [De Bona, 2020]. Briefly, a Pu additive containing 53 wt% ^{238}Pu was dissolved in HNO_3 and mixed with a uranyl nitrate solution of known concentration to achieve the desired ratios. The two targeted compositions were 2.5 and 10 wt% Pu-doped UO_2, equivalent to an actual ^{238}Pu content of about 1.25 and 5 wt%, allowing kinetic studies of the radiation damage accumulation. The $(U,Pu)O_2$ powders were then pressed to form pellets in a 5 mm diameter cylindrical die under 738 MPa and sintered at the nominal temperature of 1650 °C under Ar – 4 % H_2 during 6 h.

The total alpha-dose cumulated at the time of the experiments was performed using the decay-engine from the Nucleonica web portal [Magill, 2009] knowing the detailed isotopic composition of the examined samples. An estimation of the upper limit for the concentration of point defects created by self-irradiation can be directly obtained if the recombination processes are neglected. For instance, the α-decay dose accumulated in the 10 wt% Pu-doped UO_2 (UPu9) sample during 6 months is $5.3 \cdot 10^{17}$ g^{-1}, with a corresponding energy deposition rate of about 0.1 $W \cdot cm^{-3}$. Each α-particle (energy of 5.499 MeV) creates about 66 U displacements (assuming a displacement energy threshold of 40 eV [Soullard, 1978]) and 140 O displacements (displacement energy threshold 20 eV [Soullard, 1978]), whilst the ^{234}U recoil atom (energy of 92 keV) creates 295 U and 1180 O displacements as determined using the SRIM code [Ziegler, 2010]. If damage overlapping and recombination are not considered, the total defect concentrations are $2.0 \cdot 10^{20}$ g^{-1} for uranium and $7.3 \cdot 10^{20}$ g^{-1} for oxygen Frenkel pairs. Assuming the atomic density of UO_2 is $6.23 \cdot 10^{21}$ $atoms \cdot g^{-1}$, the displacements per atom (dpa) value is of the order of magnitude of 0.1. In fact, only a small fraction of the defects created is effectively present as point defects at these damage doses and temperature. The majority either recombines or interacts with other defects to form less costly extended configurations, and it is the specific objective of this present work to qualify and quantify their effect on the heat capacity.

The heat capacity of the samples was followed during damage accumulation. The excess of heat released was assessed and the recovery stages associated with various defects were described by integrating results from Transmission Microscopy, helium desorption, thermal diffusivity and XRD annealing studies.

Samples (composition)	Name	Synthesis method / density %theo	Decay x10^{18} αg^{-1}	dpa	Measurement
$(U_{0.975}, {}^{238}Pu_{0.0125}Pu_{0.0125})O_2$	UPu2.5-1	SG / 97.5	0.124	0.031	TEM
	UPu2.5-2		0.300	0.075	SEM, TEM
	UPu2.5-3			0-0.087	LFA
$(U_{0.9}, {}^{238}Pu_{0.05}Pu_{0.05})O_2$	UPu10-1	SG / 97.5	1.090	0.27	DSC
	UPu10-2		0.295	0.073	TEM
	UPu10-3		0.440	0.109	TEM
	UPu10-4		0.735	0.182	TEM
	UPu10-5		1.320	0.328	TEM, TDS
	UPu10-6		1.610	0.40	TEM

Table 13 – Samples and their characterisation as function of damage accumulation

SG: sol-gel; TEM: Transmission Electron Microscopy; SEM: Scanning Electron Microscopy; DSC: Differential Scanning Calorimetry; TDS: Thermal Desorption Spectrometry; LFA: Laser Flash Analysis.

In Figure 8 the apparent C_p* for two samples representing two compositions and two damage level is represented. The exothermic peaks resulting from the excess heat compared to the normal C_p correspond to the annealing of defects [Staicu, 2010]. While there is a larger contribution for the lower damaged sample at around 700 K, the sample at high damage exhibits a peak at 1300 K. The excess of heat in general increases with damage increase but the proportion of the different peak changes. This has to be understood as a change in the nature of the defects and their magnitude/size. Table 13 summarises the main defects assigned to the peaks observed by considering the other investigations performed to determine their nature (and somehow concentration).

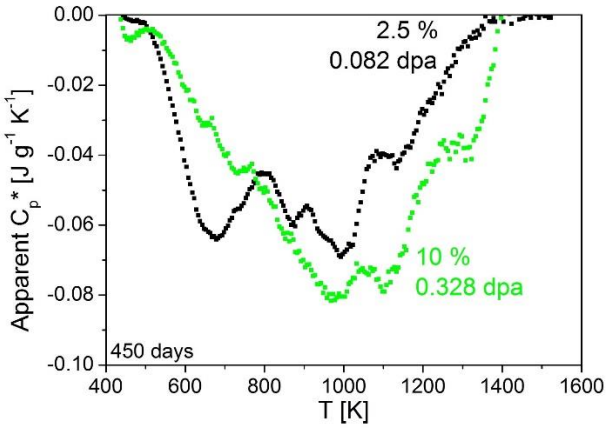

Figure 8 – Apparent C_p obtained by DSC for the two different samples and two different damage level*

The next reported data are contributing to the assessment of the nature of these defects. Figure 9 shows the evolution of the hardness of the two kind of samples as a function of the damage. With a factor of 4 in the concentration of Pu (hence ^{238}Pu) the kinetic also differs and it can be observed that the sole parameter that impacts the evolution of the hardness is the damage (no kinetic effect). All the measured hardness values fit perfectly on the curve.

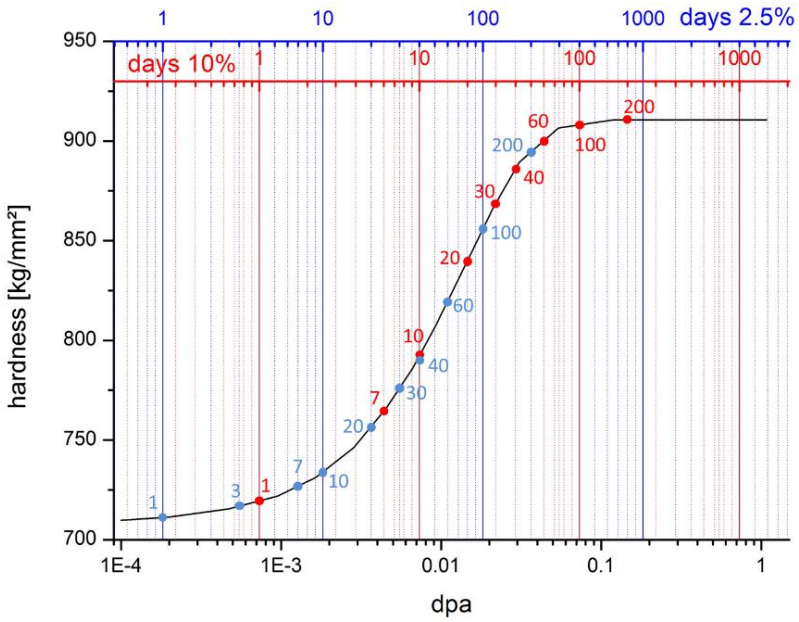

Figure 9 – Evolution of the hardness of the studied sample as a function of time

The upper scale (time) is indicative for the correspondence with damage (dpa). All points being either from 2.5% or 10% Pu-doped UO_2 perfectly sit on the same curve indicating no kinetic dependence (with these compositions).

In Figure 10, the lattice parameter of the two types of samples was monitored during time (damage accumulation) showing exactly the same behaviour as the hardness (i.e., a perfect match on the evolution regardless of the composition or kinetics of damage formation). The saturation of the lattice parameter is reached at around 0.2 dpa, which corresponds to the hardness saturation highlighting the intricate behaviour of this parameter connected to the same type of defects.

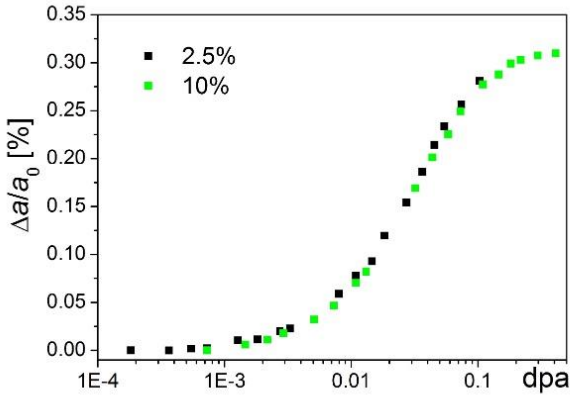

Figure 10 – Evolution of the lattice parameter of the studied sample as a function of dpa

All points being either from 2.5% or 10% Pu-doped UO_2 perfectly sit on the same curve indicating no kinetic dependence (with these compositions).

The helium desorption performed on a sample that has cumulated 0.328 dpa shows an onset for the main release peak at 1300 K (see Figure 11). This corresponds exactly to the (exothermic) peak observed during the apparent C_p measurement and is due to the annealing of a complex defect/helium. It is an important information since other parameters like lattice parameter and hardness tend to saturate around 0.2 dpa, the radiogenic helium continues to accumulate in the sample and might contribute to an increase of stored energy while standalone defects themselves reach a steady state between formation and annealing.

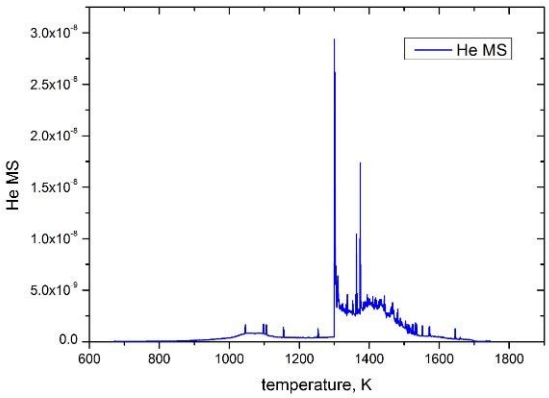

Figure 11 – Helium desorption as a function of the annealing temperature of a sample that has cumulated 0.328 dpa

The thermal diffusivity was measured for the 2.5% sample and a very rapid degradation could be observed (see Figure 12). It is recognised that point defects act as phonon scattering site and this property therefore reflect the early stage of defect formation (i.e., point defect formation). The XRD hardness would also be impacted by extended defect formation (i.e., clusters, dislocation loops). The next study performed was a TEM monitoring of the microstructure evolution as a function of damage formation. It could be clearly proven that after the formation of the very first small dislocation loops already at 0.031 dpa, their size and concentration increased and that at 0.4 dpa helium nano-bubbles could already be observed. This corroborates the previous observation and gives a good picture of the evolution of the damage patterns even with the intrinsic limitation of each technique (e.g., TEM does not resolve point defects).

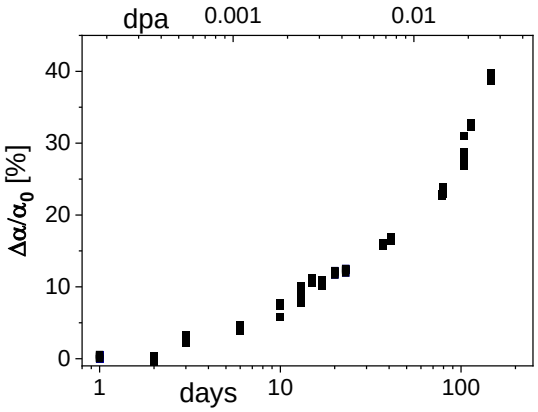

Figure 12 – Thermal diffusivity degradation as a function of time (bottom scale) or damage (top scale)

In Figure 13, a series of 6 bright field images shows the formation of dislocation loops (the dark circular "banana" shaped features). At the highest dpa (i.e., 0.4 dpa), helium nano-bubbles are indicated by a white arrow.

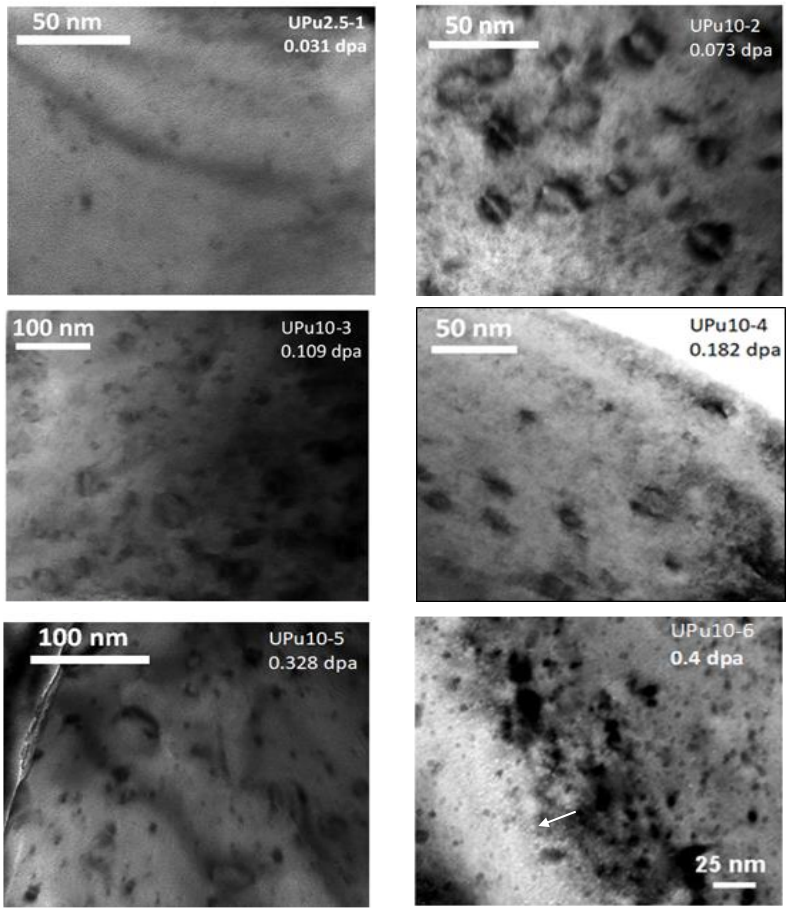

Figure 13 –TEM micrographs of alpha-damaged samples at different dpa as indicated in the images

The days and dpa are not correlated since the samples examined are of different activity (UPu2.5-1 top left and UPu10-2-6 others). Note the different scale bars. The arrow in the lower right image points to a helium bubble (white spots in the image in under-focused conditions).

A simplified description of defects annealing is proposed in Table 14, which also shows some operational temperature to confront the damage evolution and possible recovery stages.

Stage	T, K	Mechanisms	engineering temperatures
I	450 – 700	Oi migration Ui	Wet storage clad. max 473 K Dry storage clad. max 673 K [Raynaud, 2015]
II	700 – 1'000	Uv, Puv migration Ov migration	Fuel operation in LWR [Weber, 1983; Matzke, 1992b]
III	≥ 1'000	Helium desorption from extended defects	Fuel operation in FR

Table 14 – Simplified defects annealing temperature ranges for uranium-plutonium dioxides

Oi: oxygen interstitial; Ui: uranium interstitial; Uv: uranium vacancy; Puv: plutonium vacancy; Ov: oxygen vacancy.

This JRC-Karlsruhe study shows that different defect annealing stages can be identified. It could also be proven that the excess of energy stored in defects tends to saturate after rather low damage levels but that, with increasing radiogenic helium production, another contribution of stored energy appears. This can be attributed to the formation of helium-defect complexes that cannot annihilate until higher temperatures are reached. These results are useful in order to provide information on the evolution of the state of spent fuel under interim and final storage conditions. A practical application of these results is that the stored energy in spent fuels can be expected to increase during the disposal timeframe, potentially leading to changes in properties. Time range of interest for forecasting the fate of spent fuels can vary from decades to millenaries. While no damage recovery is to be expected under wet storage conditions, it can be assumed that the oxygen defects could be recovered under dry storage conditions. This would, however, not impact the formation of extended defects as observed in ion-irradiation performed at 773 K [Haddad, 2018] or at 873 K [He, 2013]. As for the stored energy, it would represent an extra 40 MJ/t of spent fuel. That is to heat 100 litres of liquid water at constant pressure from 0 °C to 100 °C or about 10 kWh of electricity.

3.3. Experimental characterisation

3.3.1. Radiochemical and chemical analysis of irradiated fuel rod components

The radionuclide inventory present in the components of irradiated fuel rods (spent nuclear fuel, cladding, and structural components) is determined by means of radiochemical and chemical analyses after digestion of the respective samples. Both acid digestion and digestion in alkaline media are applied to completely dissolve the samples. Radionuclides present in the digestion liquor (e.g., actinides, lanthanides, and sparingly soluble fission and activation products) or in gaseous samples (e.g., volatile fission and activation products, fission gases, or gaseous radionuclide reaction products such as $^{14}CO_2$) are measured consecutively after various chemical separation methods.

Concentrations of radionuclides present in the aqueous or gaseous phases are measured by various analytical techniques. Currently, new analytical techniques are being developed for radionuclides that are difficult to measure such as ^{14}C, ^{129}I or ^{36}Cl present in highly active samples. α-spectroscopy is applied to quantify $^{235,238}U$, ^{237}Np, $^{238,239,240,242}Pu$, $^{241,243}Am$, and $^{243,244}Cm$ present in aqueous samples. Usually, Pu isotopes are measured after separation from other α-emitting radionuclides. Fission products and minor actinides with characteristic γ-rays, e.g., $^{134,137}Cs$, ^{129}I, $^{241,243}Am$, ^{154}Eu, and ^{125}Sb, are quantified in digestion liquors using γ-spectroscopy. Minor actinides, activation and fission products such as ^{14}C, ^{55}Fe, ^{36}Cl, and ^{241}Pu are measured in the digestion liquor or gas phase after separation from other radionuclides, using liquid scintillation counting. In addition, isotopes such as ^{99}Tc, $^{233,234,235,236,238}U$, ^{237}Np, $^{239,240,241,242}Pu$, $^{241,243}Am$, and $^{244,245,246,248}Cm$ present in digestion liquors can be quantified using high-resolution mass spectrometry (inductively coupled plasma – sector field – mass spectrometry, ICP-SF-MS). Gas phase composition and the concentration of fission gases Kr and Xe released during the digestion of irradiated fuel rod components into the gas phase can be analysed by means of a multipurpose mass spectrometer with a customised gas inlet system.

The experimental uncertainty of the above-mentioned analytical methods is, in most cases, less than 5 %. In accordance with Section 2.5.1, the used experimental techniques are suitable for determining the inventory of the mentioned radionuclides. See also [NEA, 2011] and [Hu, 2017] for state-of-the-art measuring techniques of specific radionuclides and the uncertainties associated with these measurements. It should be emphasised, that this is only the experimental uncertainty related to the measurement of the specific radionuclides and should not be mixed up with theoretical uncertainties based on models. Later, the experimental and theoretical data will be compared to each other with its own uncertainty.

3.3.2. Fuel-cladding chemical interaction analysis

During irradiation in a nuclear reactor, the cladding is affected both by interactions with the cooling water, causing oxidation of the outer cladding surface and hydride precipitation within the Zr alloy, and by corrosion from volatile fission and activation products (e.g., caesium, chlorine, iodine compounds) at the fuel/cladding interface. These chemical reactions lead to embrittlement and weakening of the mechanical properties of the cladding.

Current experimental studies focus on the chemical interactions between Zircaloy and precipitates of volatile fission products at the plenum of an irradiated fuel rod, a location where pellet-cladding interactions cannot occur to separate effects. Samples of fuel/cladding interfaces and samples from rod plenum sections were taken from fuel rod segments irradiated in pressurised water reactors. The composition of agglomerates found on the inner surface of the plenum cladding and in fuel-cladding interaction layers were analysed by means of scanning electron microscopy and spectroscopic methods, such as X-ray photoelectron spectroscopy and synchrotron radiation-based techniques.

Preliminary investigations of the plenum cladding inner surfaces show precipitates containing Rb in addition to Zr, Ba, Cs, and U. Analyses of fuel-cladding interaction layers of a high burn-up UO_X and MOX fuel show the presence of Cs-U-O-Zr-Cl-bearing compounds in these layers, in addition to Te, Ba and U. By using various spectroscopic techniques, such as X-ray photoelectron spectroscopy (XPS) and X-ray absorption spectroscopy (XAS), it could be confirmed that the volatile activation and fission products chlorine and iodine are present as negatively charged species (i.e., chloride and iodide) [König, 2022]. Figure 14 depicts narrow scans of the binding energy range of Cl $2p_{1/2}$ and Cl $2p_{3/2}$ elemental lines for fuel residue analysed on defueled cladding samples of UO_X and MOX fuels. The narrow scans of the Cl 2p elemental lines for both specimens show Cl $2p_{3/2}$ at a binding energy of 198.1 eV, confirming chloride speciation.

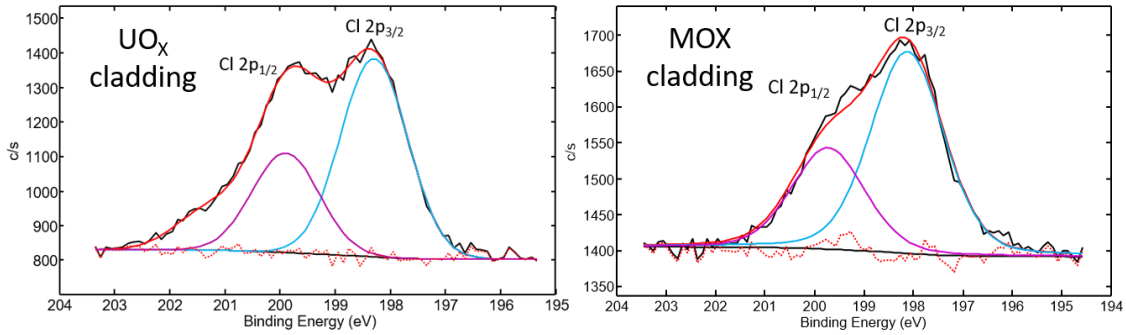

Figure 14 – Narrow scans of the binding energy range of Cl $2p_{1/2}$ and Cl $2p_{3/2}$ elemental lines for the fuel-cladding interaction layers present on UOX and MOX fuel cladding

Both XPS spectra were measured by Al Kα monochromator excitation (1486.7 eV).

For analysis of iodine compounds present in the fuel-cladding interaction layer, as well as within the fuel itself, XAS measurements were performed at the Karlsruhe research accelerator synchrotron facility for UO_X and MOX fuel specimens. As shown in Figure 15, iodine is existing in its negatively charged iodide speciation in both, the fuel as well as the fuel-cladding interaction layer, presumably as caesium iodide [König, 2021].

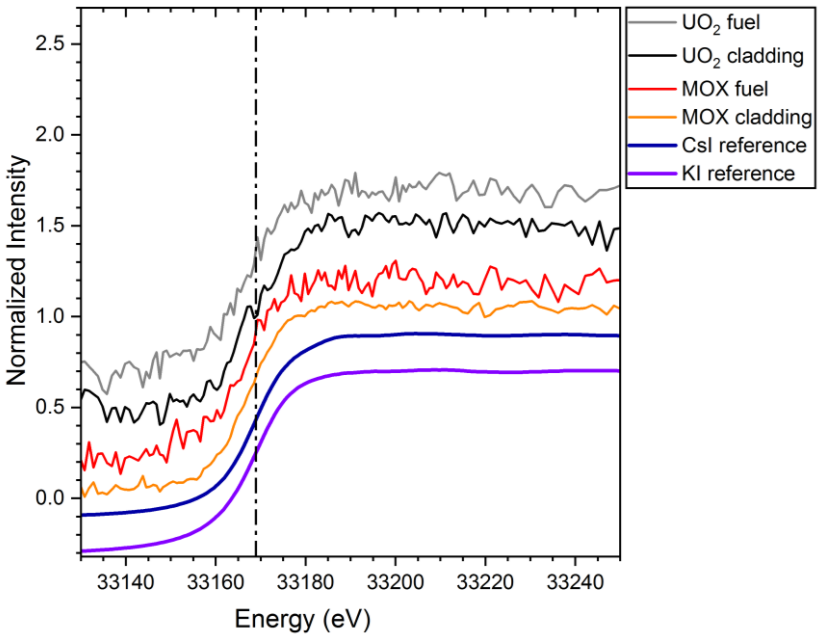

Figure 15 – Iodine K-edge spectra for fuel fragments and the fuel-cladding interaction layers present on UOX and MOX fuel cladding

CsI and KI reference spectra were added for comparison.

Both elements, chlorine and iodine, are regarded as stress corrosion cracking agents for cladding materials of nuclear fuel rods and therefore special emphasis should be given on further investigations on their impact on the mechanical stability of used fuel assemblies [Syrett, 1979; Goetzmann, 1982].

3.3.3. Thermo-mechanical creep test

Thermal creep is the progressive deformation of a material under the influence of temperature and stresses lower than the yield stress. Creep occurs in three stages (Figure 16). The primary stage shows rapid deformation and a decrease in the creep rate over time, the secondary stage has a constant creep rate and the tertiary stage has a rapidly increasing creep rate over time until fracture occurs. The creep behaviour of unirradiated cladding may be a function of many material parameters including chemical composition, metallurgical structure, and processing conditions. For irradiated cladding, the radiation effects overshadow these fabrication and chemical effects as, during irradiation, the anisotropy disappears and the material texture becomes homogeneous [Nakatsuka, 1987]. The irradiation-assisted creep in the reactor is an order of magnitude greater than thermal creep. Most codes calculate the two modes of creep separately [Martin, 2007]. In spent fuel, the irradiation becomes negligible, but the thermal creep of the irradiated material continues.

The two principal physical factors affecting the creep behaviour of the cladding in interim storage are the hoop stress and the temperature. The hoop stress results from the rod internal pressure, a combination of the original fill gas and the fission gas released during operation, and the temperature results from the decay heat of the fuel assemblies [ASTM1562, 2010]. The creep strain rate and the strain upon failure of the spent nuclear fuel cladding are affected by material parameters such as alloy composition, fabrication steps (for example, cold work, solution annealing, recrystallisation annealing), and radiation fluence [ASTM1562, 2010].

The spent fuel, which has undergone corrosion during operation, may contain some dissolved hydrogen or precipitated hydrides. It is important to quantify the effect of the hydrogen content on the creep properties. Previous studies [Kamimura, 2003; Kamimura, 2004] have shown that hydrogen does not have the same effect on BWR and PWR cladding. A hydrogen concentration above the solid solubility

limit, i.e. hydrides exist, under high stress tends to suppress creep of BWR cladding, while a hydrogen concentration below the solubility limit under high stress tends to accelerate creep. For PWR cladding, no creep-accelerating effect has been found for hydrogen concentrations below the solid solubility limit, while a remarkable creep-suppressing effect has been observed with hydrogen concentrations above the solid solubility limit. Irradiated materials have shown a certain creep-suppressing effect compared to unirradiated material, but the degree of suppression depends on temperature and stress conditions.

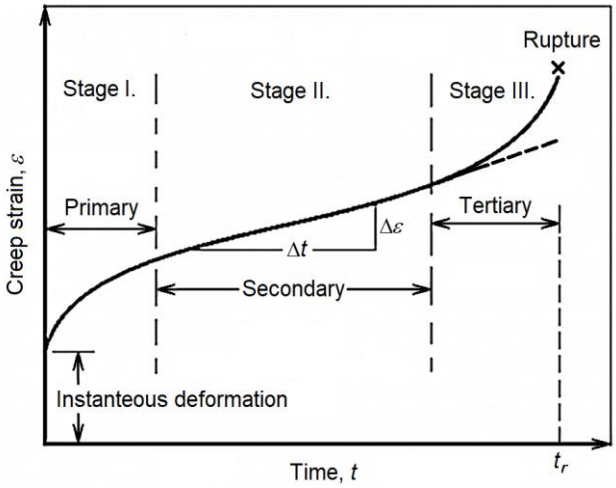

Figure 16 – The three stages of creep

[Faridani, 2011]

For preparation of creep test samples (Russian Zr1%Nb cladding E110 and its variant $E110_{opt}$), low-pressure hydrogen gas was dissolved in cladding samples in a vacuum furnace at 600 °C. The absorbed hydrogen content was verified by measuring the mass increase of the sample, and the distribution of hydrogen was measured by neutron-induced prompt gamma-ray spectroscopy. As the heat treatment during sample preparation may also have an effect, a heat-treated control sample (subjected to the same preparation process at 600 °C, but in a pure Ar atmosphere) should also be measured.

The effect of high hydrogen content in the cladding was observed at hydrogen concentrations around 1100 wppm. The effect of the thermal treatment during the hydrogen charging was also evaluated (Figure 17). The results indicate a significant hardening effect of the hydrides present in the zirconium matrix, as the secondary thermo-mechanical creep rate of as-received unirradiated claddings was three times higher than the ones charged with hydrogen.

The thermal treatment also had a significant effect; it decreased the creep rate compared to the as-received untreated cladding samples by 25%. This could be attributed to the partial recrystallisation of the originally stress relieved annealed cladding. In this test, the temperature of the measurement (the maximum allowed cladding temperature of 400 °C during dry storage), the high circumferential load (66% of the yield strength), and the high hydrogen content (double the maximum allowed hydrogen content of 600 ppm with the typical amount far below this) were well above the anticipated real values. The relatively high temperature and pressure were necessary to observe the creep, as at values closer to the realistic reference case the creep rate could be an order of magnitude lower, necessitating much longer measurement times. The high hydrogen content was necessary in this first test to clearly identify the effect of the hydrogen. Further experiments should approximate the anticipated realistic reference scenario in terms of hydrogen content and structure, although its effect will also be smaller and harder to distinguish.

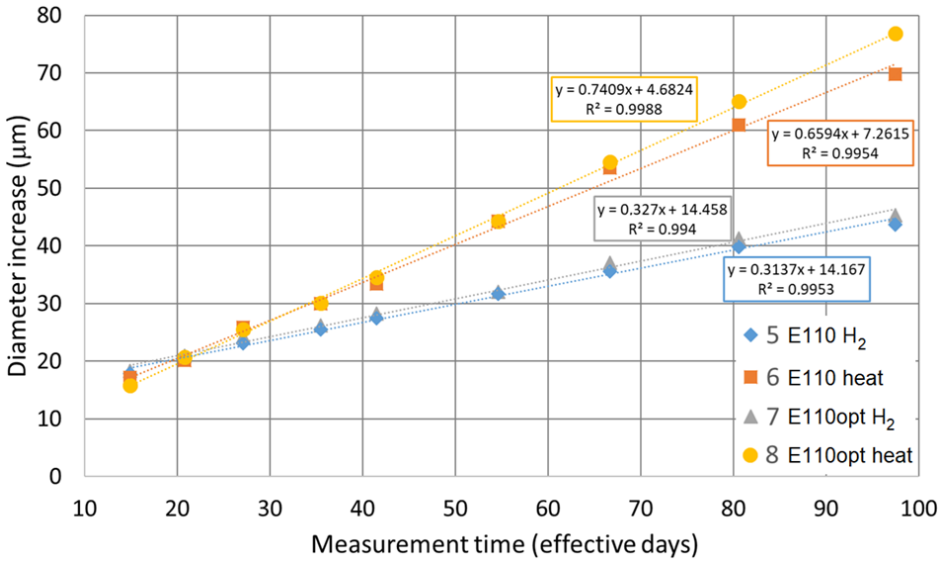

Figure 17 – Average diameter increase and secondary creep rate of hydrogenated and heat-treated cladding samples, derived from the corrected diameter data

3.3.4. Mandrel ductility test

The ductility of the cladding is an important parameter under both transport and storage conditions. During normal reactor operation, the gap between the fuel pellet and the cladding tube closes, and in the case of an incident or a sudden increase in power, the thermal expansion of the pellet could rupture the cladding wall. Another case of volumetric expansion of the pellet is due to air ingress during the high-temperature phase of dry storage, as higher uranium oxides have a lower density; this could also result in cladding rupture.

Historically, pellet-cladding mechanical interaction (PCMI) tests were often conducted using multi-element tools to determine the plasticity limits of fuel cladding tubes or rings. These tearing tools are referred to as segmented expanding mandrels. Their role is to distribute the radial load evenly along the perimeter of the tubes. The advantage of the test is that it is relatively easy to perform and does not require lengthy preparation and irradiation to obtain a properly fragmented pellet and cladding. The initial heat treatment, corrosion, amount of hydrogen and iodine absorbed by the specimens can be controlled and the specimen can be inactive or irradiated. These tests can be performed both at room temperature and near the operating temperature (350 °C).

There are several methods for generating radial stress. In one case, a soft metal cylinder (zirconium or aluminium) is pressed inside the cladding [Nobrega, 1985; Foster, 1987; Jiang, 2014] and deformed to increase its diameter, thereby transferring radial load. Alternatively [Nilsson, 2011; Catherine, 2006], a cone or spike is pressed into the centre of the tool; this approach was used in this test. The advantage is that the cone or spike is not deformed, i.e., the measured force depends only on the bank angle of the cone and the friction between the cone and the mandrels, so that the radial force applied to the sample can be determined more precisely.

Standard mandrel experiments are usually carried out until failure occurs. An important parameter can be the rate of deformation. In the case of soft metal cylinder compression, the compression is very slow, typically 0.01 mm/min, which is significantly lower than the tensile rate of 5…50 mm/min commonly used in tangential tensile tests. The slow loading, especially the so-called "ramp-and-hold" (sustained load over a longer period of time), allows crack propagation to be analysed more effectively. The higher stretch speed (above 10 %/h) simulates the cladding elongation during a power increase due to thermal expansion caused by the temperature increase. Lower speed (below 0.5 %/h) simulates the subsequent

prolonged swelling of the fuel pellet due to slow swelling and increased internal pressure. In the case of RIA or sudden power increase, the deformation may be orders of magnitude faster.

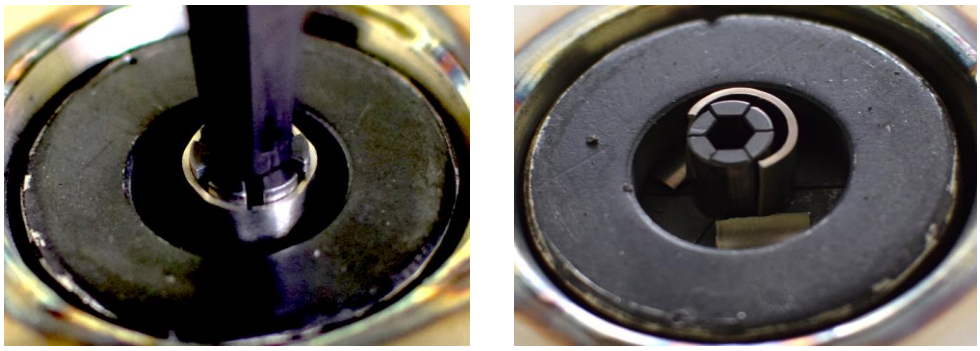

Figure 18 – The mandrel test performed with a ductile (left) and a brittle sample (right)

Courtesy of MTA-EK.

The mandrel test setup at MTA-EK can simulate the pellet-cladding mechanical interaction by expanding segmented dies (mandrels) inside cladding samples (Figure 18). This setup represents the actual mechanical conditions of the cladding better than the ring compression test which is widely used to investigate cladding ductility. The mandrels are driven apart by a pyramidal taper connected to the crosshead of a universal testing machine, and the force is measured under the mandrels. The friction coefficient between the mandrels and the base plate they move on is kept constant by applying graphite-based high-temperature-bearing grease. The temperature can also be increased up to 300 °C using a small furnace around the mandrels.

The effect of hydrogenation on the ductility of 8 mm long unirradiated Russian Zr1%Nb cladding samples (E110 and a new variant $E110_{opt}$) was evaluated (Figure 19). The transition from ductile to brittle behaviour of the samples during the test was observed and a gradual decrease in ductility was found depending on the hydrogen concentration. The maximum cladding inner diameter increase up to failure was found to be almost linearly decreasing with the increase of hydrogen content, from 0 to around 2’000 wppm. Above 2’000 wppm hydrogen content, the samples showed only minimal ductility and failed rapidly along multiple simultaneous axial cracks, reaching maximum measured forces twice as high as observed for the very ductile as-received samples. Similar trends were observed for measurements conducted at room temperature and 300 °C. A new value called integral work was also calculated from the area below the stress-strain curve. The measurement methodology was proven as an alternative ductility test method, and some version of it could be applied to tests with irradiated cladding materials in hot cells. The reiteration of the mandrel design to test longer (30 mm) samples is proposed in order to be able to better replicate the failure of fuel rods by axial cracks, as observed after PCMI. This new mandrel tool design would apply the load only in the middle of the longer sample tubes and so simulate the restrictive effect of the long fuel rods on the axial and tangential deformation.

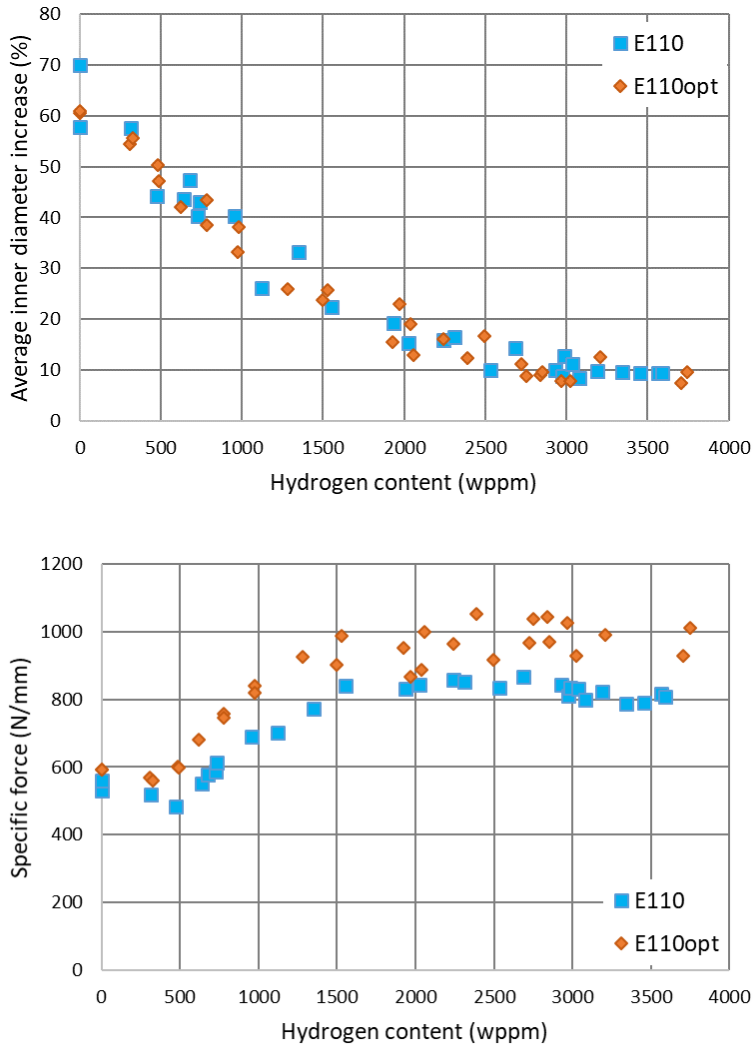

Figure 19 – Maximum diameter change (above) and specific maximum force (below) in the mandrel test at room temperature as function of the hydrogen content

3.3.5. Three-point bending and impact tests

The international research community has made several attempts, mostly consisting of modeling approaches and rather limited experimental studies, to increase the knowledge of the underlying mechanisms that influence the mechanical properties of SNF rods. The majority of the experimental studies focus on irradiated cladding properties by performing tests on defueled cladding ring specimens (i.e., ring compression tests). However, results from experiments on the complete fuel-cladding configuration (i.e., real SNF rods) are extremely rare. Direct tests on irradiated fuel rods require technologically sophisticated facilities, appliances (hot cells, specific remotely operated equipment, etc.), and highly radioactive samples of significant size; they produce a lot of spent fuel waste and are therefore quite expensive and technically difficult to perform.

At JRC – Karlsruhe, a simple free-falling hammer device inducing fuel rupture events was developed and installed in a hot cell in 2008. Impact tests were performed on irradiated commercial LWR UO_2 fuel segments with burnups between ~ 19 and ~ 74 GWd/t. Although the rigidly fixed SNF rod specimens ruptured at three points, only 3.9 … 5.6 g of coarse fuel fragments were released in total (i.e., 1.3 …1.9 g per breakage). Details of these pilot tests can be found as part of the IAEA Coordinated Research

Project SPAR III [IAEA, 2015] as well as in [Papaioannou, 2009b; Papaioannou, 2009c; Dallongeville, 2010].

Results of bending tests, using fresh and spent fuel rods with an average burnup of 50 GWd/t, were published in 2010 [Dallongeville, 2010]. The objective of this joint project was to assess the response of LWR fuel assemblies (FA) during the 9-m drop test as specified in the IAEA transport regulations. The bending test span corresponded approximately to the fuel pin inter-grid distance. Fuel rod failures were observed at about 35 mm net lateral deflection. Ring compression tests or, as the authors called them, hull-lateral compaction tests, were also performed for modelling purposes.

In 2016, a new experimental campaign was initiated at JRC – Karlsruhe to establish a basis for reference data and provide reliable conclusions by performing tests on SNF rod segments with specially developed equipment. The equipment is described in [Vlassopoulos, 2018b] and includes the capability to undertake 3-point bending and gravitational impact tests on fuelled, pressurised SNF rod segments. The new campaign aims to determine the fuel rod response to external loads until failure. Segments with different properties (burnup, fuel composition, history, cladding, etc.) are pressurised to the original rod pressure and subjected to quasi-static bending or dynamic (impact) mechanical loading experiments, determining the critical fracture load (or energy) and the fuel mass released. A thorough characterisation of the fuel rod and companion specimens is carried out before and after each experiment for a comprehensive evaluation of the SNF rod behaviour.

The force (or energy) required for the failure of a fuel rod is determined under the experimental boundary conditions. As the accident scenarios are limitless, it has been decided to study the SNF mechanical integrity under two reference conditions by applying quasi-static or dynamic loads. The acquired data are correlated to properties and processes that potentially affect the SNF mechanical stability. In addition to post-irradiation examinations performed on the fuel rod at previous stages (including many non- or destructive hot cell techniques), the fuel and cladding of the tested specimen are extensively examined after the experiment. Metallography of the failure location is undertaken to investigate the hydride morphologies, population and orientation, while the local H_2 content is determined by means of the hot-gas extraction method. After dynamic impact, the released fuel particles are observed by scanning electron microscopy (SEM), and corresponding size distributions are determined by image analysis.

The employed experimental setups are shown schematically in Figure 20. The 3-point bending apparatus consists of a force transmitter fixed to a loading column, which is driven perpendicular to the sample axis by a stepper motor at a constant slow speed between 4 and 17 μm/s. The force transmitter, termed "deflector", has a concave, round contact surface (see details in Figure 20a) adjusted to the cladding shape, so that no other side- or edge-load is applied on the fuel rod segment during the experiment. The flexible modular design of the device allows the use of different load transmitters, or, due to removable supports, different specimen lengths. The geometrical configuration of the device follows the prerequisites of a standard bending test as specified in the ISO standard 7438 [ISO7438, 2016]. The device is equipped with sensors for simultaneous acquisition of the applied load, the sample deflection, and internal pressure of the segment. The raw data are in the form of load-displacement curves. The load data is used to evaluate the stresses in the sample. The uncertainty associated with the reported flexural strength is derived based on the method described in [Vlassopoulos, 2018a].

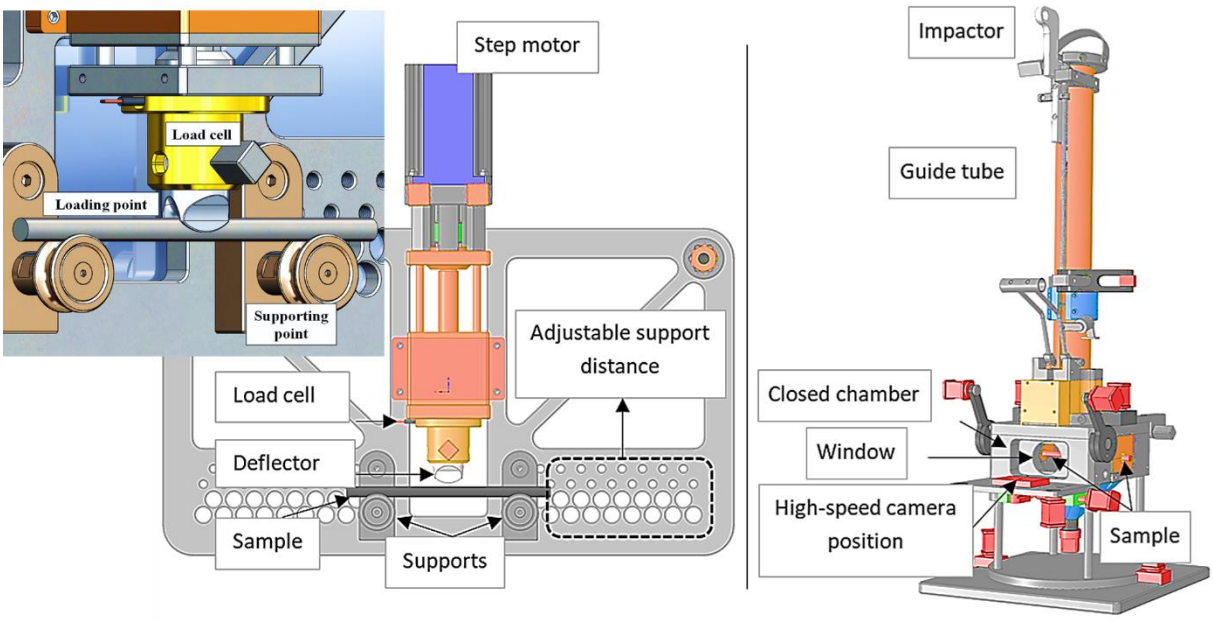

(a) (b)

Figure 20 – Overview of the 3-point bending apparatus (a) and impact tower (b)

The new apparatus for impact tests, shown in Figure 20b, is based on the same principles as the older one used to perform the experiments reported in [Papaioannou, 2009b; Papaioannou, 2009c]. A body (hammer), called the 'impactor', falling through a vertical guiding column impacts the specimen. The impact occurs in a closed chamber, where the released material (mainly fuel with some pieces of the outer-cladding oxide layer) is completely captured. The coarse fragments are collected at the bottom due to the funnel shape of the chamber interior, whereas the fine aerosol particles settle on the internal walls or are caught in the particle filter of an integrated aspiration system. The impact of the specimen is video-recorded by a high-speed digital camera (2'000 frames/s) placed on the window of the chamber and provided with its own illumination.

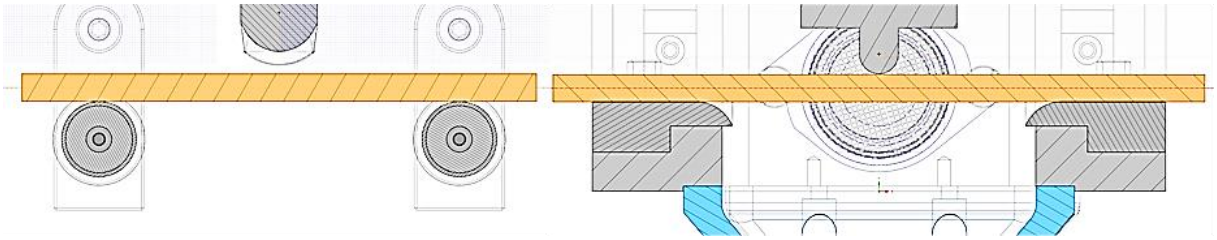

(a) *(b)*

Figure 21 – Scheme of the specimen positioning in the bending (a) and impact (b) device

Rounded supports of the same radius and the same specimen lengths are used for both experiments.

As far as possible, the design of the two devices is mutually consistent. In both experiments, the specimens are bent or impacted by rounded compactors, as shown in Figure 21. The main difference between the two experiments is related to the velocity of the impactor and the bending deflector, enabling a direct comparison of the results in both configurations. The velocity of the falling hammer at point of impact is 3.5 m/s (i.e., at least 2×10^6 times faster than in the 3-point bending test).

A typical specimen for mechanical testing is shown in Figure 22. Using exact tube fittings to preserve the required tightness, 25 to 27 cm long segments cut from SNF rods are connected to a helium gas flask, pressurised to the desired pressure and disconnected after closing the attached gas valve. A pressure transducer, fixed on the other end of the segment, provides continuous pressure control and instant detection of the rupture, which is very important for the bending tests.

Figure 22 – Gastight specimen assembly connected to the pressure gauge with attached pressure transducer, ready for mechanical testing

The investigations in the hot cells include experiments on commercial SNF rods from light water reactors, pressurised to their corresponding internal pressure as measured at the end of in-pile service. Bending and impact are conducted on sets of carefully selected rod segments, excluding segments close to the spacer grids of the fuel assembly, or, if relevant, close to locations where cladding or fuel failures are suspected. So far, studies have used UO_2 fuel rods covering an extended burnup (BU) range from 18 to over 100 GWd/t.

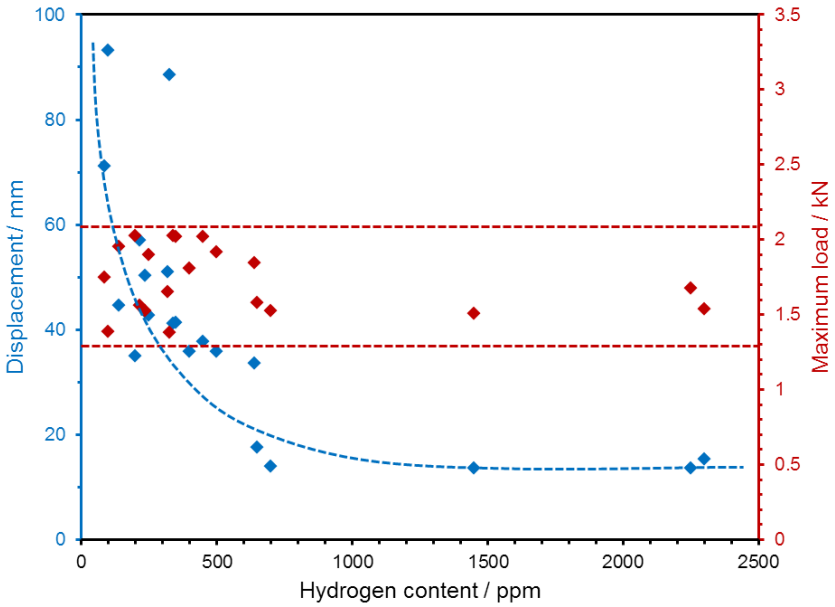

Figure 23 – Measured deflection and maximum fracture load as a function of hydrogen concentration in the cladding during the cold 3-point bending test

Prior to their installation in a hot cell, the two devices shown above were extensively tested for proper functionality and operation with tele-manipulators. Many cold trials with surrogate specimens were carried out for this purpose. The simulated tests used hydrogenated Zry-4 cladding tubes, filled with Al_2O_3 pellets and pressurised to 4 MPa. Most of the results obtained from the bending tests have already been reported [Nasyrow, 2016] in the form of displacement vs. hydrogen content diagrams (Figure 23). Despite the enormous changes in the displacement measured, the corresponding maximum loads

persist within a very narrow range between 1.3 to 2.1 kN and, contrary to the displacement, do not appear to have been affected by the hydrogen concentration in the cladding.

Two load-displacement curves from the 3-point bending experiments on SNF rod segments with low and high average burnup and corresponding hydrogen pickups, respectively, are compared in Figure *24*. These data were extensively discussed in [Vlassopoulos, 2018a; Vlassopoulos, 2018b; Rondinella, 2017]. A remarkable feature of the data is the instant drop in the applied load exactly at the point of specimen fracture, i.e. at the very early stage of crack initiation. Roughly, 20 % higher loads were applied to rupture the high BU fuel segments, whereas the total displacement was less than half of that of the low BU rods.

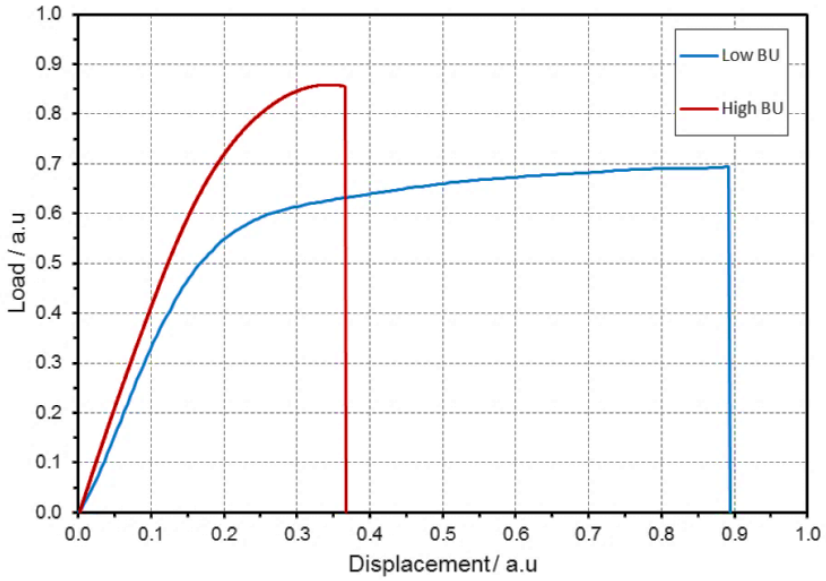

Figure 24 – Load-displacement curves of high and low BU samples during the 3-point bending test

Considering the results from the cold test in Figure 23, the overall behaviour of the SNF rods is fairly consistent. The higher displacement of the low BU specimen was expected, as the material preserves its ductility, but a relatively small change in the maximum critical load to rupture was observed. Nearly three times more energy, as calculated by integrating the area under the curve, must be transmitted to the low BU fuel rod to induce its fracture. The different slopes of the curves in the elastic region denote the higher stiffness of the specimens, which is apparently caused by the higher hydrogenation of the cladding and closure of the gap between fuel and cladding.

The impact device is not equipped with explicit sensors for the acquisition of load-displacement curves. Instead, a high-speed camera attached to the closed chamber of the apparatus records the tests. A sequence of images over a total recording time of only 6.1 ms obtained from the original video file is shown in Figure 25. The visual inspection of the impact provides extremely valuable insight into the various phenomena occurring. Image (a) shows the hammer just before touching the specimen. In the images (b) and (c), several splinters of the cladding's outer oxide layer are clearly propelled from the contact area between hammer and specimen. The crack initiation, morphology and propagation are revealed in image (c). The same photograph illustrates the moment of the "explosive" fuel release in the form of a fine particle cloud. Finally, the subsequent progression and release of coarse fuel fragments at the opening of the crack are observed in images (d) and (e).

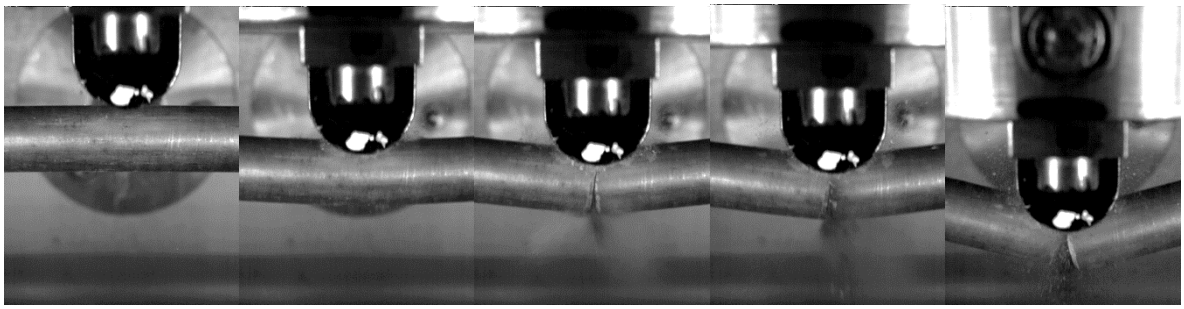

(a) (b) (c) (d) (e)

Figure 25 – Representative selected frames of the image sequence during an impact test on a SNF rod

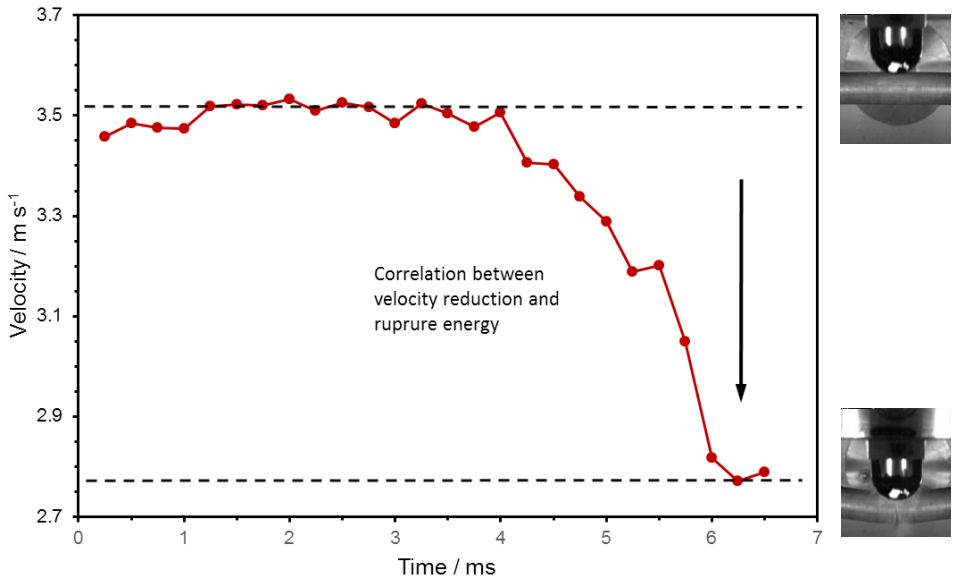

Figure 26 – Hammer velocity change (used to calculate the transmitted energy that caused the specimen rupture)

An image analysis (IA) methodology to extract velocity data from the video records has been developed. The process converts the obtained impact sequence images into instantaneous sample deflection and hammer velocity. Thus, the kinetic energy transmitted by the hammer to the specimen can be calculated from the observed velocity reduction upon impact, as illustrated in Figure 26. The quantification of the uncertainty associated with the derived IA methodology has not yet been evaluated. A direct estimation of this uncertainty is very challenging, since it depends on the minimum detectable displacement and applied object-tracking algorithms, which can differ for each case.

There is only a limited amount of experimental data available in literature characterising the mechanical behaviour of SNF. In addition, these data are restricted to specific types of fuels and loading conditions. During the EURAD project, a new experimental campaign has been performed to extend and deepen the macroscopic characterisation of the mechanical behaviour of SNF rods in a more systematic way. This study complements and extends previous experimental investigations by generating new data concerning areas where technical gaps have been identified. Particularly, it examines the response of PWR SNF rods under a wide range of burnup, from very low to extremely high, covering the spectrum of conditions that can be encountered in practice. The examined loading conditions on SNF rods represent bending sollecitations. In terms of experimental analysis, an innovative image analysis methodology was developed to examine the dynamic response of SNF under impact bending loads. In

this way, the dependence of flexural mechanical properties from strain rate was determined, which is very important to distinguish and analyse scenarios including either static (e.g., storage) or dynamic (e.g., transport or handling) loads.

The samples used for the hot-test campaign consist of commercial spent fuel rods irradiated in PWR NPPs. The campaign was designed in the frame of a collaboration between JRC-Karlsruhe and Nagra, upon agreement with Gösgen Nuclear Power Plant (KKG) and Framatome GmbH, who kindly allowed using the Framatome spent fuel rods, which had been irradiated in KKG and were temporarily stored in JRC-Karlsruhe for this study. The results from an additional PWR fuel rod, irradiated at the Grohnde NPP (KWG), have also been included. Most rods consist of UO_2 with duplex cladding with outer liner (DXD4). In addition, there is one MOX fuel rod segment from KKG having DXD4 cladding as well. The cladding DXD4 consists of two layers, an outer thin one, which is highly corrosion resistant, and a thicker inner layer of Zry-4, which forms the bulk of the cladding and provides most of the mechanical strength. The cladding of the KKG fuel rod with the highest burnup has 2.5% of Nb in the outer liner (DX Zr2.5Nb). The selected rods have different discharge dates, with cooling time up to the tests ranging from 9 to 16 years (having the test date as reference). The selected segments were subjected to three-point bending; after fracture, the remaining of the segment was used for impact tests. All SNF samples were re-pressurised with helium to the rod internal pressure (RIP) as measured at room temperature by puncture tests.

Three-point bending tests on irradiated samples

The experimental setup and test procedure are described in Figure 20a and Figure 21a. Figure 27a shows the load-displacement curves from bending tests performed on all selected SNF rod segments. For the sake of comparison, the results from the two tests performed on fresh Zry-4, with and without the presence of alumina pellets, are plotted in the same diagram. The SNF samples showed higher bending strength due to irradiation hardening. In addition, the slope of the elastic region slightly increases with the burnup of the rods. Different factors might contribute to this increasing trend, such as the slightly different cladding elastic properties due to different burnup (or irradiation time), and the slight difference in the SNF cross-section due to increased oxide layer thickness in higher burnup rods. All samples fractured under plastic deformation; the low burnup rodlet showed much higher ductility compared to the higher burnup samples, but smaller ductility if compared to fresh Zry-4 claddings. In comparison to the fresh claddings, the yield point of the low burnup sample was slightly higher (approximately 10%), however, the development of the plastic region was similar until the point of buckling (appeared at the empty cladding). This indicates that the relative contribution of the pellets to the bending strength of the samples is comparable; however, in both cases a pellet/cladding interface (PCI) is not fully developed (presence of gap). Moreover, the low burnup sample showed lower bending strength compared to the higher burnup samples, which fractured at 25 to 50% higher loads. The MOX fuel rod sample did not show any deviation in its mechanical behaviour. The displacement and load at fracture was similar to the high burnup samples.

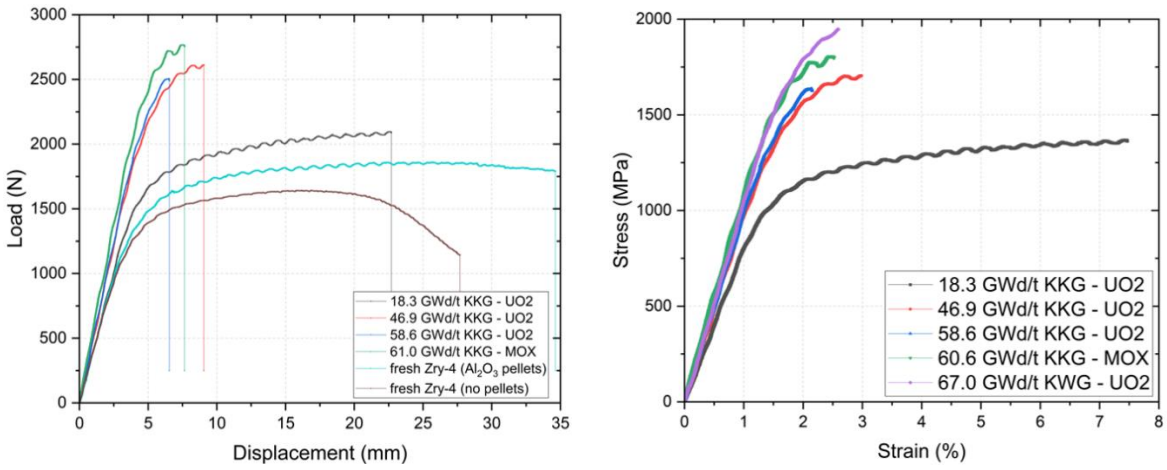

(a) *(b)*

Figure 27 – (a) Load-displacement curves from bending tests on SNF rodlets and fresh Zry-4 samples; (b) Flexural stress-strain curves for beam elements with hollow-circular cross-section derived from three-point bending tests on pressurised SNF rodlets

The flexural properties of the irradiated PWR SNF samples were derived from the three-point bending test results, based on the assumptions of the simple beam theory, as described in [Vlassopoulos, 2021]. The flexural stress-strain curves for beam elements with hollow-circular cross-sections are provided in Figure 27b. The cladding flexural elastic properties were derived assuming that beam elements with hollow-circular cross-section can well describe its elastic flexural behaviour. Results on the Young's modulus of the different DXD4 cladding samples show a nearly linear increase with burnup. This increase could possibly originate from the difference in the oxide layer and bulk Zry-4 material thickness with different burnup. The Young's modulus of the oxide layer is significantly higher compared to Zry-4, therefore, as its thickness increases with burnup, this could result in higher average elastic modulus of the claddings. Finally, as consequence of the higher irradiation damage, the yield strength and 0.2% offset yield strength reveal the higher toughness of higher burnup samples. In addition, the difference between these quantities for each sample could indirectly indicate the steepness of the transition to plastic deformation. Higher values represent less ductile behaviour and the resulting differences confirm the observations of the samples' flexural response.

Impact tests on irradiated samples

The experimental apparatus and the testing procedure are described in Figure 20b and Figure 21b. The following figures show the dynamic response of the samples subjected to impact testing with the use of representative frames before and after the samples' rupture. Typically, the sample deforms under dynamic loading and the oxide layer around the hammer area, being the region with the highest local strain, detaches from the rodlet. The sample cracks at the bottom surface subjected to tension and the depressurisation of the sample is visible as fine particulates from the fuel and cladding are floating in the closed chamber. Once the crack has propagated and the rupture is established at the sample's midspan, larger fuel fragments are released from the area in the close vicinity of the crack. The big fragments are collected at the bottom of the closed chamber, while the fine particulates and aerosol are captured by the micro-filters connected to the chamber's aspiration system or are deposited on the inner walls of the testing chamber.

The ductility of the samples can be evaluated from the amount of deformation undergone before fracture. A first qualitative indication is given by a direct comparison from the frames in which the first crack is observed. For this purpose, Figure 28 (top) is used where the image size from all frames was adjusted to the rod size and, subsequently, the samples have been aligned. The yellow line indicates the upper

position of the rodlet or the moment that the hammer touches the sample. In Figure 28 (bottom) the frames when the first crack occurred for each sample are shown. The relative ductility of the samples can be estimated from their displacement to fracture. Similarly to the three-point bending tests, the first three samples, having the same type of cladding DXD4, showed decreased ductility with higher burnup. The fourth sample, with a cladding of a different alloy (DX Zr2.5Nb) and having a very high burnup, exhibited larger deformation until fracture compared to the other high burnup samples, as observed in the three-point bending tests. These results provide valuable information on the samples' ductility as function of burnup. In addition, they provide proof that plastic deformation occurs even in cases of higher strain rates, such as the impact loading. Nevertheless, in order to quantify the resulting deformations, an image analysis is required.

Image analysis is utilised to calculate the energy absorbed from the sample until fracture, which can be derived from the difference of the hammer's kinetic energy before impact until the point of first crack (or complete rupture). In addition, the displacement to fracture can be calculated from the cumulative distance of the loading point at these frames. Results clearly reveal the effect of the strain rate, as the low burnup sample achieved approximately two times higher deformation (or bending angle) until fracture in three-point bending compared to impact test. On the other hand, the high burnup samples exhibited similar behaviour in both tests: the displacement and bending angle to fracture were slightly smaller for the impact case; however, they were comparable for all samples. As a result, the ductility of the samples is less dependent on the burnup at higher strain rates.

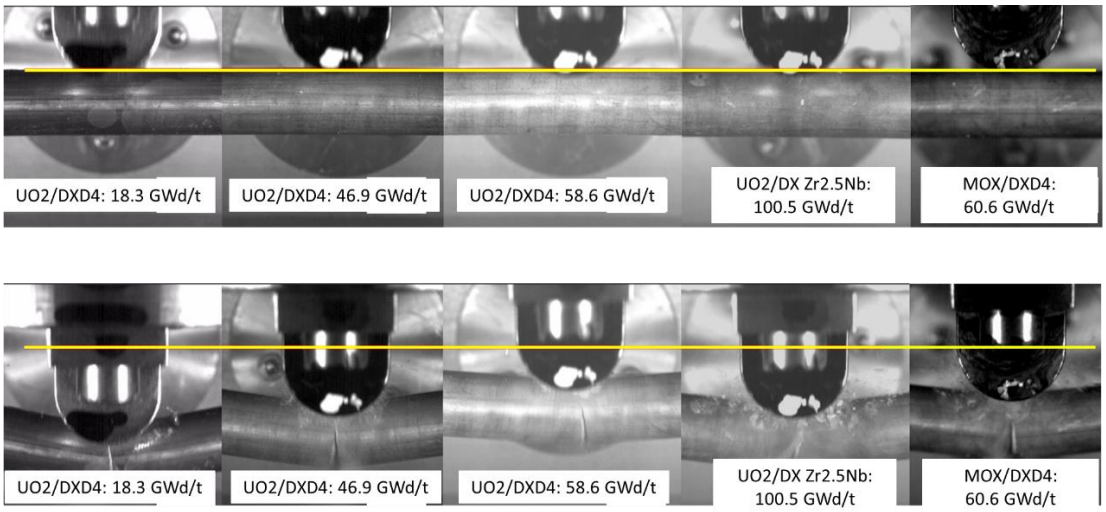

Figure 28 – Qualitative indication of KKG samples' ductility as function of burnup from direct comparison of their deformation to fracture

Top: Selected frames before impact loading adjusted to rod size for all KKG samples; Bottom: Frame when first crack observed for all KKG samples.

With regard to the work or energy absorbed from the sample until fracture, the results of the impact tests are similar to those from the three-point bending tests, showing higher energy requirements to cause sample fracture as burnup decreases. For the first three samples, which have the same cladding type, the energy depends linearly on burnup. The work in impact tests was found to be slightly higher (approximately 5…10%); however, this might be a consequence of the end-plugs use, which changed the sample geometry and total mass. Since inertia effects are relevant in dynamic loadings, the use of end-plugs affects the derived quantities.

Post-test examinations on irradiated samples

A series of post-test examinations was performed to characterise the state of the fuel rodlet upon fracture, the cladding material in terms of hydrogen concentration and hydride morphology, as well as the fuel mass release in terms of mass and size distribution. The location of the cladding crack initiation was systematically at the bottom side subjected to tension and at the pellet-pellet interphase closest to the loading axis. In all cases, the fuel mass release per fracture was limited to less than one pellet and was always relatively higher in impact tests compared to three-point bending, as shown in Figure 29. In addition, the low burnup fuel sample showed higher release compared to the two higher burnup samples, due to the open (or not well established) gap between the pellets and the cladding.

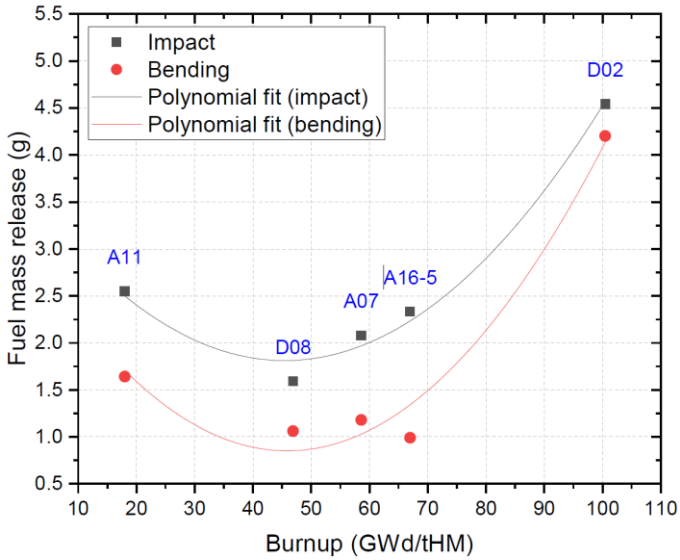

Figure 29 – Fuel mass release per fracture of SNF rod samples under impact and bending tests

In addition, the fuel fragments were characterised based on their size distribution; most of the released mass consisted of fragments larger than 1 mm. The fine particulates and aerosol that were captured after impact tests at the filter system connected to the aspiration device were analysed with SEM and BSE. Image analysis was performed to determine the equivalent circular diameter of these particulates. Moreover, the hydrogen concentration of the cladding at the fracture surfaces was measured with the hot-gas extraction method. The hydrogen content of the samples ranged from approximately 50 ppm to 240 ppm, showing an increasing trend in higher burnup samples, as illustrated in Figure 30. As expected, the hydrogen content of the first three DXD4 (A11, D08, A07) samples from KKG increases with higher burnup. The fourth KKG sample D02 with the highest burnup has lower hydrogen content due to the different cladding material (DX Zr2.5Nb). Finally, the KWG A16-5 sample from a different vendor has lower hydrogen content compared to the high burnup samples D08 and A07 from KKG.

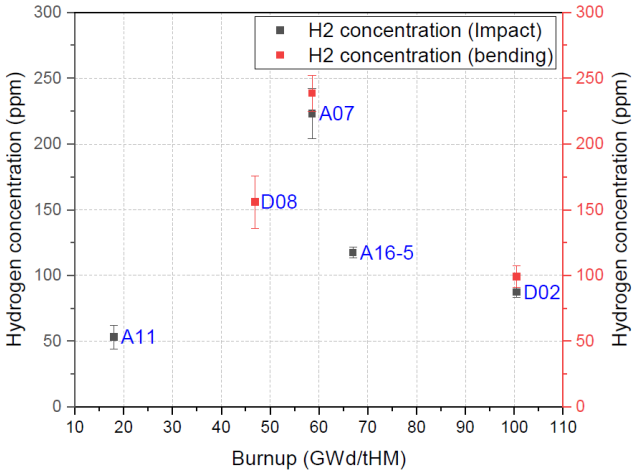

Figure 30 – Hydrogen concentration at cladding fracture region as measured with the hot-gas extraction method

Furthermore, metallographic examinations were performed at the vicinity of the cladding fracture to examine the hydride distribution and morphology. The photographs showed increased hydride precipitation at the outer liner, with long circumferential hydrides and almost no radial hydrides observed.

Three-point bending tests on unirradiated samples

At Universidad Politécnica de Madrid (UPM), three-point bending tests were performed on unirradiated ZIRLO® cladding samples (9.52 mm diameter and 0.57 mm wall thickness). The material is cold-work stress-relieved and was supplied by ENUSA Industrias Avanzadas, S.A. Tube samples (160 mm long) were charged with hydrogen by cathodic charge in the central 40 mm of the outer surface. The hydrogen content is homogeneous in the central 30 mm and it is around 105 wppm.

A new three-point bending system was built, with a design inspired by the one employed by JRC – Karlsruhe. During the test, the load applied by the upper part and its displacement are recorded. An image of the device is depicted in Figure 31a. In addition to empty cladding samples, surrogate rods (with ZrO_2 ceramic inserts) were also tested. ZrO_2 was chosen (instead of Al_2O_3, which is also reported in the literature) because its Young's modulus is closer to the one of UO_2 pellets. The ZrO_2 pellets were cylinders with 8.30 mm diameter (initial gap 200 µm) and 10 mm height and were glued to each other and to the cladding sample (see Figure 31b). Tests were performed at 20, 135 and 300 °C on as-received and pre-hydrided claddings, both hollow and with surrogate pellets. The surrogate rod samples were carefully prepared so that the interphase between two ceramic inserts was always located at the center of the sample. It was considered that this was the worst-case scenario for the bending tests.

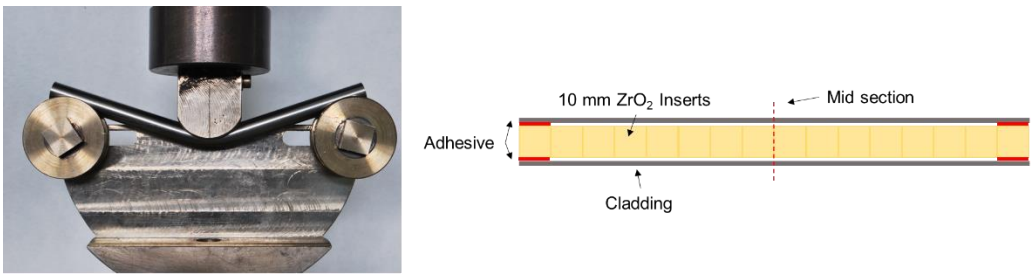

Figure 31 – Picture of the TPB device built at UPM (a) and sketch of the surrogate rod with the ZrO_2 ceramic inserts (b)

The code used to identify the TPB samples is the following: TPB_XX_Y_ZZZ_VV, where TPB means three-point bending, XX is the sample state ("AR" as-received or "PH" pre-hydrided), Y is the sample type ("H" hollow or "P" with surrogate pellets), ZZZ is the test temperature (°C), and VV is the test number.

Figure 32 shows the load-displacement plots from three-point bending tests for as-received pre-hydrided samples hollow and with ceramic inserts at a) 20 °C and b) 300 °C. The hollow as-received and pre-hydrided samples show a very similar behaviour at each testing temperature. The load increases with the displacement of the contact point until the maximum load is reached. After that, the load decreases slowly without any remarkable drop. The final load drop is due to the unloading at the end of test. The maximum load decreases with temperature, with values ranging from 1.1 kN at 20 °C to 0.8 kN at 300 °C. The displacement corresponding to the maximum load is similar for all temperatures and no significant differences are found between as-received and pre-hydrided samples. These results indicate that circumferential hydrides do not significantly affect the mechanical behaviour of cladding in three-point bending tests. This is because the direction of the maximum stress (axial in this case) is parallel to the plane where the hydrides precipitate (radial-axial). Consequently, circumferential hydrides will not have an influence in TPB tests on unirradiated pre-hydrided cladding. The load-displacement plots for samples with surrogate pellets (as-received and pre-hydrided) are also depicted in Figure 32. The behaviour is different from the one observed for the empty samples. The load increases with displacement (of the load application point) until a given value, when the sample fails suddenly and the load decreases to zero. This load drop is associated with the initiation and propagation of a crack in the central cross-section of the cladding, which coincides with the separation between two ceramic inserts. The crack starts at the lower part of the cladding, opposite to the load application point, and propagates upwards through the cladding wall. The plots are quite similar at the different temperatures, although the load and displacement at failure decrease with temperature. As this happens both for the as-received and pre-hydrided samples, it can be concluded that the mechanical response is dominated by the presence of the ceramic inserts.

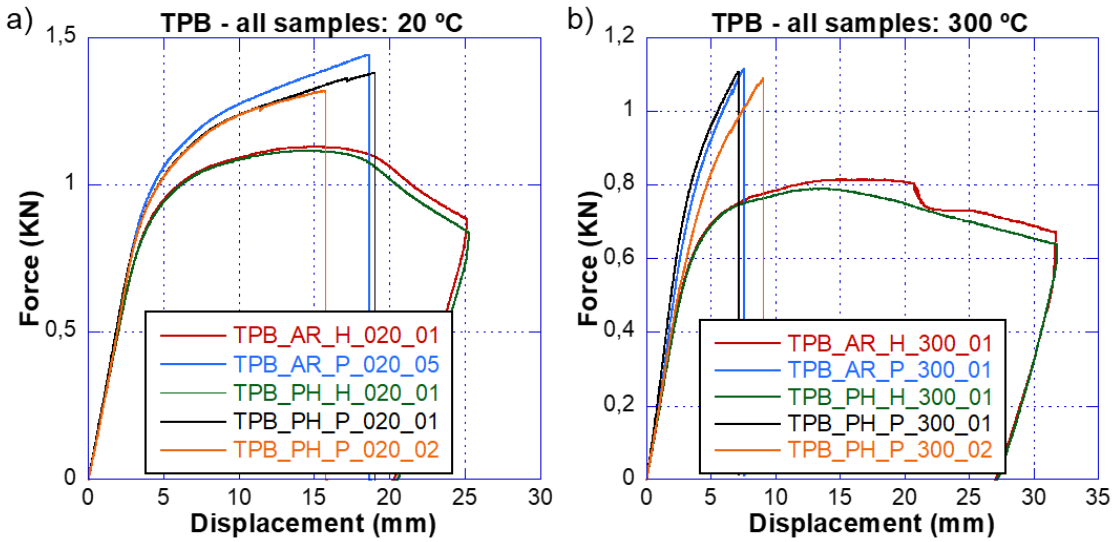

Figure 32 – Load-displacement plots from three-point bending tests for as received and pre-hydrided samples hollow and with ceramic inserts at a) 20 °C and b) 300 °C

Figure 33 shows four images taken during TPB tests at the beginning and after the maximum load. For empty samples (a) and (b), the sample deforms plastically without visible cracking. In samples with ceramic inserts (c) and (d), a crack perpendicular to the cladding axis initiates at the central cross-section (bottom of the sample) and propagates upwards, as explained previously.

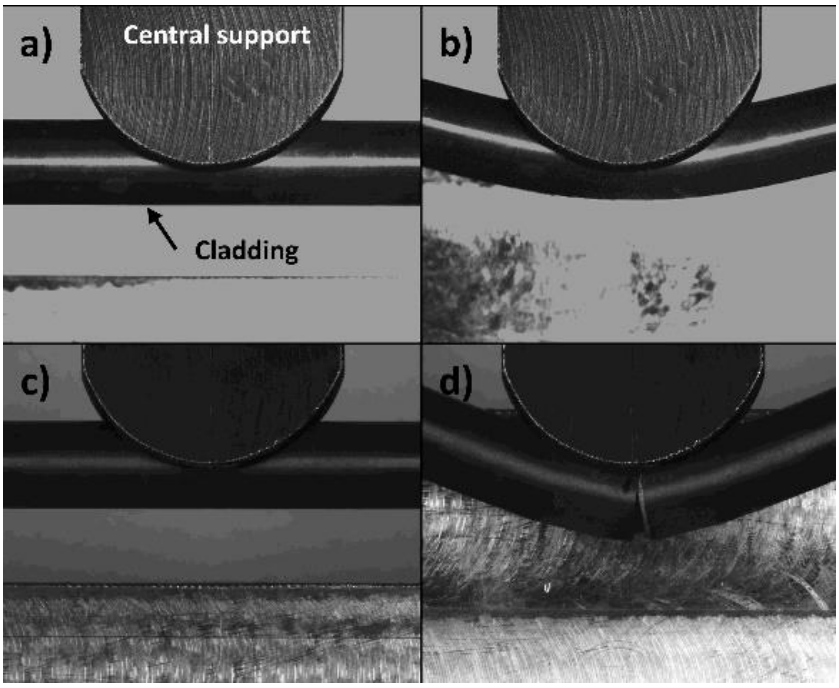

Figure 33 – Photos taken during TPB tests of empty samples (TPB_PH_H_020_01) at the beginning of the test (a) and after maximum load (b) as well as of samples with ceramic inserts (TPB_PH_P_20_01) at the beginning of the test (c) and after maximum load (d)

3.3.6. Ring compression test

Hydrogen embrittlement is known to affect the structural integrity of existing nuclear fuel cladding (zirconium alloys), as has been extensively reported in the literature, e.g. [Billone, 2013a; Ruiz, 2015; Billone, 2018; Billone, 2019]. In water-cooled reactors, an oxide layer is formed at the outer side of cladding, and zirconium hydrides (the hydrogen resulting from the reaction of cladding and cooling water) are precipitated in the cladding when the solubility limit is reached. It has been recognised that, depending on their morphology and the hydrogen content, the hydrides are the most important factor influencing the mechanical performance of the cladding. As an example, the hydrides mainly precipitate along the circumferential direction of the cladding when occuring in cold-work stress-relieved cladding (typically Zircaloy-4, ZIRLO® and E110). However, during drying operations, hydrides may redissolve in the zirconium matrix as the temperature increases, so that hydrogen is available again for precipitation when the temperature decreases. If the circumferential stress in the cladding is above a threshold value (typically around 90 MPa), the hydrides will precipitate along the radial direction when the temperature decreases. The resulting hydride morphology, see Figure 34, can be very detrimental to cladding behaviour in the case of a "pinch-loading" accident, which involves a diametral compression of the fuel rod due to contact with the grid assembly.

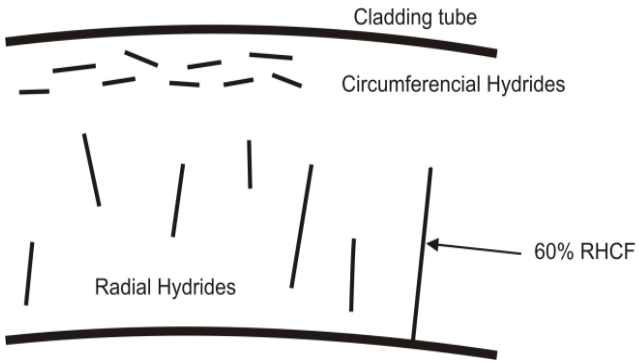

Figure 34 – Typical hydride distribution in a cladding tube

RHCF means radial hydride continuity factor.

Assuming that hydride platelets are considered as closed cracks inside the cladding material, a fracture-mechanics approach can be used to address microscopic crack growth as the failure mechanism and to consequently investigate fracture behaviour. Compact Tension (CT) specimens are commonly used for research on fracture behaviour. Using cathodic and gaseous charging processes, studies on hydrogen-charged CT specimens show a decrease of the fracture initiation parameter J_{IC} for increasing hydrogen contents and low temperatures [Bertolino, 2003]. The macroscopic fracture behaviour was considered as ductile, and therefore a transition from ductile to brittle material response could not be deduced. A negative influence on the fracture toughness of zirconium alloys could be confirmed from 25 °C up to 300 °C, and precipitations along grain boundaries have been determined as a reason for the loss in fracture toughness [Hsu, 2012]. During a pin-loading test performed with hydrogen-charged Zircaloy-4 rings, circumferential hydrides reduced the fracture toughness by 20 %. Combined radially and circumferentially aligned hydrides could reduce the fracture toughness by up to 90 % [Langlade, 2006]. Even in the case where macroscopic failure appears to be brittle, microscopic crack growth was considered to be plastic strain-driven.

Although common fracture-mechanics testing procedures allow the observation of some effects regarding hydride embrittlement, the impact of crack fields remains unanswered. In addition, the result of a CT test with its defined stress state is hardly applicable to the complex structure and geometry of a thin-walled tube. Therefore, the ring compression test (RCT) was established to consider these effects. In this test, a cylindrical sample of the cladding material is deformed within movable plates, and a loading force vs. displacement curve is obtained. Experimental results from RCTs for different hydride contents and temperatures are used to develop numerical models that help to understand and interpret the micromechanical processes inside the cladding. Based on a predictive simulation, failure criteria for the cladding material can be derived. Billone et al. [Billone, 2013a; Billone, 2013b] developed an experimental procedure for the commercially available alloys ZIRLO®, M5® and Zircaloy-4. Both samples from higher burnup fuel rods and as-fabricated, hydrogen-charged cladding segments were heated up to 400 °C and pressurised to induce peak hoop stresses from 80 MPa up to 140 MPa to simulate drying and storage. Hydrogen contents ranged from 350 wppm to 650 wppm for ZIRLO®. Afterwards, the ring segments were cooled with cooling rates of ~ 5 °C/h. RCTs were performed with as-irradiated as well as hydride-reoriented samples at distinct temperatures from room temperature up to 200 °C and with a displacement rate of 5 mm/s. The extent of radial hydrides was quantified by the radial-hydride-continuity factor (RHCF) as the ratio of continuous radial hydride length to wall thickness of the cladding, see Figure 34. It could be shown that through-cracks during the tests correlate with the extent of radially aligned hydride formation. Furthermore, the reprecipitation of platelets in the radial direction is controlled by the peak hoop stress. The highest testing temperature, at which brittle behaviour occurs, is defined as the ductile-to-brittle transition temperature (DBTT). This temperature depends on the type of material, hydrogen content, and reorientation stress. Billone et al. [Billone, 2013b] established an "offset strain" of 2 % in the RCT diagram as embrittlement criterion.

Further ring compression tests were performed by Martin-Rengel [Martin-Rengel, 2012; Martin-Rengel, 2013] and Ruiz-Hervías [Ruiz, 2015]. Ring segments of ZIRLO® were charged with hydrogen to achieve contents of up to 2'000 wppm. The heating, reorientating and cooling were performed in a similar way as described above. Two additional failure criteria were proposed based on the strain energy density and the equivalent plastic strain respectively.

Hence, the ring compression test is the established experimental method for the investigation and characterisation of the mechanical behaviour of defueled cladding tubes. The test can be carried out in hot cells with irradiated material as well as with unirradiated material under normal laboratory conditions. The effort for hot cell tests is very high, but investigations outside hot cells require unirradiated mock-up cladding tubes with material behaviour representative of the irradiated material state. Real Zircaloy claddings contain circumferential and radial hydrides due to the conditions in water-cooled reactors and subsequent vacuum-drying. Therefore, the influence of these hydrides on the material behaviour must also be reproduced.

Realistic distributions of circumferentially or radially oriented hydrides can be created by hydrogen charging of unirradiated claddings. Ruiz-Hervías [Ruiz, 2015] describes a cathodic charging method for a controlled insertion of hydrogen into an unirradiated sample. In an electrochemical reaction, the sample acts as the cathode, and a platinum wire coiled around the sample as the anode in a KOH-aqueous solution. After hydrogen charging, the sample is exposed to an inert gas atmosphere at constant elevated temperature and then slowly cooled down (approx. 1.2 °C/min). The hydrides are circumferentially oriented at this stage of the procedure. Based on a subsequent thermo-mechanical treatment with applied hoop stress (or reorientation stress), the hydrides can be dissolved and partly reoriented along the radial direction of the cladding. The resulting hydride density and orientation is similar to radial hydrides found in the cladding of irradiated fuel rods after radial-hydride treatment (cf. Figure 34). In the case of Zircaloy M5®, mostly individual long radial hydrides precipitate. For ZIRLO®, typically a mix of radial and circumferential hydrides predominates.

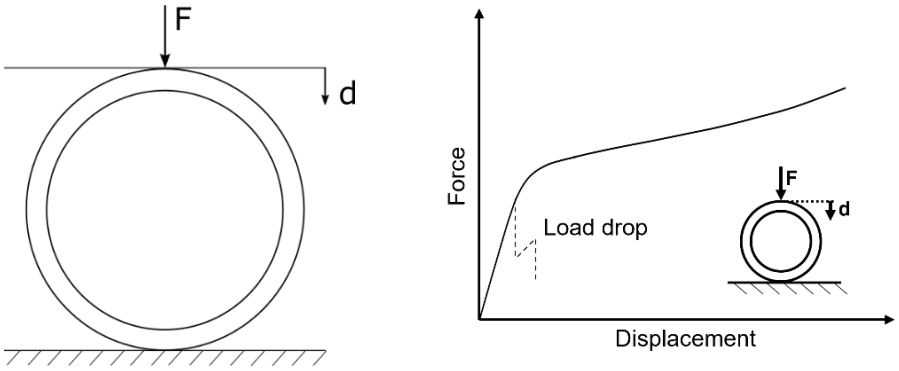

Figure 35 – Ring compression test experimental setup (left) and typical load-displacement curves (right)

The experimental setup of the ring compression test is shown schematically in Figure 35. Tests are displacement-controlled by means of two plane and parallel steel plates. The load is measured with a load cell. The upper plate moves with constant velocity, while the lower one is fixed. Maximum tensile hoop stresses occur at the inner surface of the 6 and 12 o'clock positions and at the outer surface of the 3 and 9 o'clock positions. Specimens are ring-shaped with a height of 10 mm. The dimensions of the cladding tube may vary. Typical values are an outer diameter of 9.5 mm and a wall thickness of 0.5 mm.

Figure 35 illustrates the characteristic load-displacement curve of pre-hydrided empty samples. Cladding samples with circumferentially oriented hydrides typically show ductile behaviour during a RCT. The displacement at maximum load is much larger than the typical gap between tube and fuel. After large deformation, ductile failure is detected and the load decreases gradually (not shown in the

figure). By contrast, hydrides oriented in radial direction of the cladding can cause brittle failure associated with sudden load drops. The displacements at the point of failure can be very small. After the maximum load, failure by crack initiation and subsequent crack propagation is observed.

As testing with irradiated cladding is both difficult and expensive, it is not possible to cover all possible conditions. Testing with unirradiated material may help bridge the gaps. The precise experimental simulation of the hydride structures observed in irradiated claddings is particularly important in this respect. Newer sample preparation techniques are able to simulate experimentally the drying process with independent control of the internal pressure and temperature of the cladding.

At Universidad Politécnica de Madrid (UPM), a new radial hydride treatment (RHT) to reorient circumferential into radial hydrides using internal pressure has been developed where pressure and temperature can be controlled independently. Unirradiated ZIRLO® cladding samples (9.52 mm diameter and 0.57 mm wall thickness) were used. The material is cold-work stress-relieved and was supplied by ENUSA Industrias Avanzadas, S.A. Tube samples (50 mm long) were charged with hydrogen by cathodic charge in the central 20 mm of the outer surface. The hydrogen content is homogeneous in the central 10 mm with a value around 80 wppm. Pre-hydrided samples were closed with stainless steel fittings, connected to a high-pressure valve system and introduced in an electric furnace. The radial hydride treatment consists of heating the samples without internal pressure up to 400 °C for 80 minutes. Then the samples were pressurised with argon up to a pressure equal to 19 MPa. The value of the internal pressure was calculated to produce an average circumferential stress (on the cladding wall) equal to 140 MPa. The internal pressure and the temperature were hold during 30 minutes. Finally, the sample was cooled at 5 °C/h while keeping constant the internal pressure.

Figure 36 shows two micrographs. Figure 36a corresponds to a cladding sample before the RHT, while Figure 36b corresponds to a cladding after the RHT. In the first one, zirconium hydrides can be observed as dark lines inside the cladding wall section. Hydrides are in circumferential direction and mainly located at the mid-wall thickness. In the second image, after the RHT, most of the hydrides are reoriented in the radial direction, and some almost connect the inner and outer surface of the cladding. The RHT employed produces a highly reoriented microstructure.

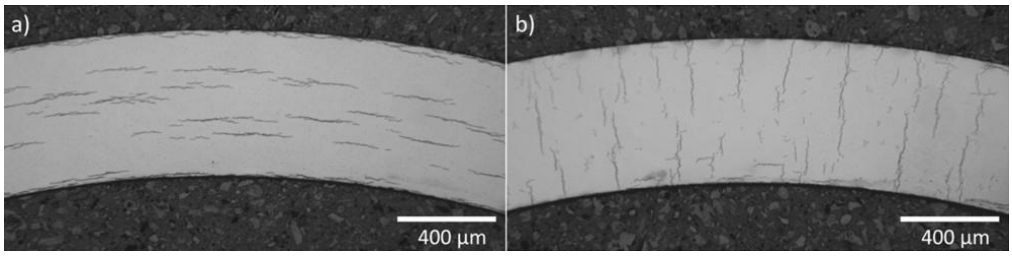

Figure 36 – Photos taken during TPB tests of empty samples (TPB_PH_H_020_01) at the beginning of the test (a) and after maximum load (b) as well as of samples with ceramic inserts (TPB_PH_P_20_01) at the beginning of the test (c) and after maximum load (d)

Ring compression tests were performed on pre-hydrided empty samples with radial and circumferential hydrides at 20, 135 and 300 °C. Tests on pre-hydrided samples with radial and circumferential hydrides containing a surrogate pellet were carried out at 20 °C. The results are summarised in Figure 37, where load vs. displacement plots are shown for a) empty samples tested at 20, 135 and 300 °C and b) samples with a surrogate pellet tested at 20 °C (along with results on empty samples for comparison). In empty samples with circumferential hydrides, the load increases monotonically with displacement (see Figure 37a). At 20 ºC, the maximum load is approximately 1 kN for a displacement of 5 mm. When the testing temperature increases, the maximum load decreases while the displacement at maximum load increases. The same behaviour is observed in empty samples with radial hydrides tested at 300 °C. However, on empty samples with radial hydrides at 20 ºC and 135 °C, sudden load drops occur in the

linear part of the load-displacement plot, where no part of the sample has yielded. They are associated to cracks that are visible in the pictures taken during the tests. The cracks appear first at the 12 and 6 o'clock locations on the inner diameter of the sample and then at the 3 and 9 o'clock locations on the outer diameter. It is worth noticing that the load corresponding to the first load drop is approximately 0.25 kN for a displacement around 0.2 mm.

In case of samples with surrogate pellet, the behaviour is completely different. No catastrophic failures occurred even for the RHT samples. The cladding-insert system was stiffer, and the maximum load was much higher than in empty samples tested at the same temperature (see Figure 37b). Consequently, mechanical behaviour is controlled by the insert and not by the radial hydrides in this case.

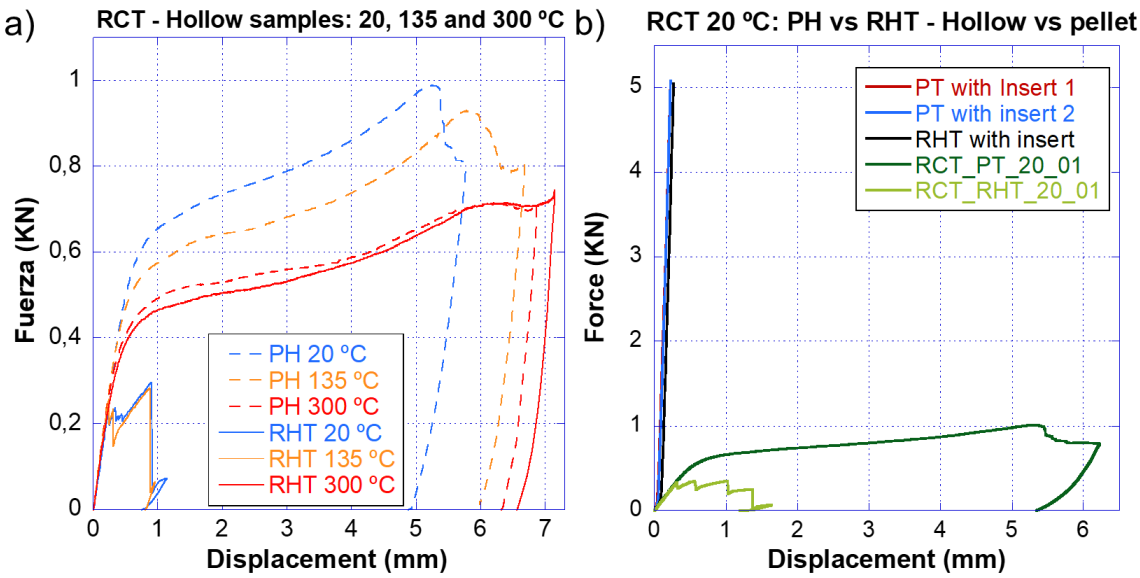

Figure 37 – Load-displacement plots in RCT for samples with circumferential (PH) and radial hydrides (RHT): a) empty, at 20, 135 and 300°C; b) empty and with surrogate pellet at 20 °C

For comparison, the samples without hydrides but with precipitation treatment (PT) are also shown.

Figure 38 shows two micrographs of the cross-section of cladding samples with radial hydrides after RCT at 20 °C and 300 °C. At 20 °C, several cracks can be observed along pre-existing radial hydrides. In this case, the cracks initiate at the outer surface of the cladding (at 9 o'clock location) and propagate towards the inner surface, following two parallel hydrides. In the sample tested at 300 °C, no cracks can be seen; the sample deforms plastically and very few hydrides are found. At this temperature, the terminal solid solubility of hydrogen in zirconium is larger than the existing hydrogen concentration (around 80 ppm) and most hydrides are redissolved in the zirconium matrix. Consequently, even with a severely reoriented hydride morphology, the samples tested in RCT at 300 °C do not show a brittle behaviour, as found at 20 ºC and 135 ºC.

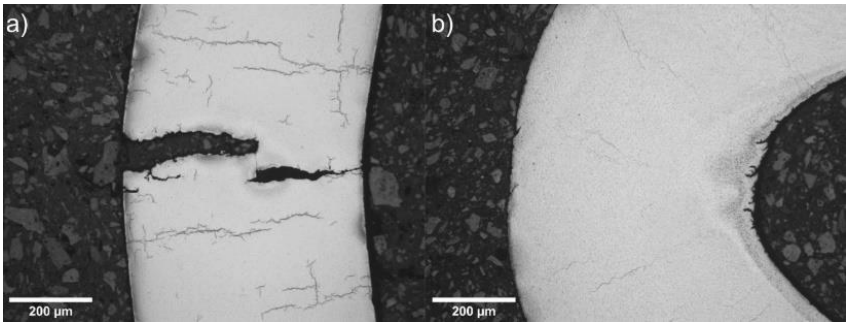

Figure 38 – Micrographs of empty cladding samples with radial hydrides after RCT at a) 20 °C and b) 300 °C

3.3.7. Oxidation and dissolution tests

The potential contact between fuel pellets and gaseous atmosphere [Aronson, 1957; Einziger, 1985; Einziger, 1986; Anderson, 1955a; Hanson, 1998; Leinders, 2016a; Leinders, 2018] or aqueous environment [IAEA, 1998; Johnson, 1977] during its temporary storage has been studied in the past to some extent. Additionally, the SNF behaviour has been studied in many previous projects funded by Euratom [Poinssot, 2005; EC, 2008; Grambow, 2010; Evins, 2014; Kienzler, 2017; Evins, 2021]; however, all of them were focused on the quantitative understanding of key processes affecting the SNF under geological repository conditions. Nevertheless, important gaps in the knowledge of interactions between UO_2 with oxidising agents (gas or aqueous) in the event of an undetected cladding breach still exist. The study of the different intrinsic (specific to SNF attributes) and extrinsic (environmental storage conditions) parameters, that can affect the SNF matrix integrity evolution, is of outermost interest for irradiated fuel under operational and accidental scenarios during the early stages of back-end of the nuclear fuel cycle such as handling, transport and storage. To ensure SNF integrity under whatever considered scenarios (e.g., moisture, aqueous dissolution of the UO_2 matrix, corrosion of the SNF, etc.), systematic identification of events and their consequential effects, that are still not well understood, should be considered in the safety assessment.

Before final disposal of SNF in a deep underground repository, and after being discharged from the reactor, the SNF is stored in cooling pools at the reactor site to allow for the decay of the heat capacity (related to very short-lived nuclides decay) below a specific level. Then, the used fuel may be transferred (transport) to wet or dry long-term interim storage for periods from 30 years up to 100 years, because of the lack of geologic repositories [Ewing, 2015; Kienzler, 2018; IAEA, 2020; Spahiu, 2021]. The SNF is theoretically able to resist long-term interim storage without important changes of its features; however, some elementary processes need to be further addressed.

Knowing that working with SNF is more representative of the realistic scenario, the chemical and structural complexity of SNF and the associated radiation fields complicate answering still open questions from experiments with SNF. In order to gain knowledge on separate and synergetic effects and also to develop/conduct fundamental research, the use of non-irradiated alternatives is important before carrying out experimentation on real irradiated systems presenting radiological risks that must be handled with particular care (in hot-cells which capability is limited to some countries). The experimental research proposed has been performed by means of various "model materials" that can represent some physico-chemical properties maintaining certain degree of conservatisms. The main objective is to reduce uncertainties and to improve the description of the most relevant processes driving the chemical evolution of SNF at the interim storage conditions (e.g., wet and dry) based on new experimental data that may have an impact on final disposal. Thus, corrosion studies were carried out using systematically prepared and precisely characterised UO_2-based model materials to understand several single and linked effects on SNF behaviour under relevant conditions of interim storage.

Table 15 shows information on the studies carried out at CIEMAT, and the experimental protocols (see more details in Deliverable D8.9).

Materials used	Measurement / Type of experiment	Techniques
UO_2 Eu-doped UO_2: 0.02; 0.2; 2 $^w/_o$ Eu_2O_3-UO_2 **Synthesis and sintering** Pellet, dry route, Sintering: 1675°C, 4h, N_2/H_2 (4.7%) Powder	**Dry: oxidation behaviour** T: RT to 900 °C $O_2(N_2)$ conc.: 1-21% **Wet: Aqueous dissolution test** H_3BO_3: 1600 and 3500 ppm pH: ~ 5.2 RT	Solid: TGA, SEM-EDX, BET, XRD, Raman Analysis in solution: pH, redox, ICP-MS

Table 15 – Experimental approaches used for studying nuclear fuel behaviour on simulated interim storage

Samples preparation and solutions

A series of UO_2 pellets doped with different amounts of Eu_2O_3 (0, 0.02, 0.2 and 2 $^w/_o$) have been sintered by "dry route", and analysed by X-ray diffraction (XRD) and Scanning Electron Microscopy (SEM). The specific surface area (SSA) was geometrically calculated (without roughness factor) and measured by N_2 BET (Brunauer–Emmett–Teller) method [Brunauer, 1938]. The density of the pellets was estimated using two different methods: 1) geometric density based on the pellet dimensions, which includes both open and closed porosity and assumes perfect cylindrical pellets; 2) immersion density measurement by Archimedes method, which allows measurements that are more precise. In agreement with prior studies [Lee, 2017; Iwasaki, 2009], the XRD data show that an increase in lanthanide (Ln) dopant concentration produces a contraction of the fluorite structure possibly due to the joint effects of smaller cation size of Eu and shorter U/Eu-O bonds and/or by hypo-stoichiometry [Olds, 2020], showed by the Rietveld-refined lattice parameters. Further details can be found in D8.9 [Rodríguez, 2024].

Thereafter, most of the as-prepared pellets were directly used for dissolution tests. However, one pellet representative of each composition of Eu-doped (and undoped) UO_2 was manually milled in an agate mortar prior to being subjected to dry oxidation experiments.

Dry oxidation behaviour of Eu doped UO_2-based model material as analogue for spent nuclear fuel

Oxidising gas intrusion such as air into a breached cladding SNF rod may cause a SNF matrix oxidation up to U_3O_8, associated with a ~36% volumetric expansion with respect to the initial UO_2 [McEachern, 1998; Milena, 2023a], and turn out with spallation and pulverisation of material [McEachern, 1998; Milena, 2023b]. This may pose a safety issue for SNF management as it could imply a confinement failure and hence dispersion of radionuclides within the environment [Taylor, 1991]. It is generally assumed that the fluorite-type lattice of UO_2 matrix is stabilised at intermediate oxidation states (U_4O_9/U_3O_7) during oxidation with the presence of dopants [Wilson, 1961; Hill, 1962; Roberts, 1961; Suresh, 2004; Jégou, 2010; Eloirdi, 2018]. Some efforts are needed to improve the knowledge about the effect of these dopants or impurities in the fuel oxidation resistance to U_3O_8, and in particular of trivalent lanthanides formed due to the nuclear fission reactions [Milena, 2023c].

Here, the effects of Eu_2O_3 doping on the thermal stability of UO_2 were investigated. For this purpose, powdered samples (UO_2-0.02 $^w/_o$ Eu_2O_3, UO_2-0.2 $^w/_o$ Eu_2O_3, and UO_2-2 $^w/_o$ Eu_2O_3) were subjected to a thermal treatment by thermogravimetric analysis (TGA) consisting of a heating ramp up to 900 °C at two

oxygen concentrations (1% and 21% O_2). Pure UO_2 powder was evaluated and used as a reference. Oxidations were conducted by heating the samples to obtain the complete conversion to U_3O_8 and study the overall reaction. Complete oxidation TGA measurements were performed by triplicate to include uncertainties (SDs) of all mean values of the total weight change (%), oxidation onset temperatures (OOTs), maximum reaction temperatures (MRTs), and reaction rate at the maximum reaction temperature (RR_{MRT}), in addition to ensuring the repeatability and reliability of the TGA results [Milena, 2023a; Costa, 2021]. TGA oxidation curves of all the materials at the two aforementioned oxygen partial concentrations are given in Figure 39.

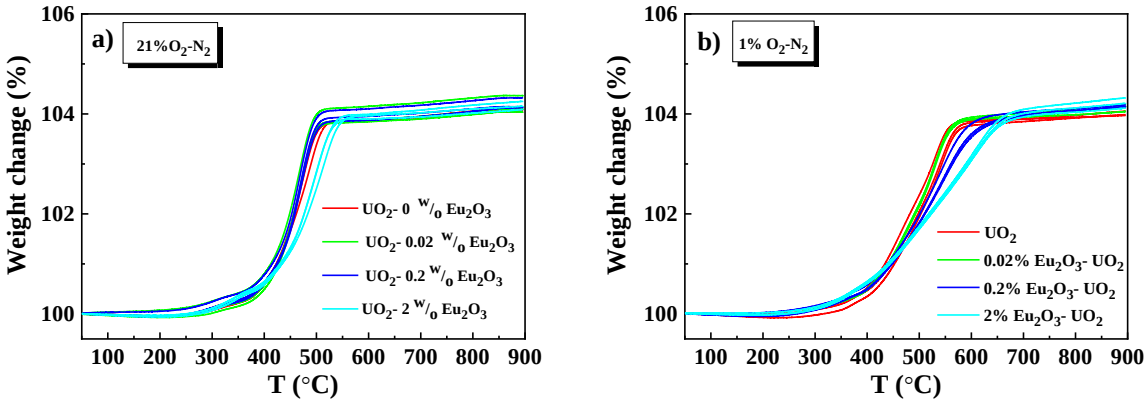

Figure 39 – Weight change curves at 21%O_2 (a) and 1%O_2 (b) of: UO_2, UO_2-0.02 $^w/_o$ Eu_2O_3, UO_2-0.2 $^w/_o$ Eu_2O_3, and UO_2-2 $^w/_o$ Eu_2O_3

These studies showed that adding Eu to UO_2 slightly retards oxidation to orthorhombic U_3O_8. This effect, attributed to the dopant, is more marked with lower oxygen concentration (as low as 1% O_2).

Dissolution behaviour of Eu doped UO_2-based model material as analogue for spent nuclear fuel

The SNF is stored underwater in the spent fuel pool for up to 10 years [IAEA, 2012], depending on the fuel design and burnup, for initial cooling. Thereafter, depending on the strategy followed by each country, it may continue at wet interim (pool) storage or it may be stored under dry interim (cask) storage conditions, for the next decades before final disposal. Boron is a neutron absorber added to the water coolant, which is required during the wet storage of SNF. Introduced in the form of boric acid (H_3BO_3) in the pool, it ensures adequate subcriticality following a contingency principle [IAEA, 1999]. A specified minimum boron concentration must be maintained, especially during spent fuel loading operations [IAEA, 1999]. In this study from CIEMAT, we compare the corrosion behaviour of Eu-doped UO_2 in two simulated pool waters, representing two different boric acid concentrations nominally containing 1'600 and 3'500 ppm boron, respectively. Further details can be found in D8.9 [Rodríguez, 2024]. The normalised dissolution rates of U ($R_L(U)$), expressed in $mg \cdot m^{-2} \cdot d^{-1}$, were calculated from concentration data and BET surface area to calculate an elemental mass loss normalised to the SSA, following the formula given in [Bosbach, 2021].

The trend and values of both U concentrations and SSA normalised dissolution rates for U are similar for both leaching media over the entire test duration, a decrease of dissolution rate with increasing Eu content in the solid solution. This suggests an oxidative dissolution resistance of Eu, similar to previous findings from the literature where other trivalent dopants like Gd are known for stabilising the UO_2 matrix towards oxidative dissolution [Barreiro, 2019; Casella, 2016].

The presence of Eu has an important impact on the rate of oxidation of U(IV) to U(VI), which is well emphasised in Figure 40, where the final values of $R_L(U)$ (at 48 days), normalised to the BET surface area, are plotted vs. the Eu_2O_3 concentration added. Overall, the $R_L(U)$ decreases with increasing Eu content. This would suggest that the presence of Eu improves the durability of UO_2, at these leachant concentrations. It can be hypothesised that this reduction in rate with increasing Eu is a result of a slowdown of its oxidation due to the presence of trivalent elements, which promotes and stabilises the formation of oxygen vacancy clusters (in order to maintain electroneutrality) [Park, 1992], as in the case of Gd_2O_3-doped UO_2 [Lee, 2017; Park, 1992; Kim, 2001; Scheele, 2021].

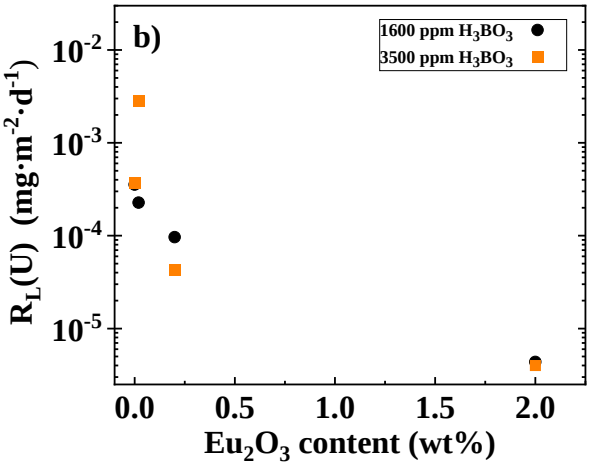

Figure 40 – Final values (after 48 days of dissolution experiment) of normalised dissolution rate of U, $R_L(U)$, as a function of Eu content, for Eu-doped and undoped UO_2 dissolved in 1'600 ppm and 3'500 ppm H_3BO_3

Post-leaching examinations by SEM of the pellets´ surface reveal that, for the samples containing 2 $^w/_o$ Eu_2O_3, some kind of aggregates appears for both boric acid concentrations (Figure 41), even after 1 day of dissolution. The evident higher abundance of these structures as a function of time and, especially, at the samples leached at 3'500 ppm H_3BO_3, leads to the assumption that it might be related to the boric acid concentration. In addition, the fact that they were only detected for the samples with 2 $^w/_o$ Eu_2O_3 content suggests that the Eu^{3+} trivalent plays a key role in the formation of such aggregates. Nevertheless, these aggregates formed on the surface of the pellet need further characterisation. Conversely, no remarkable alteration was detected for undoped, 0.02 and 0.2 $^w/_o$ Eu_2O_3-UO_2 (images not shown).

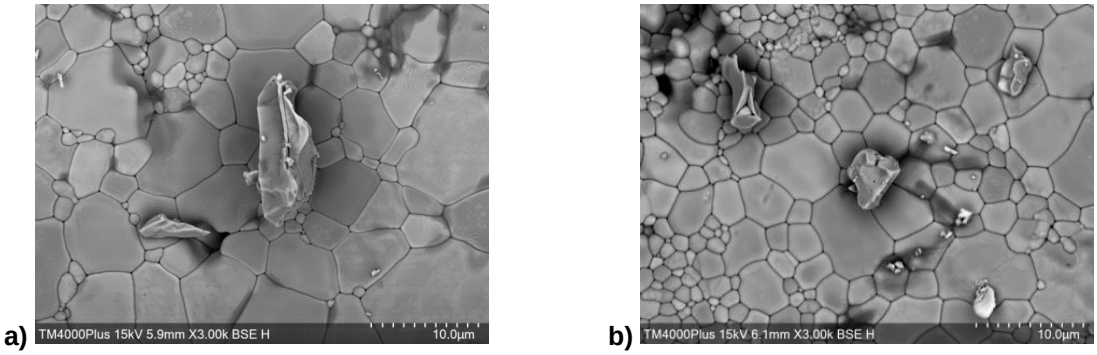

Figure 41 – SEM image of a UO_2-2 $^w/_o$ Eu_2O_3 pellet surface after 1 month of dissolution experiment in (a) 1'600 ppm and (b) 3'500 ppm H_3BO_3

3.3.8. Thermogravimetric tests

The fuel-cladding interface can be described as composed of two zones, one closer to the cladding (polycrystalline ZrO_2) and a second one nearer the fuel pellet, which is mainly formed by solid solutions of $(U,Zr)O_2$ (cubic fluorite) [Frost, 2020]. This second layer is composed by variable relative concentrations of U and Zr [Kim, 2010; NEA, 2015]. PCI is one of the causes identified as leading to potential cladding failure [IAEA, 2010; NEA, 2005]. In the framework of back-end of nuclear fuel, prior to or after the dry interim storage period, the nuclear fuel assemblies can be transferred into a transfer unit to change from transport to storage cask. The dry transfer system provides an "interface between large and small casks and between storage-only and transportation casks" [Christensen, 1999] and it can also allow fuel handling for examination and repair [Christensen, 1999; El-Samrah, 2021]. Considering possible scenarios that may take place in a dry interim storage facility, including transfer module, important variables such as time/temperature limits need further investigation to prevent SNF oxidation when it is exposed to an oxidising atmosphere. In such scenario, the degradation of both, Zircaloy cladding against gross rupture, and the irradiated UO_2, needs to be fully understood for the appropriate technical support to be adopted in order to prevent release of radioactive material [NRC, 2006; NRC, 2017; NRC, 2019]. The availability of oxygen (oxidant agent) and temperatures higher than 250 °C may entail the oxidation of the fuel matrix from UO_2 (fluorite, cubic) to U_3O_8 (orthorhombic) that implies a volume increase of around 36%, which in turn may result in pulverisation, spallation, splitting of the sheath and leakage of radioactive material. The oxidation of UO_2 constitutes a two-step reaction: $UO_2 \rightarrow U_4O_9/U_3O_7 \rightarrow U_3O_8$. The better-required final stabilised form for the uranium oxides should be limited to intermediate oxides U_4O_9, where fluorite structure is preserved. Although oxidation of UO_2 under different surrounding conditions, such as temperature and oxygen partial pressure, has been studied for more than five decades [McEachern, 1998; Sinkov, 2008], some topics still remain unclear and are not even included in fuel performance codes, like the influence of the fuel-cladding inter-diffusion zone [Hanson, 1998; Frost, 2020].

Understanding the properties of the pellet-clad bonding layers is worth studying. Specifically, the potential chemical oxidation resistance of UO_2 (matrix fuel) to U_3O_8 by the ZrO_2/Zr system, after a potential air intrusion, in case of undetected damaged cladding (zirconium alloy) or defective fuel, is relevant in terms of assessing fuel integrity covering all possible scenarios during storage. Therefore, assuming evidences on Zircaloy-fuel interaction [Kim, 2010; NRC, 2017], characterisation of ZrO_2-doped UO_2 pellets including morphological, chemical, and crystallographic analyses was conducted. Furthermore, some results of the oxidation behaviour of these powdered samples under dry conditions were shown, that prove the chemical oxidation resistance of UO_2 to U_3O_8, when it forms part of the $(U,Zr)O_2$ solution, trying to mimic the chemical bonding between ZrO_2 and UO_2. In this study, both individual and joint effect of temperature were investigated, oxygen partial pressure and Zr content to analyse complex scenarios facing matrix oxidation with competing factors [Rodríguez, 2023].

At CIEMAT, the behaviour of the pellet-cladding interface under a potential oxygen exposure during dry storage and subsequent transportation conditions has been studied. More specifically, the ultimate goal has been to provide empirical data on chemical oxidation resistance of UO_2 to U_3O_8 because of the interlayer bonding of urania and zirconia formed during reactor operation in LWR. Three issues have been addressed in detail:

1. the synthesis and microstructural characterisation of ad-hoc fuel surrogate of PCI in a representative way (i.e., UO_2 ceramics doped with different ZrO_2 contents)
2. the evolution of these ZrO_2-UO_2 systems (with a range of ZrO_2 contents) due to oxidising degradation, and
3. the overall responses of powdered samples at temperature and oxygen partial pressure coupling effects

Mixtures of ZrO_2-doped UO_2, in the full range of possible compositions across the layer (simulating the ZrO_2/UO_2 chemical bonding in LWR fuels, PCI phenomenon), and undoped UO_2 have been obtained via "powder route" and characterised at CIEMAT.

The oxidation behaviour as a function of temperature and oxygen partial pressure was performed using thermogravimetry on x wt% ZrO_2-UO_2 (x=0, 20, 40, 80 and 100) samples for in-situ monitoring of the oxidation reaction of UO_2 to U_3O_8 under "representative" conditions of a dry environment as a function of ZrO_2 content, oxidising atmosphere (1 and 21 $\%O_2$), and temperature. A series of thermogravimetric analysis (TGA) tests was performed and oxidised samples were also characterised. Solid samples were analysed under non-isothermal ($10\,^{\circ}C \cdot min^{-1}$, up to 900 °C) and isothermal (100, 300 and 400 °C) conditions.

The thermal analysis on some representative model materials of PCI showed that, under non-isothermal systems, the presence of zirconium in the UO_2 fuel matrix provides certain oxidation resistance to U_3O_8, hindering matrix oxidation (see Figure 42). No clear differences were observed between different oxidising conditions (1 and 21 $\%O_2$). The use of relatively low partial pressures of oxygen did not avoid severe degradation, although the evidences found for samples analysed suggest that, over a certain ZrO_2 content threshold, the oxidation degree is slightly influenced by oxygen pressure. For ZrO_2 contents below 40 wt% in UO_2, the higher the O_2%, the higher the oxidation degree of uranium matrix was observed, indicating that ZrO_2 can improve the thermal oxidative stability of UO_2 to some extent. Difficulties about ZrO_2 solubility in the UO_2 matrix and polymorphism of ZrO_2 can affect the subsequent oxidation responses of the tested samples.

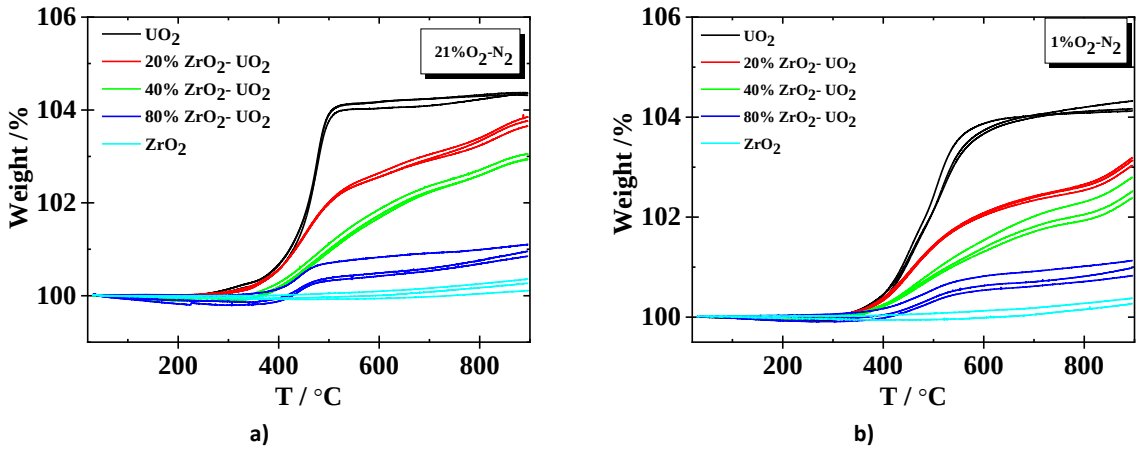

Figure 42 – Weight change curves at 21%O_2 (a) and 1%O_2 (b) of: UO_2, 20 wt% ZrO_2 -UO_2, 40 wt% ZrO_2 -UO_2, 80 wt% ZrO_2 -UO_2, ZrO_2

Under isothermal conditions, the temperature as a key affecting parameter on fuel matrix alteration is confirmed (see an example at 300 ºC in Figure 43, further details can be found in D8.10 [König, 2024]). Increasing ZrO_2 content decreases the mean oxidation degree. In general, the effect of low oxygen concentration in the gas phase induces a moderation of the oxidation degree on average, for the same Zr content but with no remarkable implications. Further experimental work is necessary to better characterise and simulate the UO_2-ZrO_2 inter-diffusion layer. Additional analyses with controlled ZrO_2 polymorphic phases will refine the data and contribute to describe the post-PCI behaviour in the context of a potential oxygen exposure during storage conditions.

Therefore, the results of this analysis are important not only for possible design/construction of loading/unloading FAs cells but also for transport of SNF in O_2 containing environments, once closure of pellet-cladding gap occurs. It also important in evaluating a conventional method to be applied for understanding the oxidation behaviour of SNF during the back-end of the fuel cycle, i.e., handling transport and storage. However, to implement this assumption on real irradiated fuel, further characterisation techniques by considering the presence of FP (e.g., Cs, I, Cd) in the Zr/ZrO_2 zone must be explored.

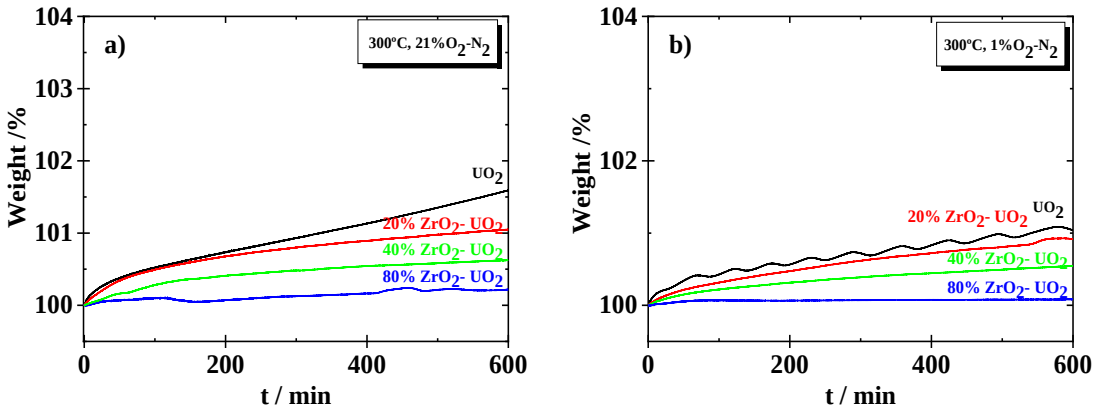

Figure 43 – Weight curves at 21% O_2 (a) and 1% O_2 (b) under isothermal conditions at 300 °C during 10 h of: UO_2, 20 wt% ZrO_2 -UO_2, 40 wt% ZrO_2 -UO_2, 80 wt% ZrO_2 -UO_2

3.3.9. Helium property measurements

Helium (He) already present in samples (coming from alpha-decay) or intentionally introduced can be measured in single crystals, polycristals and powders using several techniques. This enables the determination of He properties such as solubility, diffusion coefficient and inventory in uranium oxides.

Helium can be introduced in uranium oxides using three different methods: infusion, implantation or by alpha-decay doping:

1. He Infusion:
   Infusion was used in several studies to introduce He (see references in [Luzzi, 2018]) and different devices can be used. For example, the Helium Infusion Device (HEIDI) was developed at JRC-Karlsruhe [Maugeri, 2009]. It aims to infuse helium into a uranium oxide sample by heating it with a laser at high temperature under high He pressure up to 200 MPa. The sample temperature is measured by a pyrometer. In such conditions, a homogeneous helium profile can be obtained, if infusion time is long enough. The amount of helium infused depends on pressure and temperature as well as microstructure and damage already present in the sample. Such introduction technique allows only He to be introduced without creating defects if the

infusion time is short enough [Colle, 2013]. It is therefore particularly well suited for measurement of He solubility in uranium oxides. For example, Maugeri et al. found a He solubility of $2.29 \cdot 10^{-8} \pm 4 \cdot 10^{-10}$ mol·g^{-1} (6.3±0.1 at·ppm) at 1523 K and 10^8 Pa in UO_2 single crystal [Maugeri, 2009].

2. ^{3}He implantation:
Helium can be introduced into uranium oxides by implantation of various He isotopes. The ^{3}He isotope is of particular interest because it can be analysed using Nuclear Reaction Analysis (see dedicated section below). The implantation of energetic ions induces simultaneously damage (essentially point defects) in the samples. The energy of the ^{3}He beam can be chosen to be adapted to the analysis techniques. In most cases, ^{3}He ions of 0.5 or 1 MeV are used. The fluence can also be selected to obtain different He concentrations. Depth profiles of ^{3}He and damage (atomic displacements (dpa)) can be calculated using the SRIM simulation code [Ziegler, 2010] in the so-called KP option (quick calculation with Kinchin-Pease formalism). The displacement energy thresholds for oxygen and uranium atoms are set at 20 and 40 eV respectively [Soullard, 1985]. ^{3}He ions of 1 MeV penetrate in UO_2 up to 2 µm (called the ion range). The He concentration is very low in the first 1 µm and increases to a maximum value of 0.35 at% at 2 µm depth for a fluence of 1·1016 ^{3}He+·cm^{-2}. Damage is roughly flat at an average value of 0.014 dpa in a region down to around 1 µm depth. Implantation is usually performed by focusing the beam (1×1 mm^2) and by sweeping it over the disk surface to ensure a homogeneous dose. Implantation temperature can be controlled as CEMHTI's DIADDHEM system [Chamssedine, 2010]. The maximum He concentration introduced under these conditions is very close to the amount of He (~0.37 at%) reached in UO_2 after a burnup of 52 GWd/t and 50.000 years of storage [Ferry, 2010]. In comparison, He content reached 0.26 at% in a 17-year-old irradiated MOX fuel (after discharge from the reactor) with an average burnup of 42.6 GWd/t and a Pu content of 3.5% [Colle, 2014]. The He concentration can be increased incrementing the He fluence as it has been done in [Guilbert, 2003]. By incrementing the fluence by a factor of 5, He platelets can be formed after heating at the ion range, resulting in blistering and flaking of the top layer of the implanted sample with a thickness of the order of the ion range.

3. Alpha-decay doping:
Helium can be also introduced by doping uranium oxides with radioisotopes that decay by emitting alpha particles such as ^{238}Pu. In this case, He is introduced at the same time as irradiation damage. For example, ^{238}Pu doped UO_2 can be synthesised by a sol–gel technique. The advantage of this technique is to obtain a uniform distribution of the dopants in UO_2. After compacting and sintering the pellets, a homogeneous solid solution with a density of 94% of the theoretical value can be obtained [Talip, 2014a]. The He amount and damage depends on the Pu content, its isotopic composition, the storage time and the temperature history of the sample. For alpha-doped UO_2 samples (which contain depleted UO_2) with 0.1 wt% of additive containing 66.7 wt% of ^{238}Pu, the He amount and damage dose were estimated at 1.6 at·g^{-1} and 0.04 dpa respectively after 15 years of storage [Talip, 2014a].

Essentially, two types of techniques can be used to analyse He in materials. Nuclear reaction analysis (NRA) allows to measure the He content, while mass spectrometry can be used to determine the amount of He released when sample is heated. It has to be noticed that He bubbles can be observed using TEM but this technique does not allow the quantification of He.

Nuclear reaction analysis (NRA)

NRA can be used to detect He in materials using the nuclear reaction $^{3}He(^{2}H, ^{1}H)\alpha$ [Trocellier, 2003; Guilbert, 2004; Roudil, 2004; Martin, 2006; Pipon, 2009]. Several authors used these techniques with different versions of implementation. He content can be measured by proton or alpha particle detection, both products of the nuclear reaction. As the energy of incident ^{2}H ions is fixed at 900 keV, the amount of He can be measured in the first 3 µm of depth in uranium oxides. Using a micro-beam of deuterons, the He content can be mapped at the microscopic scale with a resolution of 2 to 3 µm as has been achieved in LPS Saclay and CENBG Bordeaux [Sauvage, 2005]. DIADDHEM, the device installed on one beam line of the Pelletron accelerator at CEMHTI, is schematized in Figure 44 and described by Chamssedine et al. [Chamssedine, 2010]. The alpha particles energy can be measured in coincidence with the protons, making it possible to determine the depth at which the reaction occurred and measuring He depth profiles. In this set-up, samples can be heated under vacuum to track He release and the change in depth profile as a function of temperature and of in situ or ex situ annealing. Interesting, Garcia et al. took advantage of three pieces of information on He release kinetics, depth profiles and lateral mapping in polycrystals to distinguish two He diffusion coefficients: one in the grains and one at the grain boundaries [Garcia, 2012].

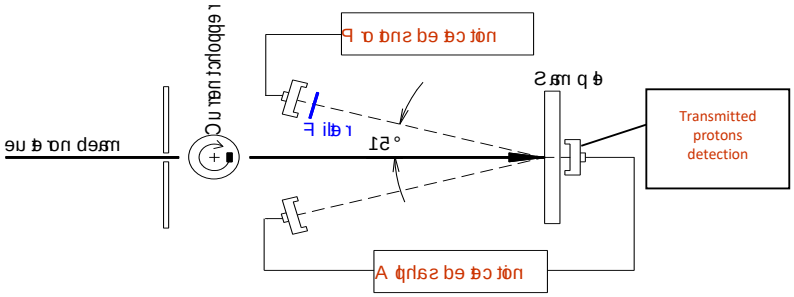

Figure 44 – Schematic view of the DIADDHEM set-up used to measure the ^{3}He content in uranium oxides

Knudsen Cell Effusion Mass-Spectrometer (KEMS)

At JRC-Karlsruhe, a set-up combining a Knudsen cell and a quadrupole mass spectrometer was developed, as described in [Colle, 2014]. The samples placed in a tungsten Knudsen cell are heated in vacuum up to ~2700 K, the temperature at which UO_2 is totally vaporised. The species, gases and vapour leave the cell and are ionised and measured with a mass spectrometer placed above the cell, cf. scheme in Figure 45. A direct semi-quantitative evaluation of the gas is possible within the KEMS. A quantitative analysis can only be performed together with an equipment (Q-GAMES) that measures the released gas together with a spike of He for calibration. The dynamic range of measurement is between 10^{-12} and 10^{-5} mol with a relative error below 2%.

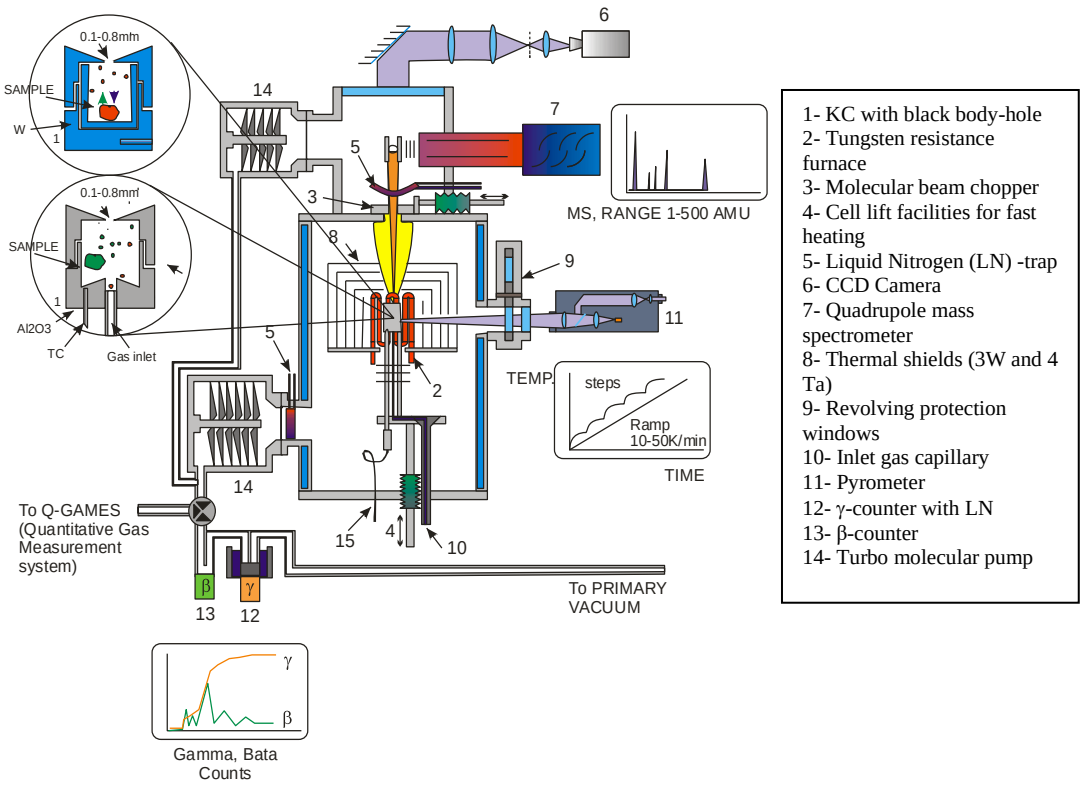

Figure 45 – Knudsen Cell Effusion Mass-Spectrometer (KEMS) used for the gas desorption

The cell used in this work was a tungsten cell.

3.3.10. Damage characterisation in uranium oxides

Damage induced in uranium oxides by alpha particles can influence the gas diffusion in spent fuel [Ferry, 2005]. The damage can be characterised using classic methods such as XRD, TEM, RBS/C (see [Matzke, 1992a] as a review). In the following, the focus is on the brief description of two techniques newly used for these materials: Raman spectroscopy and positron annihilation spectroscopy.

Raman spectroscopy

Raman spectroscopy allows determining the vibration modes in molecules through inelastic diffusion of the light. In uranium oxides, this technique was used to get information on:

- The stoichiometry: Hyper-stoichiometry is charaterised by high-frequency T_{2g} – at 445 cm^{-1} for $UO_{2.00}$ – band shift and broadening and appearance of two new Raman modes at ~575 cm^{-1} (T_{1u}LO mode) and at ~650 cm^{-1} in association with cuboctahedral type oxygen cluster defects by Desgranges et al. [Desgranges, 2012]. In hypo-stochiometric $(U,Ce)O_{2-x}$ [Elorrieta, 2018b], a new band at ~535 cm^{-1} is observed increasing with Ce concentration. In $(U,Am)O_{2-x}$ solid solutions, Epifano et al. [Epifano, 2020] observed by Raman the three bands at ~535, ~575 and at ~632 cm^{-1}, while Am^{3+} and U^{4+}/U^{5+} were present in the material. Medyk et al. showed that in $(U,Pu)O_{2-x}$ solid samples containing mostly ^{239}Pu and natural uranium, the T_{2g} band shifts toward lower frequencies [Medyk, 2020].
- The damage: This triplet band, commonly called the U1, U2 and U3 defect bands at 535, 575 and 635 cm^{-1} respectively, is also observed for irradiated UO_2 and PuO_2 samples [Mohun, 2016; Mohun, 2019; Villa, 2019; Guimbretière, 2012; Desgranges, 2014].

- The Pu content: In (U,Pu)O_{2-x} solid samples containing mostly ^{239}Pu and natural uranium, and tracks of ^{241}Am, the Pu/(U+Pu+Am) content could be determined from Raman spectra [Medyk, 2020].

  Raman spectra can be measured in two modes: i) by focusing the laser beam in the center of the larger grains, and ii) using mapping on a surface sufficiently large to analyse several grains. The wavelength of excitation laser can be fixed at various values: 488, 532, 547 or 633 nm. For example, at CEMHTI, an InVia Qontor instrument from Renishaw was used for these analyses using a 633 nm laser and a 1800 l/mm grating centered at 950 cm^{-1}, such that each spectrum spans from 327 to 1510 cm^{-1}.

Positron Annihilation Spectroscopy (PAS)

PAS is based on both fundamental properties of positron in solids: i) it annihilates with electron leading to the emission of gamma rays at the energy of around 511 keV; ii) it is trapped in vacancy defects where it annihilates enabling characterisation of vacancy defects [Hautojärvi, 1995]. Fast positrons directly emitted from ^{22}Na source or slow positron beam enable to probe thick samples (~100µm deep) and close to the surface (in the first 1.5 µm) respectively. Two different spectrometers can be used to measure two complementary signatures of the positron annihilation: the positron lifetime τ (PALS, Positron annihilation lifetime spectroscopy) and the electron-positron momentum distribution obtained by measuring the Doppler broadening (DB) of the annihilation line with a DB spectrometer. For example, at the CEMHTI laboratory a DB spectrometer is coupled to a slow positron beam (SPB-DB). A comprehensive description of the experimental setup and the basics of this powerful method are described in [Desgardin, 2001]. The Doppler broadening of the annihilation line centered at 511 keV is characterised by using two parameters *S* and *W*. *S*, defined as the ratio of counts in the central region of the spectrum to the total counts, represents the fraction of positron-electron pairs annihilated with low momentum and is thus related mostly to annihilations with valence electrons. *W*, the ratio of counts in the wing regions of the spectrum to the total counts, represents the fraction of positron-electron pairs annihilated with high momentum and hence is more specifically related to the annihilations of positrons with core electrons. For the following, the momentum ranges for the calculation of *S* and *W* correspond to ranges of energies of photons of [510.28–511.72 keV] for *S*, and [504.27–508.29 keV] and [513.71–517.73 keV] for *W*.

Each material exhibits specific τ_L, S_L and W_L values, as a signature of lifetime and momentum distribution of electrons in the perfect lattice (i.e., without vacancy defects). When positrons are trapped at vacancies, positron is trapped in vacancy where the electron density is low and the annihilation with core electrons decreases. The positron lifetime τ decreases and the positron-electron momentum distribution (or annihilation line) narrows, resulting in an increase of *S* and decrease of *W*. Each type of vacancy defects *j* is characterised by some specific values τ_j, S_j and W_j. Generally, because *S* and *W* are also sensitive to the electronic environment of the positron when it annihilates, these parameters could detect the chemical decoration of vacancy defects.

S_{ref} = 0.371±0.002, W_{ref} = 0.079±0.001 and τ_{ref} = 170 ps were measured in UO_2 reference samples annealed at 1'700 °C during 24 hours in Ar-H_2. They were associated to annihilation at non-vacancy defects [Labrim, 2001]. These non-vacancy defects were predicted to be negative ions (oxygen interstitials O_i^{2-} or valence II and III impurities) that could be dissolved in UO_2.

In UO_2 irradiated with 1 MeV He [Labrim, 2006], SPB-DB results plotted in *S(W)* graph showed experimental points aligned on the same D1 line with different position. The position depends on the damage dose from the S_{ref}, W_{ref} point for no damage to the point with a maximum S_{max} value, and minimum W_{min} obtained for a mean damage dose around 0.014 dpa in the positron probed region (0 – 1'100 nm) for the ^{3}He fluence of $1 \cdot 10^{16}$ cm^{-2} [Labrim, 2006]. S_{max} and W_{min} do not change when He fluence increases up to $1 \cdot 10^{17}$ cm^{-2} or damage dose up to 0.14. It is called He saturation point and the associated annihilation characteristics are S_{HeSat} W_{HeSat} (S_{HeSat} = 0.398 ± 0.002, W_{HeSat} = 0.069 ± 0.001).

All the experimental points aligned on this line D1 have been associated to positron annihilations as trapped in uranium vacancy related complexes by comparison with irradiation performed with electrons with sufficiently high energy to allow displacements in the U sublattice and show a positron lifetime of 316 ± 7 ps [Mohun, 2019; Wiktor, 2014]. Up to now, no oxygen related vacancy defects could be detected probably due to their positive charge state.

3.4. Numerical methods and analysis

3.4.1. Finite element analysis and mechanical state of the fuel

Extensive research studies [SCIP, 2013; Billone, 2013a; Billone, 2019] have been performed to investigate phenomena that affect the mechanical state of nuclear fuel and cladding during irradiation. The vast majority of the fuel-performance codes examine mainly the thermo-mechanical properties of the fuel/cladding during irradiation, where numerous models have been developed and validated against experimental data. However, experimental activities using SNF rods experiencing interim and/or long-term dry storage conditions are rather limited. The main reason for this is the inherent difficulty of working with highly activated materials and the associated costs for such experiments.

Over the last couple of decades, there has been an increasing need to develop a better phenomenological understanding of the SNF rod mechanical behaviour throughout the different stages of the back-end of the fuel cycle, i.e. during wet/dry storage, transport and handling. This need is mainly associated with the licensing requirements related to the extension of the SNF dry storage periods in transport and storage casks (TSCs) and to their integrity evaluation after transport and/or handling operations related to final disposal. The technical gaps have been identified and presented in [NRC, 2014; UFDC, 2012]. The need to generate experimental data, especially for the high-burnup and MOX fuels, was highlighted in order to contribute to the validation and further development of analytical and numerical models. This chapter attempts to provide a review on the SNF rod mechanical-response studies by means of numerical and/or analytical approaches complemented by experimental investigations on irradiated SNF rods.

One of the first integrated programmes addressing SNF integrity after dry storage was developed by Areva TN and International Nuclear Services in the early 2000s. The Fuel Integrity Project (FIP) studied the impact response of both irradiated and unirradiated fuel with the main objective being the development of a methodology to evaluate the nature and extent of damage to SNF assemblies during TSC drop accidents [Purcell, 2004]. The experimental work included an extensive testing programme on both fresh and spent rodlets in order to obtain information on the SNF properties (as a fuel/cladding composite material) and to determine some uncertainties (e.g., pellet/cladding friction coefficients) relative to specific loading configurations of the SNF rods (i.e. static and dynamic bending, buckling). The main results of the experimental campaign are summarised in [Purcell, 2004; Zéachandirin, 2011], where the data obtained are used to develop analytical calculations for the rod behaviour in the elastic domain of the cladding and numerical models for Finite Element Analysis (FEA) of the rod behaviour in the cladding plastic domain. The FEA models were validated against 3-point bending tests on SNF rods and lateral compression tests on claddings [Dallongeville, 2010; Dallongeville, 2005]. The FIP methodology was built upon these results, and it distinguishes cases depending on the type of load (direction), the type of fuel assembly and the irradiation state (fresh or used) of the rod [Zéachandirin, 2011; Dallongeville, 2012]. The major results of this project concerned the uncertainties in the modelling of the fuel rods, the determination of the irradiated cladding properties related to burnup and assumptions on the fuel-mass-release analysis.

Another methodology has been proposed by Structural Integrity Associates, Inc. (former ANATECH) that considers the high-burnup effects mostly associated with the hydrogen concentration and hydride orientation in the cladding [Rashid, 2004a]. A major assumption of this method is the consideration of a static analysis, rather than dynamic, which conservatively bounds the dynamic analysis results. Finite element models have been developed where the essential feature of these models is the damage

formulation, which describes the interactions of the cladding response to specific failure modes. Therefore, no a posteriori application of failure criteria is needed in comparison to the FIP methodology. The cladding-failure criteria have been derived from limited experimental data on burst tests of empty claddings [Rashid, 2004b; Rashid, 2004c], with no reference tests used for the finite element model validation. Although this method provides a step towards a quantitative analysis of the SNF rod failures for transport accidents, its application is rather complicated and experimental validation using real SNF rods is still needed.

In order to address some of the aforementioned data gaps, it was necessary to develop experimental campaigns to macroscopically and fundamentally study the mechanical response and failure processes of the fuel/cladding composite system under static and dynamic loads. JRC – Karlsruhe and Oak Ridge National Laboratory (ORNL) were among the first to independently develop such integrated campaigns and make their findings public.

JRC–Karlsruhe initiated an extensive experimental campaign to characterise the quasi-static and dynamic response of surrogate and LWR SNF rodlets using three-point bending and gravitational impact tests, respectively, as described in Section 3.3.5. In collaboration with GNS (Germany) and Areva, the first results of the impact tests were published in [Papaioannou, 2009b; Papaioannou, 2009c; Rondinella, 2012]. These studies focused on the characterisation of the fuel mass release and revealed remarkable similarities among all samples used, corresponding to $\leq$ 2 g of fuel release per fracture, and no indication associated with high-burnup rim structure in the size classification of the released particulates. Investigations following this work included the collaboration with Nagra (Switzerland) and the Federal Institute for Materials Research and Testing (BAM, Germany) to develop the three-point bending apparatus and the experimental optimisation of the impact tests [Vlassopoulos, 2017b]. Experimental results for the bending tests consist of the flexural stress-strain curves, bending angles to fracture and fuel mass release characterisation, where a correlation between the level of ductility of the sample and its burnup value was revealed [Nasyrow, 2016; Vlassopoulos 2018b]. To examine the strain-rate dependence of the SNF rod response, an Image Analysis (IA) methodology was developed to analyse the recorded high-speed videos of the impact tests. The experimental campaign is complemented by numerical studies conducted independently by Nagra and BAM using FEA [Vlassopoulos, 2018b; Ballheimer, 2016; Vlassopoulos, 2018a]. Two types of models were developed to simulate the rod response using the simple beam approach or by explicitly modelling the pellets and the cladding. The model validation was performed against the experimental data, and the cladding failure criteria were derived by analysing the stresses and strains at the bending angles of fracture.

Another major campaign was established by the U.S. Department of Energy - Office of Nuclear Energy (DOE-NE). The Used Fuel Disposition Campaign (UFDC) [Adkins, 2013] aims to conduct R&D activities related to storage, transport and disposal of SNF and high-level waste. Within this framework, ORNL has developed a SNF-vibration testing procedure to quantify the reliability of the SNF during transport [Jiang, 2014; Wang, 2018]. Experimental activities include static and dynamic SNF testing under simulated transport conditions using a cyclic integrated reversible-bending fatigue tester (CIRFT). The studies revealed a detailed understanding of the mechanical interactions between pellets and cladding, and of the effect of loading rate and loading mode on the fatigue damage evolution of high-burnup SNF under transport conditions [Wang, 2018]. Major findings have shown the importance of the SNF system interface bonding in the vibration performance, the contribution of the fuel to the SNF system stiffness and the SNF failure initiation at the pellet-cladding interface region. FEA was used to investigate the relative importance of the pellet-pellet and pellet-cladding interfacial bonding efficiency with regard to the SNF dynamic system performance, which showed a significant reduction of the SNF system flexural rigidity in case of debonding [Jiang, 2014; Jiang, 2016a; FY2014; Jiang, 2016b; FY2017]. The intensity of the contact interaction as well as the impact loading between spacer grids and SNF rods have also been investigated using FEA. A first approach towards SNF assembly modelling was made by simulating a subassembly model to investigate the SNF system's dynamic stability under normal transport conditions [Jiang, 2016a].

Complementary numerical studies within the UFDC framework, conducted as part of a collaborative effort between different U.S. national laboratories, include FEA on the rod scale [Coleman, 2014] and the SNF assembly level [Sanborn, 2014]. In these studies, the importance of the uncertainties in the SNF material properties and in the non-linear geometric behaviour of the model has been highlighted. For this reason, it was considered necessary to develop the equivalent beam properties of the detailed SNF system. In this respect, the aims of the detailed modelling are to establish reasonable lower/upper bounds and best-estimate material properties. The transport-damage prediction in a worst-case scenario during normal conditions of transport (NCT) was found to be approximately 18 % of the expected SNF fatigue limit, resulting in no SNF rod failures.

For the estimation of the SNF assembly behaviour during handling operations, CEA (with the support of EDF) has conducted three-point bending tests on six-cycle fuel rod segments complemented by FEA [Guerin, 2013]. An equivalent constitutive equation for the SNF rod system has been derived, taking into account the experimental force-displacement curve and maximum failure strain/curvature. The relative contribution of the pellets and cladding to the rod global behaviour has been estimated. The results were used to model a two-dimensional SNF assembly with a beam element in CAST3M. Bending calculations were performed and failure criteria were derived by comparing the calculated bending angles to the experimental ones at failure.

To evaluate the mechanical integrity of high-burnup SNF assemblies under accident transport conditions, BAM has developed an analytical methodology [Ballheimer, 2010; Schrödl, 2010]. The rods are considered as continuous beams, supported at the positions of the grids, and are excited dynamically through the supports (and not by directly applied external loading). The beams are modelled with only elastic material behaviour. This assumption seems to be justified by the drastic decrease in cladding ductility in high-burnup rods. In addition, radial hydrides are not considered to affect the failure mode under bending loadings. Considering certain boundary conditions, an analytical derivation of the effective static load and the beam's global displacement is possible. To estimate the fuel mass release, the critical deflection of the cladding is compared against the limiting beam deflection, and a bounding release per rod-breakage has been considered. This study clearly highlights the importance of the experimental verification of the approach as well as the importance of the accessibility of data generated by experimental testing of SNF rods.

Another extensive integrated campaign aimed at evaluating the dynamic response of SNF rods has been carried out in a collaborative effort by several Japanese institutions, as was already reported in the SPAR III programme [IAEA, 2015]. The experimental activities include basic mechanical tests on claddings and dynamic impact tests on fuel rods [Ozawa, 2013; Hirose, 2012; Hirose, 2013]. Axial and lateral loading of fuel rods were used to study the rod failure loads, strains, and the fuel mass release. The fuel material release from BWR SNF rods was equivalent to approximately two or three pellets under axial and lateral impact testing, respectively. For the PWR cases, the fuel mass release was bounded to 1.4 g. FEA was used to study the SNF rod buckling behaviour [Minamoto, 2011] as well as the dynamic response of fuel rods under side drop loading [Minamoto, 2015].

3.4.2. SNF rodlet performance under flexural loads

Numerical studies were performed to complement the experimental investigations with focus on modelling the bending behaviour and the mechanical properties of the examined spent nuclear fuel (SNF) rods. With the use of Finite Element Analysis (FEA) it is attempted to gain a better understanding of the observed experimental results, to investigate the mechanical properties of the SNF rod materials and to extend the examination of the rod’s integrity to conditions and configurations outside the domain defined by the experimental studies themselves.

From the experimental investigations at JRC-Karlsruhe (cf. Section 3.3.5), the elastic properties of the rod/cladding were approximated with the use and based on the assumptions of the simple beam theory. Among others, the most important assumption is that the material is experiencing only linear elastic deformation. In addition, the so-called "beam", refers to an unstressed, homogenous and isotropic

material with given cross-section. As a result, the range of validity of this theory lies within the elastic region of the material and it cannot be used to accurately describe the relation of flexural stress-strain developed during plastic deformation. Moreover, the SNF rods are composite beams consisting of metallic cladding tubes and ceramic pellets, which have different material properties and are significantly heterogeneous (especially the irradiated fuel). Therefore, the application of the simple beam theory in our case will simply provide information on the effective (fictitious) mechanical properties of a homogeneous beam, which deforms identically to the SNF rod. Although this analysis may not directly investigate the mechanical properties of the cladding and the pellets, it still provides valuable information, which can be used either in analytical or numerical approaches when investigating the SNF response under bending loads.

A more elaborate approach towards the derivation of the cladding mechanical properties is with the use of FEA. The 3-point bending experiments are simulated using three-dimensional static structural analysis in ANSYS® Mechanical. The calibration of the finite element models was performed on the 3-point bending experimental results with the use of "OptiSLang", an ANSYS® integrated software package for sensitivity analysis and optimisation. In short, the finite element models were parametrised so that the variation of certain variables (i.e., cladding mechanical properties) could be used to explore their effect on the results. Then, the numerical results were compared to the experimental data by implementing an objective function, which calculates the sum of the squared errors (or differences between experimental and numerical data) over all time steps. Thus, OptiSLang explored the cause of non-matching results, to understand the driving parameters, adjust the parameters for the numerical model and finally optimize the specific function of interest. The objective in this study was to examine any possible dependence of mechanical properties of the cladding on the rod's average burnup. The presented results refer exemplarily to KKG SNF rods. In the end, the cladding "effective" mechanical properties can be derived as a result of the optimization process of the model's parameters. The term "effective" refers to the fact that cladding properties can also be influenced by the modelling assumptions/simplifications that were considered in the finite element model (FEM). However, a thorough sensitivity analysis was conducted to investigate the relative importance of various numerical parameters and modelling approaches on the derived numerical results, namely the load-displacement curve of a sample in the three-point bending test. As a result, the derived cladding mechanical properties could well be used to macroscopically characterise the cladding's mechanical properties.

The development of a three-dimensional finite element model representing a fuel rod segment is a challenging task, since it includes large deformations with non-linear behaviour and undefined geometry of the cladding, pellets and their interaction. The development of the preliminary finite element models was based on the results from the three-point bending test on surrogate samples. In this case, the geometrical characteristics and mechanical properties of the pellets and cladding are known, in comparison to the irradiated samples, therefore the number of modelling uncertainties can be significantly reduced.

Figure 46a shows an overview of a FEM of a fuel rod segment simulating a surrogate rodlet in the three-point bending test. The pellets and cladding are modelled as solid elements with a flexible stiffness behaviour. The nominal mechanical and geometrical properties were used, as given in [Vlassopoulos, 2021]. The model exploits one fourth symmetry to reduce its size (or number of elements) and minimise the computational time. The symmetry planes are along the loading axis and at the pellets' mid-section (or at y- and x-axes). The former and the support are modelled as shell elements with rigid behaviour, which does not allow their deformation. Finer mesh was employed at the areas of interest, being the pellet and cladding at the loading point and at the former and support contact areas.

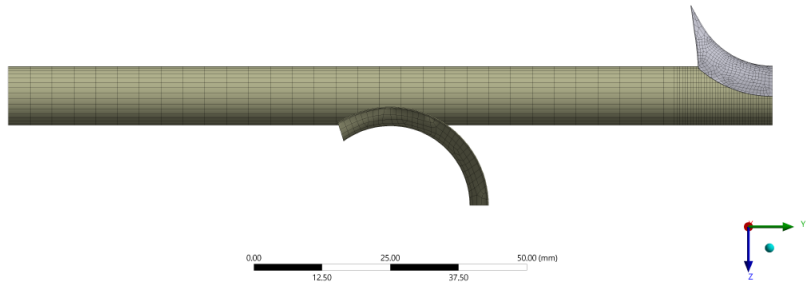

(a) Mesh elements of cladding and former/support.

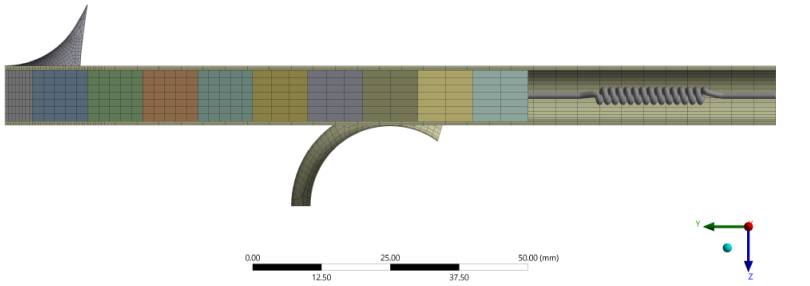

(b) Mesh elements of pellets and spring attachment.

Figure 46 – 3D implicit FEA simulating the three-point bending behaviour of a fuel rodlet

A series of boundary conditions were used to represent the experimental settings. The pellets were retained with the use of a spring attached at the end-pellet, as shown in Figure 46b. Frictionless contact was applied between the cladding and the support to simulate its rotation. Frictional contacts were used for the pellet-pellet, pellet-cladding and former-cladding interactions. In addition, the sample's internal pressure was simulated with a uniform pressure acting on the internal surface of the cladding. Moreover, a fixed support was placed at the shell element representing the support. Finally, loads are applied by assigning a maximum displacement at the former as determined in the experimental results (fracture point).

The mechanical response of the cladding in plasticity was defined using the Voce material law. ANSYS® uses the expression of Voce law as described in the following equation:

$$\sigma = \sigma_0 + R_0\varepsilon_{pl} + R_{inf}\left(1 - e^{-b\varepsilon_{pl}}\right)$$

where σ is the calculated stress, σ_o is the initial yield stress (YS), $\boldsymbol{\varepsilon}_{pl}$ is the plastic strain, R_0 is the linear coefficient, R_{inf} is the exponential coefficient and b is the exponential saturation coefficient.

Material properties of pellets were defined using the cast-iron plasticity model. This material law is widely used for modelling ceramic materials as it accounts for different plastic yield and hardening in tension and compression, while still assuming isotropic elastic behaviour. Pellet cracking is indirectly modelled by defining very low values for the compressive and tensile plastic modulus. Based on this approach and in combination with the low tangent modulus that was defined (gradient of plastic region), if the pellet yields under any type of load, then its load bearing capabilities are significantly hindered.

Based on this model, an extensive sensitivity analysis was performed on numerous numerical and physical parameters in order to examine their relative importance on the results and the uncertainty that could be introduced based on different modelling approaches. A final version of the finite element model was built upon the results of the sensitivity study, as the best compromise between computational time and solution quality.

In addition, a finite element model representing the irradiated samples was constructed based on a series of assumptions. Their validity was investigated, and the finite element model was used to simulate the mechanical response of the samples under three-point bending conditions. OptiSLang was used to

calibrate the finite element models against the bending experimental results, to understand the most important parameters of the model and finally to derive the cladding mechanical properties. For this purpose, an optimisation problem was solved aiming at reducing the differences in terms of load-displacement curves between numerical and experimental results. An objective function is created by comparing the load-displacement curve as derived from the simulation to the experimental results. OptiSLang explores the solution space of this optimisation problem by intelligently generating a number of FEA simulations by varying the parameter values. As initial values and variable range for the model parameters linked to fuel and cladding, experimental data (e.g., elastic modulus) found in the open literature are used. The driving parameters of the model are further adjusted until the model calibration is finally achieved by minimising the difference between predicted and experimental results. Figure 47a shows the load-displacement curve comparison for the generated FEA simulation against the experimental results. The "best-fit" has been highlighted in red showing an almost perfect match to the experimentally derived curve (black).

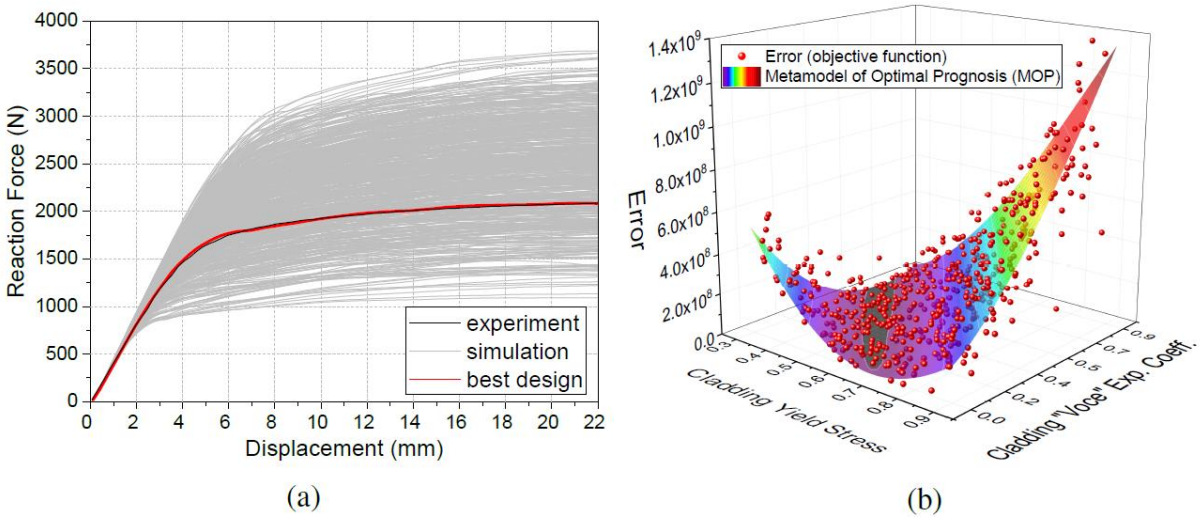

Figure 47 – (a) Force-displacement curves of the generated design points obtained from sampling the variables' range with OptiSLang and (b) Metamodel of Optimal Prognosis (MOP) showing the result deviation or error of each simulation (red points) from the experimental results

The error is plotted as function of the most important parameters of the finite element model being the cladding yield stress and the Voce exponential coefficient.

Each simulation can be described from the value of the objective function (or the error). These values can be plotted as a function of the input variables to provide a visual representation of different solution spaces describing the optimisation problem. OptiSLang produces a so-called Metamodel of Optimal Prognosis (MOP), which is a response surface as an explicit function based on the exploration of selected variables. In other words, the MOP is basically the fitted surface created by the response of the most decisive parameters (as estimated in OptiSLang) of the FEM simulation. Figure 47b shows an example of a MOP as derived after a sensitivity analysis on the material properties of the model. The data points in red represent how much the simulation deviates from experimental results. In this specific case, the effect of the cladding yield stress and Voce exponential coefficient (being the most important parameters in this model) are shown. The goal of the optimisation was to find the best possible solution that describes the cladding mechanical properties by providing the lowest possible difference against the three-point bending experimental results from of each test.

The cladding properties as derived from the best design point after the optimisation are given in Table 16. In addition, the Coefficient of Prognoses (COP) values for each parameter are given along with the

total COP, which characterises the quality of the MOP. Although the COP values depend on many factors, it can be observed that the most decisive parameters of the COPs are the Young's modulus and the yield strength (σ_0). This is particularly correct for the two high burnup samples, where there was only limited amount of plastic deformation. Consequently, the parameters describing the plastic stress development based on the Voce model are less important. These factors showed higher importance for the low burnup case, in particular the Voce exponential coefficient R_{inf}, as expected due to much higher plastic deformation.

Sample burnup	**Young's modulus** [MPa]	$\boldsymbol{\sigma_0}$ [MPa]	$\boldsymbol{R_0}$ [MPa]	$\boldsymbol{R_{inf}}$ [MPa]	$\boldsymbol{b}$ [MPa]
18.3 GWd/t	87'050	699	545	112	186
46.9 GWd/t	104'762	776	717	364	407
58.6 GWd/t	103'500	800	138	350	660

Table 16 – Cladding properties as calculated in OptiSLang

Finally, a comparison between experimentally and numerically derived effective cladding properties was performed. The results showed very good agreement on Young's modulus and a difference of 30% – 50% (depending on the burnup) on the yield strength. Such differences were expected, since the experimental results reflect the flexural beam properties derived with the simple beam theory, which cannot be used to accurately describe the relation of flexural stress-strain developed during plastic deformation.

3.4.3. Fracture mechanics modelling of the ring compression test

The mechanical integrity of the cladding tubes during handling, transport, or in accident scenarios (e.g., a cask drop) should be ensured after long-term storage, despite possible embrittlement. To assess the risk of failure, analysis methods for the ring compression test have been developed to gain an understanding of the consequences of existing hydrides in a zirconium matrix.

Nilsson [Nilsson, 2010] proposed an elastic-plastic fracture-mechanics finite element analysis (FEA). A two-dimensional plane-strain tube segment was modelled with a suitable constitutive model for Zry-4. Individual straight cracks of different lengths, locations and angles were added to the model. A stress load was applied as a boundary condition and the J-integral was calculated. It could be confirmed that circumferentially aligned cracks have no impact on fracture initiation because J values for those cracks were essentially zero. The ligament starts yielding at lower stresses for cracks close to the inner or outer surface. Fragmented hydrides were then modelled as kinked cracks with angles from -30° to +30° differing from the radial direction. Radial cracks with kinks had the same initiation values for J as straight cracks. The likelihood of crack growth is increased, however, for kinked cracks in comparison with straight cracks. Since cladding tubes can contain many hydrides, the distance between the platelets is often smaller than their individual length. Therefore, the complex interaction between cracks was analysed depending on the distance of the crack tips and the angle between neighbouring cracks. For a realistic study, pictures of hydrides were analysed and transferred to an equivalent FEA model of a crack field. It was concluded that cladding failure becomes more unstable if several radial hydrides interact. Failure might be triggered by a critical hydride configuration, even if the configuration is very local. Hydride-induced failure is strongly influenced by the yielding along the ligaments. The size of the hydrides in the radial direction is the most significant parameter for the load necessary to initiate failure.

Herb [Herb, 2014] developed a computational model based on the results of 102 RCTs. The derived failure criterion considers the ratio of burst stress, i.e. the stress at which the first drop in the load-displacement curve occurs, and the yield stress of the material to predict the ductile-to-brittle transition.

A local damage-mechanics approach has been proposed by Le Saux [Le Saux, 2015], using a modified Gurson-Tvergaard-Needleman model with extensions to incorporate plastic anisotropy and viscoplasticity. Ductile failure was reproduced for temperatures of 25, 350 and 480 °C, and a hydrogen content up to 1'200 wppm, with damage initiation induced through both hydride cracking and the debonding between the matrix and the precipitations. The damage evolution is deducted from observations of the microstructure and further parameters obtained from experiments. Implemented in a finite element analysis, the model could predict experimental results with reasonable accuracy. Due to the nature of the damage model, the impact of lower hydrogen contents with high degrees of anisotropy were not taken into consideration and could not be modelled.

Since the stress state in the sample is not homogeneous during the RCT, finite element analyses can help to understand the failure behaviour. Stress-plastic strain curves can be obtained from baseline studies (without radial hydrides) to simulate the sample deformation. Martin-Rengel et al. [Martin-Rengel, 2013] and Gómez et al. [Gomez, 2017a] demonstrated the use of a cohesive zone in a finite element model to predict the ductile failure of pre-hydrided unirradiated RCT samples. Simbruner et al. [Simbruner, 2022] improved the method and applied it to irradiated M5® cladding samples with radial hydrides to simulate brittle fracture under RCT conditions by cohesive zone modelling. Later, Zencker et al. [Zencker, 2024] applied the approach to irradiated cladding alloy ZIRLO® to demonstrate the general material-independent applicability of the method to simulate brittle fracture of RCT samples from defueled fuel rods.

The test setup is described above; see Figure 35 in Section 3.3.6. All tests considered here were carried out at room temperature (23 °C) in displacement-controlled mode at constant loading rate of 5 mm/s to the maximum displacement of 1.7 mm using a servo-hydraulic material testing machine. The fracture-mechanics analysis method is described exemplarily for ZIRLO® samples.

The samples were cut from segments of about 80 mm in length, which were taken from a defueled fuel rod with burnup of 68 GWd/t. Segment 105A was used for baseline tests to investigate the microstructure of the material and to determine stress-strain properties as documented by Billone et al. [Billone, 2012]. The average outer diameter of the corroded cladding was 9.53 ± 0.02 mm, and the outer diameter of the cladding metal was 9.44 ± 0.02 mm. The cladding metal wall thickness was 0.54 ± 0.01 mm. The corroded cladding had an average hydrogen content of 530 wppm (weight parts per million). Metallographic studies of samples from this segment have shown that there were a few radial hydrides among predominantly circumferential hydrides.

The quasi-static RCT on ZIRLO® sample 105C4 with radial hydrides, as described by Billone et al. [Billone, 2013a], was selected for the investigation of the failure behaviour of irradiated ZIRLO® cladding. Segment 105C was taken from the same HBU fuel rod from which the as-irradiated segment (105A) was sectioned. Both ends of the segment were closed with weld seams to create a rodlet. This rodlet was subjected to a radial hydride treatment (RHT) to simulate drying and storage of the fuel rod. The sealed and pressurised rodlet was heated to 400 °C to dissolve existing hydrides. The temperature was held for one hour. The rodlet was then cooled slowly at 5°C/hour to 200°C, where essentially all the hydrogen re-precipitated as hydrides, and afterwards at a faster rate to room temperature (RT). Metallographic studies have shown that this treatment creates a network of circumferential and radial hydrides, but with pronounced radial hydride structures.

Based on the experimental data, a finite element analysis was carried out to understand the complex interaction between the stress state, hydride structure, and initiation of cracks. The sudden load drops observed in force-displacement diagrams are the result of fast propagating cracks in the hydride structure, which should be reproduced by the FEA model. The model was simplified by assuming plane strain conditions. The commercial code ABAQUS® in quasi-static analysis mode was used for all calculations. The sample rests on a lower support plate that is assumed rigid. The deformation is caused by a movable upper loading plate, also assumed rigid, which is pressed onto the top of the sample. The solid section of the ring consists of plane strain elements with eight nodes, quadratic interpolation, and reduced integration. At the 12 o'clock position of the ring, a 1 µm wide gap was modelled along the wall

thickness. This gap was filled with a cohesive section of the same thickness. Tie constraints were used to connect the cohesive section and the surrounding mesh. The cohesive section was meshed using two-dimensional four-node cohesive elements. It is important to set the length of the individual sample as the out-of-plane width of the finite elements, as this scales the calculation result. The prescribed displacement of the upper plate applied the load. Figure 48 shows the complete finite element mesh with a detail around the cohesive zone. In most of the ring, 10 finite elements were used across the wall thickness. The mesh was refined around the 12 o'clock position to better reflect the complex stress state in the sample. The cohesive zone itself was very finely discretised with 1'000 cohesive elements in order to split the crack propagation into small steps and thus obtain a smooth and stable calculation result.

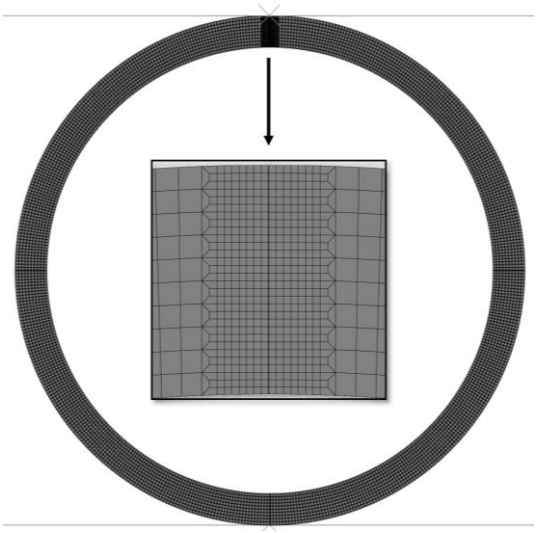

Figure 48 – Finite element mesh employed for cohesive zone modelling

The fracture mechanics analysis is a two-stage FEA approach. In the first stage, a baseline RCT was analysed numerically using the sample 105A9 (from segment 105A before RHT) to get the relevant stress-plastic strain relation (flow curve) by an automated inverse analysis method. An appropriate stress-plastic strain curve is required so that the simulated deformation behaviour of the sample matches the observed experimental behaviour as closely as possible. For that purpose, an iteration algorithm was developed based on Gómez et al. [Gomez, 2017b].

In the second stage, a RCT with pronounced radial hydride structures was simulated using sample 105C4 (from segment 105C after RHT) to examine the failure along radial hydrides. In this calculation, the deformation behaviour of the sample was based on the flow curve determined in the first stage. A cohesive zone model (CZM) with a traction-separation law was adapted to describe the failure process along radial hydride structures in irradiated cladding samples. The traction-separation approach consists of three parts: linear-elastic behaviour, damage initiation, and damage evolution. Figure 49 shows a simple traction-separation curve with triangular shape. Once an applied tensile stress reaches the cohesive strength σ_{c0}, damage is initiated within the cohesive element. The separation energy dissipated in the damage process is represented by the area under the traction-separation curve and is denoted as G_C. The degradation behaviour of a cohesive element is therefore determined by the parameters σ_{c0} and G_C for the given triangular traction-separation curve.

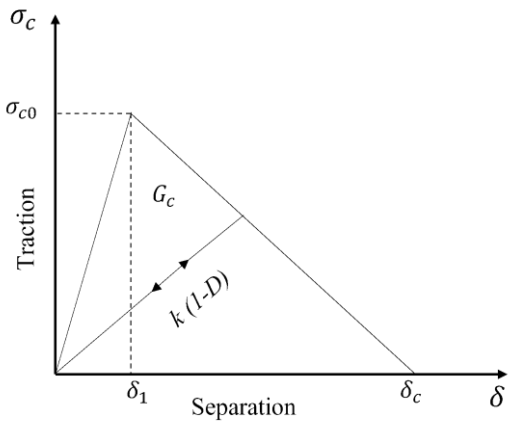

Figure 49 – Schematic traction-separation law

The failure mechanism of zirconium-based cladding alloys with radial hydrides subjected to RCT loading conditions consists of two different failure modes and was described by Ruiz et al. [Ruiz, 2021] based on the analysis of fracture surfaces. Quasi-cleavage along hydride structures was the dominating appearance of the fracture surface and an indicator of brittle failure. Some areas of the fracture surface showed void growth and coalescence associated with ductile failure and crack propagation through the zirconium matrix. Simbruner et al. [Simbruner, 2022] mapped the structure of the fracture surface of a RCT sample onto a cohesive zone to allow modelling of brittle behaviour along the hydrides and ductile behaviour along the zirconium matrix within the same cohesive zone. A separate cohesive law was used for each of the two failure modes. Various matrix-hydride distributions were investigated with assumptions on the size and distance of the hydrides and on the ratio of brittle areas to ductile areas on the fracture surface. Alternatively, the alternating failure due to quasi-brittle fracture at the hydrides and ductile failure of the zirconium matrix segments may be considered in a smeared manner, in that the failure mechanisms are not spatially resolved. This results in the approach of an effective cohesive law with only one set of cohesive zone parameters [Zencker, 2024].

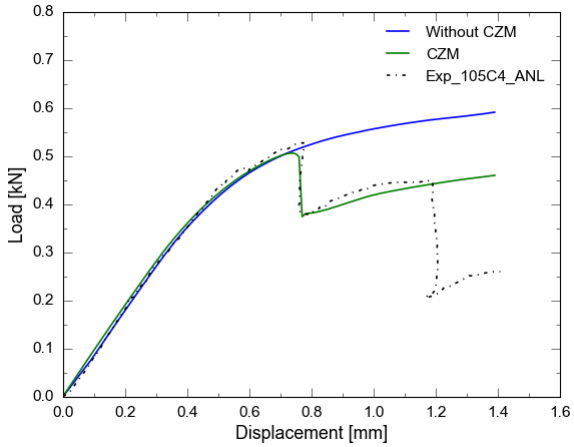

Figure 50 – FEA results with and without CZM compared to the test result

Figure 50 shows the test result together with calculation results with and without a cohesive zone. A series of simulations was carried out to determine the cohesive zone parameters for good agreement with the experimental results. The first major load drop occurred just after the yield point at around 0.75 mm of global displacement. The maximum load calculated in the FEA before crack initiation and

the load drop agree well with the experimental results. The simulation result shows a load drop of around 25 %, while the RCT showed a value of around 28 %. To consider further load drops, additional cohesive zones are necessary at the 6 o'clock position near the inside and at the 3 and 9 o'clock positions near the outside of the modelled sample. However, the determination of a unique set of cohesive zone parameters may be difficult because of complex interactions between zirconium hydrides and the surrounding zirconium matrix in the fracture zone. Simbruner et al. have shown that even minor variations in the positioning of ductile patches in the fracture zone can change the result of the RCT quantitatively and qualitatively [Simbruner, 2022]. The success of the simulation therefore depends not only on the knowledge of the cohesive parameters, but also on the hydride structure actually present in the sample.

3.4.4. Fuel performance codes

The key phenomena mentioned above often influence each other so that fuel rod performance can only be properly characterised through their proper integration into analytical tools. The strategy commonly followed to obtain these analytical capabilities is based on the extension to dry storage conditions of in-reactor thermo-mechanical codes. Since the in-reactor end-of-life (EOL) is the final outcome, they are well consolidated and their use is widespread. This extension is based on three main aspects:

- initial conditions (in-reactor EOL) provided by the code itself
- boundary conditions provided by thermal hydraulics or thermal fluid dynamics tools
- fuel performance during dry storage provided by new models implemented in the code extension

Additionally, other minor modifications are needed, such as including suppression of the cladding corrosion modelling during dry storage (i.e., inert atmosphere as coolant). A summary of fuel performance codes extended to dry storage is shown below, based on information available in the open literature.

BISON (INL)

Local effects in the cladding, such as hydrogen diffusion and precipitation, cannot be handled rigorously (including for instance azimuthal variation of hydrides) with traditional 1.5-dimensional fuel performance codes. However, hydrides may be modelled with the thermo-mechanical fuel performance code BISON, developed by the Idaho National Laboratory (INL) since 2009 [Newman, 2009]. BISON employs the finite element method and solves fully coupled thermo-mechanics and species diffusion equation systems in 2D-axisymmetric and 3D geometries. The code has been augmented with hydride modelling capability: hydrogen diffusion, precipitation into hydrides, and dissolution [Courty, 2014; Stafford, 2015]. In order to have a consistent post-irradiation state of the rod (including the cladding stress state) for the study of fuel behaviour in storage, all the successive stages are considered in a single code run: steady-state irradiation, wet storage, drying, and dry storage.

Fuel models in BISON describe temperature- and burnup-dependent thermal properties, swelling, densification, thermal and irradiation creep, relocation, fracture, and fission gas production and release [Hales, 2016]. Cladding mechanical models include plasticity, irradiation growth, and thermal and irradiation creep. The code is also able to simulate gap heat transfer, mechanical contact and the evolution of free volume pressure. With BISON, large problems can be solved as it may be run in parallel, i.e., assumptions on symmetry do not have to be made. The calculation mesh for the FEA is generated with external software such as TRELIS, ABAQUS/CAE, MSC/PATRAN or ANSYS, or, in simple cases via the input file, i.e., 2D-axisymmetric mesh with no pellet chamfers or dishings. Either first- or second-order elements may be used with BISON: 4- or 8-node quad element for 2D, and 8- or 20-node hexahedral element for 3D. In practical applications, it is typical to use 2D simulations for a full-length rod and 3D simulations for a segment of a rod for detailed study.

BISON has a boundary condition option to model the heat flux from, and the peak cladding temperatures of, a rod in the centre of a fuel assembly situated in a dry cask storage system [Hales, 2016]. Radiative and conductive effects inside the assembly, and conductive and convective effects from the assembly are considered. The cask-effective heat-transfer coefficient depends on cask type and loading and should be tuned. This option is not applied if the cladding surface temperature is given as a boundary condition. BISON contains a coolant channel model that calculates the heat transfer from cladding to coolant. Again, if the cladding temperature is given, this model is not used.

Currently, the models in BISON cannot predict radial hydride concentrations. Failure estimation due to hydrides can only be studied indirectly by comparing the calculated cladding stress to some stress criteria. A new model for improved hydride rim modelling, the modified Hydride Nucleation-Growth-Dissolution (mHNGD) model, has recently been implemented by Passelaigue et al. [Passelaigue, 2022].

For the cladding mechanical behaviour, in order to model the cladding creep-out during interim dry storage, a cladding creep model suitable for out-of-reactor conditions has to be used. A creep model developed by CIEMAT was implemented in the code BISON within the EURAD programme. However, this is not part of the standard distribution of the code.

FRAPCON (PNNL)

FRAPCON is a steady-state fuel-performance code developed by PNNL (Pacific Northwest National Laboratory) for the NRC [Geelhood, 2015]; it is applied to light water reactor (LWR) fuel rods. The capability to model spent fuel during dry storage has been added in the last version (4.0) and also in the new code FAST, which merges FRAPCON and the transient code FRAPTRAN. The new capabilities added are:

- coupling with the DATING sub-code, which uses empirical correlations for cladding creep and temperature decay curves for the analysis of fuel cladding under storage conditions
- implementation of the ANS-5.1-2004 Draft Standard to model the decay heat; so far, it is not used to estimate the fuel rod temperature in dry storage
- implementation of empirical correlations to add the effect of helium production and release due to α-decay and the swelling of the pellets via a build-up of the helium decay product

FRAPCON-xt (CIEMAT)

FRAPCON-xt is CIEMAT's extension to the FRAPCON code [Herranz, 2010; Feria, 2018]. The extension is based on the inclusion of models (most of them derived from and/or adapted by CIEMAT):

- an empirical cladding creep law that allows a direct feedback with the stress relaxation due to temperature decay and cladding creep-out
- an engineering correlation to calculate the temperature decay (based on thermal fluid dynamics calculations conducted with ANSYS FLUENT for concrete and metallic casks)
- a diffusion/precipitation model that is coupled with the code to estimate the hydrogen distribution throughout the cladding
- an empirical model of hydride radial reorientation in dry storage [Desquines, 2014]
- an empirical criterion based on available data on cladding-defect propagation onset due to UO_2 oxidation

Additionally, a Best Estimate Plus Uncertainty methodology has been set to quantify the code's uncertainties [Feria, 2017].

Due to the importance of the initial conditions of spent fuel when studying its behaviour under dry storage conditions, studies from CIEMAT have been conducted to improve the accuracy of the FRAPCON-xt code in these terms. Specifically, due to the relevance of the cladding hoop stress (and consequently

the rod internal pressure) for the evolution of certain mechanisms such as creep or hydrides' radial reorientation which could evolve in the degradation of the cladding, these studies have focused on improving the accuracy of rod internal pressure calculations.

A database of 11 fuel rods irradiated in commercial PWR reactors has been collected and their respective inputs created for the code FRAPCON-xt. This database has enough information on the design parameters and irradiation histories to create reliable inputs, and data of post-irradiation examinations related to the rod internal pressures at end-of-life (mostly fission gas release information from puncturing tests). FRAPCON-xt predictability in terms of rod internal pressure has been assessed with this database, showing a reasonable agreement between the experimental data and the code results (maximum deviations of 11% approximately). The results obtained also show an increasing trend of the deviation with the burnup for the three different designs present in the database [Aguado, 2021]. While the accuracy in pressures is acceptable (relative deviations smaller than 12%), fission gas release (FGR) and void volume calculations present differences (around 60% and 17%, respectively) that should be taken into account for code improvements. The rod internal pressures modeling with FRAPCON-xt was further studied, conducting a calibration of the void volume and FGR models for burnups higher than 60 GWd/t. This calibration was performed using the previously mentioned database, and an additional fuel rod was added in order to verify the calibration [Feria, 2022].

The results obtained with the code FRAPCON-xt regarding the initial spent fuel characterisation have also been compared with those given by the code BISON in terms of rod internal pressure and hydrogen distribution within the cladding at end of life in reactor [Aguado, 2022]. In the case of rod internal pressures, similar average relative deviations with the experimental data were obtained (around 5%), the results of both codes show significant underpredictions for burnups higher than 60 GWd/t. Regarding the hydrogen distribution within the cladding thickness, CIEMAT developed the model HYDCLAD to calculate the hydrogen distribution/precipitation and hydrides reorientation within the cladding [Feria, 2018; Feria, 2020; Feria, 2023]. Comparing the results of the hydrogen distribution given by HYDCLAD and BISON against experimental data, the in-clad hydrogen distribution is better captured by HYDCLAD, especially regarding the hydride rim, which is not well captured with the BISON code.

The comparison between FRAPCON-xt and BISON has been recently extended to dry storage, in terms of the cladding creep. The results obtained show that, for the rod studied, stored in dry conditions for 20 years, BISON modelling of the creep results in more than the double cladding hoop strain than those given by FRAPCON-xt simulation. Such big differences between both codes mainly come from different predictions in the irradiation hardening during the in-reactor stage and from a different evolution of the stress during dry storage. It should be noted that there are no actual data that allow to determine which of the two codes is more accurate. However, from a qualitative point of view, it has been observed that FRAPCON-xt includes the feedback between cladding strain and stress during dry storage, while the BISON adaptation carried out in the project (alternative creep law for dry storage) seems not to account for that. Concerning the irradiation hardening, this is one of the aspects to be taken into account in further work along with further validation using data that become available in future projects.

ENIGMA (NNL, VTT)

The ENIGMA fuel performance code was originally developed by Berkeley Nuclear Laboratories and Nuclear Electric [Kilgour, 1992] to calculate the thermo-mechanical behaviour of a LWR fuel rod under steady-state conditions.

NNL (UK National Nuclear Laboratory) has extended ENIGMA for modelling dry storage scenarios [Rossiter, 2011], which is mainly based on the incorporation of an empirical creep model valid for dry storage (derived by EDF [Bouffioux, 2001]). The thermal conditions are provided through in-house and commercial thermal analysis or computational fluid dynamics (CFD) codes, including ANSYS FLUENT. The calculation of the decay heat of the spent fuel is based on the FISPIN code, with nuclear cross sections supplied by CASMO.

A recent extension of ENIGMA to dry storage has been carried out by VTT [Arkoma, 2018]. The so-called VTT-ENIGMA was modified in order to model the cladding creep during dry storage. Two creep models were implemented into the code: one from EDF [Bouffioux, 2001] and one from CIEMAT [Feria, 2015]. The thermal conditions were determined by CFD calculations with OpenFOAM, which was fed by decay heat calculations with the SERPENT code.

TESPA-ROD (GRS)

The TESPA-ROD code analyses the thermo-mechanical behaviour of LWR fuel rods under operational conditions and design-basis accidents (RIA, LOCA), and it was extended to dry storage conditions [Sonnenburg, 2017]. To do this, the creep of the cladding material was modelled under prevailing conditions (implementation of empirical creep law), as well as the pellet swelling due to helium production during long-term storage. The fuel rod temperature was determined through the sub-channel thermal hydraulic code COBRA-SFS and supported by calculations from a burnup code such as KENOREST.

TRANSURANUS (ITU-JRC)

TRANSURANUS is a fuel-performance code developed by ITU-JRC (Institute for Transuranium Elements-Joint Research Centre) that is applicable to LWR fuel rods. In order to extend the code to dry storage, an analysis of the empirical cladding creep model was used by the code [Lassmann, 1977] and a comparison was performed with other creep models with a wider range of application [Mayuzumi, 1990; Martin, 2007]. With this study, it was possible to identify the best option to apply depending on the prevailing conditions.

Synthesis

Table 17 provides a synthesis of the information explained above. The following should be highlighted:

- The cladding creep in dry storage is modelled based on practically all the codes shown. In spite of this, further modelling and validation are needed, especially concerning the effect of the irradiation damage annealing and the hydrogen concentration and orientation.
- The in-cladding hydrogen behaviour is only modelled based on BISON and FRAPCON-xt, and further understanding, modelling and validation are needed regarding concerns in dry storage such as hydride radial reorientation or hydride blister formation, for which the accuracy enhancement of the hydrogen migration/precipitation models is of the utmost interest.
- The pellet-related phenomena seem to be less modelled. The α-decay is only modelled based on two codes; the main research interest is focused on MOX fuel, with significantly higher helium production than UO_2. Regarding the effect of UO_2 oxidation, only FRAPCON-xt takes it into account with a cladding failure criterion, although supported on a scarce database of low-burnup fuel, and further research is thus needed to model this phenomenon. In the case of the pellet-cladding bonding, only BISON has the capability to analyse its effect; indeed, the complexity of this mechanism requires further research to be done in this regard.

Code	Key phenomena							
	Cladding					Pellet		
	Creep	Hydrogen migration/ precipitation	Hydride radial reorientation	Hydride blister formation	DHC	Pellet-cladding bonding	UO_2 oxidation	α decay
FRAPCON-xt (CIEMAT)	X	X	X				X	
FRAPCON/FAST (PNNL)	X							X
ENIGMA (NNL)	X							
VTT-ENIGMA (VTT)	X							
TESPA-ROD (GRS)	X							X
TRANSURANUS (ITU-JRC)	X							
BISON (INL)		X		X	X	X		

Table 17 – Synthesis of fuel performance codes and key phenomena simulated in dry storage

Finally, it should be noted that a proper integrated validation of the codes shown is not possible due to the lack of data. Therefore, further work should be performed to derive qualified experimental databases for the assessment of the code extensions to dry storage.

3.5. Summary and conclusions

The characterisation of spent fuel rods is a key aspect of understanding their performance in storage and final disposal. Significant effects of temperature on the softening of the cladding material with increasing temperature and the embrittlement with decreasing temperature were investigated. In particular, radial hydrides in the cladding under hoop stress at low temperature can lead to the formation of cracks, which is disadvantageous for a transport after storage. The measured fuel mass release in case of cladding fracture corresponds to a fraction of a pellet.

Hydrides, regardless of their orientation, may hinder the movement of dislocations and therefore reduce the creep rate due to hardening. In this sense, the precipitation of hydrides during dry storage can be advantageous, because a phenomenon known as clad lift-off may be prevented. Clad lift-off does not occur if the outward creep rate of the cladding is lower than the swelling rate of the fuel. In this case, the pellet-cladding gap remains closed and the fission gas release is impeded.

Finite element analyses are essential to study failure modes and derive mechanical properties of rod and cladding. A potential brittle cladding failure in the ring compression test due to radial hydrides could be modelled with the novel cohesive zone approach. A fracture-mechanical analysis of the sudden failure by brittle fracture revealed the underlying processes and is a necessary link to understanding and predicting the macroscopic behaviour of the cladding under operational and accident conditions on

its way towards final disposal. The FRAPCON-xt predictive capability to model early stages of dry storage has been enhanced. On one side, fission gas release and free volume modelling have been adapted to deal with burnups higher than 60 GWd/t; its better performance has been proved against an open database built ad-hoc. On the other side, the spent fuel and cladding creep models have been benchmarked against BISON.

Quantitative data about environmental impact of spent fuel rods in dry storage installations or wet storage facilities are needed for the stage following the period of in-reactor operation, considering not only normal operation, but also potential accidents, when the SNF is eventually discharged [Hill, 1962]. Progress was made towards the understanding of the role of trivalent lanthanides and microstructure within the context of traditional LWR fuels interim storage.

1. Several types of UO_2 model materials representative of used fuels were prepared by different routes and characterised. Generally, three different model materials were obtained: a) Solid solutions with lanthanides in UO_2 (including pure UO_2); b) UO_2 doped with lanthanides, PGM bearing (metallic particles) and Mo; and 3) SIMFUEL (UO_2 doped with Mo, Zr, Ru, Ba and Nd).
2. Dissolution tests performed on UO_2 model materials under some relevant wet storage conditions (spent fuel pools) suggest a beneficial impact of Ln elements on the chemical durability of the ceramics. Additionally, no significant impact of PGM elements and molybdenum on the chemical durability of the leached samples was observed.
3. From the oxidation tests conducted under dry storage conditions it can be concluded that the presence of Ln such as Eu in the UO_2 structure, the grain size of UO_2 and the synthesis route of samples affect the oxidation of the fuel matrix.

The work on trivalent lanthanides and microstructure within the context of traditional LWR fuels interim storage does not aim to accurately reproduce all the features and experimental behaviour of SNF, but allows an estimate of dopant, microstructure and He effects on fuel pellet durability to degradation by oxidant gases or water. To bridge the gap between "model materials" and the complex real systems, inter-comparative analysis should be done to definitively verify the experimental conclusions reached and associated uncertainties, or data obtained could be validated through the response of predictive models on irradiated fuel. The quantitative reproduction of the obtained experimental data with the conceptual models would help to explain key chemical reaction mechanisms, both kinetics and thermodynamics. Reliable behaviour characterisation of SNF at long-term in different environments needs to be further addressed.

The thermal analysis on some representative model materials of PCI showed that the presence of zirconium in the UO_2 fuel matrix provides certain oxidation resistance to U_3O_8, hindering matrix oxidation, under formation of a $(U, Zr)O_2$ solid solution.

Furthermore, it was demonstrated by mandrel ductility tests that by increasing the H_2 content within cladding samples, a linear relationship between ductility decrease of the specimens and incorporated hydrogen up to 2’000 wppm could be identified, indicating the presence of radially orientated hydrides. After application of 1’500 to 2’000 wppm of hydrogen to the specimens, no change in mechanical behaviour was seen; thus, it is concluded, that the ductile-to-brittle transition threshold is then reached. In addition, state-of-the-art spectroscopic investigations, such as synchrotron-based spectroscopy, on the fuel-cladding interaction layer showed the presence of chlorine as well as iodine bearing compounds and gave further insights into hydride orientation within irradiated fuel. In case of the identified iodine compounds, it could be confirmed that it is present in its negatively charged iodide speciation, presumably as CsI. Through radiolytically enhanced dissociation of CsI, free iodine can be formed, which may enable pitting corrosion effects on the inner side of the cladding tube. As for the determined chlorine compound, analyses showed the presence of a Cs-U-O-Zr-Cl-bearing mixed phase.

In summary, EURAD SFC Task 3 has brought, among others, the following progress:

- Improvement of experimental methods (sample preparation for ring compression test, hydride visibility with neutron radiography),
- Better understanding of mechanical behaviour by enhanced numerical capabilities (creep, brittle cladding failure with radial hydrides),
- Investigation of radiochemical ageing and degradation mechanisms during dry storage and wet pool storage (model materials to support SNF corrosion studies), and
- New insights into pellet-cladding interface (a new complex mixed phase was found).

For future studies, experiments with fueled samples to better understand the pellet contribution to the structural behaviour of SNF rods are recommended. Further post-irradiation examination data are required to validate and extend various models in fuel performance codes. Corrosion studies using "model materials" are still needed to understand the separate and combined effects, which can hardly be done with real SNF. Numerical simulations should complement experimental investigations for better understanding what is happening in each system. There is a demand for intercomparative studies using model materials and irradiated fuel at the same conditions. Further experiments are needed to examine the effect of fission and activation products precipitated at the fuel-cladding interface on the cladding integrity.

4. Accident scenarios

The term "scenario" means a "*postulated or assumed set of conditions and/or events that can lead to human exposure or environmental contamination*" [IAEA, 2013] or, differently phrased, "a set of conditions and/or events that involves a potential risk of radiation exposure of human beings and/or the environment".

Each scenario must reflect certain conditions arising either during the normal operation of a facility or as a consequence of a specific event leading to a deviation from normal operating conditions. The choice of an appropriate range of scenarios and associated assessment cases is essential for the safety assessment of any nuclear facility (e.g. power plant, wet storage, dry storage, encapsulation facility, etc.) or specific activity/process (e.g. SNF transport, handling, etc.). Once identified, these scenarios should take into account existing and potential hazards arising from the facility/process, and also their interrelation and evolution over the lifetime of the facility or defined processes according to the safety case.

A systematic approach to accident scenarios may be as follows: 1) Identification and screening of hazards with respect to the facility design and defined processes (for instance, the types of hazard have to be identified with respect to the SNF inventory, activity, physical conditions and location, together with any additional hazards arising indirectly from activities or processes for their management); 2) Identification of initiating events with the potential for causing harm to humans and/or the environment; 3) Quantification of the hazards; 4) Safety analysis of all relevant scenarios arising from either processes or accident situations in which the screened hazards could occur.

Unlike the previous chapters, this chapter aims to give a generic overview of accident scenarios that have been identified so far in the pre-disposal activities for SNF. Hazards and initiating events are strongly site-specific and have thus been left out of the scope of this chapter.

4.1. Safety standards for pre-disposal management of SNF

The safety requirements for the pre-disposal management of SNF necessitate the development of a safety case – together with the necessary supporting safety assessment – for each facility or activity [IAEA, 2016]. The safety case and supporting safety assessment provide the basis for the demonstration of safety and for licensing (siting, location, design and operation) of SNF dry storage or packaging facilities, as well as other types of nuclear facilities. Spent fuel storage facilities have to demonstrate the safe, stable and secure storage of spent fuel [IAEA, 2020]. The design features and the operation of the facility should be such as to ensure the containment of radioactive material and optimum radiation protection of workers, members of the public and the environment within the dose constraints in accordance with established requirements (see [IAEA, 2009b]), in order to maintain subcriticality and ensure the removal of decay heat and retrievability of the spent fuel. These safety functions should be maintained during all operational states and accident conditions.

Safety Guides are provided by the IAEA [IAEA, 2013] for guidance and recommendations on the development and review of the safety case and supporting safety assessment prepared or conducted for a pre-disposal waste management facility and related processes/activities. All aspects of the safety case and safety assessment must be covered in a general sense, including planning, design, construction, commissioning, operation and modification of the facility.

This guidance requires demonstration of acceptability following defined accident scenarios (for example SNF transport accidents or a SFA dropping from height). As the IAEA recommendations have a common basis, the Safety Standards are used as the main reference in this report, although certain criteria to be met (such as dose limits) are country-specific.

4.2. Accident scenarios for fuel in interim storage

A safety analysis of an interim dry storage facility for SNF must be performed with respect to potential accident scenarios. Several stages, both from the point of view of the design and the site, have to be taken into account: source definition, radioactivity inventory assessment, analysis of the radioactive release scenarios and their consequences in the geosphere and biosphere, dose assessment for preparation, transport/transfer and proper interim storage of spent fuel. The radionuclide inventory and related uncertainty can be evaluated using several methodologies (numerical and experimental), as described in Chapter 2.

According to the IAEA Safety Standards [IAEA, 2013], scenarios should be developed for normal operation, anticipated operational occurrences and accident conditions. The safety analysis should address the consequences of normal operation and the frequencies and consequences associated with all anticipated operational occurrences and accident conditions. The degree of detail of the analysis should depend on the magnitude of the radiation risks associated with the facility or activity, the frequency with which events occur, the complexity of the facility or activity and the uncertainties inherent in the processes.

Three types of potential accident scenarios can be considered according to the nature of the operations:

I. scenarios for normal operation
II. scenarios for anticipated operational occurrences and design-basis accidents
III. scenarios for beyond-design-basis accidents

Scenarios should also be evaluated according to accidents due to natural or man-made events and accidents due to external and internal human-induced events.

In order to analyse the accident scenarios, conservative assumptions should be considered. To perform a probabilistic analysis, the effective doses and risks have to be evaluated. As a consequence of the results obtained and of the measures taken for the design, it must be demonstrated that humans and the environment will remain safe and protected in all cases.

The three above-mentioned scenarios are defined in [IAEA, 2013] in a general context and summarised here as follows.

I. Scenarios for normal operation

Scenarios for normal operation should address all conditions under which the systems and equipment of the facility operate (activities carried out as expected), with no internal or external challenges [IAEA, 2013]. This includes all aspects of operation for which the facility is designed to conduct over the course of normal operation, including maintenance over the lifetime of the facility and all stages of activities. The effects of variations in the input materials (feedstock, source material, receipts, etc.) on normal operation should be considered.

Scenarios for normal operation should be defined with the goal of assessing whether the activities can be carried out safely or the facility can be operated safely under normal operation. This includes an assessment of whether radiation doses to workers and members of the public and planned discharges will lie within prescribed limits and constraints and can be maintained as low as reasonably achievable. It also includes verification that the elements of defence-in-depth will be maintained and that adequate safety margins will remain at all times.

II. Scenarios for anticipated operational occurrences and design-basis accidents

The facility conditions considered in the design-basis assessment are typically divided into two categories: anticipated operational occurrences and design-basis accidents. The division between the two categories of scenarios is based on the frequency of occurrence and the extent of the challenge to safety from the initiating events causing the condition [IAEA, 2013].

Anticipated operational occurrences are processes deviating from normal operation that are expected to occur at least once during the operating lifetime of the facility, but which, in view of appropriate design provisions, do not cause any significant damage to items important to safety or do not lead to accident conditions. Scenarios for anticipated occurrences should also be considered for SNF management activities.

A design-basis accident is an accident condition against which a facility is designed according to established design criteria, and for which the damage to the radioactive waste inventory and the release of radioactive material is kept within authorised limits. Design-basis accidents have a lower frequency than anticipated operational occurrences, and they are not expected to occur during the lifetime of the facility but must be considered in its design.

The safety analysis should identify the anticipated operational occurrences and accident conditions. This should include all internal and external events and processes that may impact physical barriers that confine the radioactive material or otherwise increase radiation risks. The selection of events and processes considered in the safety analysis should be based on a systematic, logical and structured approach, and justification should be provided that the identification of scenarios is sufficiently comprehensive. The analysis should be based on an appropriate grouping and bounding of the events and processes, and partial failures of components or barriers as well as complete failures should be considered.

The assessment should demonstrate that the design of the facility and associated safety processes/procedures meet all safety criteria. For instance, the design-basis assessment should demonstrate that the potential for release of radioactive material or loss of shielding is controlled, that any operational discharges of effluents will remain below prescribed limits, that the limiting criteria for design-basis accident conditions will be met and the radiological limits applied will not be exceeded, and that some or all of the barriers put in place to limit exposure and the release of radioactive material from the facility will maintain their integrity to the extent required. A conservative assessment should take account of the uncertainties associated with the assessment itself.

For new facilities or activities, a comprehensive identification and assessment of all design-basis accidents should be carried out. For modifications of existing facilities or activities, the assessment should focus on those design-basis accidents that might either directly or indirectly affect these modifications.

The assessment carried out for anticipated operational occurrences (AOOs) is essentially the same as that for design-basis accidents (DBAs) and requires many of the same conservative assumptions, especially those that relate to the structures, systems and components important to safety. Differences might exist, though, in the consideration of non-safety-related structures, systems and components in safety analyses of AOOs and DBAs.

III. Scenarios for beyond-design-basis accidents

Accidents beyond the design basis (BDBA: Beyond-Design-Basis Accident) are those that are not considered for design-basis accidents, but are considered in the design process of the plant in accordance with best-estimate methodology, and for which releases of radioactive material are kept within acceptable limits [IAEA, 2013]. Design-extension conditions can be divided into two general groups: (a) Those with a high enough probability of occurrence and sufficiently severe consequences, for which corrective or remedial actions have to be considered. This may be appropriate even though the probability of occurrence is lower than that of design-basis accidents. (b) Those that have a very low probability of occurrence, but potential consequences could be severe.

The distinction between design-basis accidents (DBA) and accidents beyond design basis is based on the probability of occurrence and the consequences. The distinction is significantly facility- or activity-dependent and site-dependent. If the probability of an accident occurring is considered to be unacceptably high, the design has to make provisions for preventing any significant consequences. If

the probability of occurrence of an accident is much lower but the consequences would be significant, it may be advisable to incorporate features into the design that accommodate this eventuality.

The set of representative fault sequences depends on the design of the facility. These sequences can result in substantial radiological consequences, including those with multiple component failures and/or wrong accident management. Important event sequences that could lead to serious accidents should be identified using a combination of probabilistic and deterministic methods and sound engineering judgement. The details of serious-accident sequences that have to be analysed are unique for each type of facility.

If necessary, the accident assessment should model the wide range of physical processes that could lead to a release of radioactive material to the environment or define the limiting criteria where a release can be assumed.

The assessment should generally be carried out using realistically conservative assumptions, representative data, best-estimate methods and decision criteria. Where this is not possible, reasonably conservative assumptions should be made that take account of the uncertainties in the understanding of any relevant physical process and equipment failure modes being modelled. However, it should be emphasised that the complexity of BDBAs might be such that assumptions made cannot be ensured to be conservative.

Radiological impact assessment

The assessment of radiological impacts constitutes a major part of the safety case for a pre-disposal SNF management facility and related processes. Qualitative assessments and the quantitative analysis of possible challenges to the safety functions and the resulting potential radiological impacts have to be carried out by means of conceptual and mathematical models. The dose rates for the given assessment endpoint have to be calculated both for workers and the public. For accident scenarios, effective doses (Sv) covering the whole exposure time must be calculated, while for normal operation scenarios the annual effective doses (Sv/year) have to be considered. Doses from internal exposure are generally defined as committed effective doses affecting workers over a period of 50 years and the public over a period of 70 years. The exposure assessment differs from the hazard characterisation in that the assessments do not consider standardised conservative conditions, but realistic conditions expected to occur in the given scenario.

Remarks on accident scenario analysis

Currently, accident analyses focus on determining the consequences on the storage system itself, so that safety functions are maintained, and thus meeting the limits set by the regulator.

The licensing requirements are passed on to the designers of the dry storage systems, who also take international standards and guidance as a reference for the definition of the accident scenarios, and therefore need to be assessed on a case-by-case basis.

The fuel condition used in the analysis does not typically correspond to a real situation, since conservative assumptions are employed to account for degradation phenomena that alter the physical properties of the constituent materials (e.g. failure of a significant number of rods or even 100% of the rods). Therefore, for the analysis of accidents during interim storage, it is recommended to establish a clear understanding of the relationships between the postulated accidents for storage facilities and systems, and their effect on the spent fuel, while taking into consideration its condition.

During the assessment of accidents and to facilitate the technical understanding of accident selection, it may be helpful to apply a risk assessment methodology to each specific case and regulatory framework. Damage to the storage system and to the stored fuel have to be considered both.

4.3. Accident scenarios for SNF during transport

It is assumed that, after dry interim storage, the SNF loaded in the transport and storage casks has to be moved from the interim storage facility to a conditioning facility. These transports must comply with the same requirements as the transports before dry interim storage. This applies to behavior under normal transport conditions and in the event of transport accidents. The transport of fissile material is governed by the authorities of the individual countries, who generally comply with the requirements specified in IAEA SSR-6 [IAEA, 2018b].

The main focus of the related research activities is on the behavior and performance of the cladding tubes, i.e. whether they remain intact, only let gas (noble gas and volatiles) escape or whether significant quantities of fissile material can escape from the cladding tubes in addition to the gas (see Chapter 3 for a more detailed description of these activities).

Since cladding tubes are exposed to significantly higher loads in the case of a transport accident than during handling under final conditioning, comparing the analysis of transport accidents can help to conservatively estimate potential SNF damage.

This section focuses on the U.S. NRC approach [NUREG, 2014] as well as on EPRI studies [EPRI, 2007]. The NRC Risk Assessment Report takes into account three different types of containers, various transport routes in the United States and extensive radiological analyses. The guidelines assume a 9-m drop with an orientation that can cause the greatest damage to the transport/storage cask (TSC) (see Figure 51).

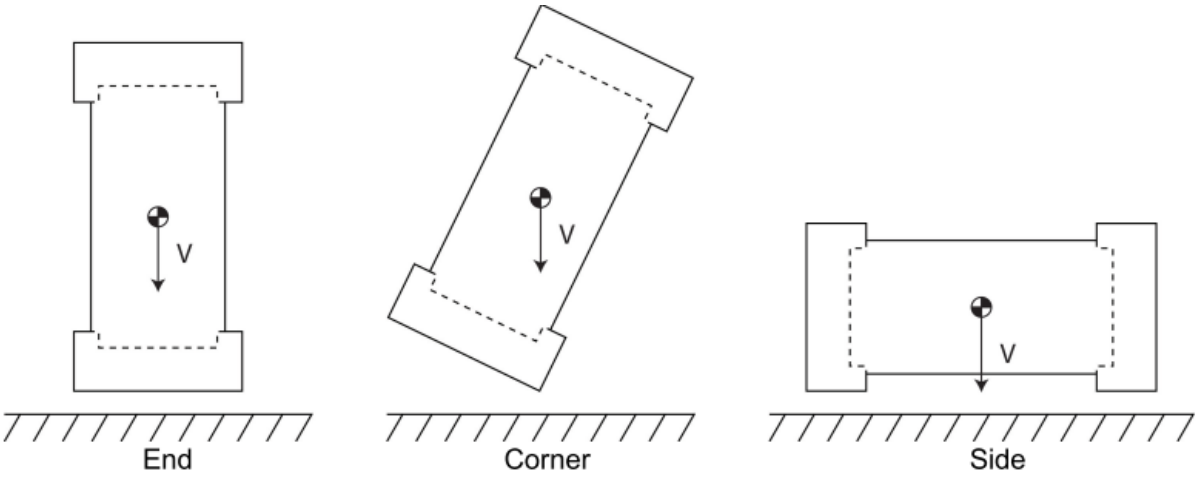

Figure 51 – Different orientations of the TSC for the drop from a 9-m height

[NUREG, 2014]

While a drop on the corner is considered worst for the cask, a drop on the side is more likely to damage the SNF. Therefore, the side case is used for the set of calculations. In the case of the end drop, the fuel rods are guided in the FA structure, which is why the possible failure-relevant bending of the fuel rods, according to the NUREG report, is severely restricted. In addition, the side-drop loads are more relevant in the case of settled formation of radial hydrides in the fuel cladding. The hydride reorientation describes the stress-related rearrangement of hydrides from an orientation in the circumferential direction or from an irregular arrangement into hydride rows which are radially oriented. Such radial hydrides can have an impact on the ductility properties of the cladding (above a certain threshold).

Figure 52 shows different loading modes of a fuel rod.

EPRI also worked extensively on the transport accident behavior of spent fuel elements (see synthesis report [EPRI, 2007]). This study takes into account the failure modes and the failure criteria for the effects of transport accidents on the fuel rods, including changes in the material of the cladding tube during the dry storage period. The study covers normal transport conditions (falling from a height of 30 cm, according to 10 CFR 71) and accident conditions, as well as an analysis of the cladding behavior during dry interim storage.

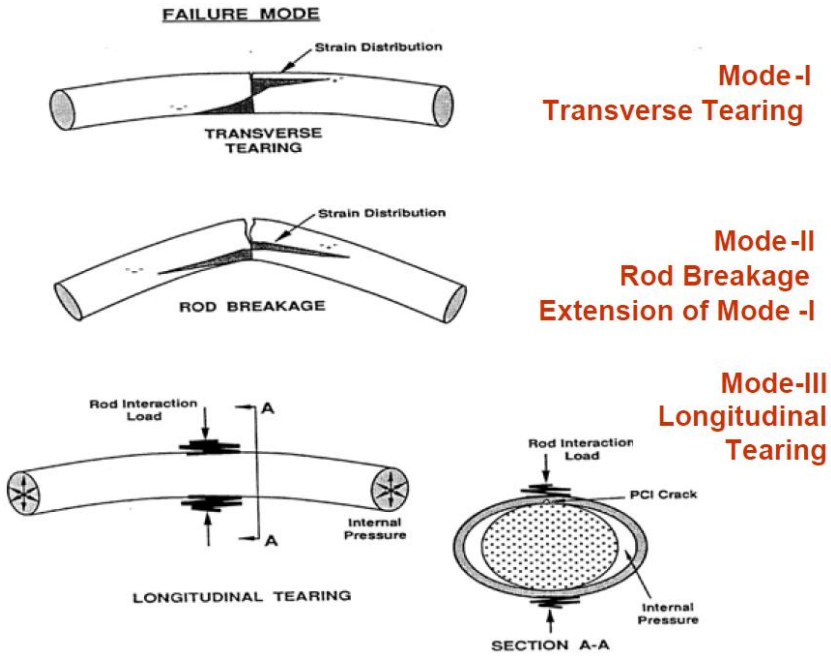

Figure 52 – Different loading modes of the fuel rod

Mode-I describes a bending load that leads to a crack (perpendicular to the rod axis). Mode-II describes the behavior of the fuel rod under bending load when the above-mentioned crack has passed through the wall thickness: Mode-III describes the loading of the cladding tube under radial pressure (as in the ring compression test).

As part of the work performed within Task 4, IDOM has developed a methodology to assess the severity of potential accidents from both dry storage systems (DSS) and spent nuclear fuel (SNF) perspectives, specifically applied to the context of Spain but broadly relevant to other countries. The analysis includes scenarios such as vertical and horisontal drops, tip-over accidents, impacts from various sized objects, fire, explosion, flooding, and extreme temperature changes.

One of the most severe scenarios analysed is the DSS tip-over, which has the highest impact on both the DSS and the fuel, potentially causing significant mechanical damage to the fuel assemblies and altering criticality control due to changes in fuel configuration. This scenario can lead to overstress and deformation of structural components, compromising multiple safety functions such as confinement, criticality control, and heat transfer.

Drop accidents, whether vertical, horisontal, or corner, can induce high accelerations, leading to deformation of the fuel assemblies and potential breaches in fuel cladding. These scenarios particularly affect structural and fuel integrity and heat transfer functions. A fire, while capable of causing component overheating and loss of polymeric shielding materials, is generally less severe due to the DSS's thermal inertia, which prevents critical temperatures and pressures from being reached.

An explosion, though less likely to compromise DSS safety functions due to the systems' high structural strength, is still being considered. The analysis carried out within the EURAD project shows no significant impact on the DSS or SNF under typical explosion parameters. Flooding can compromise

the confinement and criticality control functions of the DSS, yet the fuel elements, subjected to pressures lower than those experienced during reactor operation, are not expected to suffer significant damage.

Other scenarios, such as object impacts, lightning, and extreme temperature changes, generally have minimal impact on the DSS and SNF. Lightning strikes, for instance, cause localised heating but do not compromise safety functions, while object impacts and extreme temperature changes are within the design tolerances of the DSS.

The study concludes that some accidents pose significant threats to the DSS safety functions; however, they might not necessarily result in SNF damage. This dual-perspective approach in safety analyses ensures that both the storage system and the fuel are adequately protected against a wide range of potential accidents. The findings serve as a valuable resource for stakeholders in the nuclear industry, informing the development of more resilient and secure storage solutions.

4.4. Accident Analysis Methodology Development

Another important outcome from the work performed within Task 4, is the development of two independent methodologies aiming at evaluating the structural response of key elements of the SNF. On one hand, Nagra is using Finite Element Analysis (FEA) to study the mechanical behaviour of Pressurised Water Reactor (PWR) spent fuel assemblies under different accident conditions. On the other hand, CIEMAT developed a methodology to predict the probability of fuel rod failure in spent nuclear fuel (SNF) during accident scenarios.

4.4.1. Structural performance of SFA with Finite Element Analysis

Nagra performed a comprehensive study aimed at analysing the response of spent nuclear fuel (SNF) under mechanical stress and assessing the consequences of fuel rod failure. This research is crucial for providing valuable input data to optimise the management of SNF and temporary storage casks (TSCs) for safe handling and disposal. The study was conducted through a collaborative effort involving Nagra, JRC-Karlsruhe, and the Swiss Federal Institute of Technology in Lausanne (EPFL). Utilising commercial spent fuel rod samples, this experimental campaign sought to address technical gaps identified in previous investigations and extend the understanding of SNF behaviour under a wide range of burnup levels (BU), from quite low to very high.

The primary objective of the experimental campaign was to examine the mechanical response of pressurised water reactor (PWR) spent nuclear fuel (SNF) rods across various burnup levels. The experimental procedure included performing three-point bending tests on rodlets until fracture, with additional tests on empty cladding to determine the effect of pellets on the samples' response. Throughout the testing, force and displacement were measured, and post-fracture analyses included assessing the released fuel mass, particle size distribution, oxide layer thickness, and hydride orientation. Additional tests on surrogate samples with varying hydrogen concentrations were conducted to study the effects of hydrogen embrittlement on cladding performance (see Section 3.3.5 for details).

The experimental findings revealed that the contribution of pellets to the bending response of fuel rods is significant during plastic deformation, where they increase bending stiffness and prevent cladding buckling. Conversely, the elastic properties of the samples were governed solely by the cladding, with the Young's modulus showing a nearly linear increase with BU mainly due to the thicker oxide layer. The force-displacement curves demonstrated that ductility decreases with both increased BU and hydrogen concentration, whereas toughness increases with BU, driven primarily by irradiation hardening of the cladding. Failure mode analysis indicated that cracks typically initiate at the pellet-to-pellet interface under tension, with limited fuel mass release due to effective pellet-to-cladding bonding at high BU and cladding deformation at low BU.

To further analyse the mechanical properties of SNF, the experimental data were combined with Finite Element Analysis (FEA) to develop a Finite Element Model (FEM) simulating the three-point bending experiments using Ansys® Mechanical (see Section 3.4.1). This 3D implicit static structural FEM

required defining the geometry and material properties of the samples, contacts between different parts, meshing of the geometry, and boundary conditions. Calibration of the model against experimental data was a significant achievement, as few studies integrate both experimental and numerical investigations. Sensitivity analyses on various modelling parameters ensured the generated FEM provided valuable insights into the mechanical properties of SNF and could be used to examine responses under conditions beyond those tested experimentally.

The 3D model offered the advantage of simulating multiple loading configurations and provided a foundation for modelling entire fuel assemblies. However, due to the extensive simulation time required for large-scale assemblies, a series of simplified 1D models were created with different cross-sections: annular cylindrical, cylindrical, and a combined model with both elements. These models underwent sensitivity analyses and calibration processes to fit the three-point bending experimental data. The annular cylinder model best replicated the rodlets' response under bending tests and allowed for direct assignment of cladding elastic properties derived from experimental data, thus reducing the number of optimisation parameters.

The development of larger-scale FEMs, such as a 15x15 PWR SFA model, enabled the evaluation of individual fuel rods' behaviour under significant deformation caused by bending loads. These simulations demonstrated that guide tubes, as the main load-bearing components, experienced higher strains than fuel rods under the same bending loads. Furthermore, fuel rods only entered plasticity after substantial deformation of the top end piece, with the number of rods entering plasticity plateauing before increasing again at higher deformations. These findings suggest that under normal handling conditions, no rods are expected to enter plasticity, highlighting the robustness of the fuel assembly design.

Automated Python scripts facilitated the extraction and summarisation of the FEM results, including strain, shear force, and bending moment diagrams for individual rods and guide tubes. These results are crucial for determining whether a rod has reached its failure point and for future data analysis.

The study concludes with recommendations for future FEM development and experimental extensions. Automating the modelling process, performing experiments on fuel assembly models under typical handling or accident loads, and creating numerical models for dynamic loading scenarios will enhance the confidence in FEM results and provide deeper insights into SNF behaviour. These efforts will significantly contribute to the optimisation of SNF management and disposal strategies, ensuring safe handling and long-term storage.

4.4.2. Stochastic approach to determine fuel

CIEMAT has developed a methodology to estimate the probability of cladding failure in spent nuclear fuel (SNF) during postulated accident scenarios. This methodology can estimate cladding failure probability leverages FRAPCON-xt, an in-house extension of the FRAPCON code tailored for dry storage; HYDCLAD, a CIEMAT model for hydrogen distribution and precipitation; and DAKOTA, a statistical toolbox developed by Sandia National Laboratories (SNL). The methodology consists of three primary pillars: thermo-mechanical characterisation of the fuel rod at the onset of the accident, modelling cladding mechanical properties and failure criteria, and extending the analysis to cladding failure probability using statistical methods. The fuel performance simulation under irradiation and dry storage conditions is conducted using FRAPCON-xt, which is coupled with HYDCLAD to model hydride distribution and reorientation within the cladding. The predictive capability of FRAPCON-xt has been enhanced to include rod internal pressure (RIP) beyond 60 GWd/tU for extended burnups.

The cladding stress is selected as the Figure of Merit (FOM). The stress-strain behaviour in FRAPCON is modelled using Hooke’s law for the elastic regime and a specific equation for the plastic regime. The yield stress calculation differentiates between uniaxial and flexural loads. For uniaxial loads, FRAPCON includes correlations for irradiated material properties, while for flexural loads, a correlation between yield stress and burnup has been derived from experimental stress-strain data from bending tests (refer to previous section).

The failure criteria are embedded within the methodology, utilising information from the open literature and project-specific data. The primary criterion limits the cladding hoop stress to 90 MPa to prevent brittle failure due to hydride radial reorientation. Additional criteria include the temperature of ductile-to-brittle transition and deformation limits for brittle cladding with reoriented hydrides. The failure probability is determined by comparing cladding stress and strain against these criteria.

Statistical analysis is conducted by coupling FRAPCON-xt with the DAKOTA toolbox, allowing the propagation of thermo-mechanical input variabilities through Monte Carlo simulations. The input variabilities include fuel rod design, irradiation history, cladding temperature evolution during dry storage, and cladding temperature at the time of the accident. This approach facilitates an estimation of failure probability based on the selected FOM. Figure 53 illustrates the statistical approach followed in this methodology.

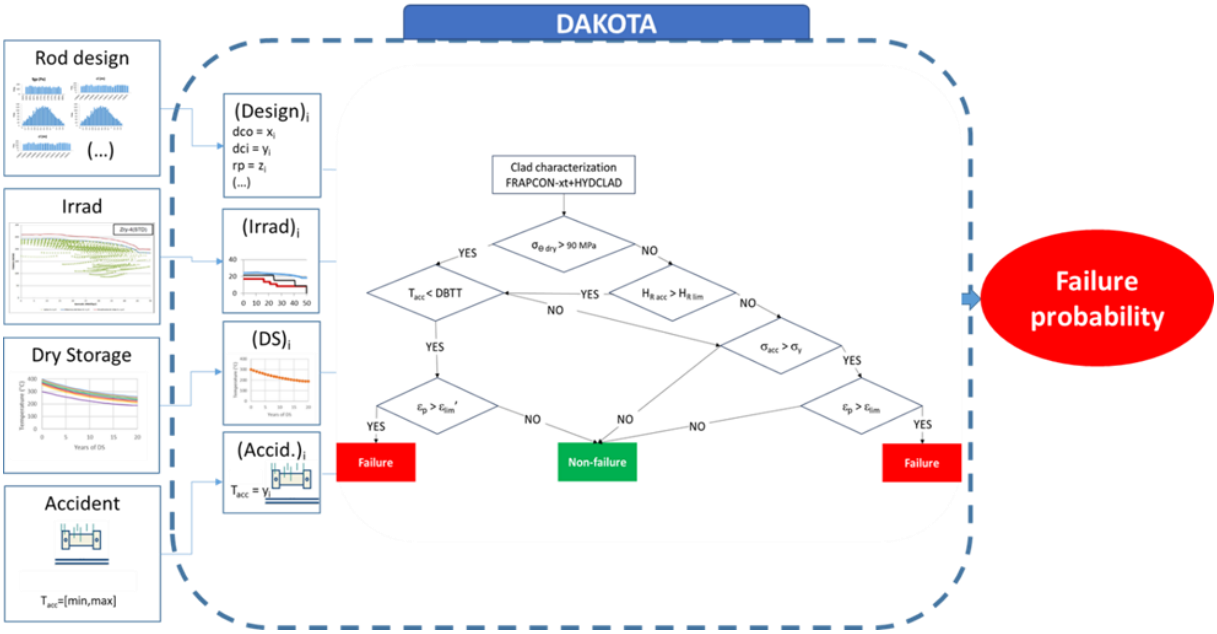

Figure 53 – Statistical approach scheme.

The methodology was applied to an irradiated PWR fuel rod under a side drop accident scenario after 20 years of dry storage in a metallic cask. A total of 1000 cases were simulated. The results, shown in Figure 54, indicate large safety margins, with maximum cladding hoop stress at dry storage onset significantly below the threshold for hydride reorientation, and minimum yield stress during the accident providing ample safety margin.

Further analysis examined the impact of different stages on the assessment, including irradiation, storage, and accident stages. For the irradiation stage, the impact of the fission gas release (FGR) model on hydride radial reorientation embrittlement at high burnup was analysed, showing minor differences between models. The storage stage analysis assessed the effect of irradiation damage annealing on yield stress, indicating that annealing might play a significant role in ensuring cladding integrity. Finally, the accident stage analysis compared yield stresses at room temperature and under flexural loads, demonstrating that plasticity would not be reached under accident conditions.

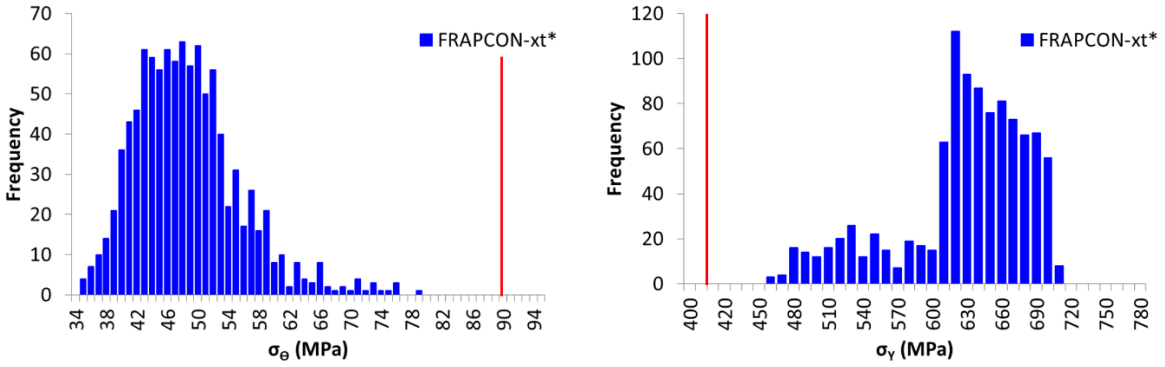

Figure 54 – Cladding hoop stress at dry storage onset (left) and yield stress at the moment of the accident (right); red lines represent the ductile-to-brittle threshold set (left) and the accident maximum stress applied (right).

4.5. Analysis of potential fire accident scenario in dry-storage facility

The Technical University of Sofia (TUS) has studied a scenario for a fire and associated risk assessment in the Dry Spent Fuel Storage Facility (DSFSF) at Kozloduy Nuclear Power Plant (NPP) in Bulgaria. This study assess the impacts on the storage facility and its contents and evaluate the effectiveness of existing safety measures.

By using the PyroSim software to model fire growth, smoke movement, and thermal effects within the storage facility, the IDOM's methodology was used for risk assessment and impact qualification. Real data from Kozloduy NPP ensures the scenario's accuracy.

Simulation results indicate that a fire in the DSFSF can significantly affect the facility's safety functions, particularly thermal loading and smoke propagation. Thermal effects may compromise storage cask integrity, and smoke can obscure detection systems and hinder emergency responses. The risk assessment identifies critical factors contributing to the fire's severity, while the impact qualification evaluates the potential consequences on safety functions like containment and heat removal.

The study emphasises the need for comprehensive fire risk assessments for dry spent fuel storage facilities and recommends a robust fire detection and suppression systems, effective ventilation, and regular maintenance.

4.6. Exploratory studies of postulated DSFSF-related accident scenarios facility

Potential recriticality during storage and transportation accidents of SNF has been studied by MCNP analyses both in ENUN 32P (PWR) and HI-STAR 100 MPC68 (BWR). The study concluded that the only possibility of achieving critical conditions is in case of internal flooding plus fresh fuel conditions. The effective criticality constant for optimum moderation has been worked out as a function of water density. According to the observations, additional safety measures can be added to avoid these scenarios. Anyway, the accident scenario identified is very unlikely and uncertain. Availability of data concerning the degradation of inner rack components would notably reduce the existing uncertainties.

An exploratory analysis of a postulated accident in a SNF vault storage system has been carried out assuming fuel rods and capsules failed. The radioactive material transport has been modelled with MELCOR 2.2, an integral severe accident code that has proved to be capable of simulating the scenario proposed. The MELCOR model of the scenario, based on a single tube with two vertically stacked spent fuel canisters, was very simple since no quantitative results were pursued in the study. Nonetheless, the model was sound enough to produce insights into a postulated accident scenario. The scenario

considers the release of cesium particles from a ruptured canister, as well as a crack in the tube that could lead to the release of fission products into the environment. The results show that most of Cs mass (over 99%) is primarily deposited by gravitational settling on the bottom of the canisters within the tube. The fraction eventually released to the environment (<0.3%) was noted to be primarily dependent on variables like crack size and particle size.

4.7. Management of high level nuclear waste resulting from Chernobyl-4 NPP accident

Management of spent nuclear fuel (SNF), including damaged SNF, fuel containing materials (FCM), High Level or Low Level Waste (HLW/LLW), after the Chernobyl-4 NPP accident is a reference to consider, if needed. A specific compilation study has been conducted. The report outlines the general solutions for spent nuclear fuel management in Ukraine, and the specific implementation of these solutions at the Chernobyl NPP. The report describes the old "wet" SNF storage facility - ISF-1, and the new, "dry" storage facility - ISF –2, including the technologies and procedures being used. A special emphasis is given to the management of damaged spent nuclear (DSNF) fuel at the Chernobyl NPP.

5. Acknowledgements

The authors express their gratitude to Stefano Caruso/KKG, Henrik Liljenfeldt/ Noemi Analytics, Laura Mc Manniman/IAEA, David Hambley/NNL UK) and Márton Király/MTA-EK for their extremely valuable contributions to reviewing the manuscript. The authors are also grateful to Monica Storz/Nagra who supported us to a great extent in the finalisation of the report.

6. Conclusions

This report described how state-of-the-art in the field of spent nuclear fuel characterisation and assessment during the pre-disposal phase has been improved by contributions from the WP8. Chapter 2, presented an overview of the advancements made, focusing on improving experimental methods for characterising spent nuclear fuel (SNF) and assessing the performance of depletion codes used for fuel characterisation. The key conclusions emphasize the importance of high-quality experimental data for validating depletion codes used in spent nuclear fuel characterisation. Improvements in non-destructive assay methods and experimental techniques, such as neutron emission measurements and radiochemical analysis, are critical for reducing uncertainties. Systematic errors in depletion calculations, due to variations in nuclear data and burnup conditions, require more accurate nuclear data libraries. Recommendations include expanding experimental data diversity, refining NDA methods, and improving terminology and uncertainty handling to enhance code validation and fuel characterisation procedures.

Chapter 3 focused on advancements in the area of the behaviour of SNF and cladding after discharge. The characterisation of spent nuclear fuel rods is crucial for understanding their performance in storage and disposal. Key findings show that cladding softens at high temperatures and becomes brittle at low temperatures, particularly due to radial hydrides, which can cause cracking during transport. Hydrides can also reduce creep and prevent clad lift-off in dry storage. Enhanced modeling techniques have improved the prediction of cladding failure and fuel behavior in storage, while experimental studies on UO_2 materials show that lanthanides improve fuel durability. Future research should focus on experiments with irradiated fuel, further corrosion studies, and combined experimental and numerical analyses to better understand spent fuel rod integrity.

Finally, Chapter 4 provided updates in the area of accident scenarios analysis. Great advancements have been achieved related to the development of different methodological approaches to investigate the structural integrity of SNF during postulated accident scenarios. Those methodological approaches benefit both from experimental and numerical data derived within this WP aiming to characterise the thermomechanical properties of the fuel and their evolution after discharge. To improve the safety of SNF storage systems, it is recommended to incorporate probabilistic risk assessments and detailed accident scenario analyses into the design and certification processes. Additionally, continuous monitoring and data collection programs should be established to refine models and methodologies, with a particular focus on irradiation damage recovery and long-term oxidation behaviour. Future efforts should aim to expand the scope of accident scenarios and incorporate advanced modelling techniques. Collaboration with industry partners and regulatory bodies will be essential to integrate these methods into standard safety practices and ensure the continued safety of SNF storage and transport systems.

A. Relevant Radionuclides

A list of relevant radionuclides for safety studies of a long-term storage installation for Belgian waste was set up by NIRAS/ONDRAF [Vandoorne, 2018]. These radionuclides, together with nuclear properties (half-live and decay mode) and the origin of these nuclides, are listed [Govers, 2019].

Nuclide	Half-life	Decay mode	Major source	Main location	Mostly present as
^{54}Mn	312 d	β^+, EC	^{54}Fe	ST, CL, FU	AL/IM, AP
^{94}Nb	2.00 10^4 a	β^-	^{93}Nb	CL	AL, AP
^{59}Ni	7.6 10^4 a	β^+, EC	^{58}Ni	ST, CL, FU	AL/IM, AP
^{93}Zr	1.53 10^6 a	β^-	^{92}Zr, FP	FU, CL	FP, AL, AP.
^{63}Ni	101 a	β^-	^{62}Ni	ST, CL, FU	AL/IM, AP
^{10}Be	1.6 10^6 a	β^-	^{9}Be	FU	IM, AP
^{14}C	5700 a	β^-	^{14}N, ^{13}C	FU, CL	IM, AP
^{36}Cl	3.01 10^5 a	β^-, β^+, EC	^{35}Cl	FU, CL	IM, AP
^{41}Ca	1.03 10^5 a	ec	^{40}Ca	FU	IM, AP
^{60}Co	5.27 a	β^-	^{59}Co	ST, CL, FU	IM, AP
^{93}Mo	4000 a	EC	^{92}Mo, ^{93}Nb	ST, CL	AL/IM, AP
^{108m}Ag	418 a	β^-	^{107}Ag	FU, CL	IM, AP
^{110m}Ag	250 d	β^-	FP	FU	FP
^{125}Sb	2.76 a	β^-	FP, ^{124}Sb	FU, CL	AL/IM, AP, FP
^{3}H	12.3 a	β^-	FP	FU	FP
^{79}Se	3.56 10^6 a	β^-	FP	FU	FP
^{85}Kr	10.8 a	β^-	FP	FU, plenum	FP
^{90}Sr	28.8 a	β^-	FP	FU	FP
^{99}Tc	2.14 10^5 a	β^-	FP	FU	FP
^{106}Ru	1.06 a	β^-	FP	FU	FP
^{107}Pd	6.5 10^6 a	β^-	FP	FU	FP
^{126}Sn	2.3 10^5 a	β^-	FP	FU	FP
^{129}I	1.61 10^7 a	β^-	FP	FU	FP

Nuclide	Half-life	Decay mode	Major source	Main location	Mostly present as
^{134}Cs	2.07 a	β^-	FP	FU	FP
^{135}Cs	2.3 10^6 a	β^-	FP	FU	FP
^{137}Cs	30.0 a	β^-	FP	FU	FP
^{144}Ce	285 d	β^-	FP	FU	FP
^{147}Pm	2.62 a	β^-	FP	FU	FP
^{151}Sm	90.0 a	β^-	FP	FU	FP
^{154}Eu	8.59 a	β^-	FP	FU	FP
^{155}Eu	4.75 a	β^-	FP	FU	FP
^{226}Ra	1600 a	β^-	(4n+2) DS	FU	AC
^{229}Th	7340 a	α	(4n+1) DS	FU	AC
^{230}Th	7.54 10^4 a	EC, β^+, β^-, α	(4n+2) DS	FU	AC
^{232}Th	1.41 10^{10} a	α	(4n) DS	FU	AC
^{231}Pa	3.28 10^4 a	α	(4n+3) DS	FU	AC
^{233}U	1.59 10^5 a	α	(4n+1) DS	FU	AC
^{234}U	2.46 10^5 a	α	(4n+2) DS	FU	AC
^{235}U	7.04 10^8 a	α	Fabrication	FU	AC
^{236}U	2.37 10^7 a	α	^{235}U	FU	AC
^{238}U	4.47 10^9 a	α	Fabrication	FU	AC
^{237}Np	2.14 10^6 a	α	^{236}U, ^{241}Am	FU	AC
^{238}Pu	87.7 a	α	^{237}Np	FU	AC
^{239}Pu	2.41 10^4 a	α	^{238}U	FU	AC
^{240}Pu	6563 a	α	^{239}Pu	FU	AC
^{241}Pu	14.3 a	β^-	^{240}Pu	FU	AC
^{242}Pu	3.74 10^5 a	α	^{241}Pu	FU	AC
^{244}Pu	8.00 10^7 a	α	^{242}Pu	FU	AC
^{241}Am	433 a	α	^{241}Pu	FU	AC
^{242m}Am	141 a	IT	^{241}Pu	FU	AC

Nuclide	Half-life	Decay mode	Major source	Main location	Mostly present as
^{243}Am	7365 a	α	^{242m}Am, ^{242}Pu	FU	AC
^{242}Cm	163 d	α	^{242m}Am	FU	AC
^{243}Cm	30.0 a	α	^{242}Cm	FU	AC
^{244}Cm	18 a	α	^{243}Cm, ^{244}Am	FU	AC
^{245}Cm	8500 a	α	^{244}Cm	FU	AC
^{246}Cm	4730 a	α	^{245}Cm	FU	AC
^{247}Cm	1.6 10^{7} a	α	^{246}Cm	FU	AC
^{248}Cm	3.4 10^{5} a	α	^{247}Cm	FU	AC

EC: Electron Capture
IT: Isomeric Transition
DS: Decay series
FP: Fission Product
AL: Alloying
IM: Impurity
AP: Activation Product
ST: Structures
CL: Cladding
FU: Fuel

References

[Adkins, 2013] Adkins, H., Geelhood, K.J., Koeppel, B., Coleman, J., Bignell, J., Flores, G., Wang, J.-A., Sanborn, S. Spears, R., Klymyshyn, N.: Used Nuclear Fuel Loading and Structural Performance Under Normal Conditions of Transport – Demonstration of Approach and Results on Used Fuel Performance Characterisation, 2013.

[Agrenius, 2002] Agrenius, L.: Criticality safety calculations of storage canisters, Technical Report TR02-17, April 2002.

[Aguado, 2021] Aguado, C., Feria, F., Herranz, L.E.: Assessment of FRAPCON predictive capabilities for spent fuel characterisation, Proc. TopFuel 2021, Santander, 24.-28.10.2021.

[Aguado, 2022] Aguado, C., Feria, F., Herranz, L.E.: Strengthening the initial thermo-mechanical characterisation of spent fuel facing dry storage, Proc. 47th Annual Meeting of the Spanish Nuclear Society, Cartagena, 28.-30.09.2022.

[Álvarez-Velarde, 2014] Álvarez-Velarde, F., González-Romero, E.M., Rodríguez, I.M.: Validation of the burn-up code EVOLCODE 2.0 with PWR experimental data and with a Sensitivity/Uncertainty analysis, Annals of Nuclear Energy, 73 (2014) 175-188.

[Álvarez-Velarde] Álvarez-Velarde, F., Panizo-Prieto, S: "Contribution of CIEMAT to EURAD WP8 Task 2.1 on Uncertainty Propagation in Depletion Analysis", CIEMAT internal report DFN/IN-01/11-21

[Ancius, 2019] Ancius, D., Aymanns, K., Checcis, P., Gonella, F., Jussofie, A., Montecassiano, F., Murtezi, M., Schwalbach, P., Schoop, K., Vanini, S., Zumerle, G.: Modelling of safeguards verification of spent fuel dry storage casks using muon trackers, Proceedings 41th ESARDA Symposium, 14. – 16. May 2019, Stresa, Italy, pp. 142-148, 2019.

[Anderson, 1955a] Anderson, J.S., Roberts, L.E.J.,Harper, E.A.: The oxides of uranium. Part VII: The oxidation of uranium dioxide. Journal of the Chemical Society (resumed), pp. 3946-3959, 1955.

[Anderson, 1955b] Anderson, J.S., Harper, E.A., Moorbath, S., Roberts, L.E.J.: The properties and microstructure of uranium dioxide; their dependence upon the mode of preparation. UK Atomic Energy Authority Report, AERE C/R 886, 1955.

[Andersson 2020] Andersson, P., Rathore, B., Senis, L., Anastasiadis, A., Sundén, E.A., Atak, H., Holcombe, S., Håkansson, A., Jansson P., Nyberg, J.: Simulation of the response of a segmented High-Purity Germanium detector for gamma emission tomography of nuclear fuel. Submitted for publication in SN Applied Sciences, 2020.

[Andersson, 2016] Andersson, P., Holcombe, S., Tverberg, T.: Inspection of a LOCA Test Rod at the Halden Reactor Project using Gamma Emission Tomography", Conference Top Fuel 2016 – LWR Fuels with Enhanced Safety and Performance, American Nuclear Society, 11. – 16. September 2016 Boise, Idaho, USA.

[Ansari, 2007] S.A. Ansari, M. Asif, T. Rashid, K.G. Qasim, “Burnup studies of spent fuels of vayring types and enrichment”, Annals of Nuclear Energy 34 (2007) 641 – 651

[Arkoma, 2018] Arkoma, A., Huhtanen, R., Leppänen, J., Peltola, J., Pättikangas, T.: Calculation chain for the analysis of spent nuclear fuel in long-term interim dry storage. Annals of Nuclear Energy, Vol. 119, pp. 129-138, 2018.

[Aronson, 1957] Aronson, S., Roof, R., Belle, J.: Kinetic Study of the Oxidation of Uranium Dioxide, The Journal of Chemical Physics 27 (1957) 137-144.

[ASTM 1969] ASTM, Standard Test Method for Atom Percent Fission in Uranium and Plutonium Fuel (Neodymium-148 Method), Annual Book of ASTM Standards 12.02, E321-69, 1969.

[ASTM, 2010] ASTM 1562, Standard Guide for Evaluation of Materials Used in Extended Service of Interim Spent Nuclear Fuel Dry Storage Systems, ASTM C1562-10, 2010.

[ASTM, 2012] ASTM, Standard Test Method for Atom Percent Fission in Uranium and Plutonium Fuel (Neodymium-148 Method), Annual Book of ASTM Standards, 12.02 E321-96, 2012,

[Aures, 2017] Aures, A., Bostelmann, F., Hursin, M., Leray, O.: Benchmarking and application of the state-of-the-art uncertainty analysis methods XSUSA and SHARK-X, Annals of Nuclear Energy 101 (2017) 262-269.

[Bae, 1994] Bae, K.K., Kim, B.G., Lee, Y.W., Yang, M.S., Park, H.S.: Oxidation behavior of unirradiated UO2 pellets. Journal of Nuclear Materials, Vol. 209, pp. 274-279, 1994.

[Baeten, 2003] Baeten, P., D'hondt, P., Sannen, L., Marloye, D., Lance, B., Renard, A., Bassellier, J.: The REBUS Experimental Programme for Burn-up Credit, Proceedings of the 7th International Conference on Nuclear Criticality Safety (ICNC2003), Tokai-mura, Japan, 20.-24. October 2003, JAERI – Conf 2003 – 019, pp. 645-649.

[Bahadir, 2009] Bahadir, T., Lindahl, S.O.: Studsvik's next generation nodal code SIMULATE-5, in Proceedings of the ANFM-2009 conference, Advances in Nuclear Fuel Management IV, Hilton Head Island, South Carolina, USA, 2009.

[Ballheimer, 2010] Ballheimer, V., Wille, F., Droste, B.: Mechanical safety analysis for high burn-up spent fuel assemblies under accident transport conditions. Packaging, Transport, Storage & Security of Radioactive Material, Vol. 21, pp. 212-217, 2010.

[Ballheimer, 2016] Ballheimer, V., Wille, F., Sterthaus, J., Linnemann, K., Rolle, A., Vlassopoulos, E., Nasyrow, R., Papaioannou, D., Rondinella, V.V.: Analysis of parameters affecting the bending behavior of spent fuel rods. In: Proc. 18th International Symposium on the Packaging and Transportation of Radioactive Materials (PATRAM 2016), Kobe, Japan, September 18. – 23., 2016.

[Bannister, 1968] Bannister, M.J.: The storage behaviour of uranium dioxide powders — review article. Journal of Nuclear Materials, Vol. 26, pp. 174-184, 1968.

[Barnes, 1970] Barnes, B.K., Hom, D.M., Sanders, W.M., Clinton, D.D., Swansen, J.E.: Techniques for two-dimensional gamma-ray scanning of reactor fuel element sections, Nuclear Applications and Technology 9 (1970) 746-754.

[Barnes, 1982] Barnes, B.K., Phillips, J.R., Barnes, M.L.: Reconstruction of radial fission product distributions in reactor fuels from a small number of projections, Journal of Nuclear Materials 106 (1982) 147-156.

[Barreiro, 2019] Barreiro Fidalgo, A., Jonsson, M.: Radiation induced dissolution of (U, Gd)O2 pellets in aqueous solution – A comparison to standard UO2 pellets, Journal of Nuclear Materials 514 (2019) 216-223.

[Bateman, 1910] Bateman, H.: The solution of a system of differential equations occurring in the theory of radioactive transformations, Proc. Cambridge Philos. Soc. 15 (1910) pp. 423-427.

[Bé, 2015] Bé, M.M., Isnard, H., Cassette, P., Mougeot, X., Lourenço, V., Altzitzoglou, T., Pommé, S., Rožkov, A., Auerbach, P., Sochorová, J., Dziel, T., Dersch, R., Kossert, K., Nähle, O., Krivošik, M., Ometáková, J., Stadelmann, G., Nonell, A., Chartier, F.: Determination of the ^{141}Sm half-life, Radiochemica Acta 103 (2015) 619-626.

[Becker, 2009] Becker, B., Dagan, R., Lohnert, G: Proof and implementation of the stochastic formula for ideal gas, energy dependent scattering kernel, Annals of Nuclear Energy, 36 (2009) 470-474.

[Belgonucléaire, 2000] Belgonucléaire, "ARIANE international programme final report", AR2000/15, BN Ref. 0000253/221, Rev. B, December 2000.

[Bell, 1973] Bell, M.J.: ORIGEN – The ORNL isotope generation and depletion code, ORNL-4628, May 1973.

[Bengtston, 2022] Bengtston, M., Jansson, P., Bäckstrom, U., Johanssson, F., Sjöland, A.: "Experimental Method for Verification of Calculated 137Cs Content in Nuclear Fuel Assemblies", Nuclear Technology 208 (2022) 295-302

[Berger, 2015] Berger, M.J.: ESTAR, PSTAR, and ASTAR", in: NIST, 2015. http://physics.nist.gov/Star.

[Berndt, 1988] Berndt, R.: Verification of spent PWR fuel data using the ^{154}Eu, ^{134}Cs and ^{137}Cs activities, Kernenergie 31 (1988) 59-63.

[Bertolino, 2003] Bertolino, G., Meyer, G., Ipina, J.P.: Effects of hydrogen content and temperature on fracture toughness of Zircaloy-4. Journal of Nuclear Materials, Vol. 320, pp. 272-279, 2003.

[Bevard, 2009] Bevard, B.B., Wagner, J.C., Parks, C.V., Aissa, M.: Review of information for spent nuclear fuel burnup confirmation, Report NUREG/CR-6998, December 2009.

[Billone, 2012] Billone, M.C., Burtseva, T.A., Liu, Y.Y.: Baseline Studies for Ring Compression Testing of High-Burnup Fuel Cladding. Report FCRD-USED-2013-000040, ANL 12/58, Argonne National Laboratory, Lemont, 2012.

[Billone, 2013a] Billone, M.C., Burtseva, T.A., Han, Z., Liu, Y.Y.: Used fuel disposition campaign – embrittlement and DBTT of high-burnup PWR fuel cladding alloys. Report FCRD-UFD-2013-000401, ANL-13/16, Argonne National Laboratory, Lemont, 2013.

[Billone, 2013b] Billone, M.C., Burtseva, T.A., Einziger, R.E.: Ductile-to-brittle transition temperature for high-burnup cladding alloys exposed to simulated drying-storage conditions. Journal of Nuclear Materials, Vol. 433, pp. 431-448, 2013.

[Billone, 2018] Billone, M.C., Burtseva, T.A.: Results of Ring Compression Tests – Spent Fuel and Waste Disposition. Report SFWD-SFWST-2018-000510, ANL-18/36, Argonne National Laboratory, Lemont, 2018.

[Billone, 2019] Billone, M.C.: Ductility of High-Burnup-Fuel ZIRLO™ following Drying and Storage – Spent Fuel and Waste Disposition. Report M2SF-19AN010201011, ANL-19/14, Argonne National Laboratory, Lemont, 2019.

[Bolind, 2014] Bolind, A.M.: Development of an analytical theory to describe the PNAR and CIPN nondestructive assay techniques, Annals of Nuclear Energy 66 (2014) 167-176.

[Bolind, 2015] Bolind A.M., Seya, M.: The State of the Art of Nondestructive Assay of Spent Nuclear Fuel Assemblies – A Critical Review of the Spent Fuel NDA Project of the U.S. Department of Energy's Next Generation Safeguards Initiative, JAEA-Review-2015-027, December 2015.

[Borella, 2011] Borella, A., Carchon, R., DeLimelette, C., Symens, D., van der Meer, K.: "Spent Fuel Measurements with the Fork Detector at the Nuclear Power Plant of Doel", in ESARDA 33rd annual meeting. Luxembourg, 2011 - ESARDA - European Safeguards Research & Development Association, Budapest, Hungary, 2011-05-16

[Borella, 2012] Borella, A., van der Meer, K.: "The Fork Detector for Spent Fuel Measurements: Measurements and Simulations", in Proceeding of the 53rd INMM Annual Meeting, 15-19 July 2012, Orlando, Florida, USA.

[Borella, 2017] Borella, A., Calleja, A., Fiorito, L.: Sensitivity studies on the production of Cm isotopes in spent fuel for safeguards applications, International Conference on Mathematics and Computational Methods Applied to Nuclear Science & Engineering, Jeju, Korea, April 16. – 20., 2017.

[Borms, 1999] Borms, L., Oeyen, J.: The design of a multipurpose tomography installation, Nuclear Instruments and Methods in Physics Research A422 (1999) 489-492.

[Børresen, 2004] Børresen, S.: Spent Nuclear Fuel Analyses based on In-Core Fuel Management Calculations, in: PHYSOR-2004, Chicago, Il, USA, 2004.

[Borresen, 2014] Borresen, S.: Spent nuclear fuel analyses based on in-core fuel management calculations, in Proceedings of the PHYSOR-2014 conference (The Westin Miyako, Kyoto, Japan, 2014).

[Bosbach, 2021] Bosbach, D., Cachoir, C., Myllykylä, E., Jegou, C., Rodríguez-Villagra, N., Farnan, I. et al.: DISCO Project Report - Model materials experiments: Final dissolution results, European Commission 2021.

[Bosler, 1991] Bosler, G.E., Rinard, P.M.: Burnup measurements with the Los Alamos FORK detector, Report LA-UR-91-2508, December 1991.

[Bouffioux, 2000] Bouffioux, P., Rupa, N.: Impact of Hydrogen on Plasticity and Creep of Unirradiated Zircaloy-4 Cladding Tubes. Zirconium in the Nuclear Industry: Twelfth International Symposium. Ed. Sabol, G., Moan, G., 100 Barr Harbor Drive, PO Box C700, West Conshohocken, PA 19428-2959: ASTM International, 2000.

[Bouffioux, 2001] Bouffioux, P., Leclercq, S., Cappelaere, C., Bredel, T.: Interim dry storage of PWR spent fuel assemblies – development of a long term creep law to assess the fuel cladding integrity. In: Proc. 8th international conference on radioactive waste management and environmental remediation (ICEM'01), Bruges, Belgium, Sep. 30. – Oct. 4., 2001.

[Boulanger, 2004] Boulanger, D., Lippens, M., Mertens, L., Basselier, J., Lance, B.: High Burnup PWR and BWR MOX Fuel Performance: A Review of Belgonucleaire Recent Experimental Programs, Proceedings. International Meeting LWR Fuel Performance, Orlando, Florida, September 19. – 22., 2004, American Nuclear Society, 2004.

[Bowman, 2011] Bowman, S.M.: SCALE 6: comprehensive nuclear safety analysis code system, Nuclear Technology 174 (2011) 126-146.

[Briesmeister, 2000] Briesmeister, J.F.: MCNP - A General Monte Carlo N-Particle Code, Program Manual, LA-13709-M, LANL (2000).

[Broadhead, 1995] Broadhead, B.L., DeHart, M.D., Ryman, J.C., Tang, J.S., Parks, C.V.: Investigation of Nuclide Importance to Functional Requirements Related to Transport and Long-Term Storage of LWR Spent Fuel, Report ORNL/TM-12742, 1995.

[Broustaut, 2012] Broustaut, M.: Benchmarking of the ALEPH Burn-Up code, SCK•CEN/36467063, 2012.

[Brun, 2015] Brun, E., Damian, F., Diop, C.M., Dumonteil, E., Hugot, F.X., Jouanne, C., Lee, Y.K., Malvagi, F., Mazzolo, A., Petit, O., Trama, J.C., Visonneau, T., Zoia, A.: TRIPOLI-4®, CEA, EDF and AREVA reference Monte Carlo code" Annals of Nuclear Energy, 82 (2015) 151-160.

[Brunauer, 1938] Brunauer, S., Emmet, P., Teller, E.: Adsorption of Gases in Multimolecular Layers, Journal of the American Chemical Society 60 (1938) 309.

[Buurveld, 1993] Buurveld, H.A., Dassel, G.: Emission Computer Tomography on a Dodewaard Mixed Oxide Fuel Pin, Report ECN-C-93065, Petten, 1993.

[Cabellos, 2011] Cabellos, O., Martinez, J.S., Diez, C.J.: Isotopic uncertainty assessment due to nuclear data uncertainties in high-burnup samples, International Conference on Nuclear Criticality, Edinburgh, 19. – 23. September 2011.

[Caldwell, 1986] Caldwell, J.T., Hastings, R.D., Herrera, G.C., Kunz, W.E., Shunk, E.R.: The Los Alamos second-generation system for passive and active neutron assays of drum-size containers, Report LA10774-MS, September 1986.

[Čalič, 2022] Čalič, D., Kromar, M.: "Spent fuel characterisation analysis using various nuclear data libraries", Nuclear Energy Technology 54 (2022) 3260 - 3271.

[Camp, 2002] Camp, D.C., Martz, H.E., Roberson, G.P., Decman, D.J., Bernardi, R.T.: Nondestructive waste-drum assay for transuranic content by gamma-ray active and passive computed tomography, Nuclear Instruments and Methods in Physics Research A495 (2002).

[Campbell, 1989] Campbell, T. K., Gilbert, E. R., White, G. D.,Piepel, G. F. and Wrona, B. J.: Oxidation Behavior of Nonirradiated UO2, Nuclear Technology, vol. 85, pp. 160-171, 1989.

[Carlson, 2018] Carlson, A.D., Pronyaev, V.G., Capote, R. et al.: Evaluation of the neutron data standards, Nuclear Data Sheets 148 (2018) 143-188.

[Caruso, 2007] Caruso, S., Murphy, M., Jatuff, F., Chawla, R.: Validation of ^{134}Cs, ^{137}Cs and ^{154}Eu single ratios as burnup monitors for ultra-high burnup UO_2 fuel, Annals of Nuclear Energy 34 (2007) 28-35.

[Caruso, 2008] Caruso, S., Günther-Leopold, I., Murphy, M., Jatuff, F., Chawla, R.: Comparison of optimised germanium gamma spectrum try and multicollector inductively coupled plasma mass spectrometry for the determination of ^{134}Cs, ^{137}Cs and ^{154}Eu single ratios in highly-burnt UO_2, Nuclear Instruments and Methods in Physics Research A589 (2008) 425-435.

[Caruso, 2009] Caruso, S., Murphy, M., Jatuff, F., Chawla, R.: Determination of within-rod caesium and europium isotopic distributions in high burnup fuel rods through computerised gamma-ray emission tomography, Nuclear Engineering and Design 239 (2009) 1220-1228.

[Caruso, 2014a] Caruso, S., Jatuff, F.: Design, development and utilisation of a tomography station for γ-ray emission and transmission analyses of light water reactor spent fuel rods, Progress in Nuclear Energy 72 (2014) 49-54.

[Caruso, 2014b] Caruso, S., Panadero, A.L.: Development and Validation of Ad Hoc ORIGEN-ARP Libraries for Very High Burnup UO_2 PWR Fuel with SCALE/TRITON, PHYSOR 2014, Kyoto, Japan, 28.09-03.10 2014.

[Caruso, 2016] Caruso, S.: Estimation of the radionuclide inventory in LWR spent fuel assembly structural materials for long-term safety analysis, EPJ Nuclear Science and Technology 2 (2016).

[Casella, 2016] Casella, A., Hanson, B., Miller, W.: The effect of fuel chemistry on UO2 dissolution, Journal of Nuclear Materials 476 (2016) 45-55.

[Catherine, 2006] Catherine, C., Le Boulch, D., Carassou, S., Ramasubramanian, N., Lemaignan, C.: An internal conical mandrel technique for fracture toughness measurements on nuclear fuel cladding. Journal of Testing and Evaluation, Vol. 34, pp. 373-382, 2006.

[CEA, 2009] CEA, Nuclear fuels. Paris, 2009.

[Cetnar, 2000] Cetnar, J., Gronek, P.: BISON-C one dimensional transport and burnup calculation code with consideration of actinides and fission, Nuclear Science and Engineering, 134 (2000) 23-25.

[Cetnar, 2006] Cetnar, J.: General solution of Bateman equations for nuclear transformation, Annals of Nuclear Energy 33 (2006) 640-645.

[Chadwick, 2011] Chadwick, M.B. et al.: ENDF/B-VII.1 Nuclear Data for Science and Technology: Cross Sections, Covariances, Fission Product Yields and Decay Data, Nuclear Data Sheets. 112 (2011) 2887-2996. doi:10.1016/j.nds.2011.11.002.

[Chamssedine, 2010] Chamssedine, F., Sauvage, T., Peuget, S.: DIADDHEM set-up: New IBA facility for studying the helium behavior in nuclear glasses, Nucl. Instrum. Methods Phys. Res. Sect. B Beam Interact. Mater. At. 268 (2010) 1862–1866.

[Chatzidakis, 2016] Chatzidakis, S., Choi, C.K., Tsoukalas, L.H.: Interactioin of cosmic ray muons with spent fuel dry casks and determination of lower detection limit, Nuclear Instruments and Methods in Physics Research A 828 (2016) 37-45.

[Checchia, 2017] Checchia, P., Gonella, F., Rigoni, A., Vanini, S., Zumerle, G.: Muon tomography for spent nuclear fuel control, ESARDA Bulletin 54 (2017) 2-5

[Checchia, 2018] Checchia, P., Ancius, D., Goonella, F., Zumerle, G., Aymanns, K., Erdmann, N. Schwalbach, P., Vanini, S.: Muography of spent fuel containers for Safeguards purposes, IAEA Symposium on International Safeguards, IAEA-CN-267-048, 2018

[Choi, 1996] Choi, J.-W., McEachern, R.J., Taylor, P., Wood, D.D.: The effect of fission products on the rate of U3O8 formation in SIMFUEL oxidized in air at 250°C. Journal of Nuclear Materials, Vol. 230, pp. 250-258, 1996.

[Choi, 2018] Choi, H. et al.: Benchmarking DRAGON/PARCS Against KRITZ and FFTF Measurements, Journal of Nuclear Technology 205 (2018) 486-505.

[Christensen, 1999] Christensen, M. R., McKinnon, M. A.: Spent Nuclear Fuel Dry Transfer System Cold Demonstration Project, Final Report, USA, 1999.

[Cobos, 1998] Cobos, J., Papaioannou, D., Spino, J., Coquerelle, M.: Phase characterisation of simulated high burn-up UO2 fuel. Journal of Alloys and Compounds, Vol. 271-273, pp. 610-615, 1998.

[Coleman, 2014] Coleman, J.L., Spears, R.E.: Detailed PWR Fuel Rod and Grid Finite Element Analysis to Provide Equivalent Rod Stiffness and Damping and Equivalent Grid Shell Thickness to PWR Used Nuclear Fuel (UNF) Assembly – 14525 Idaho National Laboratory. In: Proc. Waste Management Symposia 2014 (WM2014), Phoenix, Arizona, USA, March 2. – 6., 2014.

[Colle, 2013] Colle, J.-Y., Hiernaut, J.-P., Wiss, T., Beneš, O., Thiele, H., Papaioannou, D., Rondinella, V.V., Sasahara, A., Sonoda, T., Konings, R.J.M.: Fission product release and microstructure changes of irradiated MOX fuel at high temperatures, J. Nucl. Mater. 442 (2013) 330–340.

[Colle, 2014] Colle, J.-Y., Maugeri, E.A., Thiriet, C., Talip, Z., Capone, F., Hiernaut, J.-P., Konings, R.J.M., Wiss, T.: A mass spectrometry method for quantitative and kinetic analysis of gas release from nuclear materials and its application to helium desorption from UO 2 and fission gas release from irradiated fuel, J. Nucl. Sci. Technol. 51 (2014) 700–711.

[Costa, 2021] Costa, D. R., Hedberg, M., Middleburgh, S. C., Wallenius, J., Olsson, P., Lopes, D. A.: Oxidation of UN/U2N3-UO2 composites: an evaluation of UO2 as an oxidation barrier for the nitride phases, Journal of Nuclear Materials 544 (2021) 152700.

[Courty, 2014] Courty, O., Motta, A.T., Hales, J.D.: Modeling and simulation of hydrogen behavior in Zircaloy-4 fuel cladding. Journal of Nuclear Materials, Vol. 452, pp. 311-320, 2014.

[Croff, 1983] Croff, A.G.: ORIGEN2: a versatile computer code for calculating the nuclide compositions and characteristics of nuclear materials, Nuclear Technology, 62 (1983) 335-352.

[Dagan, 2005] Dagan, R.: On the use of S(a,b) tables for nuclides with well pronounced resonances, Annals of Nuclear Energy 32 (2005) 367-377.

[Dallongeville, 2005] Dallongeville, M., Werle, J., McCreesh, G.: Fuel Integrity Project: Analysis of Results of Tests on Light Water Reactor Fuel Rods. Packaging, Transport, Storage & Security of Radioactive Material, Vol. 16, pp. 125-134, 2005.

[Dallongeville, 2010] Dallongeville, M., Zeachandirin, A., Purcell, P., Cory, A.: Finite elements analysis of intergrid bending tests on used fuel rods samples. In: Proc. 16th International Symposium on the Packaging and Transportation of Radioactive Materials (PATRAM 2010), London, UK, October 3. –8., 2010.

[Dallongeville, 2012] Dallongeville, M., Zeachandirin, A., Laurent, M.: Simplified approach to study fuel rod rupture risks by bending or Euler buckling, Proc. 9th International Conference on the Radioactive Materials Transport and Storage (RAMTRANSPORT 2012), Kensington, London, UK, 22. – 24. May, 2012.

[De Bona, 2020] De Bona, E., et al.: Radiation effects in alpha-doped UO2, Nucl. Instrum. Methods Phys. Res. Sect. B Beam Interact. Mater. At. 468 (2020) 54-59.

[Degueldre, 2016] Degueldre, C., Bertsch, J., Martin, M.: Post irradiation examination of nuclear fuel: Toward a complete analysis, Progress in Nuclear Energy 92 (2016) 242-253.

[Desgardin, 2001] Desgardin, P., Liszkay, L., Barthe, M.F., Henry, L., Briaud, J., Saillard, M., Lepolotec, L., Corbel, C., Blondiaux, G., Colder, A., Marie, P., Levalois, M.: Slow positron beam facility in Orleans, PosMaterial Sci. Forum. 363–365 (2001) 523–525.

[Desgranges, 2012] Desgranges, L., Baldinozzi, G., Simon, P., Guimbretière, G., Canizares, A.: Raman spectrum of U4O9: a new interpretation of damage lines in UO2: Raman spectrum of U4O9, J. Raman Spectrosc. 43 (2012) 455–458.

[Desgranges, 2014] Desgranges, L., Guimbretière, G., Simon, P., Duval, F., Canizares, A., Omnee, R., Jégou, C., Caraballo, R.: Annealing of the defects observed by Raman spectroscopy in UO2 irradiated by 25MeV He2+ ions, Nucl. Instrum. Methods Phys. Res. Sect. B Beam Interact. Mater. At. 327 (2014) 74–77.

[Desquines, 2014] Desquines, J., Drouan, D., Billone, M., Puls, M.P., March, P., Fourgeaud, S., Getrey, C., Elbaz, V., Philippe, M.: Influence of temperature and hydrogen content on stress-induced radial hydride precipitation in Zircaloy-4 cladding. Journal of Nuclear Materials, 453, 131-150, 2014.

[Díez, 2015] Díez, C.J., Buss, O., Hoefer, A., Porsch, D., Cabellos, O.: Comparison of nuclear data uncertainty propagation methodologies for PWR burn-up simulations, Annals of Nuclear Energy 77 (2015) 101-114.

[Dilg, 1973] Dilg, W., Mannhart, W., Steinchele, E., Arnold, P.: Precision neutron total cross section measurements on gold and cobalt in the 40 µeV – 5 meV range, Zeitschrift für Physik 264 (1973) 427-444.

[Dilg, 1974] Dilg, W., W. Mannhart, W.: Neutron total cross sections of Sc, V, Cu and Rh at µeV energies, Zeitschrift für Physik 266 (1974) 157-160.

[Dimitriou, 2014] Dimitriou, P., Nichols, A.L.: Total absorption gamma-ray spectroscopy for decay heat calculations and other applications, Summary report of a consultants' Meeting, 15. – 17. December 2014, IAEA, Vienna, INDC(NDS) – 0676.

[Dobrin, 1997] Dobrin, R., Craciunescu T., Tuturici, I.L.: The Analysis of Failed Nuclear Fuel Rods by Gamma Computed Tomography, Journal of Nuclear Materials 246 (1997) 37-42.

[Dokhane, 2018] Dokhane, A., Grandi, G., Vasiliev, A., Rochman, D., Ferroukhi, H.: Validation of PSI best estimate plus uncertainty methodology against SPERT-III reactivity initiated accident experiments, Annals of Nuclear Energy 118 (2018) 178.

[Donnelly, 2000] Donnelly, J.V. abd, Ovanes, M.: Validation of 3-Dimensional Neutron Transport Calculations of CANDU Reactivity Devices, 2000 ANS International Topical Meeting on Advances in Reactor Physics and Mathematics and Computation into the Next Millenium (PHYSOR 2000), May 7. – 12., 2000. Pittsburg, OA, USA, 2000.

[Ducros, 1985] Ducros, G.: ISARD, a method of tomographic reconstruction of the position of gamma emitters in a nuclear fuel pin from transversal gamma scanning, Nuclear Technology 68 (1985) 370-384.

[Durham, 2018] Durham, J.M., Poulson, D., Bacon, J., Chichester, D.L., Guardincerri, E., Morris, L, Plaud-Ramos, K., Schwendiman, W., Tolman, J.D., Winston, P.: Verification of Spent Nuclear Fuel in Sealed Dry Storage Casks via Measurements of Cosmic-Ray Muon Scattering, Physical Review Applied 9 (2018) 044013.

[Ebiwonjumi, 2019] Ebiwonjumi, B., Choi, S., Lemaire, M., Lee, D., Shin, H.C., Lee, H.S.: Verification and validation of radiation source term capabilities in STREAM, Annals of Nuclear Energy 124 (2019) 80-87.

[EC, 2008] European Commission: Understanding and Physical and Numerical Modelling of the Key

Processes in the Near Field and their Coupling for Different Host Rocks and Repository Strategies (NF-PRO). Final report., 2008.

[Eigenbrodt, 2014] Eigenbrodt, J., Tobin, S.J., Charlton, W.S., Bolind, A.M., Menlove, H.O., Seya, M., Trellue, H.R.: PNAR Measurements of Fugen Fuel, 55th Annual Meeting of the Institute of Nuclear Materials Management, Atlanta, Georgia, 20. – 14. July 2014.

[Eigenbrodt, 2016] Eigenbrodt, J., Menlove, H.O.: Spent fuel measurements: passive neutron albedo reactivity (PNAR) and photon signatures, Report LA-UR-16-22112, May 2016.

[Einziger, 1985] Einziger, R. E., Cook, J. A.: Behavior of Breached Light Water Reactor Spent Fuel Rods in Air and Inert Atmospheres at 229°C, Nuclear Technology 69 (1985) 55-71.

[Einziger, 1986] Einziger, R. E., Strain, R. V.: Behavior of breached PWR spent-fuel rods in an air atmosphere between 250ºC and 360ºC, Nuclear Technology 75 (1986) 82-95.

[Eloirdi, 2018] Eloirdi, R., Cakir, P., Huber, F., Seibert, A., Konings, R., Gouder, T.: X-ray photoelectron spectroscopy study of the reduction and oxidation of uranium and cerium single oxide compared to (U-Ce) mixed oxide films. Applied Surface Science, Vol. 457, pp. 566-571, 2018.

[Elorrieta, 2016] Elorrieta, J. M., Bonales, L. J., Rodriguez-Villagra, N. Baonza, V. G., Cobos, J.: A detailed Raman and X-ray study of UO_{2+x} oxides and related structure transitions. Physical Chemistry Chemical Physics, Vol. 18, pp. 28209-28216, 2016.

[Elorrieta, 2017] Elorrieta, J.M., Manara, D., Bonales, L.J., Vigier, J.F., Dieste, O., Naji, M., et al.: Raman study of the oxidation in (U, Pu)O2 as a function of Pu content. Journal of Nuclear Materials, Vol. 495, pp. 484-491, 2017.

[Elorrieta, 2018a] Elorrieta, J.M., Bonales, L.J., Baonza, V.G., Cobos, J.: Temperature dependence of the Raman spectrum of UO2. Journal of Nuclear Materials, Vol. 503, pp. 191-194, 2018.

[Elorrieta, 2018b] Elorrieta, J.M., Bonales, L.J., Fernández, S., Rodríguez-Villagra, N., Cobos, J.: Pre- and post-oxidation Raman analysis of (U, Ce)O2 oxides. Journal of Nuclear Materials, Vol. 508, pp. 116-122, 2018.

[El-Samrah, 2021] El-Samrah, M. G., Tawfic, A. F., Chidiac, S. E.: Spent nuclear fuel interim dry storage; Design requirements, most common methods, and evolution: A review, Annals of Nuclear Energy 160 (2021) 108408.

[Epifano, 2020] Epifano, E., Vauchy, R., Lebreton, F., Joly, A., Guéneau, C., Valot, Ch., Martin, Ch.: Behaviour of (U,Am)O2 in oxidizing conditions: a high-temperature XRD study, J. Nucl. Mater. 531 (2020) 151991.

[EPRI, 2007] Spent Fuel Transportation Applications - Assessment of Cladding Performance under normal and hypothetical accident conditions, EPRI Synthesis Report 1015048, 2007.

[Espriu-Gascon, 2015] Espriu-Gascon, A. Llorca, J., Domínguez, M., Giménez, J., Casas, I., de Pablo, J.: UO2 surface oxidation by mixtures of water vapor and hydrogen as a function of temperature. Journal of Nuclear Materials, Vol. 467, pp. 240-243, 2015.

[Evins, 2014] Evins, L. Z., Juhola, P., Vähänen, M.: REDUPP. Final report., Posiva Oy, 2014.

[Evins, 2021] Evins, L. Z., Bosbach D., Duro, L., Farnan I, Metz V, Riba O.: DISCO Final Scientific Report, Grant Agreement 755443., 2021.

[Ewing, 2015] Ewing, R. C.: Long-term storage of spent nuclear fuel. Nat Mater, Vol. 14, pp. 252-257, 2015.

[Eyserman, 2022a] Eysermans, J., Verwerft, M., Govers, K., Ichou, R., Ilas, G., Meryturek, U., Messaoudi, N., Romojaro, P., Slosse, N.: "REGAL International Program, Analysis of experimental data for depletion code validation", Annals of Nuclear Energy 172 (2022) 109057

[Eysermans, 2022b] Eysermans, J., Verwerft, M.: "Databook of flat burnup samples from rod D05 extracted from fuel assembly FT1X57, Tihange 1 NPP", Report R-8189 (rev.1), SCK CEN November, 2022

[Faridani, 2011] Faridani, M.N.: Classification and probabilistic model development for creep failures of structures: Study of X-70 carbon steel and 7075-T6 aluminum alloys. University of Maryland, 2011.

[Feria, 2015] Feria, F., Herranz, L.E., Penalva, J.: On the way to enabling FRAPCON-3 to model spent fuel under dry storage conditions: the thermal evolution. Annals of Nuclear Energy 85, 995-1002, 2015.

[Feria, 2017] Feria, F., Herranz, L.E.: Application of the BEPU methodology to assess fuel performance in dry storage. Annals of Nuclear Energy, 99, 240-246, 2017.

[Feria, 2018] Feria, F., Herranz, L.E..: Effect of the oxidation front penetration on in-clad hydrogen migration. Journal of Nuclear Materials, Vol. 500, pp. 349-360, 2018.

[Feria, 2020] Feria, F., Aguado, C., Herranz, L.E.: Extension of FRAPCON-xt to hydride radial reorientation in dry storage, Ann. Nucl. Energy 145 (2020) 107559.

[Feria, 2022] Feria, F., Aguado, C., Herranz, L.E.: Spent fuel rod initial characterisation in dry storage. Insights into the fission gas release modelling, Proc. 6th SEDS Workshop, Garching, Germany, 01.-03-06.2022.

[Feria, 2023] Feria, F., Herranz, L.E.: Assessment of hydride precipitation modelling across fuel cladding: Hydriding in non-defective and defective fuel rods, Ann. Nucl. Energy 188 (2023) 109810.

[Ferroukhi, 2008a] Ferroukhi, H., Hofer, K., Hollard, J.M., Vasiliev, A., Zimmermann, M.A.: Core Modelling and Analysis of the Swiss Nuclear Power Plants for Qualified R& D Applications, in Proc. Int. Conf. on the Physics of Reactors, PHYSOR'08, 2008, Interlaken, Switzerland.

[Ferroukhi, 2008b] Ferroukhi, H., Hofer, K., Hollard, J-M., Vasiliev, A., Zimmerman, M.A.: "Core Modelling and Analysis of the Swiss Nuclear Power Plants for Qualified R&D Applications", in Proc. Int. Conf. on the Physics of Reactors, PHYSOR'08, Interlaken, Switzerland

[Ferry, 2005] Ferry, C., Lovera, P., Poinssot, C., Garcia, P.: Enhanced diffusion under alpha self-irradiation in spent nuclear fuel: Theoretical approaches, J. Nucl. Mater. 346 (2005) 48–55.

[Ferry, 2010] Ferry, C., Piron, J.-P., Ambard, A.: Effect of helium on the microstructure of spent fuel in a repository: An operational approach, J. Nucl. Mater. 407 (2010) 100–109.

[Fiorito, 2014] Fiorito, L, Diez, C.J., Cabellos, O., Stankovskiy, A., Van den Eynde, G., Labeau, P.S.: Fission yield covariance generation and uncertainty propagation through fission pulse decay heat calculation, Annals of Nuclear Energy 69 (2014) 331-343.

[Fiorito, 2015] Fiorito, L, Piedra, D., Cabellos, O., Diez, C.J.: Inventory calculation and nuclear data uncertainty propagation on light water reactor fuel using ALEPH-2 and SCALE 6.2, Annals of Nuclear Energy 83 (2015) 137-146.

[Fiorito, 2016] Fiorito, L., Stankovskiy, A., Van den Eynde, G., Diez, C.J., Cabellos, O. abd, Labeau, P.E.: Generation of fission yield covariances to correct discrepancies in the nuclear data libraries, Annals of Nuclear Energy 88 (2016) 12-23.

[Fiorito, 2017] Fiorito, L, Žerovnik, G., Stankovskiy, A., van den Eynde, G., Labeau, P.E.: Nuclear data uncertainty propagation to integral responses using SANDY, Annals of Nuclear Energy 101 (2017) 359-366

[Fiorito, 2021] Fiorito, L., Romojaro, P., Cabellos, O., García-Hormigos, M., Hernandez-Solis, A., Sánchez-Fernández, S., Stankovskiy, A., Van den Eynde, G., Žerovnik, G.: "On the use of criticality and depletion benchmarks for verification of nuclear data", Annals of Nuclear Energy, 161 (2021) 108415

[Fiorito] Fiorito, L.: Private communication.

[Foster,1987] Foster, J.P.: Segmented expanding mandrel test methods (letter to editors). Journal of Nuclear Materials, Vol. 150, pp. 342-350, 1987.

[Freyss, 2006] Freyss, M., Vergnet, N., Petit, T.: Ab initio modeling of the behavior of helium and xenon in actinide dioxide nuclear fuels, J. Nucl. Mater. 352 (2006) 144–150.

[Fröhner, 2000] Fröhner, F.H.: Evaluation and analysis of nuclear resonance data, JEFF Report 18, NEA/OECD, 2000.

[Frost, 2020] Frost, D. G., Galvin, C. O. T., Cooper, M. W. D., Obbard, E. G., Burr, P. A.: Thermophysical properties of urania-zirconia (U,Zr)O2 mixed oxides by molecular dynamics, Journal of Nuclear Materials 528 (2020) 151876.

[Fujino, 1992] Fujino, T., Sato, N.: Analyses of the oxygen potential of the solid solutions MyU1−yO2+x (M = M3+andM2+) by statistics of defects and defect complexes. Journal of Nuclear Materials, Vol. 189, pp. 103-115, 1992.

[FY2014] FY 2014 Status Report : Quantification of CIRFT System Biases and Uncertainties When Testing High-Burnup Spent Nuclear Fuel, 2014.

[FY2017] FY 2017 Status Report : CIRFT Data Update and Data Analyses for Spent Nuclear Fuel Vibration Reliability Study, 2017.

[Galvin, 2016] Galvin, C.O.T., Cooper, M.W.D., Fossati, P.C.M., Stanek, C.R., Grimes, R.W., Andersson, D.A.: Pipe and grain boundary diffusion of He in UO 2, J. Phys. Condens. Matter. 28 (2016) 405002.

[Gandini, 1975] Gandini, A.: Time-dependent generalized perturbation methods for burn-up analysis, NEACRP-L-130, 1975.

[Garcia, 2012] Garcia, P., Martin, G., Desgardin, P., Carlot, G., Sauvage, T., Sabathier, C., Castellier, E., Khodja, H., Barthe, M.-F.: A study of helium mobility in polycrystalline uranium dioxide, J. Nucl. Mater. 430 (2012) 156–165.

[Garrido, 2004] Garrido, F., Nowicki, L., Sattonnay, G., Sauvage, T., Thomé, L.: Lattice location of helium in uranium dioxide single crystals, Nucl. Instrum. Methods Phys. Res. Sect. B Beam Interact. Mater. At. 219–220 (2004) 196–199.

[Gauld, 2001] Gauld, I.C., Ryman, J.C.: Nuclide importance to criticality safety, decay heating, and source terms related to transport and interim storage of high-burnup LWR fuel, Report NUREG/CR-6700, January 2001.

[Gauld, 2003] Gauld, I.C.: Strategies for Applications of Isotopic Uncertainties in Burnup Credit, Report NUREG/CR-6811, June 2003.

[Gauld, 2005] Gauld, I.C. Mueller, D.E.: Evaluation of Cross-Section Sensitivities in Computing Burnup Credit Fission Product Concentrations, ORNL/TM-2005/48, August 2005.

[Gauld, 2006] Gauld, I.C., Bowman, S.M., Murphy, B.D., Schwalbach, P.: Applications of ORIGEN to spent fuel safeguards and non-proliferation", in Proceedings of the INMM 47th Annual Meeting, 16. – 20. July 2006, Nashville, Tennessee.

[Gauld, 2010] Gauld, I.C., Ilas, G., Murphy, B.D., Weber, C.F.: Validation of SCALE 5 decay heat predictions for LWR spent nuclear fuel, Report, TM-2008/015, February 2010.

[Gauld, 2011a] Gauld, I.C., Ilas, G., Radulesu, G.: Uncertainties in predicted isotopic compositions for high burnup PWR spent nuclear fuel, Report NUREG/CR-7012, January 2011.

[Gauld, 2011b] Gauld, I.C., Radulescu, G., Ilas, G., Murphy, B.D., Williams, M.L., Wiarda, D.: Isotopic depletion and decay methods and analysis capabilities in scale, Nuclear Technology 174 (2011) 169-195.

[Gauld, 2015] Gauld, J.C., Hu, J., DeBaere, P., Vaccaro, S., Schwalbach, P., Liljenfeldt, H., Tobin, S.: In-field performance testing of the FORK detector for quantitative spent fuel verification, in Proceedings of the 37th Annual ESARDA Symposium, Manchester, 2015.

[Gauld, 2016] Gauld, I.C., Giaquinto, J.M., Delashmitt, J.S., Hu, J., Ilas, G., Haverlock, T.J., Romano, C.: Re-evaluation of spent nuclear fuel assay data for the Three Mile Island unit reactor 1 and application to code validation, Annals of Nuclear Energy 87 (2016) 267-281.

[Gauld, 2017] Gauld, I.C., Williams, M.L., Michel-Sendis, F., Martinez, J.S.: Integral nuclear data validation using experimental spent nuclear fuel compositions, Nucear Engineering and Technology 49 (2017) 1226-1233.

[Gauld, 2019] Gauld, I.C. Mertyurek, U.: Validation of BWR spent nuclear fuel isotopic predictions with applications to burnup credit, Nuclear Engineering and Design 345 (2019) 110-124.

[Geelhood, 2015] Geelhood, K.J., Luscher, W.G., Raynaud, P.A., Porter, I.E.: FRAPCON-4.0: A Computer Code for the Calculation of Steady-State, Thermal – Mechanical Behavior of Oxide Fuel Rods for High Burnup. PNNL-19418, Vol. 1, Rev. 2, 2015.

[Gérard, 2018] Gérard, D.: Validation expérimentale du code ALEPH2 d'évolution du combustible pour le calcul de chaleur résiduelle, UCL 17217, 2018.

[Giorgi, 2022] Giorgi, R., Cechet, A., Cognini, L., Magni, A., Pizzocri, D., Zullo, G., Schubert, A., Van Uffelen, P., Luzzi, L.: Physics-based modelling and validation of inter-granular helium behaviour in SCIANTIX, Nucl. Eng. Technol. 54 (2022) 2367–2375.

[Goetzmann, 1982[Goetzmann, O.: Die Bedeutung der Brennstoff-Verunreinigungen für das Brennstabverhalten. Journal of Nuclear Materials 53 (1982) 301-308.

[Gómez, 2008] Gómez, F., Quiñones, J., Iglesias, E., Rodriguez, N.: Dependence of the specific surface area of the nuclear fuel with the matrix oxidation. In: ATALANTE 2008: Nuclear Fuel Cycle for a Sustainable Future, Montpellier, France, 2008.

[Gomez, 2017] Gomez, F.J., Rengel, M.A.M., Ruiz-Hervias, J., Puerta, M.A.: Study of the hoop fracture behaviour of nuclear fuel cladding from ring compression tests by means of non-linear optimization techniques. Journal of Nuclear Materials, Vol. 489, pp. 150-57, 2017.

[Gomez, 2017b] Gómez-Sánchez, F.J., Martin-Rengel, M.A., Ruiz-Hervías, J.: A new procedure to calculate the constitutive equation of nuclear fuel cladding from ring compression tests, Progress in Nuclear Energy 97 (2017) 245-251.

[Govers, 2009] Govers, K., Lemehov, S., Hou, M., Verwerft, M.: Molecular dynamics simulation of helium and oxygen diffusion in, J. Nucl. Mater. 395 (2009) 131–139.

[Govers, 2015] Govers, K., Dobney, A., Gysemans, M., Verwerft, M.: Technical scope of the REGAL base program, Revision 1.2, External Report SCK•CEN-ER-110, January 2015.

[Govers, 2019] Govers, K., Boulanger, D., Meert, K., Leinders, G., Verwerft, M.: Characterisation of Belgian spent fuel assemblies, SCK•CEN, Mol, Report BLG-1142, 2019.

[Grambow, 2010] Grambow, J. B. B., Duro, L., Merino, J., Tamayo, A., Martin, C., Pepin, G., Schumacher, S., Smidt, O., Ferry, C., Jegou, C., Quiñones, J., Iglesias, E., Rodriguez Villagra, N., Nieto, J. M., Martínez-Esparza, A., Loida, A., Metz, V., Kienzler, B., Bracke, G., Pellegrini, D., Mathieu, G., Wasselin-Trupin, V., Serres, C., Wegen, D., Jonsson, M., Johnson, L., Lemmens, K., Liu, J., Spahiu, K., Ekeroth, E., Casas, I., de Pablo, J., Watson, C., Robinson, P., Hodgkinson, D.: MICADO: Model Uncertainty for the Mechanism of Dissolution of Spent Fuel in Nuclear Waste Repository, EURATOM Final activity report (Contract No.: FI6W-036366), Brussels, Belgium, 2010.

[Grandi, 2011] Grandi, G., Lindahl, S.O.: Benchmark of SIMULATE5 thermal hydraulics against the Frigg and NUPEC full bundle test experiments, International Topical Meeting on Nuclear Reactor Thermalhydraulics, Toronto, Ontario (Canada), 25. – 30. September 2011, NURETH-14.

[Grimaldi, 2022] Grimaldi, F.: "Nuclear data uncertainty quantification in fuel depletion calculations", MSc Thesis, Politecnico di Torino, August 2022, SCK CEN/50213296 Rev. 1.0, 2022F.

[Grimaldi, 2023] Grimaldi, F., Romojaro, P., Fiorito, L., Belfiore, E., Bruggeman, C., Dulla, S.: "Nuclear data uncertainty quantification on PWR spent nuclear fuel as a function of burnup", Frontiers in Energy Research 11 (2023) 1146598

[Gruel, 2011] Gruel, A., Leconte, P., Bernard, D., Archier, P., Noguère, G.: Interpretation of Fission Product Oscillations in the MINERVE Reactor, from Thermal to Epithermal Spectra, Nuclear Science and Engineering 169 (2011) 229-244.

[Guerin, 2013] Guerin, C., Laporte, T., Cappelaere, C., Vaille, C., Mongabure, P., Miquet, A., Bouffioux, P.: CAST3M modelling of a spent fuel assembly bending during a handling accident. Rod failure risk evaluation from the experimental results of spent fuel rod bending test, Mechanics & Industry, Vol. 305, pp. 301-305, 2013.

[Guilbert, 2003] Guilbert, S., Sauvage, T., Erramli, H., Barthe, M.F., Desgardin, P., Blondiaux, G., Corbel, C., Piron, J.P.: Helium behavior in UO2 polycrystalline disks, J. Nucl. Mater. 321 (2003) 121–128.

[Guilbert, 2004] Guilbert, S., Sauvage, T., Garcia, P., Carlot, P., Barthe, M.F., Desgardin, P., Blondiaux, G., Corbel, C., Piron, C., Gras, J.M.: He migration in implanted UO2 sintered disks, J. Nucl. Mater. 327 (2004) 88–96.

[Guimbretière, 2012] Guimbretière, G., Desgranges, L., Canizarès, A., Carlot, G., Caraballo, R., Jégou, C., Duval, F., Raimboux, N., Ammar, M.R., Simon, P.: Determination of in-depth damaged profile by Raman line scan in a pre-cut He2+ irradiated UO2, Appl. Phys. Lett. 100 (2012) 251914.

[Haddad, 2018] Haddad, Y., et al.: In situ characterisation of irradiation-induced microstructural evolution in urania single crystals at 773 K, Nuclear Instruments and Methods in Physics Research Section B: Beam Interactions with Materials and Atoms 435 (2018) 25-30.

[Haeck, 2012] Haeck, W., Cochet, B., Aguiar, L.: Monte Carlo depletion calculations using VESTA 2.1 new features and perspectives, International Conference on the Physics of Reactors 2012, PHYSOR 2012, Advances in Reactor Physics.

[Hairer, 1996] Hairer, E., Wanner, G.: 'Solving Ordinary Differential Equations II: Stiff and Differential-Algebraic Problems", Springer Series in Computational Mathematics 14, Springer-Verlag, Second Edition (1996).

[Hairer, 1999] Hairer, E., Wanner, G.: Stiff differential equations solved by Radau methods, Journal of Computational and Applied Mathematics 111 (1999) 93-111.

[Häkkinen, 2021a] Häkkinen, S.: "Gundremmingen-A assembly B23 sample I2680 depletion calculation with Serpent2", VTT Technical Research Centre of Finland. VTT Research Report No. VTT-R-00631-21, 2021

[Häkkinen, 2021b] Häkkinen, S.: "Sensitivity and uncertainty analysis of Gundremmingen-A assembly B23 sample I2680 depletion calculation with Serpent 2", VTT Technical Research Centre of Finland. VTT Research Report No. VTT-R-00632-21, 2021

[Hales, 2016] Hales, J.D., Gamble, K. A., Spencer, B. W., Novascone, S. R., Pastore, G., Liu, W., Stafford, D. S., Williamson, R. L., Perez, D. M., Gardner, R. J., Casagranda, A., Galloway, J., Matthews, C., Unal, C., Carlson, N.: BISON Users Manual, BISON Release 1.3. INL/MIS-13-30307 Rev. 3, 2016.

[Ham, 2011] Ham, Y.S., Sitaraman, S.: Partial defect tester: a novel approach to detect partial defects inpressurized water reactor spent fuel, Nuclear Technology 175 (2011) 401-418.

[Ham, 2015] Ham, Y., Sitaraman, S., Kerr, P., Rossa, R.: Partial defect verification of spent fuel assemblies by PDET: principle and field testing in interim fuel storage facility (CLAB) Sweden, ANIMMA conference, April 2015.

[Ham, 2019] Ham, Y., Sitaraman S., Kerr, P.: Verification of spent fuel inside dry storage casks using fast neutrons, ESARDA Bulletin 59 (2019) 47-56.

[Hanson, 1998] Hanson, B.D.: The Burnup Dependence of Light Water Reactor Spent Fuel Oxidation. Report PNNL-11929, Pacific Northwest National Laboratory, 1998.

[Hanson, 2003] Hanson, B.D., Cumblidge, S.E., Scheele, R.D., Sell, R.L.: The Effect of Rare Earth Dopants on UO2 Oxidation. United States, 2003.

[Hanson, 2012] Hanson, B., Alsaed, H., Stockman, C., Enos, D., Meyer, R., Sorenson, K.: Gap analysis to support extended storage of used nuclear fuel. Report PNNL-20509, Pacific Northwest National Laboratory, 2012.

[Hannstein, 2023] V. Hannstein, M. Behler, R. Henrt and F. Sommer, ”Validation of the burnup code MOTIVE with respect to fuel assembly decay heat data”, Frontiers in Energy Research, 11 (2023) 1083249.

[Harkness, 2018] Harkness, Zhu, T., Liang, Y., Rauch, E., Enqvist, A., Jordan, K.A.: Development of neutrón energy spectral signatures for passive monitoring of spent fuel nuclear fuels in dry cask storage, EPJ Web of Conferences 170 (2018) 07004.

[Hautamäki, 2000] Hautamäki, J., Tiitta, A.: Spent fuel verification options for final repository safeguards in Finland, STUK-YTO – TR 173, December 2000.

[Hautojärvi, 1995] Hautojärvi, P., Corbel, C.: Positron Spectroscopy of Defects in Metals and Semiconductors, Proc. Int. Sch. Phys. Enrico Fermi. 125 (1995) 491–532.

[He, 2013] He, L.-F., et al.: In situ TEM observation of dislocation evolution in Kr-irradiated UO2 single crystal. Journal of Nuclear Materials 443 (2013) 71-77.

[Hébert, 2006] Hébert, A.: 'Towards DRAGON Version4', Proceedings of Topical Meeting on Advances in Nuclear Analysis and Simulation (PHYSOR), Vancouver, Canada, September 10. – 14., 2006.

[Heck, 1974] Heck, D., Börner, H.R., Rousille, R.: Neutron capture cross section of 147Nd, Atomkernenergie 24 (1974) 141.

[Henzl, 2013] Henzl, V., Croft, S., Richard, J., Swinhoe, M.T., Tobin, S.J.: Determination of the plutonium content in a spent fuel assembly by passive and active interrogation using a differential die-away instrument", Nuclear Instruments and Methods in Physics Research A 712 (2013) 83-92.

[Herb, 2014] Herb, J., Sievers, J., Sonnenburg, H.G.: A new cladding embrittlement criterion derived from ring compression tests, Nuclear Engineering and Design, Vol. 273, pp. 615-630, 2014.

[Herranz, 2009] Herranz, E., Feria, F.: Spent fuel rod splitting due to UO2 oxidation during dry storage: Assessment of the database. Progress in Nuclear Energy, Vol. 51, pp. 201-206, 2009.

[Herranz, 2010] Herranz, L.E., Feria, F.: Extension of the FRAPCON-3.3 creep model to dry storage conditions. Progress in Nuclear Energy 52, 634-639, 2010.

[Herrero, 2015] Herrero, J.J., Pecchia, M., Ferrouki, H., Canepaad, S., Vasiliev, A., Caruso, S.: Computational Scheme for Burnup Credit Applied to Long Term Waste Disposal, Proceeding International Conference on Nuclear Criticality Safety, ICNC 2015, Charlotte, US, 2015.

[Herrero, 2017] Herrero, J.J., Vasiliev, A., Pecchia, M., Rochman, D., Ferroukhi, H., Johnson, L., Caruso, S.: Criticality Safety Assessment for Geological Disposal of spent Fuel using the PSI BUCSS R Methodology, Nagra Arbeitsbericht NAB 17-23, October 2017.

[Hicks, 2018] Hicks, T.W., Baldwin, T.D.: Review of Burn-up Credit Applications in Criticality Safety Assessments for Spent Fuel Management and Disposal, Contractor Report to RWM, Contractor Report no. GSL-1649-4-V3.1, January 2018.

[Higham, 2005] Higham, N.J.: The scaling and squaring method for the matrix exponential revisited, SIAM Journal on Matrix Analysis and Applications, 2 (2005) 1179-1193.

[Higham, 2009] Higham, N.: Cholesky Factorization, Vol. 1, John Wiley & Sons, Inc., 2009, pp. 251-254.

[Hill, 1962] Hill, D. C.: Phase Relations and Crystal Chemistry in the System Uranium Oxide–Lanthanum Oxide, Journal of the American Ceramic Society 45 (1962) 258-263.

[Hirose, 2012] Hirose, T., Ozawa, M., Miura, H., Baba, T., Kamimura, K.: Dynamic load impact tests on high burnup spent fuel rods of BWR and PWR. In: Proc. The Nuclear Materials Conference (NuMat 2012), Osaka, Japan, 2012.

[Hirose, 2013] Hirose, T., Ozawa, M., Miura, H., Baba, T., Kamimura, K.: Research on integrity of high burnup spent fuel under long term dry storage and transport. In: OECD/NEA International Workshop on Safety of Long Term Interim Storage Facilities, Munich, Germany, 2013.

[Hoekstra, 1961] Hoekstra, H.R., Santoro, A., Siegel, S.: The low temperature oxidation of UO2 and U4O9. Journal of Inorganic and Nuclear Chemistry, Vol. 18, pp. 166-178, 1961.

[Holcombe, 2015] Holcombe, S., Jacobsson, S., Svärd, J., Hallstadius, L.: A novel gamma emission tomography instrument for enhanced fuel characterisation capabilities within the OECD Halden Reactor Project, Annals of Nuclear Energy 85 (2015) 837-845.

[Holcombe, 2016] Holcombe, S., Andersson, P., Svärd, S.J., Hallstadius, L.: Determination of the rod-wise fission gas release fraction in a complete fuel assembly using non-destructive gamma emission, Nuclear Instruments and Methods in Physics Research A 837 (2016) 99-108.

[Hong, 2002] Hong, I.S.: Validation of DRAGON code in Connection with WIMS-AECL/RFSP Code System based on ENDF/B-VI Library and Two Group Model, Report KAERI/TR-2218/2002, Korean Atomic Energy Research Institute (2002).

[Honkamaa, 2014] Honkamaa, T., Lévay, F., Berndt, R., Schwalbach, P., Vaccaro, S., Turunen, A.: A Prototype for Passive Gamma Emission Tomography, Symposium on International Safeguards, IAEA, Vienna, 2014.

[Hsu, 2012] Hsu, H.H., Tsay, L.W.: Fracture properties of hydrided Zircaloy-4 cladding in recrystallization and stress-relief anneal conditions. Journal of Nuclear Materials, Vol. 422, pp. 116-123, 2012.

[Hu, 2014] Hu, J., Gauld, I.C.: Impact of nuclear data uncertainties on calculated spent fuel nuclide inventories and advanced NDA instrument response, ESARDA Bulletin 51 (2014) 9-18.

[Hu, 2016] Hu, J., Gauld, I.C., Peterson, J.L., Bowman, S.M.: "US commercial spent nuclear fuel assembly characteristics: 1968 – 2013", Report NUREG/CR-7227, September 2016.

[Hu, 2017] Hu, J., Giaquinto, J.M., Gauld, I.C., Ilas, G., Keever, T.J.: Analysis of new measurements of Calvert Cliffs spent fuel samples using SCALE 6.2, Annals of Nuclear Energy 106 (2017) 221-234.

[Hue, 1978] Hue, S.T., Crane, T.W., Talbert Jr. W.L., Lee, J.C.: Nondestructive assay methods for irradiated nuclear fuels, Report LA – 6923, January 1978.

[Hykes, 2013] Hykes, J.M., Ferrer, R.M.: Solving the Bateman equations in CASMO5 using implicit ODE numerical methods for stiff systems, M&C 2013, International Conference on Mathematics & Computational Methods Applied to Nuclear Science & Engineering, Sun Valley, Idaho, US, 5. – 9. May, 2013.

[IAEA, 1998] International Atomic Energy Agency, Durability of Spent Nuclear Fuels and Facility Components in Wet Storage, IAEA, Vienna, 1998.

[IAEA, 1999] International Atomic Energy Agency, Storage of Spent Fuel from Power Reactors, Proceedings of a symposium held in Vienna, 9-13 November 1998, IAEA, Vienna, 1999.

[IAEA, 2009] International Atomic Energy Agency, Predisposal Management of Radioactive Waste, IAEA Safety Standards Series No. GSR Part 5, IAEA, Vienna, 2009.

[IAEA, 2010] Review of Fuel Failures in Water Cooled Reactors Vol. No. NF-T-2.1. International Atomic Energy Agency, Vienna, 2010.

[IAEA, 2012] International Atomic Energy Agency, Storage of Spent Nuclear Fuel, IAEA, Vienna, 2012.

[IAEA, 2013] International Atomic Energy Agency, General Safety Guide GSG-3, "The Safety Case and Safety Assessment for the Predisposal Management of Radioactive Waste", 2013.

[IAEA, 2015] IAEA: Final Report CRP Spent Fuel Performance Final Report of a Coordinated Assessment and Research SPAR III (2009 – 2014). IAEA-Tecdoc-1771, IAEA, Vienna, 2015.

[IAEA, 2016] International Atomic Energy Agency, Safety Assessment for Facilities and Activities, IAEA Safety Standards Series No. GSR Part 4 – Rev.1, IAEA, Vienna, 2016.

[IAEA, 2018a] IAEA Safeguards, Research and Development Plan, Enhancing capabilities for nuclear verification, Report STR-385, January 2018.

[IAEA, 2018b] IAEA Safety Standards SSR-6 Rev.1 "Regulations for the Safe Transport of Radioactive Material", 2018.

[IAEA, 2019a] IAEA: Behaviour of spent power reactor fuel during storage extracts from the final reports of coordinated research projects on behaviour of spent fuel assemblies in storage (BEFAST I–III) and spent fuel performance assessment and research (SPAR I–III) – 1981-2014. IAEA-Tecdoc-1862, Vienna, 2019.

[IAEA, 2019b] IAEA: Demonstrating Performance of Spent Fuel and Related Storage System Components during Very Long Term Storage, Vienna, 2019.

[IAEA, 2020] IAEA Safety Standards SSG-15 "Storage of Spent Nuclear Fuel (Rev.1)", 2020.

[Iglesias, 2008] Iglesias,E., Quiñones, J.: Analogous materials for studying spent nuclear fuel: The influence of particle size distribution on the specific surface area of irradiated nuclear fuel. Applied surface science, Vol. 254, pp. 6890-6896, 2008.

[Ilas, 2008] Ilas, G., Gauld, I.C.: SCALE analysis of CLAB decay heat measurements for LWR spent fuel assemblies, Annals of Nuclear Energy 35 (2008) 37-48.

[Ilas, 2010] Ilas, G., Gauld, I.C., Murphy, B.D.: Analysis of experimental data for high burnup PWR spent fuel isotopic validation) ARIANE and REBUS programs (UO_2 fuel), Report NUREG/CR-6969, February 2010.

[Ilas, 2011] Ilas, G., Gauld, I.C.: Analysis of experimental data for high-burnup PWR spent fuel isotopic validation – Vandellós II reactor, Report NUREG/CR – 7013, January 2011.

[Ilas, 2012] Ilas, G., Gauld, I.C., Radulescu, G.: Validation of new depletion capabilities and ENDF/B-VII data libraries in SCALE, Annals of Nuclear Energy 46 (2012) 43-55.

[Ilas, 2014] Ilas, G., Gauld, I.C., Lijenfeldt, H.: Validation of ORIGEN for LWR used fuel decay heat analysis with SCALE, Nuclear Engineering and Design 273 (2014) 58-67.

[Ilas, 2017] Ilas, G., Liljenfeldt, H.: Decay heat uncertainty for BWR used fuel due to modeling and nuclear data uncertainties, Nuclear Engineering and Design 319 (2017) 176-184.

[ISO 7438, 2016] ISO 7438:2016. Metallic materials - Bend test.

[Isotalo, 2011] Isotalo. A.E., Aarnio, P.A.: Comparison of depletion algorithms for large systems of nuclides, Annals of Nulcear Energy 38 (2011) 261-268.

[Isotalo, 2015] Isotalo, A.E., Wieselquist, W.A.: A method for including external feed in depletion calculations with CRAM and implementation in ORIGEN, Annals of Nuclear Energy 85 (2015) 68-77.

[Isotalo, 2016] Isotalo, A., Pusa, M.: Improving the accuracy of the Chebyshev Rational Approximation Method using substeps, Nuclear Science and Engineering 183 (2016) 65-77.

[Ito, 2004] Ito, K., Kamimura, K., Tsukuda, Y.: Evaluation of irradiation effect on spent fuel cladding creep properties. Proceedings of the 2004 International Meeting on LWR Fuel Performance, Orlando, Florida, September 19. – 22., 2004.

[Ivanov, 2013] Ivanov, K., Avramorva, M., Kamerow, S., Kodeli, I., Sartori, E., Ivanov, E., Cabellos, O.: Benchmarks for Uncertainty Analysis in Modelling (UAM) for the design, operation and safety analysis of LWRs, NEA/NSC/DOC(2013)7, May 2013.

[Iwasaki, 2009] Iwasaki, K., Matsui, T., Yanai, K., Yuda, R., Arita, Y., Nagasaki, T. et al.: Effect of Gd2 O3 Dispersion on the Thermal Conductivity of UO2, Journal of Nuclear Science and Technology 46 (2009) 673-676.

[Jaboulay, 2012] Jaboulay, J.C., Bourganel, S.: Analysis of MERCI decay heat measurements for PWR UO_2 fuel rod, Nuclear Technology 177 (2012) 73-82.

[Jansson, 2016] Peter Jansson, Michael L. Fugate, Andrea Favalli, Stephen J. Tobin, Anders Sjöland and Henrik Liljenfeldt, “Axial and Azimuthal Gamma Scanning of Nuclear Fuel – Implications for Spent Fuel Characterisation”, Journal of Nuclear Material Management, 45 (No; 1) (2016) 34 – 47.

[Jansson, 2020] Jansson, P., Bengtsson, M., Bäckström, U., Svensson, K., Lycksell, M., Sjöland, A.: Data from calorimetric decay heat measurements of five used PWR 17x17 nuclear fuel assemblies, Data in Brief 28 (2020) 104917.

[Jansson, 2022] Jansson, P., Bengtsson, M., Böckström, U., Álvarez-Velarde, F., Čalič, D., Caruso, S., Dagan, R., Fiorito, L., Giot, L, Govers, K., Hernandez Solis, A., Hannstein, V., Ilas, G., Kromar, M., Leppänen, J., Mosconi, M., Ortego, P., Plukienė, R., Plukis, A., Ranta-Aho, A., Rochman, D., Ros, L., Sato, S., Schillebeeckx, P., Shama, A., Simeonov, T., Stankovskiy, A., Trellue, H., Vaccaro, S., Vallet, V., Verwerft, M., Žerovnik, G., Sjöland, A.: "Blind Benchmark Exercise for Spent Nuclear Fuel Decay Heat", Nuclear Science and Engineering 196 (2022) 1125-1145

[Jaynes, 1968] Jaynes, J.E.T.: Prior Probabilities, IEEE T. Syst. Sci. Cyb., 4 (1968) 227-241.

[Jégou, 2010] Jégou, C., Caraballo, R., Peuget, S., Roudil, D., Desgranges, L., Magnin, M.: Raman spectroscopy characterisation of actinide oxides (U1−yPuy)O2: Resistance to oxidation by the laser beam and examination of defects, Journal of Nuclear Materials 405 (2010) 235-243.

[Jessee, 2014] Jessee, M.A., Wieselquist, W.A., et. al.: Polaris: A New Two-Dimensional Lattice Physics Analysis Capability for the SCALE Code System, PHYSOR 2014, Kyoto, Japan.

[Jiang, 2014] Jiang, H., Wang, J.J.: Methodology for mechanical property testing of fuel cladding using an expanding plug wedge test. Journal of Nuclear Materials, Vol. 446, pp. 27-37, 2014

[Jiang, 2016a] Jiang, H., Wang, J.A.J.: Spent nuclear fuel system dynamic stability under normal conditions of transportation. Nuclear Engineering and Design, Vol. 310, pp. 1-14, 2016.

[Jiang, 2016b] Jiang, H., Wang, J.A.J., Wang, H.: The impact of interface bonding efficiency on high-burnup spent nuclear fuel dynamic performance. Nuclear Engineering and Design, Vol. 309, pp. 40-52, 2016.

[Johnson, 1977] Johnson, J. et al.: Behavior of spent nuclear fuel in water pool storage, USA, 1977.

[Jordan, 2008] Jordan, K.A., Gozani, T., J. Vujic, J.: Differential die-away analysis system response modeling and detector design, Nuclear Instruments and Methods in Physics Research A 598 (2008) 436-444.

[Jung, 2013] Jung, H., Shukla, P., Ahn, T., Tipton, L., Das, K., He, X., et al.: Extended storage and transportation: Evaluation of drying adequacy. In: 14th International High-Level Radioactive Waste Management Conference (IHLRWMC), Albuquerque, New Mexico, 2013.

[Kaiser, 2018] Kaiser, R.: Muography: overview and future directions, Philosophical Transactions A 377 (2018) 20180049.

[Kamimura, 2003] Kamimura, K., Kohno, N., Itoh, K., Tsukuda, Y., Aomi, M., Yasuda, T., Murai, K., Fujii, H., Irisa, Y.: Thermal creep tests of BWR and PWR spent fuel cladding. Proc. International conference on storage of spent fuel from power reactors (Vienna, Austria, 2-6 Jun 2003), pp. 50-51, 2003.

[Kamimura, 2004] Ito, K., Kamimura, K., Tsukuda, Y.: Evaluation of irradiation effect on spent fuel cladding creep properties. Proc. 2004 International Meeting on LWR Fuel Performance, Orlando, Florida, September 19. – 22., 2004.

[Kapklan, 2014] Kapklan, A.C., Henzl, V., Menlove, H.O., Swinhoe, M.T., Belian, A.P., Flaska, M., Pozzi, S.A.: Determination of total plutonium content in spent nuclear fuel assemblies with the differential die-away self-interrogation instrument, Nuclear Instruments and Methods in Physics Research A 764 (2014) 347-351.

[Kashima, 2015] Kashima, T., Suyama, K., Mochizuli, H.: Validation of burnup calculation code SWAT4 by evaluation of isotopic composition data of mixed oxide fuel irradiated in pressurized water reactor, Energy Procedia 71 (2015) 159-167.

[Kellett, 2017] Kellett, M.A., Bersillon, O.: The Decay Data Evaluation Project (DDEP) and the JEFF-3.3 radioactive decay data library: combining international collaborative effort on evaluated data, EPJ Web of Conferences 146 (2017) 02009.

[Kępisty, 2007] Kępisty, G., Cetnar, J.: On the discrepancies between FIMA and specific burnup", Progress in Nuclear Energy 98 (2007) 187-192.

[Kienzler, 2017] Kienzler, B., Duro, L., Lemmens, K., Metz, V., De Pablo, J., Valls, A., Wegen, D. H., Johnson, L., Spahiu, K.: Summary of the Euratom Collaborative Project FIRST-Nuclides and Conclusions for the Safety Case, Nuclear Technology 198:3 (2017) 260-276.

[Kienzler, 2018] Kienzler, B., Geckeis, H.: Radioactive wastes and disposal options, EPJ Web Conf. 189 (2018) 00014.

[Kilgour, 1992] Kilgour, W.J., White, R.J., Shea, J.H., Turnbull, J.A.: The ENIGMA fuel performance code, code description, version 5.8d. Berkeley Nuclear Laboratories, TD/NS/REP/0035, 1992.

[Kim, 1995] Kim, H.S., Yoon, Y.K., Lee, Y.W.: Defect structures of U1 − yEryO2 ± x solid solutions. Journal of Nuclear Materials, Vol. 226, pp. 206-215, 1995.

[Kim, 2001] Kim, J.-G., Ha, Y.-K., Park, S.-D., Jee, K.-Y., Kim, W.-H.: Effect of a trivalent dopant, Gd3+, on the oxidation of uranium dioxide. Journal of Nuclear Materials, Vol. 297, pp. 327-331, 2001.

[Kim, 2007] Kim, J.S., Jeon, Y.S., Park, S.D., Han, S.H., Kim, J.G.: Burnup determination of high burnup a dry processed fuels based on isotope dilution mass spectrometric measurements, Journal of Nuclear Science and Technology, 44 (2007) 1015-1023.

[Kim, 2010] Kim, K.-T.: UO2/Zry-4 chemical interaction layers for intact and leak PWR fuel rods, Journal of Nuclear Materials 404 (2010) 128-137.

[Kim, 2015] Kim, J.S., Jeon, Y.S., Park, S.D., Ha, Y.K., Song, K.: Analysis of high burnup pressurized water reactor fuel using uranium, plutonium, neodymium and cesium isotope correlations with burnup, Nuclear Energy Technology 47 (2015) 924-933.

[Kirchknopf, 2022] Péter Kirchknopf, Istváv Almási, Gábor Radócz, Imre Nemes, Péter Völgyesi, Imre Szalóki, “Determining burnup, cooling time and operational history of VVER-440 spent fuel assemblies

based on in-situ gamma spectrometry at Paks Nuclear Power Plant", Annals of Nuclear Energy 170 (2022) 108975.

[Kleykamp, 1979] Kleykamp, H.: The chemical state of LWR high-power rods under irradiation. Journal of Nuclear Materials, Vol. 84, pp. 109-117, 1979.

[Koch, 1981] Koch, J.L., Schoof, S.: The Isotope Correlation Experiment ICE – Final Report, Technical Report EUR 7766 EN, 1981.

[Kodeli, 2001] Kodeli, I.: Multidimensional deterministic nuclear data sensitivity and uncertainty code system: method and application, Nuclear Science and Engineering 138 (2001) 45-66.

[Koleška, 2016] Michal Koleška, Ladislav Viererbl, Milan Marek, Jaroslov Ernest, Michal Šunka, "Determination of IRT-2M fuel burnup by gamma spectroscopy", Applied Radiation and Isotopes, 107 (2016) 92 – 97.

[König, 2021] König, T., Dagan, R., Dardenne, K., Herm, M., Metz, V., Pruessmann, T., Rothe, J., Schild, D., Walschburger, A., Geckeis, H.: Spectroscopic and chemical investigations on volatile fission and activation products within the fuel-cladding interface of irradiated pressurised water reactor fuel rod segments, Saf. Nucl. Waste Disposal, 1 (2021) 5–6.

[König, 2022] König, T.: "Examination of the radionuclide inventory and chemical interactions on the interface between nuclear fuel and Zircaloy-4 cladding in irradiated LWR-fuel samples", PhD Thesis, Karlsruher Instituts für Technologie (KIT), 26 April 2022

[König, 2022] König, T.: Examination of the radionuclide inventory and chemical interactions on the interface between nuclear fuel and Zircaloy-4 cladding in irradiated LWR-fuel samples, Report, Karlsruhe Institute of Technology, 2022.

[König, 2024] König T., Herm M., Metz V., Rodriguez Villagra N., Elorrieta J. M., Milena-Pérez A., Bonales L. J., Gutiérrez L., Fernández-Carretero S., Núñez A., Galán H., Király M., Bertsch J., Duarte L. I., Goutam K., Schneider C., Zencker U.: Final version as of 10.05.2024 of deliverable D8.10 of the HORIZON 2020 project EURAD. EC Grant agreement no: 847593, 2024.

[Koning, 2012] Koning, A.J., Rochman, D.: Modern Nuclear Data Evaluation with the TALYS Code System, Nuclear Data Sheets. 113 (2012) 2841-2934. doi:10.1016/j.nds.2012.11.002.

[Kromar, 2015] Kromar, M., Kurinčič, B.: Determination of the NPP Krško Spent Fuel Activity, Proceedings of 24th International Conference Nuclear Energy for New Europe – NENE 2015, Portorož, Slovenia, 2015, pp. 410.1-410.9.

[Kromar, 2017] Kromar, M., Kurinčič, B.: Determination of the NPP Krško spent fuel decay heat, Proceedings of AIP conference: Thermophysics 2017, 22nd International Meeting of Thermophysics 2017, Terchova, Slovakia, 2017, pp. 050005-1.

[Kromar, 2019] Kromar, M., Kurinčič, B.: Determination of the NPP Krško spent fuel characteristics with the Serpent and SCALE code systems, Proceedings of the 28th International Conference Nuclear Energy for New Europe – NENE 2019, Portorož, Slovenia, 2019 (to be published).

[Kromar, 2022] M. Kromar and A.T. Godfrey, "Determination of the spent fuel decay heat with the VERA code simulator", Frontiers in Energy Research, 10 (2022) 1046506.

[Krzykacz, 1994] Krzykacz, B., Hofer, E., Kloos, M.: A Software System for Probabilistic Uncertainty and Sensitivity Analysis of Results from Computer Models, Proceedings of International Conference on Probabilistic Safety Assessment and Management (PSAM-II), San Diego, USA, 1994.

[Kum, 2018] Kum, O.: Development of easy-to-use interface for nuclear transmutation computing, VCINDER code, Nuclear Engineering and Technology 50 (2018) 25-34.

[Kvashnina, 2013] Kvashnina, K.O., Butorin, S.M., Martin, P., Glatzel, P.: Chemical State of Complex Uranium Oxides. Physical Review Letters, Vol. 111, p. 253002, 2013.

[Labrim, 2001] Labrim, H., Corbel, C., Piron, J.P.: Determination of the positrons annihilation characteristics of the UO2 lattice, Mater. Sci. Forum. 363–365 (2001) 523–525.

[Labrim, 2006] Labrim, H., Barthe, M.F., Desgardin, P., Sauvage, T., Blondiaux, G., Corbel, C., Piron, J.P.: Vacancy defects induced in sintered polished UO2 disks by helium implantation, Appl. Surf. Sci. 252 (2006) 3256–3261.

[Lahaye, 2017] Lahaye, S., Tsilanizara, A., Bellier, P., Bittar, T.: Implementation of a CRAM solver in MENDEL depletion code system, M&C 2017, International Conference on Mathematics & Computational Methods Applied to Nuclear Science and Engineering, Jeju, Korea, 16. – 20. April, 2017.

[Langlade, 2006] Langlade, C., Bouffioux, P., Clavel, M.: Fracture toughness of hydrided Zircaloy-4 experimental and numerical study. Springer Netherlands, Dordrecht, pp. 1133-1134, 2006.

[Lassmann, 1977] Lassmann, K., Moreno, A.: The light-water-reactor version of the URANUS integral fuel-rod code, Atomkernenergie, Vol. 30, p. 207-215, 1977.

[Le Saux, 2015] Le Saux, M., Besson, J., Carassou, S.: A model to describe the mechanical behavior and the ductile failure of hydrided Zircaloy-4 fuel claddings between 25 °C and 480 °C. Journal of Nuclear Materials, Vol. 466, pp. 43-55, 2015.

[Lebrun, 2001a] Lebrun, A., Bignan, G.: Nondestructive Assay of Nuclear Low-Enriched Uranium Spent Fuels for Burnup Credit Application, Nuclear Technology 13 (2001) 216-229.

[Lebrun, 2001b] Lebrun, A., Merellli, M., Szabo, J.L., Huver, M., Arlt, R., Areans-Carrasco, J.: SMOPY a new NDA tool for safeguards of LEU and MOX spent fuel, Report IAEA-SM-367/CD, IAEA, 2001.

[Lebrun, 2013] Lebrun, A., Jung, S., Zykov, S., Berlizov, A.: Status of NDA techniques in use for IAEA verification of light water reactor spent fuel, in: Proceedings of the 54th Annual Meeting of the Institute of Nuclear Materials Management, INMM 2013, Atlanta, Georgia, July 2013.

[Lee, 1982] Lee, D.M., Lindqvist, L.O.: Self-interrogation of spent fuel, Report LA-9494-MS, August 1982

[Lee, 2015] Lee, Y.G., Jagenbrein, S., Kamya, S., Kamya, S.A., Ahn, S.H., Kim, K.H., Park, J.B., Lee, N.Y.: Development of "Fission Chamber Free" Fork Detector (FDET) for Safeguards Measures on LWR Spent Fuel Assemblies, Report IAEA-CN-220, March 2015.

[Lee, 2017] Lee, J., Kim, J., Youn, Y.-S., Liu, N., Kim, J.-G., Ha, Y.-K. et al.: Raman study on structure of U1−yGdyO2−x (y=0.005, 0.01, 0.03, 0.05 and 0.1) solid solutions, Journal of Nuclear Materials 486 (2017) 216-221.

[Leinders, 2016a] Leinders, G., Pakarinen, J., Delville, R., Cardinaels, T., Binnemans, K., Verwerft, M.: Low-Temperature Oxidation of Fine UO2 Powders: A Process of Nanosized Domain Development. Inorganic Chemistry, Vol. 55, pp. 3915-3927, 2016.

[Leinders, 2016b] Leinders, G., Delville, R., Pakarinen, J., Cardinaels, T., Binnemans, K., Verwerft, M.: Assessment of the U3O7 Crystal Structure by X-ray and Electron Diffraction. Inorganic Chemistry, Vol. 55, pp. 9923-9936, 2016.

[Leinders, 2016c] Leinders, G.: Low-temperature oxidation of fine UO2 powders. KU Leuven, Belgium, 2016.

[Leinders, 2018] Leinders, G.: Cardinaels, T., Binnemans, K., Verwerft, M.: Low-Temperature Oxidation of Fine UO2 Powders: Thermochemistry and Kinetics, Inorganic Chemistry 57 (2018) 4196-4204.

[Leppänen, 2010] Leppänen, J.: Performance of Woodcock delta-tracking in lattice physics applications using the Serpent Monte Carlo reactor physics burnup calculation code, Annals of Nuclear Energy 37 (2010) 715-722.

[Leppänen, 2015a] Leppänen, J.: Serpent – a Continuous-energy Monte Carlo Reactor Physics Burnup Calculation Code, User's Manual, VTT Technical Research Centre of Finland (2015a).

[Leppänen, 2015b] Leppänen, J., Pusa, M., Viitanen, T., Valtavirta, V., Kaltiaisenaho, T.: 'The Serpent Monte Carlo code: Status, development and applications in 2013,' Annals Nuclear Energy 82 (2015b) 142-150.

[Leray, 2016] Leray, O., Rochman, D, Grimm, P., Ferroukhi, H., Vasiliev, A., Hursin, M., Perret, G., Pautz, A.: Nuclear data uncertainty propagation on spent fuel nuclide compositions, Annals of Nuclear Energy 94 (2016) 603-611.

[Leray, 2017] Leray, O., Ferroukhi, H., Hursin, M., Vasiliev, A., Rochman, D.: "Methodology for core analyses with nuclear data uncertainty quantification and application to Swiss PWR operated cycles", Annals of Nuclear Energy 110 (2017) 547-559

[Leray, 2017a] Leray, O., Ferroukhi, H., Hursin, M., Vasiliev, A., Rochman, D.: Methodology for Core Analyses with Nuclear Data Uncertainty Quantification and Application to Swiss PWR Operated Cycles, Annals of Nuclear Energy 110 (2017) 547.

[Leray, 2017b] Leray, O., Fiorito, L., Rochman, D., Ferroukhi, H., Stankovskiy, A., Van den Eynde, G.: Uncertainty propagation of fission product yields to nuclide composition and decay heat for a PWR UO_2 fuel assembly, Progress in Nuclear Energy 101 (2017) 488-495.

[Lévay, 1993] Lévay, F., Dési, S., Tarvainen, M., Arlt, R.: Use of high energy gamma emission tomography for partical defect verification of spent fuel assemblies, Report STUK-YTO-TR 56, November 1993.

[Lindgren, 2019] Lindgren, S., af Ekenstam, G., Hildingsson, L., Fagerholm, R., Sjöland, A., Stål, J.O.: Aspects on declared accountancy data for the Final Spent Fuel Disposal in Sweden, Presented at the 41st ESARDA annual meeting symposium on safeguards and nuclear material management, 14. – 16. May, Stresa, Italy, 2019.

[Liu, 2017] Liu, N., Kim, J., Lee, J., Youn, Y.-S., Kim, J.-G., Kim, J.-Y., Noël, J.J., Shoesmith, D.W.: Influence of Gd Doping on the Structure and Electrochemical Behavior of UO2, Electrochimica Acta. 247 (2017) 496–504.

[Luzzi, 2018] Luzzi, L., Cognini, L., Pizzocri, D., Barani, T., Pastore, G., Schubert, A., Wiss, T., Van Uffelen, P.: Helium diffusivity in oxide nuclear fuel: Critical data analysis and new correlations, Nucl. Eng. Des. 330 (2018) 265–271.

[Lyon, 2018] Lyon, W., Mai, A, Liu, W., Capps, N., Rashid, J., Machiels, A., Waldrop, K.: Impact of Fuel-Cladding Bonding on the Response of High Burnup Spent Fuel Subjected to Transportation Accidents. Top Fuel meeting, paper A0118, 2018.

[Ma, 2019] Ma, F., Kopecky, S., Alaerts, G., Harada, H., Heyse, J., Kitatani, F., Noguere, G., Paradela, C., Šalamon, L., Schillebeeckx, P., Tsuchiya, H, Wynants, R.: Non-destructive analysis of samples with a complex geometry by NRTA, accepted for publication in Journal of Analytical and Atomic Spetrometry (2019).

[MacFarlane, 2010] MacFarlane, R.E., Kahler, A.C.: Methods for processing ENDF/B-VII with NJOY, Nuclear Data Sheets 111 (2010) 2739-2890.

[Maeda, 2004] Maeda, S., Sekine, T., Aoyala, T.: Measurement and analysis of decay heat of fast reactor spent MOX fuel, Annals of Nuclear Energy 31 (2004) 1119-1133.

[Magill, 2009] Magill, J., Dreher, R.: The NUCLEONICA Nuclear Science Portal, Current Status, Trends, and Needs in Radiochemical Education: The Us and Abroad 1164 (2009) 100-109.

[Mallipudi, 2012] Mallipudi, V., Valance, S. Bertsch, J.: Meso-scale analysis of the creep behavior of hydrogenated Zircaloy-4, Mechanics of Materials 51 (2012) 15–28.

[Martin, 1948] Martin, G.L.: The deterioration of UO2 in storage. Mallinckrodt Chemical Works, USA, 1948.

[Martin, 2006] Martin, G., Garcia, P., Labrim, H., Sauvage, T., Carlot, G., Desgardin, P., Barthe, M.F., Piron, J.P.: A NRA study of temperature and heavy ion irradiation effects on helium migration in sintered uranium dioxide, J. Nucl. Mater. 357 (2006) 198–205.

[Martin, 2007] Martin, O., Nilsson, K.F., Györi, C., van Uffelen, P., Schubert, A.: Creep Simulation of Nuclear Fuel Cladding under long term storage conditions with TRANSURANUS. JRC Scientific and Technical Reports, EUR 23926 EN, 2007.

[Martin, 2011] Martin, N.: Application de la méthode des sous-groupes au calcul Monte-Carlo multigroupe, EPM PhD Thesis, 2011.

[Martinik, 2015] Martinik, T., Henzl, V., Grape, S., Svärd, S.J., Jansson, P., Swinhoe, M.T., Tobin, S.J.: Simulation of differential die-away instrument's response of asymmetrically burned spent nuclear fuel, Nuclear Instruments and Methods in Physics Research A 788 (2015) 79-85.

[Martinik, 2016] Martinik, T., Henzl, V., Grape, S., Jansson, P., Swinhoe, M.T., Goodsell, A.V., Tobin, S.J.: Design of a prototype Differential Die-Away instrument proposed for Swedisch spent nuclear fuel characterisation, Nuclear Instruments and Methods in Physics Research A 821 (2016) 55-65.

[Martin-Rengel, 2012] Martin-Rengel, M.A., Sanchez, F.J.G., Ruiz-Hervias, J., Caballero, L., Valiente, A.: Revisiting the method to obtain the mechanical properties of hydrided fuel cladding in the hoop direction. Journal of Nuclear Materials, Vol. 429, pp. 276-283, 2012.

[Martin-Rengel, 2013] Martin-Rengel, M.A., Sanchez, F.J.G., Ruiz-Hervias, J., Caballero, L.: Determination of the hoop fracture properties of unirradiated hydrogen-charged nuclear fuel cladding from ring compression tests. Journal of Nuclear Materials, Vol. 436, pp. 123-129, 2013.

[Martin-Rengel, 2017] Martin-Rengel, M.A., Gomez, F.J., Rico, A., Ruiz-Hervias, J., Rodriguez, J.: Obtention of the constitutive equation of hydride blisters in fuel cladding from nanoindentation tests. Journal of Nuclear Materials, Vol. 487, pp. 220-228, 2017.

[Massih, 2018] Massih, A.R.: UO2 fuel oxidation and fission gas release. Quantum Technologies AB. Uppsala Science Park, Uppsala, Sweden, 2018.

[Massinon, 2018] Massinon, L.: Validation of ALEPH2 depletion code on the spent fuel isotopic content of samples irradiated in Gösgen PWR core, UCL 13305, 2018.

[Matsson, 1997] Matsson, I., Grapengiesser, B.: Developments in gamma scanning of irradiated nuclear fuel, Applied Radiation Isotopes 48 (1997) 1289-1298.

[Matzke, 1992a] Matzke, Hj.: Radiation damage in nuclear materials, Nucl. Instrum. Methods Phys. Res. Sect. B Beam Interact. Mater. At. 65 (1992) 30–39.

[Matzke, 1992b] Matzke, Hj., Turos, A.: Ion implantation studies of UO_2 and UN, J. Nucl. Mater. 188 (1992) 285-292.

[Maugeri, 2009] Maugeri, E., Wiss, T., Hiernaut, J.-P., Desai, K., Thiriet, C., Rondinella, V.V., Colle, J.-Y., Konings, R.J.M.: Helium solubility and behaviour in uranium dioxide, J. Nucl. Mater. 385 (2009) 461–466.

[Mayuzumi, 1990] Mayuzumi, M., Onchi, T.: Creep deformation of an unirradiated Zircaloy nuclear fuel cladding tube under dry storage conditions. Journal of Nuclear Materials, Vol. 171, 1990, p. 381-388, 1990.

[McEachern, 1998] McEachern, R.J., Taylor, P.: A review of the oxidation of uranium dioxide at temperatures below 400°C. Journal of Nuclear Materials, Vol. 254, pp. 87-121, 1998.

[McKinnon, 1986] McKinnon, M.A., Doman, J.W., Heeb, C.M., Creer, J.M.: Monticello BWR spent fuel assembly decay heat predictions and measurements, Report PNL-5799, June 1986.

[Medyk, 2020] Medyk, L., Manara, D., Colle, J.-Y., Bouexière, D., Vigier, J.F., Marchetti, L., Simon, P., Martin, Ph.: Determination of the plutonium content and O/M ratio of $(U,Pu)O_{2-x}$ using Raman

spectroscopy, J. Nucl. Mater. 541 (2020) 152439.

[Menlove, 1997] Menlove, H.O., Beddingfield, D.H.: Passive neutron reactivity measurement technique. In Proceedings of the Institute of Nuclear Materials Management Annual Meeting, 1997.

[Menlove, 2009] Menlove, H.O., Menlove, S.H., Tobin, S.J.: Fissile and fertile nuclear material measurements using a new differential die-away-self-interrogation technique, Nuclear Instruments and Methods in Physics Research A 602 (2009) 588-593.

[Michel, 2020] Michel, A.V., Carlot, G., Onofri, C., Sabathier, C., Cabié, M., Dumont, M.: TEM characterisation of helium platelets in implanted uranium dioxide, J. Nucl. Mater. 528 (2020) 151832.

[Michel-Sendis, 2017a] Michel-Sendis, F. et al.: SFCOMPO-2.0: An OECD NEA database of spent nuclear fuel isotopic assays, reactor design specifications, and operating data, Annals of Nuclear Energy 110 (2017) 779-788.

[Michel-Sendis, 2017b] Michel-Sendis, F., Gauld, I., Martinez, J.S., Alejano, C., Bossant, M., Boulanger, D., Cabellos, O., Chrapciak, V., Conde, J., Fast, I., Gren, M., Govers, K., Gysemans, M., Hannstein, V., Havlu, F., Hennebach, M., Hordosy, G., Ilas, G., Kilger, R., Mills, R., Mountford, D., Ortego, P., Radulescu, G., Rahimi, M., Ranta-Aho, A., Rantamäki, K., Ruprecht, B., Soppera, N., Stuke, M., Suyama, K., Tittelbach, S., Tore, C., Van Winckel, S., Vasiliev, A., Watanabe, T., Yamamoto, T.: "SFCOMPO-2.0: An OECD NEA database of spent nuclear fuel isotopic assays, reactor design specifications, and operating data", Annals of Nuclear Energy 110 (2017) 779 - 788

[Milena, 2023a] Milena-Pérez, A., Rodríguez-Villagra, N., Fernández-Carretero, S., Núñez, A.: Thermal air oxidation of UO2: Joint effect of precursor's nature and particle size distribution, Progress in Nuclear Energy 159 (2023) 104629.

[Milena, 2023b] Milena-Pérez, A., Bonales, L. J., Rodríguez-Villagra, N., Galán, H.: Exploring the impact of temperature and oxygen partial pressure on the spent nuclear fuel oxidation during its dry management, Scientific Reports 13 (2023) 1966.

[Milena, 2023c] Milena-Pérez, A., Rodríguez-Villagra, N., Feria, F., Aguado, C., Herranz, L. E.: Critical review of fuel oxidation database under dry storage conditions, Progress in Nuclear Energy 165 (2023) 104914.

[Min, 1998] D. K. Min, H.J. Park, K.J. Park, S.G. Ro, H.S. Park, ”Determination of burnup, cooling time and initial enrichment of PWR spent fuel by use of gamma-ray activity ratios”, Proceedings of the International symposium on storage of spent fuel from power reactors; Vienna (Austria); 9-13 November 1998, IAEA-SM-352/9P, pp. 421 – 426.

[Minamoto, 2011] Minamoto, H., Yasuda, T., Nakatsuka, M., Kawamura, S.: Buckling behavior of fuel rods under impact loads (numerical study on the effect of material properties). Nihon Kikai Gakkai Ronbunshu, A Hen/Transactions of the Japan Society of Mechanical Engineers, Part A, Vol. 77, pp. 16-26, 2011.

[Minamoto, 2015] Minamoto, H., Nakatsuka, M.: Numerical analysis on the dynamic response of nuclear fuel rods under side drop loading. Transactions of the JSME (in Japanese), Vol. 81, pp. 14-00676, 2015.

[Mohun, 2016] Mohun, R., Desgranges, L., Léchelle, J., Simon, P., Guimbretière, P., Canizarès, A., Duval, F., Jegou, C., Magnin, M., Clavier, N., Dacheux, N., Valot, C., Vauchy, R.: Charged defects during alpha-irradiation of actinide oxides as revealed by Raman and luminescence spectroscopy, Nucl. Instrum. Methods Phys. Res. Sect. B Beam Interact. Mater. At. 374 (2016) 67–70.

[Mohun, 2019] Mohun, R., Desgranges, L., Jégou, C., Boizot, B., Cavani, B., Canizarès, B., Duval, F., He, C., Desgardin, P., Barthe, M.-F., Simon, P.: Quantification of irradiation-induced defects in UO2 using Raman and positron annihilation spectroscopies, Acta Mater. 164 (2019) 512–519.

[Moler, 2003] Moler, C., Van Loan, C.: Nineteen dubious ways to compute the exponential of a matrix, twenty-five years later, SIAM Review (2003) 3-49.

[Mongiello, 2013] Mongiello, R., Finch, R., Baldwin, G.: Safeguards approaches for geological repositories: status and gap analysis, Technical report, SAND 2013-5185P, June 2013.

[Moore, 1995] Moore, L., Schnitzler, B.G., Wemple, C.A., Babcock, R.S., Wessol, D.E.: MOCUP: MCNP-ORIGEN2 coupled utility program, INEL-95/0523, September 1995.

[Morgan, 2015] Morgan, L.W.G., Kotlyar, D.: 'Weighted-delta-tracking for Monte Carlo particle transport,' Annals of Nuclear Energy 85 (2015) 1184-1188.

[Muñoz, 2020] Muñoz, A. (ENRESA/EUNSA): "Specification of measured isotopic concentrations of BWR Spent Fuel", 19 June 2020, Enresa_INF-TD-10032.pdf, Dissemination level: Subtask 2.1 modelling participants

[Muñoz, 2022] Muñoz, A. (ENRESA/EUNSA): "Specification of measured isotopic concentrations of BWR Spent Fuel", 21 March 2022, Enresa_INF-TD-10574.pdf, Dissemination level: Subtask 2.4 modelling participants

[Muñoz, 2023] Muñoz, A. (Enresa): "Enresa Experimental Results on BWR samples by Laser Ablation", 8 February March 2023, Dissemination level: Subtask 2.2 BWR Isotopic Measurements

[Murphy, 2009] Murphy, B.D., Gauld, I.C.: Spent fuel decay heat measurements performed at the Swedish central interim storage facility, Report NUREG/CR-6971, June 2009.

[Nakatsuka, 1987] Nakatsuka, M., Nagai, M.: Reduction of plastic anisotropy of zircaloy cladding by neutron irradiation (I). Journal of Nuclear Science and Technology, Vol. 24, pp. 832-838, 1987.

[Nasyrow, 2016] Nasyrow, R., Papaioannou, D., Rondinella, V.V., Vlassopoulos, E., Linnemann, K., Ballheimer, V., Sterthaus, J., Rolle, A., Wille, F., Caruso, S.: Bending test device for mechanical integrity studies of spent nuclear fuel rods, In: Proc. 18th International Symposium on the Packaging and Transportation of Radioactive Materials (PATRAM 2016), Kobe, Japan, September 18-23, 2016.

[NEA, 2005] OCDE/NEA: Pellet-clad Interaction in Water Reactor Fuels: Seminar Proceedings. Aix-en-Provence, France, 9-11 March 2004: OCDE, Paris, 2005.

[NEA, 2007] NEA/OECD, WPEC Subgroup 25, "Assessment of fission product decay data for decay heat calculations", Nuclear Science Report, NEA/WPEC-25, ISBN 978-92-64-99034-0, 2007.

[NEA, 2011] NEA Nuclear Science Committee, "Spent Nuclear Fuel Assay Data for Isotopic Validation, State-of-the-art Report", Nuclear Science, NEA/NSC/WPNCS/DOC(2011)5, June 2011

[NEA, 2011] NEA Nuclear Science Committee, "Spent Nuclear Fuel Assay Data for Isotopic Validation, State-of-the-art Report", Nuclear Science, NEA/NSC/WPNCS/DOC(2011)5, June 2011.

[NEA, 2015] NEA: State-of-the-Art Report on Multi-scale Modelling of Nuclear Fuels, OECD Publishing, Paris, 2015.

[NEA, 2018] OECD-NEA, Pellet-Clad Interaction (PCI) in Water-Cooled Reactors, Vol. NEA/CSNI/R (2018) 9, 2018.

[Newman, 2009] Newman, C., Hansen, G., Gaston, D.: Three dimensional coupled simulation of thermomechanics, heat, and oxygen diffusion in UO2 nuclear fuel rods. Journal of Nuclear Materials, Vol. 392, pp. 6-15, 2009.

[Nichols, 2002] Nichols, A.L.: Nuclear data requirements for decay heat calculations, Lectures at the Workshop on Nuclear Reaction Data and Nuclear Reactors: Physics, Design and Safety, Trieste, Italy, 25. February – 28. March 2002.

[Niemeyer, 2016] Niemeyer, I., Deissmann, G.: Bridging nuclear safety, security and safeguards at geological disposal of high-level radioactive waste and spent nuclear fuel, Presented at the International Conference on the Safety of Radioactive Waste Management, Vienna, Austria, 21. – 25. November 2016.

[Nilsson, 2010] Nilsson, K.F., Jaksic, N., Vokal, V.: An elasto-plastic fracture mechanics based model for assessment of hydride embrittlement in zircaloy cladding tubes. Journal of Nuclear Materials, Vol. 396, pp. 71-85, 2010.

[Nilsson, 2011] Nilsson, K.-F., Martin, O., Chenel-Ramos, C., Mendes, J.: The segmented expanding cone-mandrel test revisited as material characterisation and component test for fuel claddings. Nuclear Engineering and Design, Vol. 241, pp. 445-458, 2011.

[Nobrega,1985] Nobrega, B.N., King, J.S., Was, G.S., Wisner, S.B.: Improvements in the design and analysis of the segmented expanding mandrel test. Journal of Nuclear Materials, Vol. 131, pp. 99-104, 1985.

[Norris, 1983] Norris, D.I.R., Kay, P.: Oxygen potential and lattice parameter measurements in (U, Ce)O2 – zx. Journal of Nuclear Materials, Vol. 116, pp. 184-194, 1983.

[NRC, 2006] US NRC: Spent Fuel Project Office Interim Staff Guidance - 22: Potential rod splitting due to exposure to an oxidizing atmosphere during short-term cask loading operations in LWR or other uranium oxide based fuel. Washington, DC, 2006.

[NRC, 2014] US NRC: Identification and Prioritization of the Technical Information Needs Affecting Potential Regulation of Extended Storage and Transportation of Spent Nuclear Fuel. Washington, DC, 2014. https://www.nrc.gov/docs/ML1404/ML14043A423.pdf.

[NRC, 2017] US NRC: Standard Review Plan for Spent Fuel Dry Storage Systems and Facilities. Washington, DC, 2017.

[NRC, 2019a] US NRC: Managing Aging Processes In Storage (MAPS) Report. Washington, DC, 2019.

[NRC, 2019b] US NRC: Standard Review Plan for Spent Fuel Transportation. Washington, DC, 2019.

[NSFPOISG, 2006] N. S. F. P. O. I. S. G.-22: Potential rod splitting due to exposure to an oxidizing atmosphere during short-term cask loading operations in LWR or other uranium oxide based fuel. ed., 2006.

[NUREG, 2014] Spent Fuel Transportation Risk Assessment, U.S. NRC NUREG-2125, 01/2014.

[NUREG/CR-6971, 2009]: NUREG/CR-6971, "Spent Fuel Decay Heat Measurements Performed at the Swedish Central Interim Storage Facility", ORNL, 2009

[Olander, 1976] Olander, D.R.: Fundamental aspects of nuclear reactor fuel elements, chapter 15. In: Technical Information Center - Energy Research and Development Administration, ed. University of California, Berkeley, 1976.

[Olander, 1999] Olander, D.R., Soo Kim, Y., Wang, W.-E., Yagnik, S.K.: Steam oxidation of fuel in defective LWR rods. Journal of Nuclear Materials, Vol. 270, pp. 11-20, 1999.

[Olds, 2020] Olds, T. A., Karcher, S. E., Kriegsman, K. W., Guo, X., McCloy, J. S.: Oxidation and anion lattice defect signatures of hypostoichiometric lanthanide-doped UO2, Journal of Nuclear Materials 530 (2020) 151959.

[Olsen, 2018] Olsen, A.M., Schwerdt, I.J., Richards, B., McDonald, L.W.: Quantification of high temperature oxidation of U3O8 and UO2. Journal of Nuclear Materials, Vol. 508, pp. 574-582, 2018.

[Ortensi, 2010] Ortensi, J. et al.: Deterministic Modeling of the High Temperature Test Reactor, INL/EXT-10-18969, Idaho National Laboratories, 2010.

[Osaka, 2008] Osaka, M., Tanaka, K.: Oxygen potential of hypo-stoichiometric Lu-doped UO2, J. Nucl. Mater. 378 (2008) 193–196.

[Ozawa, 2013] Ozawa, M., Hirose, T., Miura, H., Baba, T., Kamimura, K., Yasuda, T., Murakami, T.K., Shinohara, Y.: Fuel rod mechanical performance under dynamic load condition on high burn-up spent

fuel of BWR and PWR. In: Proc. 17th International Symposium on the Packaging and Transportation of Radioactive Materials (PATRAM 2016), San Francisco, California, USA, August 18. – 25., 2013.

[Panizo, 2023] Panizo, S., Álvarez-Velarde, F.: "Evaluation of the impact of the nuclear data library cinder.dat in MCNP burn-up calculations", Progress in Nuclear Energy 155 (2023) 104503

[Papaioannou, 2009b] Papaioannou, D., Nasyrow, R., Rondinella, V.V.: Fuel release experiments on irradiated fuel rodlets under transient impact conditions. Report JRC-ITU-TPW-2009/01, Joint Research Centre of the European Commission, Karlsruhe, 2009.

[Papaioannou, 2009c] Papaioannou, D., Nasyrow, R., Rondinella, V.V., Goll, W., Winkler, H.P., Liedtke, R., Hoffmann, D.: Fuel release experiments on irradiated fuel rodlets under transient impact conditions. Proc. KTG 2009, May 12-14, 2009, Dresden, Germany, INIS Vol.42, INIS Issue.16., 2009.

[Park, 1992] Park, K., Olander, D.R.: Defect models for the oxygen potentials of gadolinium-and europium-doped urania. Journal of Nuclear Materials, Vol. 187, pp. 89-96, 1992.

[Parker, 2015] Parker, H., Joyce, M.J.: The use of ionising radiation to image nuclear fuel: A review, Progress in Nuclear Energy 85 (2015) 297-318.

[Passelaigue, 2022] Passelaigue, F., Simon, P.-C. Motta, A.: Predicting the hydride rim by improving the solubility limits in the Hydride Nucleation-Growth-Dissolution (HNGD) model, Journal of Nuclear Materials 558 (2022) 153363.

[Patterson, 2015] Patterson, C., Garzarolli, F.: Dry Storage Handbook. Performance of Spent Nuclear Fuel during Dry Storage, 2015.

[Peerani, 2007] Peerani, P., Galletta, M.: Re-establishment of the continuity of knowledge in the safeguards interim storages using NDA techniques, Nuclear Engineering and Design 237 (2007) 94-99.

[Petit, 2008] Petit, O., Hugot, F.X., Lee, Y.K., Jouanne, C., Mazzolo, A.: TRIPOLI-4 version 4 User Guide, Report CEA-R-6169, E. Brun, E. dumonteil and F. Malvagi, "Systematic uncertainty due to statistics in Monte Carlo burnup codes: application to a simple benchmark with TRIPOLI-4-D, Janvier 2008.

[Phillips, 1979] Phillips, J.R.: Passive Nondestructive Assay of Nuclear Materials, LA-UR-90-732, p. 529.

[Phillips, 1983] Phillips, J.R., Bosler, G.E., Halbig, J.K., Klosterbuer, S.F., Menlove, H.O., Rinard, P.M.: Experience using a spent fuel measurement system, Nuclear Materials Management XII (1983) 175-181.

[Pipon, 2009] Pipon, Y., Raepsaet, C., Roudil, D., Khodja, H.: The use of NRA to study thermal diffusion of helium in (U,Pu)O2, Nucl. Instrum. Methods Phys. Res. Sect. B Beam Interact. Mater. At. 267 (2009) 2250–2254.

[Poinssot, 2005] Poinssot, C., Ferry, C., Kelm, M., Cavedon, J. M., Corbel, C., Jegou, C. et al.: Spent fuel stability under repository conditions - final report of the European project, France, 2005.

[Poston, 1999] Poston, D.L., Trellue, H.R.: User's Manual, Version 2.0 for MONTEBURNS Version 1.0, LA-UR-99-4999, September 1999.

[Poulson, 2018] Poulson, D., Bacon, J., Durham, M., Guardincerri, E., Morris, C.L., Trellue, H.R.: Application of muon tomography to fuel cask monitoring, Philosophical Transactions A 377 (2018) 20180052.

[Purcell, 2004] Purcell, P.C., Dallongeville, M: Testing of Lwr Fuel Rods to Support Criticality Safety Analysis of Transport Accident Conditions. Packaging, Transport, Storage & Security of Radioactive Material, Vol. 15, pp. 265-272, 2004.

[Pusa, 2010] Pusa, M., Leppänen, J.: Computing the matrix exponential in burnup calculations", Nuclear Science and Engineering 164 (2010) 140-150.

[Pusa, 2013] Pusa, M., Leppänen, J.: Solving linear systems with sparse Gaussian elimination in the Chebyshev Rational Approximation Method, Nuclear Science and Engineering 175 (2013) 250-258.

[Pusa, 2016] Pusa, M.: Higher-order Chebyshev Rational Approximation Method and applicatioins to burnup equations, Nuclear Science and Engineering 182 (2016) 297-318.

[Puse, 2011] Pusa, M.: Rational approximations to the matrix exponential in burnup calculations, Nuclear Science and Engineering 169 (2011) 155-167.

[Ramthum, 1967] Ramthum, H.: Microcalorimetric determination of the mean β-energy of 90Sr + 90Y, Proceedings of a Symposium on Standardisation of radionuclides, 10. – 14. October 1967, IAEA Vienna (AU), pp. 589-599.

[Rashid, 2004a] Rashid, J.Y.R., Machiels, J.: A methodology for the evaluation of fuel rod failures under transportation accidents. In: Proc. 14th International Symposium on the Packaging and Transportation of Radioactive Materials (PATRAM 2004), Berlin, Germany, September 19. – 24., 2004.

[Rashid, 2004b] Rashid, J., Rashid, D.R.M.: Failure Criteria for Zircaloy Cladding Using a Damage-based Metal/Hydride Mixture Model. EPRI, Palo Alto, CA, 1009693, 2004.

[Rashid, 2004c] Rashid, J., Rashid, D.R.M.: Development of a Metal/Hydride Mixture Model for Zircaloy Cladding With Mixed Hydride Structure. EPRI, Palo Alto, CA, 1009694, 2004.

[Raynaud, 2015] Raynaud, P.A.C., Einziger, R.E.: Cladding stress during extended storage of high burnup spent nuclear fuel, J. Nucl. Mater. 464 (2015) 304-312.

[Rearden, 2011] Rearden, B.T., Williams, M.L., Jesse, M.A., Mueller, D.E., Wiarda, D.A.: Sensitivity and uncertainty analysis capabilities and data in SCALE, Nuclear Technology 174 (2011) 236-288.

[Rearden, 2015] Rearden, B., Bekar, K., Celik, C., Clarno, K., Dunn, M., Hart, S., Ibrahim, A., Johnson, S., Langley, B., Lefebvre, J., Lefebvre, R., Marshall, W., Mertyurek, U., Mueller, D., Peplow, D., Perfetti, C., Petrie, L., Thompson, A., Wiarda, D., Wieselquist, W., Williams, M.: Criticality safety enhancements for SCALE 6.2 and beyond, Proceedings of ICNC 2015, Charlotte, NC, USA, 2015, pp. 1255-1269

[Rearden, 2016] Rearden, B.T., Jessee, M.A.: SCALE Code System, ORNL/TM-2005/39 Versioin 6.2, April 2016.

[Restani, 2016] R. Restani, M. Horvath, W. Goll, J. Bertsch, D. Gavillet, A. Hermann, M. Martin, C.T. Walker, “On the condition of UO 2 nuclear fuel irradiated in a PWR to a burn-up in excess of 110 MWd/kgHM”, Journal of Nuclear Materials (2016) 88 – 100.

[Rhodes, 2006] Rhodes, J., Smith, K., Lee, D.: CASMO-5 development and applications, in Proceedings of the PHYSOR-2006 conference, ANS Topical Meeting on Reactor Physics, Vancouver, BC, Canada, 2006, p. B144.

[Rimpler, 2002] Rimpler, A.: Bonner sphere neutron spectrometry at spent fuel casks, Nuclear Instruments and Methods in Physics Research A 476 (2002) 468-473.

[Rinard, 1988] Rinard, P.M., Bosler, G.E.: Safeguarding LWR spent fuel with the FORK detector, Report LA-11096-MS, March 1988.

[Ro, 2009] Ro, T.IK., Danon, Y., Liu, E., Barry, D., Dagan, R.: Measurements of the Neutron Scattering Spectrum from U238 and Comparison of the results with a Calculation at the 36.68-eV Resonance, Journal of the Korean Physical Society Vol. 55 No.4 October 2009.

[Roberts, 1961] Roberts, L. E. J.: The actinide oxides, Quarterly Reviews Chemical Society 15 (1961) 442-460.

[Rochman, 2011] Rochman, D., Koning, A.J., van der Marck, S.C., Sciolla, C.M.: Nuclear data uncertainty propagation: perturbation vs. Monte Carlo, Annals of Nuclear Energy 38 (2011) 942-952.

[Rochman, 2013] Rochman, D., Sciolla, C.M.: Nuclear data uncertainty propagation for a typical PWR fuel assembly with burnup, Nuclear Engineering and Technology 46 (2013) 353-362.

[Rochman, 2016a] Rochman, D., Leray, O., Perret, G., Vasiliev, A., Ferroukhi, H., Koning, A.J.: Re-evaluation of the thermal neutron capture cross section of ^{147}Nd, Annals of Nuclear Energy 94 (2016) 612-617.

[Rochman, 2016b] Rochman, D., Leray, O., Vasiliev, A., Ferroukhi, H., Koning, A.J., Fleming, M., Sublet, J.C.: A Bayesian Monte Carlo method for fission yield covariance information, Annals of Nuclear Energy 95 (2016) 215-134.

[Rochman, 2018a] Rochman, D., Vasiliev, A., Ferroukhi H., Pecchia, M.: Consistent criticality and radiation studies of Swiss spent nuclear fuel: the CS2M approach, Journal of Hazardous Materials 357 (2018) 384.

[Rochman, 2018b] Rochman, D.A., Vasiliev, A., Dkhane, A., Ferroukhi, H.: Uncertainties for Swiss LWR spent nuclear fuels due to nuclear data, European Physics Journal Nuclear Science and Technology, 4 (2018) 6-15.

[Rochman, 2019a] Rochman, D.: Validation of CASMO5/SIMULATE5 models for KKB2 from Cycle 12 to Cycle 42, PSI Internal Report, TM-41-18-22, April 2019.

[Rochman, 2019b] Rochman, D.: Validation of CASMO5/SIMULATE5 models for KKB1 from Cycle 16 to Cycle 42, PSI Internal Report, TM-41-18-21, April 2019.

[Rochman, 2020a] Rochman, D., Dokhane, A., Vasiliev, A., Ferroukhi, H., Hursin, M.: Nuclear data uncertainties for Swiss BWR spent nuclear fuel characteristics, to be published in EPJ, 2020.

[Rochman, 2020b] Rochman, D., Vasiliev, A., Ferroukhi, H., Seidl, M., Basualdo, J.: Improvement of PIE analysis with a full core simulation: the U1 case, to be submitted in ANE, January 2020.

[Rochman, 2021] Rochman, D., Vasiliev, A., Ferroukhi, H., Hursin, M.: "Analysis for the ARIANE BM1 and BM3 samples: nuclide inventory and decay heat", EPJ Nuclear Science & Technology 7, (2021) 18

[Rochman, 2021a] Rochman, D., Vasiliev, A., Ferroukhi, H., Hursin, M.: "Analysis for the ARIANE GU1 sample: nuclide inventory and decay heat", Annals of Nuclear Energy 160 (2021) 108359

[Rochman, 2021b] Rochman, D., Vasiliev, A., Ferroukhi, H., Hursin, M., Ichou, R., Taforeau, J., Simeonov, T.: "Analysis for the ARIANE GU3 sample: nuclide inventory and decay heat", EPJ Nuclear Science & Technology 7 (2021) 14

[Rochman, 2022] Rochman, D., Vasiliev, A., Ferroukhi, H., Muñoz, A., Vazquez Antolin, M., Berrios Torres, M., Casado Sanchez, C., Simeonov, T., Shama, A. "Analysis of ENRESA BWR samples: nuclide inventory and decay heat", EPJ Nuclear Science & Technology 8 (2022) 9

[Rochman, 2023] Rochman, D., Taforeau, J., Simeonov, T., Shama, A.: "Comparison of calculated and measured spent nuclear fuel decay heat with CASMO5, SNF and standard methods", Nuclear Engineering and Design, 410 (2023) 112392.

[Rodríguez, 2023] Rodríguez-Villagra, N., Bonales, L. J., Fernández-Carretero, S., Milena-Pérez, A., Gutierrez, L., Galán, H.: Exploring a surrogate of Pellet–Cladding interaction: Characterisation and oxidation behavior, MRS Advances 8 (2023) 238-242.

[Rodríguez, 2024] Rodríguez-Villagra, N. Dacheux, N., Prieur, D., Barthe, M.F., Amany, M.L. Anta, L., Bonales, L.J., De Bona, E. ,Claparède, L., Desgardin, P., Durán, S., Elorrieta, J.M., Fernández-Carretero, S., Galán, H., Gutiérrez, L., Hennig, C., Imbert, H., Joseph, J., Lomonaco, J., Milena-Pérez, A., Núñez, A., Podor, R., Popov, D., Sauvage, T., Sarrazin, R., Szenknect, S., Walter, O., Wendling, O.: Behaviour of doped UO_2-based model materials as analogues for spent nuclear fuel under interim storage conditions, Final version as of 31.05.2024 of deliverable D8.9 of the HORIZON 2020 project EURAD. EC Grant agreement no: 847593, 2024.

[Romojaro, 2022] Romojaro, P., Ambrožič, K., Čalič, D., Fiorito, L., Govers, K., Hernandez-Solis, A., Kos, B., Schillebeeckx, P., Stankovskiy, A., Žerovnik, G., Kromar, M.: "Sensitivity and uncertainty analysis of PWR spent fuel observables to operational and input parameters", Proceedings International Conference on Physics of Reactors 2022 (PHYSOR 2022), Pittsburg, PA, May 15. – 20., 2022, pp. 1854-1863.

[Rondinella, 2011] Rondinella, V.V.: Effects of Helium Build-up on Nuclear Fuel Evolution During Storage. In: Proc. of the 13th International High-Level Radioactive Waste Management Conference (IHLRWMC), Albuquerque, New Mexico, American Nuclear Society, April 10 – 14, 2011.

[Rondinella, 2012] Rondinella, V.V., Wiss, T., Papaioannou, D., Nasyrow, R.: Studies on nuclear fuel evolution during storage and testing of used fuel response to impact loadings. Proc. 11th International Probabilistic Safety Assessment and Management Conference and the Annual European Safety and Reliability Conference 2012, PSAM11 ESREL 2012, 2012.

[Rondinella, 2017] Rondinella, V.V., Nasyrow, R., Papaioannou, D., Vlassopoulos, E., Cappia, F., Dieste-Blanco, O., Wiss, T.A.G.: Mechanical integrity studies on spent nuclear fuel rods, Proc. IHLRWMC 2017, Charlotte, North Carolina, American Nuclear Society, April 9. – 13., 2017.

[Rossiter, 2011] Rossiter, G.: Development of the ENIGMA fuel performance code for whole core analysis and dry storage assessment. Nuclear Engineering and Technology, 43, 489, 2011.

[Rothenstein, 1998] Rothenstein, W., Dagan, R.: Ideal gas scattering kernel for energy dependent cross-sections, Annals of Nuclear Energy 25 (1998) 209-222.

[Rothenstein, 2004] Rothenstein, W.: Proof of the formula for the ideal gas scattering kernel for nuclides with strongly energy dependent scattering cross sections, Annals of Nuclear Energy 31 (2004) 9-23.

[Roudil, 2004] Roudil, D., Deschanels, X., Trocellier, P., Jégou, C., Peuget, S., Bart, J.-M.: Helium thermal diffusion in a uranium dioxide matrix, J. Nucl. Mater. 325 (2004) 148–158.

[Ruiz, 2015] Ruiz-Hervias, J., Martin-Rengel, M.A., Gomez-Sanchez, F.J.: Failure criteria for unirradiated PWR cladding subjected to ring compression tests. Paper PVP2015-45793, Proc. of the ASME 2015 Pressure Vessels and Piping Conference, Boston, 2015.

[Ruiz, 2021] Ruiz-Hervías, J, Simbruner, K., Cristobal-Beneyto, M., Perez-Gallego, D., Zencker, U.: Failure mechanisms in unirradiated ZIRLO® cladding with radial hydrides, Journal of Nuclear Materials, 544 (2021) 152668.

[Šalamon, 2019] Šalamon, L.: Neutron resonance transmission analysis of cylindrical samples used for reactivity worth measurements, Journal of Radioanalytical and Nuclear Chemistry 321 (2019) 519-530.

[Sanborn, 2014] Sanborn, S. Koeppel, B., Klymyshyn, N., Adkins, H., Geelhood, K.: Assembly Level Modeling and Transportation Damage Prediction of Used Nuclear Fuel (UNF) Cladding – 14569. In: Proc. Waste Management Symposia 2014 (WM2014), Phoenix, Arizona, USA, March 2. – 6., 2014.

[Sanders, 1990] Sanders, T.L., Westfall, R.M.: Feasibility and Incentives for Burnup Credit in Spent-Fuel Transport Casks", Nuclear Science and Engineering 104 (1990) 66-77.

[Sani, 2010] Santi, P.A., Browne, M.C., Parker, R.F., Williams, R.B.: Testing of the dual slab verification detector for atended measuremens of teh BN-530 dry storage casks, Report LA-UR-09-03480, 2010.

[Sanz, 2008] Sanz, J.: ACAB-2008: Activation Abacus Code V2008", NEA Data Bank NEA-1839.

[Sauvage, 2005] Sauvage, T., Desgardin, P., Martin, G., Garcia, G., Carlot, G., Labriin, H., Khodja, H., Moretto, P., Barthe, P., Blondiaux, P., Errainli, P., Piron, J.P.: Microstructure effects on He diffusion in sintered UO2 by mu NRA, Nucl. Instrum. Methods Phys. Res. Sect. B-Beam Interact. Mater. At. 240 (2005) 271–276.

[Scaglione, 2009] Scaglione, J.M., Wagner, J.C.: Burnup Credit Approach used in the Yucca Mountain License Application, International Workshop on Advances in Applications of Burnup Credit for Spent Fuel Storage, Transport, Reprocessing, and Disposition, Córdoba, Spain, 27. – 30. October 2009.

[Scheele, 2004] Scheele, R.D., Hanson, B.D., Cumblidge, S.E., Jenson, E.D., Kozelisky, A.E., Sell, R.L., MacFarlan, P.J., Snow, L.A.: Effect of gadolinium doping on the air oxidation of uranium dioxide, MRS Online Proceedings Library 824 (2004) 514–519.

[Scheele, 2021] Scheele, R. D., Hanson, B. D., Casella, A. M.: Effect of added gadolinium oxide on the thermal air oxidation of uranium dioxide, Journal of Nuclear Materials 552 (2021) 153008.

[Schillebeeckx, 2012] Schillebeeckx, P, Becker, B., Danon, Y., Guber, K., Harada, H., Heyse, J., Junghans, A.R., Kopecky, S., Massimi, C., Moxon, M., Otuka, N., Sirakov, I., Volev, K.: Determination of resonance parameters and their covariance from neutron induced reaction cross section data, Nuclear Data Sheets, 113 (2012) 3054-3100.

[Schillebeeckx, 2018] Schillebeeckx, P., Alaerts, G., Borella, A., Fiorito, L., Govers, K., Paepen, J., Pedersen, B., Stankovskiy, A., Van den Eynde, G., Verwerft, M., Wynants, R., Žerovnik, G.: Characterisation of spent nuclear fuel by theoretical calculations and non-destructive analysis, Proceedings of the International Workshop on Numerical Modelling of NDA Instrumentation and Methods for Nuclear Safeguards, 16. – 17. May 2018, Luxembourg, pp. 101-113.

[Schillebeeckx, 2020] Schillebeeckx, P., Verwerft, M., Žerovnik, G., Parthoens, Y., Pedersen, B., Alaerts, G., Cools, G., Govers, K., Paepen, J., Varasano, G., Wynants, R.: "A non-destructive method to determine the neutron production rate of a sample of spent nuclear fuel under standard controlled area conditions", JRC Technical Report EUR 30379 EN, European Atomic Energy Community, Luxembourg, 2020, ISBN 978-92-76-22349-8 (where available), doi:10.2760/6148853, JRC121586

[Schillebeeckx, 2023] Schillebeeckx, P., Verwerft, M., Romojaro, P., Žerovnik, G., Messaoudi, N., Alaerts, G., Fiorito, L., Govers, K., Paepen, J., Parthoens, Y., Pedersen, B., Stankovskiy, A., Van den Eynde, G., Wynants, R.: "An absolute measurement of the neutron production rate of a spent nuclear fuel sample used for depletion code validation", Frontiers in Energy Research, 11 (2023) 1162367

[Schrödl, 2010] Schrödl, E., Brücher, W., Koch, W., Ballheimer, V.: Experimentelle Untersuchungen zum Verhalten von Brennstäben mit hohem Abbrand bei mechanischen Unfallbelastungen beim Transport, GRS - A – 3490, 2010.

[SCIP, 2013] SCIP III – Technical Description, Studsvik Report, STUDSVIK/N-13/172, 2013.

[Seidl, 2023] Seidl, M., Schillebeeckx, P., Rochman, D.: "Note on the potential to increase the accuracy of source terms calculations for spent nuclear fuel", Frontiers in Nuclear Energy 11 (2023) 1143312

[Shama, 2021] Shama, A., Rochman, D., Pudollek, S., Caruso, S., Pautz, A.: "Uncertainty analyses of spent nuclear fuel decay heat calculations using SCALE modules", Nuclear Energy and Technology 53 (2021) 2816-2829

[Shama, 2022] Shama, A., Rochman, D., Caruso, S., Pautz, A.: "Validation of spent nuclear fuel decay heat calculations using Polaris, ORIGEN and CASMO5", Annals of Nuclear Energy 165 (2022) 108758

[Simakov, 2017] Simakov, S.P., van den Berg, Q.Y.: Update of the α-n yields for reactor fuel materials for the interest of nuclear safeguards, Nuclear Data Sheets 139 (2017) 190-203.

[Simbruner, 2022] Simbruner, K., Billone, M.C., Zencker, U., Liu, Y.Y., Völzke, H.: Brittle failure analysis of high-burnup PWR fuel cladding alloys, Trans., 26th International Conference on Structural Mechanics in Reactor Technology (SMiRT), Session Tu.4.I.1, Berlin/Potsdam, Germany, 10-15 July 2022.

[Simeonov, 2017] Simeonov, T., Wemple, C.: Update and Evaluation of Decay Data for Spent Nuclear Fuel Analyses, EPJ Web of conferences 146 (2017) 09011.

[Sinkov, 2008] Sinkov, S. I., Delegard, C. H., Schmidt, A. J.: Preparation and Characterisation of

Uranium Oxides in Support of the K Basin Sludge Treatment Project, USA, 2008.

[Sirakov, 2017] Sirakov, I., Capote, R., Gritzay, O., Kim, H.I., Kopecky, S., Kos, B., Paradela, C., Pronyaev, V.,G., Schillebeeckx, P., Trkov, A.: Evaluation of cross sections for neutron interactions with ^{238}U in the energy region between 5 keV and 150 keV, European Physics Journal A 53 (2017) 199.

[SKB, 2006a] SKB, "Measurements of Decay Heat in Spent Nuclear Fuel at the Swedish Interim Storage Facility, Clab", SKB report R-05-62, December 2006 https://www.skb.se/publikation/1472024/R-05-62.pdf

[SKB, 2006b] SKB, Measurements of Decay Heat in Spent Nuclear Fuel at the Swedish Interim Storage Facility, Clab", SKB report R-05-62, December 2006 https://www.skb.se/publikation/1472024/R-05-62.pdf.

[Smith, 2011] Smith, R.E.: Annotated Bibliography for Drying Nuclear Fuel. United States, 2011.

[Smith, 2013] Smith, H.J., Gauld, I.C., Mertyutrk, U.: Analysis of experimental data for high burnup BWR spent fuel isotopic validation – SVEA-96 and GE14 assembly designs, Report NUREG/CR-7162, March 2013.

[Solans, 2022] Solans, V., Grape, S., Sjöstrand, H., Branger, E., Schillebeeckx, P., Borella, A., Rossa, R., Sjöland, A.: "Rossi-alpha distribution analysis of DDSI data for spent nuclear fuel investigation", Symposium on International Safeguards: Reflecting on the Past and Anticipating the future, IAEA, Vienna 2022

[Solans, 2023] Solans, V., Sjöstrand, H., Jansson, P., Schillebeeckx, P., Grape, S., Branger, E., Sjöstrand, A.: "Spent Nuclear Fuel passive gamma analysis and reproducibility: Application to SKB-50 assemblies", Annals of Nuclear Energy 192 (2023) 109941

[Sonnenburg, 2017] Sonnenburg, H.G., Boldt, F.: Brennstabverhalten im Normalbetrieb, bei Störfällen und bei Langzeitlagerung. GRS-Bericht: GRS – 464, ISBN 978-3-946607-47-2, 2017.

[Soullard, 1978] Soullard, J., Alamo, A.: Radiat. Eff. 38 (1978) 133.

[Soullard, 1985] Soullard, J.: High voltage electron microscope observations of UO2, J. Nucl. Mater. 135 (1985) 190–196.

[Spahiu, 2021] Spahiu, K.: State of the Knowledge Report - Spent Nuclear Fuel Domain 3.1.1. EURAD-European Joint Programme on Radioactive Waste Management (847593), 2021.

[Spykman, 2018] Spykman, G.: Dry storage of spent nuclear fuel and high active waste in Germany – Current situation and technical aspects on inventories integrity for a prolonged storage time. Nucl. Engin. Tech. 50 (2018) 313 – 317.

[Stafford, 2015] Stafford, D.S.: Multidimensional simulations of hydrides during fuel rod lifecycle. Journal of Nuclear Materials, Vol. 466, pp. 362-372, 2015.

[Staicu, 2010] Staicu, D., et al.: Impact of auto-irradiation on the thermophysical properties of oxide nuclear reactor fuels, Journal of Nuclear Materials 397 (2010) 8-18.

[Stankovskiy, 2011] Stankovskiy, A., Van den Eynde, G., Vidmar, T.: Development and validation of ALEPH Monte Carlo burnup code, Proc. Int. Workshop NEMEA-6, Krakow, Poland, 25. – 28. October 2010, NEA/NSC/DOC(2011)4, pp. 161-169, 2011.

[Stankovskiy, 2012] Stankovskiy, A., Van den Eynde, G.: 'Advanced Method for Calculations of Core Burn-Up, Activation of Structural Materials, and Spallation Products Accumulation in Accelerator-Driven Systems, Science and Technology of Nuclear Installations 2012 (2012) 545103.

[Sublet, 2009] Sublet, J.C., Blomquist, R.N., Goluoglu, S., Macfarlane, R.E.: Unresolved resonance range cross section probability and self-shielding factors, CEA Cadararache, Report CEA-R-6227, Juillet 2009.

[Sublet, 2017] Sublet, J.Ch., Eastwood, J.W., Morgan, J.G., Gilbert, M.R., Fleming, M., Arter, W.: FISPACT-II: An Advanced Simulation System for Activation, Transmutation and Material Modelling, Nuclear Data Sheets 139 (2017) 77-137.

[Suman, 2018] Suman, S., Khan, M.K., Pathak, M., Singh, R.N.: Effects of hydrogen on thermal creep behaviour of Zircaloy fuel cladding. Journal of Nuclear Materials, Vol. 498, pp. 20-32, 2018.

[Suman, 2020] Suman, S.: Understanding the role of hydrogen on creep behaviour of Zircaloy-4 cladding tubes using nanoindentation, Nuclear Engineering and Technology 52 (2020) 2041-2046.

[Suresh, 2004] Suresh Kumar, K., Mathews, T., Nawada, H.P., Bhat, N.P.: Oxidation behaviour of uranium in the internally gelated urania-ceria solid solutions – XRD and XPS studies. Journal of Nuclear Materials, Vol. 324, pp. 177-182, 2004.

[Suyama, 2005] Suyama, K., Mochizuki, H.: Effect of neutron induced reactions of noedynium-147 and 148 on burnup evaluation, Journal of Nuclear Science and Technology 42 (2005) 661-669.

[Suyama, 2006] Suyama, K., Mochizuki, H.: Corrections to the ^{148}Nd method evaluation of burnup for the PIE damples from Mihama-3 and Genkai-1, Annals of Nuclear Energy 33 (2006) 335-342.

[Svärd, 2005] Svärd, S.J., Håkansson, A., Bäcklin, A., Osifo, O., Willman, Ch.: Nondestructive experimental determination of the pin-power distribution in nuclear fuel assemblies, Nuclear Technology 151 (2005) 70-76.

[Syrett, 1979] Syrett, B.S., Cubicciotti, D., Jones, R.L.: ANS Topical Meeting on Light Water Reactor Fuel Performance, Portland, Oregon (1979), p. 169.

[Talip, 2014a] Talip, Z., Wiss, T., Di Marcello, V., Janssen, A., Colle, J.-Y., Van Uffelen, P., Raison, P., Konings, R.J.M.: Thermal diffusion of helium in 238Pu-doped UO2, J. Nucl. Mater. 445 (2014) 117–127.

[Talip, 2014b] Talip, Z., Wiss, T., Maugeri, E.-A., Colle, J.-Y., Raison, P.-E., Gilabert, E., Ernstberger, M., Staicu, D., Konings, R.J.M.: Helium behaviour in stoichiometric and hyper-stoichiometric UO2, J. Eur. Ceram. Soc. 34 (2014) 1265–1277.

[Talip, 2015a] Talip, Z., Wiss, T., Raison, P.E., Paillier, J., Manara, D., Somers, J., Konings, R.J.M.: Raman and X-ray Studies of Uranium-Lanthanum-Mixed Oxides Before and After Air Oxidation, J. Am. Ceram. Soc. 98 (2015) 2278–2285.

[Talip, 2015b] Talip, Z., Wiss, T., Janssen, A., Colle, J.-Y., Somers, J., Konings, R.J.M.: The dissolution of helium in La-doped UO2 as a surrogate of hypo-stoichiometric UO2, Nucl. Mater. Energy. 3–4 (2015) 12–16.

[Talip, 2018] Talip, Z., Peuget, S., Magnin, M., Tribet, M., Valot, C., Vauchy, R., et al.: Characterisation of un-irradiated MIMAS MOX fuel by Raman spectroscopy and EPMA. Journal of Nuclear Materials, Vol. 499, pp. 88-97, 2018.

[Tanke, 1991] Tanke, R.H., Jasper, J.E., Gaalman, P.A.M., Killian, D.: Applications of tomography in nuclear research, Kerntechnik, 56, 1991.

[Tardy, 2015] Tardy, M., Kitsos, S., Grassi, G., Santamarina, A., San Felice, L., Riffard, C.: First burnup credit application including actinides and fission products for transport and storage cask by using French experiments, Journal of Nuclear Science and Techonology 52 (2015) 1008-2017.

[Tarvainen, 1997] Tarvainen, M., Lévay, F., Valentine, T.E., Abhold, M., Moran, B.: NDA techniques for spent fuel verification and radiation monitoring, STUK-YTO-TR 133, August 1997.

[Taylor, 1980] Taylor, P., Burgess, E.A., Owen, D. G.: An X-ray diffraction study of the formation of βUO2.33 on UO2 pellet surfaces in air at 229 to 275°C. Journal of Nuclear Materials, Vol. 88, pp. 153-160, 1980.

[Taylor, 1991] Taylor, P., Wood, D. D., Owen, D. G., Park, G.-I.: Crystallization of U3O8 and hydrated UO3 on UO2 fuel in aerated water near 200°C, Journal of Nuclear Materials 183 (1991) 105-114.

[Thomas, 1993] Thomas, L.E., Einziger, R.E. Buchanan, H.C.: Effect of fission products on air-oxidation of LWR spent fuel. Journal of Nuclear Materials, Vol. 201, pp. 310-319, 1993.

[Tiitta, 2001] Tiitta, A., Hautamäki, J., Turunen, A., Arlt, R., Carrasco, J.A., Esmailpour-Kazerouni, K., Schwalbach, P.: "Spent BWR fuel characterisation combining a FORK detector with gamma spectrometry, Report STUK-YTO-TR 175, February 2001.

[Tiitta, 2002] Tiitta, A., Saarinen, J., Tarvainen, M., Axell, K., Jansson, P., Carchon, R., Gerits, J., Kulikov, Y., Lee, Y.G.: Investigation on the possibility to use FORK detector for partial defect verification of spent LWR fuel assemblies, Report STUK-YTO-TR 191, September 2002.

[Tobin 2016] Tobin, S.J., Fugate, M.L., Trellue, H.R., DeBaere, P., Sjöland, A., Liljenfeldt, H., Hu, J., Backstrom, U., Bengtsson, M., Burr, T., Eliasson, A., Favalli, A., Gauld, I., Grogan, B., Jansson, P., Junell, H., Schwalbach, P., Vaccaro, S., Vo, D.T., Wildlestrant, H.: Nondestructive assay data integration with the SKB-50 assmblies – FY16 update, Report LA-UR-16-28290, October 2016.

[Tobin, 2009] Tobin, S.J.: Determination of plutonium content in spent fuel with non-destructive assay, Presented at the 50th INMM Annual Meeting, Tucson, AZ, 11. – 17. July 2009, Report LA-UR- 09-03748 (2009).

[Tobin, 2011] Tobin, S.J., Menlove, H.O., Swinhoe, M.T., Schear, M.A.: Next Generation Safeguards Initiative research to determine the Pu mass in spent fuel assemblies: purpose, approach, constraints, implementation and calibration, Nuclear Instruments and Methods in Physics Research A 652 (2011) 73-75.

[Tobin, 2018] Tobin, S.J., Peura, P., Bélanger-Champagne, C., Moring, M., Dendooven, P., Honkama, T.: "Measuring spent fuel assembly multiplication in borated water with a passive neutron albedo reactivity instrument", Nuclear Instruments and Methods in Physics Research A 897 (2018) 32-37

[Tobin, 2018a] Tobin, S.J., Peura, P., Bélanger-Champagne, C., Moring, M., Dendooven, P., Honkamaa, T.: Utility of including Passive Neutron Albedo Reactivity in an integrated NDA system for encapsulation safeguards, ESARDA Bulletin 56 (2018) 12-18.

[Tobin, 2018b] Tobin, S.J., Peura, P., Bélanger-Champagne, C., Moring, M., Dendooven, P., Honkamaa, T.: Measuring spent fuel assembly multiplication in borated water with a passive neutron albedo reactivity instrument , Nuclear Instruments and Methods in Physics Research A 897 (2018) 32-37.

[Tobin, 2018c] Tobin, S.J., Peura, P., Hnkamaa, T., Dendooven, P., Moring, M., Bélanger-Champagne, C.: Passive Neutron Albedo Reactivity in the Finnish encapsulation context, Finnish Radiation and Nuclear Safety Authority, ISBN 978-952-309-406-2, January 2018.

[Tobin, 2019] Tobin, S.J., Tupasela, T., Dendooven, P., Honkamaa, T.: PNAR measurement report, Report LA-UR-19-30861, October 2019.

[Töre, 2013] Töre, C., Rodríguez, A.: Evaluation of REBUS measurements, sample M11, Technical Report SEA – 45, Rev. B, October 2013.

[Trahan, 2020a] Trahan, A.C., McMath, G.E., Mendoza, P.M., Trellue, H.R., Backstrom, U., Balkeståhl, L.P., Grape, S., Henzl, V., Leyba, D., Root, M.A., Sjoland, A.: "Results of the Swedish spent fuel measurement field trials with the Differential Die-Away Self-Interrogation Instrument", Nuclear Instruments and Methods in Physics Research A 795 (2020) 163329

[Trahan, 2020b] Trahan, A.C., McMath, G.E., Mendoza, P.M., Trellue, H.R., Backstrom, U., Balkeståhl, L.P., Grape, S., Henzl, V., Leyba, D., Root, M.A., Sjöland, A.: Results of the Swedish spent fuel measurement field trials with the Differential die-Away Self-interrogation Instrument, Nuclear Instruments and Methods in Physics Research A 955 (2020) 163329.

[Trellue, 2013] Trellue, H.R., Galloway, J.D., Fischer, N.A., Tobin, S.: Advances in spent fuel libraries, in Proceedings of the 54th Annual Meeting of the Institute of Nuclear Materials Management, pp. 1603-1612, 2013.

[Trocellier, 2003] Trocellier, P., Gosset, D., Simeone, D., Costantini, J.M., Deschanels, X., Roudil, D., Serruys, Y., Grynszpan, R., Saudé, S., Beauvy, M.: Application of nuclear reaction geometry for 3He depth profiling in nuclear ceramics, Nucl. Instrum. Methods Phys. Res. Sect. B Beam Interact. Mater. At. 206 (2003) 1077–1082.

[Tsilanizara, 2000] Tsilanizara, A., Diop, C.M., Nimal, B., Detoc, M., Lunéville, L, Chiraon, M., Huynh, T.D., Brésard, I., Eid, E., Klein, J.C., Roque, B, Marimbeau, P., Garzenne, C., Parize, J.M., Vergne,C.: DARWIN: An evalution code system for a large range of applications, Journal Nuclear Science and Technology, 37 (Supp. 1) (2000) 845-849.

[Tsilanizara, 2016] Tsilanizara, A., Gilardi, N., Huynh, T.D., Jouanne, C., Lahaye, S., Martinez, J., Diop, C.M.: Probabilistic approach for decay heat uncertainty estimation under URANIE platform by using MENDEL depletion code, Annals of Nuclear Energy 90 (2016) 62-70.

[Tuli, 2001] Tuli, J.K.: Evaluated Nuclear Structure Data File, BNL-NCS-51655-01/02-Rev, BNL, 2001.

[Tupasela, 2009] Tupasela, T.: Passive neutron albedo reactivity assay of spent nuclear fuel, Master Thesis, Aalto University, 2 July, 2009.

[UFDC, 2012] UFDC: Review of Used Nuclear Fuel Storage and Transportation Technical Gap Analyses, United States of America - Department of Energy, 2012.
https://www.energy.gov/sites/prod/files/Gap Comparison Rev 0.pdf.

[Une, 1983] Une, K., Oguma, M.: Oxygen potentials of (U, Gd)O2+/- x solid solutions in the temperature range 1000-1500°C., J. Nucl. Mater. 115 (1983) 84.

[Vaccaro, 2016] Vaccaro, S., Tobin, S.J., Favalli, A., Grogan, B., Jansson, P., Liljenfeldt, H., Mozin, V., Hu, J., Schwalbach, P., Sjöland, A., Trellue, H., Vo, D.: "PWR and BWR spent fuel assembly gamma spectra measurements", Nuclear Instruments and Methods in Physics Research A 833 (2016) 208-225

[Vaccaro, 2016] Vaccaro, S., Tobin, S.J., Favalli, A., Grogan, B., Jansson, P., Liljenfeldt, H., Mozin, V., Hu, J., Schwalbach, P., Sjöland, A., Trellue, H., Vo, D.: PWR and BWR spent fuel assembly gamma spectra measurements", Nuclear Instruments and Methods in Physics Research A 833 (2016) 208-225.

[Vaccaro, 2018a] Vaccaro, S., Gauld, I.C. , Hu, J., DeBaere, P., Petersen, J., Schwalbach, P., Smejkal, A., Tomanin, A., Sjöland, A., Tobin, S., Wiarda, D.: "Adavancing the FORK detector for quantitative spent nuclear fuel verification", Nuclear Instruments and Methods in Physics Research A 888 (2018) 202-217

[Vaccaro, 2018b] Vaccaro, S., Gauld, I.C., Hu, J., DeBaere, P., Petersen, J., Schwalbach, P., Smejkal, A., Tomanin, A., Sjöland, A., Tobin, S., Wiarda, D.: Adavancing the FORK detector for quantitative spent nuclear fuel verification, Nuclear Instruments and Methods in Physics Research A 888 (2018) 202-217.

[Vandoorne, 2018] Vandoorne, T.: Calculation of spent fuel and reprocessing waste inventory for SFC-1, ONDRAF/NIRAS, Report 2017-1497 rev1), 2018.

[Vasiliev, 2019] Vasiliev, A., Herrero, J., Pecchia, M., Rochman, D., Ferroukhi, H., Caruso, S.: Preliminary Assessment of Criticality Safety Constraints for Swiss Spent Nuclear Fuel Loading in Disposal Canisters, Materials 12 (2019) 494.

[Vela Mora, 2011] Mariano Vela Mora, Alebrto Gallardo Padilla, José Luis Castro Palomino, “Nondestructive burnup measurements by gamma-ray spectroscopy on spent fuel elements of the RP-10 research reactor”, Progress in Nuclear Energy, 53 (2011) 344 – 353.

[Viitanen, 2009] Viitanen, T.: Implementing a Doppler-preprocessor of cross section libraries in reactor physics code Serpent, M.Sc. Thesis, Helsinki University of Technology, 2009.

[Villa, 2019] Villa-Aleman, E., Houk, A.L., Bridges, N.J., Shehee, T.C.: Raman spectroscopy: A tool to investigate alpha decay damage in a PuO 2 crystal lattice and determining sample age since calcination, J. Raman Spectrosc. 50 (2019) 899–901.

[Vlassopoulos, 2017b] Vlassopoulos, E., Nasyrow, R., Papaioannou, D., Rondinella, V.V., Caruso, S. Pautz, A.: Destructive tests for determining mechanical integrity of spent nuclear fuel rods. In: ANS IHLRWM 2017 - 16th International High-Level Radioactive Waste Management Conference: Creating a Safe and Secure Energy Future for Generations to Come - Driving Toward Long-Term Storage and Disposal, pp. 726-733, 2017.

[Vlassopoulos, 2018a] Vlassopoulos, E., Papaioannou, D., Nasyrow, R., Caruso, S., Raffuzzi, V., Gretter, R., Fongaro, L., Somers, J., Rondinella, V.V., Grünberg, P., Pautz, A., Helfenstein, J., Schwizer, P.: Mechanical Integrity of Spent Nuclear Fuel: From Experimental to Numerical Studies. TOPFUEL 2018, ENS, Prague, 2018.

[Vlassopoulos, 2018b] Vlassopoulos, E., Nasyrow, R., Papaioannou, D., Gretter, R., Fongaro, L., Somers, J., Rondinella, V.V., Caruso, S., Grünberg, P., Helfenstein, J., Schwizer, P., Pautz, A.: Response of irradiated nuclear fuel rods to quasi-static and dynamic loads. Kerntechnik, Vol. 83, pp. 507-512, 2018.

[Vlassopoulos, 2021] Vlassopoulos, E.: Structural performance and mechanical properties investiagation of spent nuclear fuel rods under static and dynamic bending loads, PhD thesis, EPFL, Lausanne, 2021.

[Wang, 2018] Wang, J., Wang, H., Jiang, H., Bevard, B.: High burn-up spent nuclear fuel transport reliability investigation. Nuclear Engineering and Design, Vol. 330, pp. 497-515, 2018.

[Wasywich, 1993] Wasywich, K. M., Hocking, W. H., Shoesmith, D. W., and Taylor, P.: Differences in Oxidation Behavior of Used CANDU Fuel During Prolonged Storage in Moisture-Saturated Air and Dry Air at 150°C, Nuclear Technology, vol. 104, pp. 309-329, 1993.

[Weber, 1983] Weber, W.J.: Thermal recovery of lattice defects in alpha-irradiated UO2 crystals, J. Nucl. Mater. 114 (1983) 213-221.

[Werner, 2017] Werner, C.: MCNP6 User's Manual, Code version 6.2, Report. LA-UR-17-29981, 2017.

[White, 2018] White, T., Mayorov, M., Lebrun, A.R., Peura, P.: Verification of Spent Nuclear Fuel Using Passive Gamma Emission Tomography (PGET), IAEA Symposium on International Safeguards, 2018,

[Wieselquist, 2013] Wieselquist, W., Zhu, T., Vasiliev, A., Ferroukhi, H.: PSI methodologies for nuclear data uncertainty propagation with CASMO-5M and MCNPX: results for OECD/NEA UAM benchmark phase I, Science and Technology of Nuclear Installations, 2013 (2012) 549793.

[Wigner, 1944] Wigner, E.P., Wilkins, E.J.: AECD-2275, Clinton Laboratory, 1944,

[Wiktor, 2014] Wiktor, J., Barthe, M.-F., Jomard, G., Torrent, M., Freyss, M., Bertolus, M.: Coupled experimental and DFT plus U investigation of positron lifetimes in UO2, Phys. Rev. B. 90 (2014) 184101.

[William, 2006a] William, C., Håkansson, A., Osifo, O., Bäcklin, A., Svärd, S.J.: Nondestructive assay of spent nuclear fuel with gamma-ray spectroscopy, Annals of Nuclear Energy 33 (2006) 427-438.

[William, 2006b] William, C., Håkansson, A., Osifo, O., Bäcklin, A., Svärd, S.J.: A non-destructive method for discriminating MOX fuel from LEU fuel for safeguards purposes, Annals of Nuclear Energy 33 (2006) 766-773.

[Williams, 1978] Williams, M.L., Weisbin, C.R.: Sensitivity and uncertainty analysis for functionals of the time-dependent nuclide density field, ORNL-5393, April 1978.

[Williams, 2011] Williams, M.L.: Resonance Self-Shielding Methodologies in SCALE6, Nuclear Technology 174 (2011) 149-168.

[Williams, 2013a] Williams, M.L., Kim, K.S.: The Embedded Self-Shielding Method, PHYSOR 2012, Knoxville, Tennessee, USA.

[Williams, 2013b] Williams, M.L., Ilas, G., Jesse, M.A., Rearden, B.T., Wiarda, D., Zwermann, W., Gallner, L, Klein, M., Krzykarcz-Hausmann, B., Pautz, A.: A Statistical Sampling Method for Uncertainty Analysis with SCALE and XSUSA, Nuclear Technology 183 (2013) 515-526.

[Wilson, 1961] Wilson, W.B., Alexander, C.A., Gerds, A.F.: Stabilization of UO2. Journal of Inorganic and Nuclear Chemistry, Vol. 20, pp. 242-251, 1961.

[Wilson, 2008] Wilson, W.B., Cowell, S.T., England, T.R., Hayes, A.C., Moller, P.: A Manual for CINDER'90 Version 07.4 Codes and Data, LA-UR-07-8412 (December 2007, Version 07.4.2 updated March 2008).

[Wiss, 2014] Wiss, T., Hiernaut, J.-P., Roudil, D., Colle, J.-Y., Maugeri, E., Talip, Z., et al.: Evolution of spent nuclear fuel in dry storage conditions for millennia and beyond, Journal of Nuclear Materials, vol. 451, pp. 198-206, 2014.

[Wood, 1986] Wood, P., Banniste, G.H.: Release of Fission Products During and After Oxidation of Trace-Irradiated Uranium Dioxide at 300 – 900 °C. In: Proceedings of IAEA Specialists' Meeting on Fission Product Release and Transport in Gas Cooled Reactors (Berkeley, United Kingdom, October 22.-25.,1985), Austria, 1986.

[Woodcock, 1965] Woodcock, E.R. et al.: Techniques used in the GEM code for Monte Carlo neutronics calculations in reactors and other systems of complex geometry, ANL-7050, Argonne National Laboratory, 1965.

[Yaakoubi, 2019] Yaakoubi, H.E. et al.: Validation study of the reactor physics lattice transport code DRAGON5 & the Monte Carlo code OpenMC by critical experiments of light water reactors", Journal of King Saud University, Vol. 33 (1), pp. 1271–1275, 2019.

[Yakub, 2010] Yakub, E., Ronchi, C., Staicu, D.: Diffusion of helium in non-stoichiometric uranium dioxide, J. Nucl. Mater. 400 (2010) 189–195.

[Yamamoto, 2007] Yamamoto, A., Tatsumi, M., Sugimura, N.: Numerical solution of stiff burnup equation with short half lived nuclides by the Krylov subspace method, Journal of Nuclear Science and Technology 44 (2007) 147-154.

[Yoshida, 2011] Yoshida, K., Arima, T., Inagaki, Y., Idemitsu, K., Osaka, M., Miwa, S.: Oxygen potential of hypo-stoichiometric La-doped UO2, J. Nucl. Mater. 418 (2011) 22–26.

[You, 2000] You, G.-S., Kim, K.-S., Min, D.-K., Ro, S.-G.: Oxidation kinetic changes of UO2 by additive addition and irradiation. Journal of Nuclear Materials, Vol. 277, pp. 325-332, 2000.

[Zain, 2018] Zain, J.A. et al.: Validation of DRAGON4/DONJON4 simulation methodology for a typical MNSR by calculating reactivity feedback coefficient and neutron flux, Journal of Results in Physics 9 (2018) 1155-1160.

[Zéachandirin, 2011] Zéachandirin, A., Dallongeville, M., Purcell, P., Cory, A.: Description of Fuel Integrity Project methodology principles. Packaging, Transport, Storage & Security of Radioactive Material, Vol. 22, pp. 184-191, 2011.

[Zencker, 2024] Zencker, U., Völzke, H., Gaddampally, M.R.: Failure analysis on irradiated claddings subjected to long-term dry interim storage, Trans. 27th International Conference on Structural Mechanics in Reactor Technology (SMiRT), Session We.2.H.1, Yokohama, Japan, 3-8 March 2024.

[Žerovnik , 2018] Žerovnik, G., Schillebeeckx, P., Govers, K., Borella, A., Ćalić, D., Fiorito, L, Kos, B., Stankovskiy, A., Van den Eynde, G., Verwerft, M.: Observables of interest for the characterisation of Spent Nuclear Fuel, JRC Technical Reports, EUR 29301 EN, 2018.

[Žerovnik, 2019] Žerovnik, G., Ambrožič, K., Čalič, D., Fiorito, L., Govers, K., Hernandez Solis, A., Kos, B., Kromar, M., Schillebeeckx, P., Stankovskiy, A.: Characterisation of spent PWR fuel for decay heat, neutron and gamma-ray emission rate: code comparison,' Proceedings of the International Conference on Mathematics and Computational Methods applied to Nuclear Science and Engineering (M&C 2019), Portland, USA, 25. – 29. August 2019, pp. 2736-2745.

[Zhu, 2015] Zhu, T., Vasiliev, A., Ferroukhi, H., Pautz, A.: NUSS: A tool for propagating multigroup nuclear data covariances in pointwise ACE-formatted nuclear data using stochastic sampling method, Annalf of Nuclear Energy 75 (2015) 713-722.

[Ziegler, 2010] Ziegler, J.F., Ziegler, M.D., Biersack, J.P.: SRIM – The stopping and range of ions in matter (2010), Nucl. Instrum. Methods Phys. Res. Sect. B Beam Interact. Mater. At. 268 (2010) 1818–1823.

[Ziock, 2005] Ziock, K.P., Vanier, P., Forman, L., Caffrey, G., Wharton, J., Lebrun, A.: The feasibility of cask "Fingerprinting" as a spent-fuel, dry-storage cask safeguards technique, Report UCRL-TR-215943, 5 October, 2005.

[Zoia, 2013] Zoia, A., Brun, E., Jouanne, C., Malvagi, F.: Doppler broadening of neutron elastic scattering kernel in TRIPOLI-4, Annals of Nuclear Energy 54 (2013) 218-226.

[Zu, 2016] Zu, T., Yang, C., Cao, L., Wu, H.: Nuclear data uncertainty propagation analysis for depletion calculation in PWR and FR pin-cells, Annals of Nuclear Energy 94 (2016) 399-408.

[Zwermann, 2014] Zwermann, W., Aures, A., Gallner, L., Hannstein, V., Krzykacz-Hausmann, B., Velkov, K., Martinez, J.: Nuclear data uncertainty and sensitivity analysis with XSUSA for the fuel assembly depletion calculations, Nuclear Engineering Technology 46 (2014) 343-352.

[Zwicky, 2010] Zwicky, H.U., Low, J., Granfors, M., Alejano, C., Conde, J.M., Casado, C., Sabater, J., Lloret, M., Quecedo, M., Gago, J.A.: Nuclide analysis in high burnup fuel samples irradiated in Vandellós 2, Journal of Nuclear Materials 402 (2010) 60-73.

http://www.oecd-nea.org/dbdata/data/evaluated.htm

https://www-nds.iaea.org/